Intergovernmental Oceanographic Commission
technical series

48

Neotectonics and fluid flow through seafloor sediments in the Eastern Mediterranean and Black Seas

Part I: Eastern Mediterranean Sea

Preliminary results of geological and geophysical investigations during the ANAXIPROBE/TTR-6 cruise of R/V Gelendzhik, July-August 1996

Editors: J.M. Woodside
M.K. Ivanov
A.F. Limonov

SC-97/WS/67 Part I

UNESCO 1997

For bibliographic purposes, this document should be cited as follows:
Neotectonics and fluid flow through seafloor sediments in the Eastern Mediterranean and Black Seas - Parts I and II.
IOC Technical Series No. 48, UNESCO 1997
(English)

Published in 1997
by the United Nations Educational,
Scientific and Cultural Organization
7, place de Fontenoy, 75352 Paris 07 SP

Printed in UNESCO's Workshops

Printed in France

DEDICATION

This report is dedicated to the memory of our good friend and colleague Rob Kidd, late Professor of Marine Geology at the University of Wales, Cardiff. Rob became an active participant in the Training Through Research programme in 1993, joining both the TTR-3 and TTR-4 expeditions. He was instrumental in both planning and execution of the TTR scientific plans in both those years. He acted as host for the TTR post-cruise meeting on "Deep-Sea Depositional Systems and Mud Volcanism in the Mediterranean and Black Seas" which took place in Cardiff in January-February 1995; and he was involved in the TTR exercises in long-range planning at that time, thus influencing the direction of the programme.

Despite his close association with both the Deep Sea Drilling Program (DSDP) and the Ocean Drilling Program (ODP), leading to his chairmanship of ODP's PCOM and management of the JOIDES Office when he brought it to Cardiff, Rob maintained close ties with the Training Through Research programme until his premature death in June 1996. He used to say that one of the reasons he liked the TTR programme was that it had the spirit and enthusiasm typical of the early days of DSDP.

Everybody associated with him will miss his infectious enthusiasm for good scientific research, his encouraging and stimulating way with students, and his strong leadership and expertise balanced by a warm and friendly spirit and an excellent sense of humour.

TABLE OF CONTENTS

ABSTRACT

The ANAXIPROBE/TTR-6 Cruise of the R/V Gelendzhik was carried out in July-August 1996. Sixty scientists and students from seven countries took part in this marine expedition. The main objectives of the cruise included the investigation of the origin, morphology, and neotectonics of the Anaximander Mountains in the northeastern Mediterranean Sea (as a continuation of the Dutch ANAXIPROBE-95 Programme), and the study of the shallow structure and possible fluid venting in the Black Sea, on the Crimean continental margin and in the Pallas Uplift area, off the Kerch Strait. A secondary objective of the cruise embraced bathymetric mapping, with a multibeam echosounder, of parts of the Mediterranean Ridge, of the mud volcano area in the central Black Sea, and of the Russian economic zone in the eastern Black Sea.

Dredging and coring on the Anaximander Mountains have conclusively proven that this part of the Mediterranean seafloor is a prolongation of the Bey Daglari and Antalya Nappes Complex of mainland Turkey. The area is very active tectonically. Several mud volcanoes, which were inferred from remote sea floor observations, were confirmed by sampling; and active gas venting at these mud volcanoes was demonstrated by the first samples of gas hydrates ever taken from the Mediterranean floor and chemosynthetic benthic communities with Lamellibrachia (vestimentifera worms) and a new species of Lucinid. Numerous acoustic anomalies in subbottom profiler data from different parts of the area testify to the presence of gas. Shallow gas causes large-scale mass movement of sediment in a wide valley between the mountains.

In the Sorokin Trough (Crimean continental margin), many mud volcanoes were also discovered and cored. These mud volcanoes are situated on the tops of clay diapiric folds. The variable trends of the folds are controlled by uplifts in the underlying deposits. The folds resulted from a lateral, roughly south-north compression. A rich collection of gas hydrates was gathered from the mud volcanoes; and some bacterial mats were observed for the first time on authigenic carbonate crust from mud breccia.

The shallow structure of the sedimentary cover in the area of the Pallas Uplift demonstrates several stacked fans belonging to the Pleistocene Don and Kuban Rivers. No evidence of shallow gas occurs in this area.

Brief results of the bathymetric mapping on the Caucasus margin are also described in the report.

ACKNOWLEDGEMENTS

The 1996 Training Through Research cruise was supported by the Intergovernmental Oceanographic Commission of UNESCO, the Netherlands Earth Sciences Foundation (Stichting GOA), the Russian Committee on Geology, the Russian Ministry of Science and Technical Policy, and the Turkish Government. Additional support was obtained from the Free University of Amsterdam and Moscow State University; and ANAXIPROBE was funded entirely by Stichting GOA as project number 750.195.02.

Grateful acknowledgement is due to several people in the various organizations responsible for making the cruise possible. Those people whose efforts on behalf of the Training Through Research Programme were important for the success of TTR-6 include Prof. Dr. I.F. Glumov (the Russian Committee on Geology), Dr. J. Stel (Director of Stichting GOA), Dr. A. Suzyumov (UNESCO), and Prof. Dr. G. Kullenberg (Executive Secretary of IOC).

Thanks should are also due to C. van Bergen Henegouw of the Netherlands Institute for Sea Research (NIOZ) for logistic assistance, K. Gelisli and his colleagues at the Karadeniz Teknik Universitesi in Trabzon for organizing an excursion at very short notice, and to B. Ecevitoglu (Istanbul Technical University), N. Cagatay and B. Alpar (Istanbul University) and M. Ergün (Dokuz Eylul University in Izmir) for assistance with the port call and various arrangements for cruise participants in Istanbul. The Turkish Petroleum Organization, through Dr. S. Turgut, was very helpful in expediting the shipment of rock samples from Istanbul to Amsterdam. Prof. Dr. M. Ergün was instrumental in the successful liaison with the Turkish authorities regarding all aspects of the cruise in Turkish waters. P. Rosov arranged for travel of the participants between Novorossiysk and Istanbul at the end of the cruise.

Finally, Captain Yu. Shikera, his officers, the technicians, and crew of the R/V Gelendzhik are thanked for their role in obtaining the data set; and the Central Marine Geological/Geophysical Expedition and NIPIOkeangeofizika (Gelendzhik) for their provision and management of the equipment.

Preparation of this report was made possible with the help of a grant provided by the UNESCO Venice Office.

INTRODUCTION

J.M. Woodside, M.K. Ivanov, and A.F. Limonov

The sixth ANAXIPROBE/Training-through-Research expedition took place aboard R/V Gelendzhik between 5 July and 20 August 1996, as a cruise of two legs. The first leg of the cruise was in the Eastern Mediterranean and the second was in the Black Sea. The Black Sea leg was further divided into two parts separated by a port stop in Trabzon, during which some participants disembarked and an excursion took place. Thirty one scientists and technicians and twenty nine students from eight countries and sixteen organizations took part in the cruise. A list of the participants on different legs of the cruise is given at the end of the chapter.

The two themes of research were the neotectonics of the eastern Mediterranean collision zone and mud volcanoes and fluid venting in the deep Black Sea and on the Crimean margin. A third theme was the bathymetry mapping of the Causasus margin. The two main themes coincided on the first leg in the Mediterranean because sampling of mud volcanoes was expected to provide a window on the deeper geology of the Anaximander Mountains, and because of the unexpected occurrence of gas in sediments involved in mass sediment movement between the mountains. Also unexpected was the degree of slope instability on the Crimean margin as a result of gas in the sediments there. The cruise therefore evolved as an investigation principally of these processes in both the Mediterranean and Black Seas, as well as the study of the origin and evolution of the Anaximander Mountains.

The cruise began in Naples, Italy, for logistical reasons. This provided the opportunity to obtain a multibeam bathymetric swath along the crest of the Mediterranean Ridge over three previously investigated fields of mud volcanoes (i.e. on the western Mediterranean Ridge (*Limonov et al.,1995*), in the Mediterranean Ridge Mud Diapiric Belt (*Limonov et al., 1994; Cita et al., 1996*), and in the United Nations Rise area (*Limonov et al., 1996*). Similarly, the transect to the Crimean margin study area provided an opportunity to make three multibeam swaths over mud volcanoes previously examined using other methods (e.g. *Ivanov et al., 1992; Limonov et al., 1994*). The cruise ended in Novorossiysk, Russia.

As usual, the quality of the research element of the cruise was all-important; however, the training element was always in mind. One of the most important cornerstones of the Training-through-Research Programme (UNESCO-IOC Floating University Project) is that good training of young scientists is best achieved as part of a good research programme. Besides the normal hands-on experience of taking part in the research, 31 daily seminars were held on various topics from the themes and results of the cruise to related research by participants.

In planning the sixth cruise of the series, the intention was to shift the Training-through-Research Programme into a new mode in which cruises would be built around larger, previously funded projects which would provide

both a focus and momentum. This year the Dutch ANAXIPROBE project provided much of the motivation and support for the cruise. It was also thematically consistent with the general objectives of Training-through-Research, and organized on the basis of work carried out during the first Training-through-Research expedition in 1991.

This report presents the research methods, background geological information, and intitial results of the cruise. It should be understood that most of the data analysis remains to be done and that the scientific conclusions may change as a result of both the analyses and the ensuing interpretations. For each leg, a geological introduction is given, followed by a description of the data and preliminary interpretations.

The initial reports of previous expeditions in the series were issued as numbers 56, 62, 64, 67, and 68 of UNESCO Reports in Marine Science; and abstracts of presentations given at post cruise meetings can be found in numbers 91, 94, 99, and 100 of UNESCO's Marinf report series. Publication of results takes place ultimately in the open scientific literature. References to some of the publications dealing with related research within the Training-through-Research Programme may be found in the references section of this report.

List of participants of the ANAXIPROBE/TTR-6 Cruise in the Mediterranean and Black Seas

	Leg*
France	
J.-F. Dumont (Laboratoire de Géodinamique sous-marine, Villefranche-sur-Mer)	M
J.-P. Foucher (IFREMER, Brest)	B
Georgia	
E. Sakvarelidze (Tbilisi State University)	B
Germany	
M. Lüdde (University of Hamburg)	M, B
Italy	
A. Mazzini (University of Genoa)	M
The Netherlands	
J.M. Woodside** (Free University, Amsterdam)	M, B
B.B. Swaak (Free University, Amsterdam)	M, B
A.J. Doest (Free University, Amsterdam)	M, B
E. Ivanova (Free University, Amsterdam)	M

E. van der Schans (Free University, Amsterdam)	M
T.L.P. Kleeven (Free University, Amsterdam)	M
H. van den Bosch (Free University, Amsterdam)	M
J. Henderiks (Free University, Amsterdam)	M
S. Woodside (University of Amsterdam)	M, B

Russian Federation

B. Shirokozhukhov (CGGE, Gelendzhik)	M, B
A. Shanin (CGGE, Gelendzhik)	M, B
V. Skorkin (CGGE, Gelendzhik)	M, B
O. Zuev (CGGE, Gelendzhik)	M, B
A. Pavlov (CGGE, Gelendzhik)	M, B
V. Gubenkov (CGGE, Gelendzhik)	M, B
S. Maraev (CGGE, Gelendzhik)	M, B
V. Vasilyev (CGGE, Gelendzhik)	M, B
P. Lygin (CGGE, Gelendzhik)	M, B
R. Kazantsev (CGGE, Gelendzhik)	M, B
A. Rudnev (CGGE, Gelendzhik)	M, B
V. Tsyganenkov (CGGE, Gelendzhik)	M, B
V. Sirotin (NIPIOkeangeofizika, Gelendzhik)	M, B
V. Petrenko (NIPIOkeangeofizika, Gelendzhik)	M, B
V. Kharlamov (NIPIOkeangeofizika, Gelendzhik)	M, B
V. Noskov (NIPIOkeangeofizika, Gelendzhik)	M, B
L. Meisner (NIPIOkeangeofizika, Gelendzhik)	B
M. Ivanov** (Moscow State University)	M, B
V. Gainanov (Moscow State University)	M, B
S. Buryak (Moscow State University)	M, B
A. Volkonskaya (Moscow State University)	M, B
E. Mityakina (Moscow State University)	M, B
A. Trofimuk (Moscow State University)	M, B
R. Almendinger (Moscow State University)	M, B
P. Shashkin (Moscow State University)	M, B
E. Kotochigov (Moscow State University)	M, B
A. Burlakov (Moscow State University)	M, B
A. Limonov (Moscow State University)	M, B
O. Krylov (Moscow State University)	B
G. Akhmanov (Moscow State University)	M, B
E. Kozlova (Moscow State University)	M, B
A. Akhmetjanov (Moscow State University)	M, B
A. Korkin (Moscow State University)	M, B
E. Belokrinitskiy (Moscow State University)	M, B
A. Sautkin (Moscow State University)	M, B
A. Stadnitskaya (Moscow State University)	M, B
I. Belen'kaya (Moscow State University)	M, B
A. Dorofeeva (Moscow State University)	M, B
E. Udilovich (Moscow State University)	M

S. Gablina (Paleontological Institute, Russian Academy of Sciences)	M, B

Switzerland

S. Wagner (Geological Institute, University of Neuchatel)	B

Turkey

M. Ergün (Piri Reis Foundation, Izmir)	M
G. Çifçi (Dokuz Eylul University, Izmir)	B
B. Alpar Saban (Marine Science and Managdement Institute, Istanbul)	B
S. Turgut (TPAO, Ankara)	M

---

*M - Mediterranean Leg; B - Black Sea Leg.
**Chief scientist.

TECHNICAL REPORT

Not all the methods and equipment used during the cruise are described in this report. Those that have been used previously on Training Through Research expeditions are documented in previous reports in this series. Thus the deep-tow MAK-1 sidescan sonar and subbottom profiling system is described in *Limonov et al. (1993)*, the report of the second cruise (TTR-2). A description of the ship is given in *Ivanov et al. (1992)*. In cases where the methodology has changed slightly, revisions will be found in this report.

Two new methods were used this year for the first time in the Training Through Research programme: multibeam bathymetric mapping and dredging. A SIMRAD EM-12S(120) multibeam system was installed on the R/V Gelendzhik in early 1996 and used for the first time on an Italian cruise prior to TTR-6. This was used principally on a transit along the Mediterranean Ridge and for efficient bathymetric surveying in the Black Sea. Dredging was an important addition to the sampling programme because of the requirement this year to obtain samples of rock outcrops. Although dredging is a well-known method, it is not often used because it can be difficult, time-consuming, and not very precise; however, it was effective on Leg 1 of this cruise.

The ship positioning during the cruise was fulfilled with the GPS 4400.

1. Seismic reflection system

V.G. Gainanov

Seismic profiling equipment

For carrying out the seismic profiling during the cruise, a Pulse-5 air-gun and a PSS-12 hydrophone streamer were used.

The towing depth of the seismic source and streamer was 3 m, which is shallower than the calculated one (about 7 m at a predominant signal frequency of 50 Hz) but this allowed us to achieve a better vertical resolution. The towing speed was 7-7.5 knots.

Pulse-5 air-gun

Working volume, l.....3.0
Working pressure, mPa.....15
Signal frequency range, Hz.....20-250
First positive pulse amplitude at a distance
of 1 m, mPa.....5.0
Weight, kg.....45

PSS-12 hydrophone streamer

Number of receiving sections.....2
Number of empty sections.....6

Number of depressing sections.....1
Number of channels per receiving section.....6
Numbers of hydrophones per channel.....15
Type of hydrophones.....PDS-22
Sensitivity of hydrophones, mV/Pa.....350
Length of receiving section, m.....50
Length of empty section, m.....100
Length of depressing section, m.....10

All six sections of the streamer were connected in parallel, providing a single-channel mode of the signal recording.

Digital data acquisition and processing system: principle of operation

The digital data acquisition and processing system was of our own design. The air-gun was activated by the air-gun control unit in response to a command from our AT486 computer via a parallel interface.

Seismic signals, received by the seismic streamer, were transmitted via the line coupler to the seismic amplifier. After the amplifying and band pass filtering, the signals passed to the analog-digital converter (ADC). The computer processed the digitized signals and wrote them down in a special field format on a hard disk or magneto-optical disk.

The signals were simultaneously displayed on a computer monitor and printer paper in the form of a seismic time-section.

Data acquisition parameters

Amplifier coefficient, dB.....54
Band pass filter, Hz.....15-250
Sampling period, ms.....1
Trace length (samples), s.....3000 (3)
Shot interval, s.....10

Digital data acquisition and processing software

The software contained 2 main programs and several additional ones. The main programs were as follows: seis96.exe and rseis96.exe.

Data acquisition and real time processing program seis96.exe performs the following principal operations:

1. Before the registration starts, it provides the passibility for the input and modification of all data acquisition parameters, such as sampling period, shot interval, etc. It also allows some parameters (e.g. delay) to be changed during the registration not interrupting the process.

2. The program follows a computer system timepiece and sends commands for the air-gun activation over fixed time intervals. Simultaneously it resets the ADC and provides the data input in direct memory access (DMA) mode.

3. When a new seismic trace is received in DMA mode, the program is concurrently processing the previously received trace and is visualising it on the monitor and printer as a seismic time-section.

4. After completing a new trace input, the program processes it to form the special data registration format (field format), putting in it the additional information, such as date, time, trace number, and so on, and writes it down on hard disk.

5. After this, the program comes back to operation 2 of this description, if there is no the command to stop the process.

During the data registration and processing, the following parameters can be changed by giving the corresponding commands from a computer's keyboard:
-delay value;
-mode of data output on monitor and printer.

For example, the time-section signal imagery on a monitor can be changed into 'oscilloscope' mode, which provides possibility for the signal form, source, and receiver control.

Program rseis96.exe was used for the seismic data processing, which were available on a hard disk. Generally, it works similarly to the one above described.

There were also programs in use for predictive deconvolution, signal spectrum analysis, transformation of the data into SEG-Y format, etc.

Procedure of the onboard seismic data processing

- reading the data from disk;
- normalizing the time sections to a single time (delay);
- predictive deconvolution;
- band pass filtering;
- preparing the data for output on a printer (gain regulation of traces; vertical and horizontal scales adjustment);
- data output on a printer.

2. Simrad EM-12S multibeam system

R.M. Almendinger

Application

The multibeam echosounder SIMRAD EM-12S(120) is designed for obtaining both high resolution bathymetric and reflectivity maps of the sea floor. The major application of the system is for studying seafloor relief for geological, geomorphological, and geotechnical purposes.

Principle of operation

The basic model of the echosounder EM-12 is the EM-12S, which has an angular coverage sector of 90° with 81 beams and is composed of following units:

- Transmitter subsystem
- Transducer arrays (for transmission and for reception separately)
- Receiver subsystem including beam-former and special digital signal processors
- Storage and display subsystem consisting of a Bottom Detection Unit (BDU), an Operator Unit (OPU), a Quality Assurance Unit (QAU), and a Sidescan Unit (SSU).

The model EM-12S(120) installed onboard the Gelendzhik and used during the cruise is a version of the EM-12S with a software option which extends the angular coverage of EM-12S to 120° with a swath width of 3.5 times water depth. The beam spacing is either 1.5° or equidistant horizontally. The system installed on Gelendzhik does not include a Sidescan Unit. The transmitter subsystem insonifies the seafloor through the transducer array for transmission along the swath which is narrow in the fore- and aft direction and wide in athwartship direction. The echo returned from the insonified area is received through the transducer array for reception by the receiver subsystem. The beam-forming along each swath is accomplished automatically using algorithms of time domain phase shift and amplitude weighting. Each of the beams is used to detect both depth and reflectivity of a part of the seafloor within the insonified area.

The beam-forming is arranged in such a way that each beam is composed of two half beams, with each half beam being generated by approximately 70% of the transducer. The sum of these two half beams is used to estimate the amplitude of the returned echo and the difference in their phases is used to estimate the phase data. Both amplitude and phase data are used in bottom detection for each beam. In the amplitude detection, the center of gravity of the returned echo is used. The phase detection is based on interferometric principle. The final bottom detection range and an estimate of seabed reflectivity, made on the basis of the amplitude data for each beam, are transferred for rebinding correction and digital storage on an optical disk together with position data. Values of the ship's attitude (pitch, roll, etc.) measured at the times of transmission and reception allow an exact calculation to be made of the bottom hit-points in all directions.

Specifications

The SIMRAD EM-12S(120) echosounder provides high resolution bathymetric and acoustic reflectivity maps of the seafloor in 50 to 11,000 m water depth range.

Swath width.....3.5 times water depth
Depth definition accuracy.....0.25% of depth or 60 cm (whichever is greater)
Transmission pulse length:
shallow mode.....2 ms
deep mode.....10 ms
Transmission beam width in
fore-and-aft direction.....1.8°
Transmission beam
stabilization accuracy.....0.5°
Number of transducer elements
for transmission..... 384
Maximum total power input
on transmission.....10 kW
Number of elements in
the receiver array.....210
Number of channels
for reception.....42
Number of beams
for reception.....120
Reception beams width:
fore-and-aft direction.....20°
athwartship direction.....3.5 to 5.0°
Reception beams spacing.....1.5° or equidistant horizontally

Bottom definition accuracy
(reception beams spacing accuracy).....0.2°.

All data produced by the sounding system were recorded on 3.5" magneto-optical disks. The data comprise water depth information, signal strength data, parameter settings, sound velocity profiles used and position data.

Methods of work were chosen to ensure as much as possible complete coverage of the entire areas of investigation by multibeam echosounder data. Because the swath range of the EM-12S depends on depth, the lines were laid out taking this factor into account using a priori information about water depth. In order to ensure accurate and reliable bathymetric data, sound velocity measurements in water were made for every new study area. However EM-12 is very sensitive to sound velocity changes in the water column, and it was not

possible to avoid all distortions in the bathymetric data caused by uncertainties in the sound velocity profile. These distortions probably can be improved by further postprocessing of data.

3. Sampling facility

H. van den Bosch, A.V. Korkin, A.M. Akhmetjanov, and J.-F. Dumont

The bottom sampling was carried out with a dredge and a gravity corer. The dredge was used for obtaining the clasts of consolidated rocks outcropping on steep escarpments while the samples of soft sediments were taken by gravity corer. The gravity corer also recovered numerous clasts from deep below the seafloor when sampling material erupted from mud volcanoes.

The pipe dredge used was 75 cm in diameter and 100 cm long. The bottom end of the dredge was covered with a steel gridwork to keep the larger rock fragments from escaping but allowing the water and fines through; and a nylon mesh bag was attached to catch small rocks that passed though the grid. The leading edge of the open (upper) front end of the dredge was toothed to enable the dredge to catch on the rock surface, to aid in detaching fragments of rock. Between the tow cable and the chain attached to the leading edge of the dredge there was a rope weak-link which could pull up to about 2.5 tons.

The dredging sites were chosen on the basis of an analysis of the detailed seafloor relief and reflectivity pattern obtained from the corresponding Simrad EM-12D data (*Woodside, 1995*). The dredging was carried out in different structural-morphological zones of the mountains, along lines oriented perpendicular to maximum slope angle in areas with a strong seafloor reflectivity suggestive of outcropping bedrock or coarse talus. When the dredge reached the sea bottom (observed by a decrease in cable tension) at the deepest point on the dredge haul, the speed of the ship and the rate of cable release from the winch were equalized in order to keep the cable straight until about 500 m of cable were laid down on the seafloor. The dredge was then pulled at the lowest ship speed until it reached the final selected point at the end of the dredge haul. All 'bites' of the dredge (very strong tugs on the cable) were noted. The actual coordinates of the start and end points of the dredging were calculated taking into consideration the ship position and course, cable length, and the water depth.

After the retrieval of the dredge on deck, soft sediment was washed out using a jet of water from a hose, and only the remaining hard rock samples were retained. The rock samples were immediately classified lithologically and checked for fossils, in order to get an overview of the geological units as early as possible.

A gravity corer was normally used for sampling soft sediment. It had a length of 660 cm, an exterior diameter of 16.8 cm, and a weight of about 1500 kg. A stiff detachable plastic liner was used inside the iron core barrel of the corer during sampling. When the corer was brought on deck, the liner was then removed from the barrel and laid on a trestle especially designed for this purpose. The core was then extruded using a piston operated either by hand or with the help of a special worm gear and crank. Sixty centimetre core subsections of the extruded sediment were taken to the geological laboratory where they were split in half using either a nylon line for soft sediments or an iron wire for mud breccia cores. One half was then labelled and placed in a special core tray where it was photographed by a camera mounted on a frame above it. A general,

plane picture was taken of the entire split core. Every two sections were photographed together in more detail. After being photographed, this half of the core was described in detail, and key horizons were sampled for smear-slide analysis. Further subsampling of this half for other kinds of analysis was made after complete core description.

The other half was split again, to provide two quarter sections. One quarter was packed for archiving at Moscow State University, and the rest of the core was used for all other sampling for various analyses, such as mineralogical, grain-size, X-ray, and geochemical.

SCIENTIFIC REPORT

I. MEDITERRANEAN LEG (ANAXIPROBE-96)

1. Multibeam echosounder regional line along the Mediterranean Ridge

A.F. Limonov and M.K. Ivanov

An underway survey with the EM-12S multibeam echosounder was carried out on the transit from Naples to the Anaximander Mountains. The regional echosounder line was run from the base of the Calabrian Rise (Ionian Sea) almost to the Strabo Trench south of the sea mountains (Fig. 1). The total length of the line is about 1300 km. The line was aimed to obtain a precise bathymetric and bottom reflectivity swath in geologically interesting areas, some of which were studied during the previous TTR cruises: the western termination of the Mediterranean Ridge, the Cobblestone area 3, the Olimpi mud volcano field, the United Nations Rise (*Ivanov et al.*, 1996), and the eastern termination of the Mediterranean Ridge.

The base of the Calabrian Rise (the outer Calabrian Arc) is characterized by rather isometric topographic features with relief of 100-200 m. At the point with coordinates 37°12′ N/17°13′ E, a water depth of 3500 m was recorded, which gives a positive difference of about 300 m from that indicated in the International Bathymetric Chart of the Mediterranean (*IOC-UNESCO, 1981*). To the east of 17°30′ E the topographic trends become more southwestern-northeastern, and this pattern remains over the whole transitional zone from the Calabrian Rise to the Mediterranean Ridge.

The reflectivity imagery clearly shows regular southwestern-northeastern structural trends east of 18°45′ E. A circular, concentric negative feature was recorded at 37°00′ N/18°40′ E (Fig. 2). It is about 7 km across, and its nature remains uncertain.

The transition to the Mediterranean Ridge (at a longitude of about 19°45′) is gradual and is marked by a progressive decrease of the waterdepth from 3700-3800 m to 3300 m, the depth continuing to decrease southeastward along the line. The topographic trends change into northwestern-southeastern, parallel to the general trend of the ridge. The Outer Deformation Front, which is well expressed in the more eastern segment of the ridge, is evidently absent in the area which we crossed.

The next NW-SE oriented portion of the line runs across the Cobblestone area 3. The well-known Prometheus dome was recorded at 35°51.5′ N/20°51.2′ E (*cf.* 35°51′ N/20°48′ E in *Cita and Camerlenghi, 1992*). Its slopes, particularly the western one, are marked by high reflectivity, whereas the reflectivity on its top is low. In addition to this, the bathymetric contours show numerous circular positive relief features, about 2.5 km in diameter and 50-200 m high, at least six of them being notable for high reflectivity. They are thought to be mud volcanoes, because many such structures were observed in the OKEAN sonograph in 1994, and the mud volcanic nature of some of them was proven by coring (*Limonov et al., 1995*).

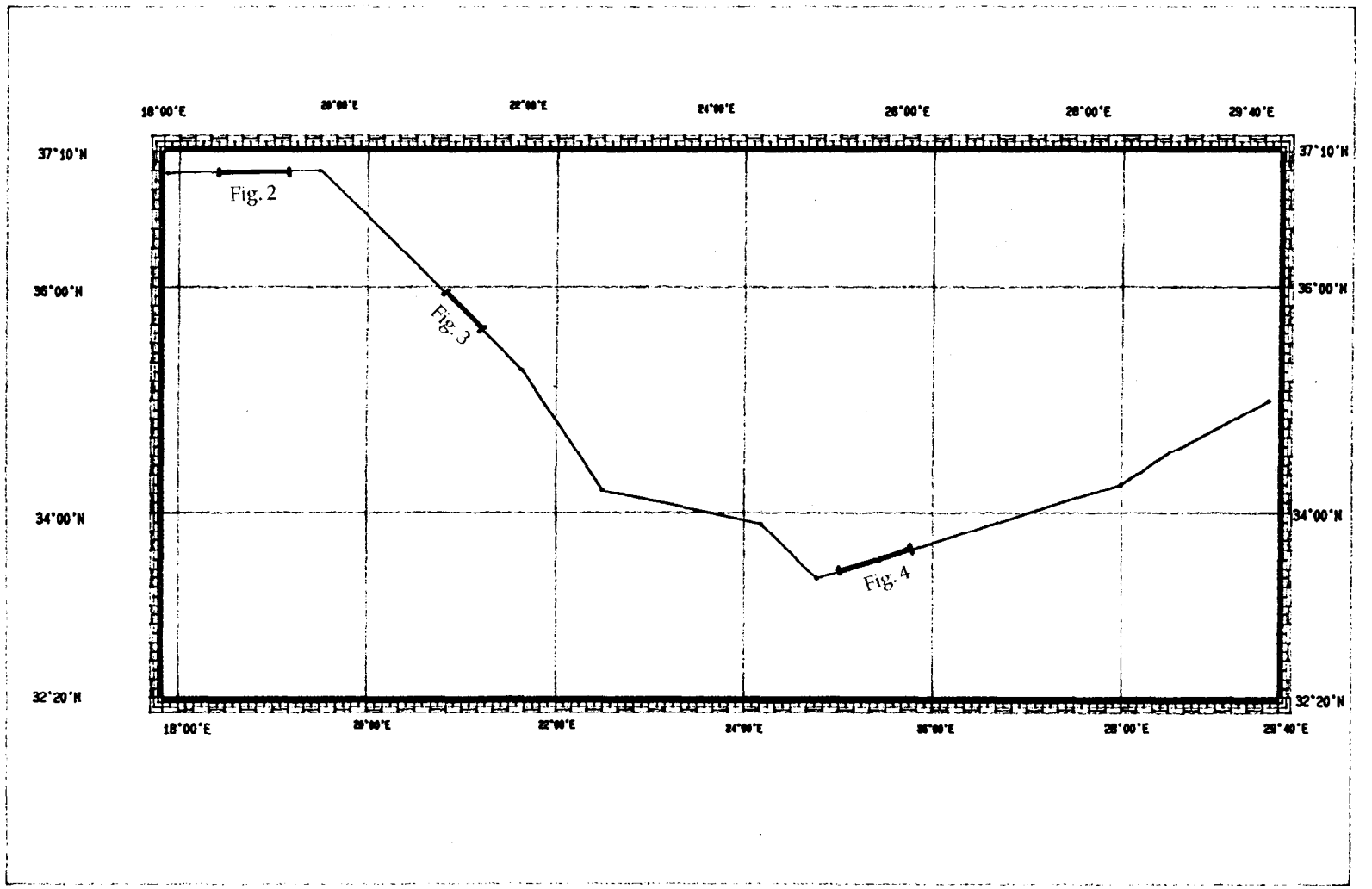

Fig. 1. Location map of the Simrad EM-12S line along the Mediterranean Ridge. The thick segments of the line are referred to Figures 2 - 4

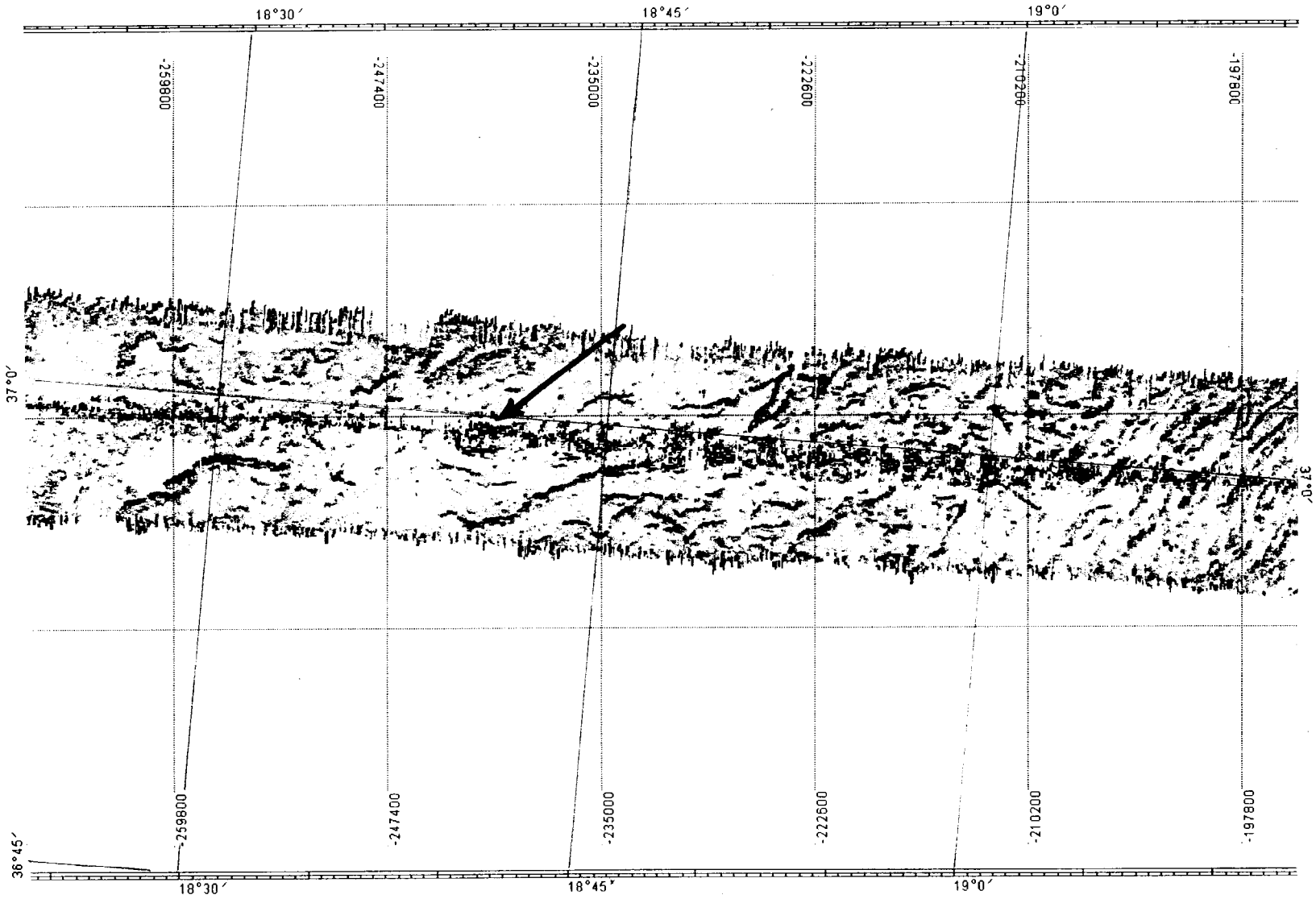

Fig. 2. Circular, concentric feature with a negative seafloor relief, about 7 km across (arrow). Its nature remained uncertain (sink hole?). Note also the change of the topographic trends at 18°45′E. The regular SW-NE structural-geomorphologic trends east of 18°45′E are clear evidence that this area of the Mediterranean seafloor is affected by the Calabrian subduction rather than the Hellenic one

To the southeast of 21° E, the line follows slightly obliquely the Inner Deformation Front of the Mediterranean Ridge. The Inner Deformation Front is seen as a steep, east-northeast-facing scarp more than 750 m high. The reflectivity swath demonstrates that the front is represented by several *en echelon* highly reflective linear features, which are interpreted as the edges of backthrust sheets (Fig. 3). One of the assumed mud volcanoes is clearly related to the thrust plane. No mud volcanoes are observed inward (northeast of) the deformation front.

The next line segment stretches between 35°18′ N/21°34′ E and 34°12′ N/22°30′ E. The western part of the Discovery brine lake (*MEDRIFF Consortium, 1995*), more than 200 m deep is well seen at the very beginning of the segment. Its reflectivity is unknown because the reflectivity imagery was plotted only for the final quarter of the line segment. The first half of this line segment shows a subdued relief with the waterdepth averaging 3200 m. The relief becomes higher and more complex toward the southeast. Deep slightly elongate depressions on the seafloor may represent karst forms in the shallow buried or exposed Messinian evaporites. Exposures of the Messinian may also be expected on the steep walls of seafloor highs bounded by faults, which are marked by strong reflectivity. This system of highs belongs to the Inner Deformation Front that separates the Inner (Lower) Plateau from the crestal part of the Mediterranean Ridge (the Upper Plateau) in this part of the ridge (*Limonov et al., 1994*). Circular relief features, which could be related to mud volcanoes, are not observed.

The next line segment runs over the flat Inner Plateau, crosses the Inner Deformation Front again at 34°04′ N/23°20′ E, and attains the western boundary of the Olimpi/Prometheus 2 mud volcano field. A number of isometric or slightly elongate seafloor depressions, from 50 to 250 m deep, are recorded within the Deformation Front. They might be attributed to karst forms.

Within the Olimpi/Prometheus 2 mud volcano field, the line runs from the Gelendzhik mud volcano plateau to the Toronto mud volcano. The Gelendzhik plateau is accompanied by a 100 m deep depression to the west of it. The western margin of this plateau has enhanced reflectivity on the reflectivity imagery. The Toronto mud volcano, which has the elevation of 130 m, is displayed as a very dark spot with irregular edges.

After the crossing of the Toronto dome, the line passes over the United Nations Rise, which is a part of the Inner Deformation Front (*Ivanov et al., 1996a*). The Inner Deformation Front can be traced on the basis of its characteristic topography from 33°34′ N/25°17′ E to 33°48′ N/26°17′ E. The steep western edge of the rise, rising to about 300 m above the neighbouring seafloor area, implies the presence of a large fault zone. This fault system, confirmed also by the reflectivity imagery, was recorded on the OKEAN sonographs and seismic sections in 1995, and, as was shown then, bounds the United Nation Rise, separating it from the rest of the Mediterranean Ridge (*Ivanov et al., 1996a*). No preferred orientation of topographic trends is observed on the United Nations rise: its topography is dominated by steep, rather isometric highs and lows with relief of 150-250 m (Fig. 4). At longitude of 25°50′ E, one of the branches of the Strabo Trench, with a waterdepth of up to 2825 m wedges into the United Nations Rise from the southeast.

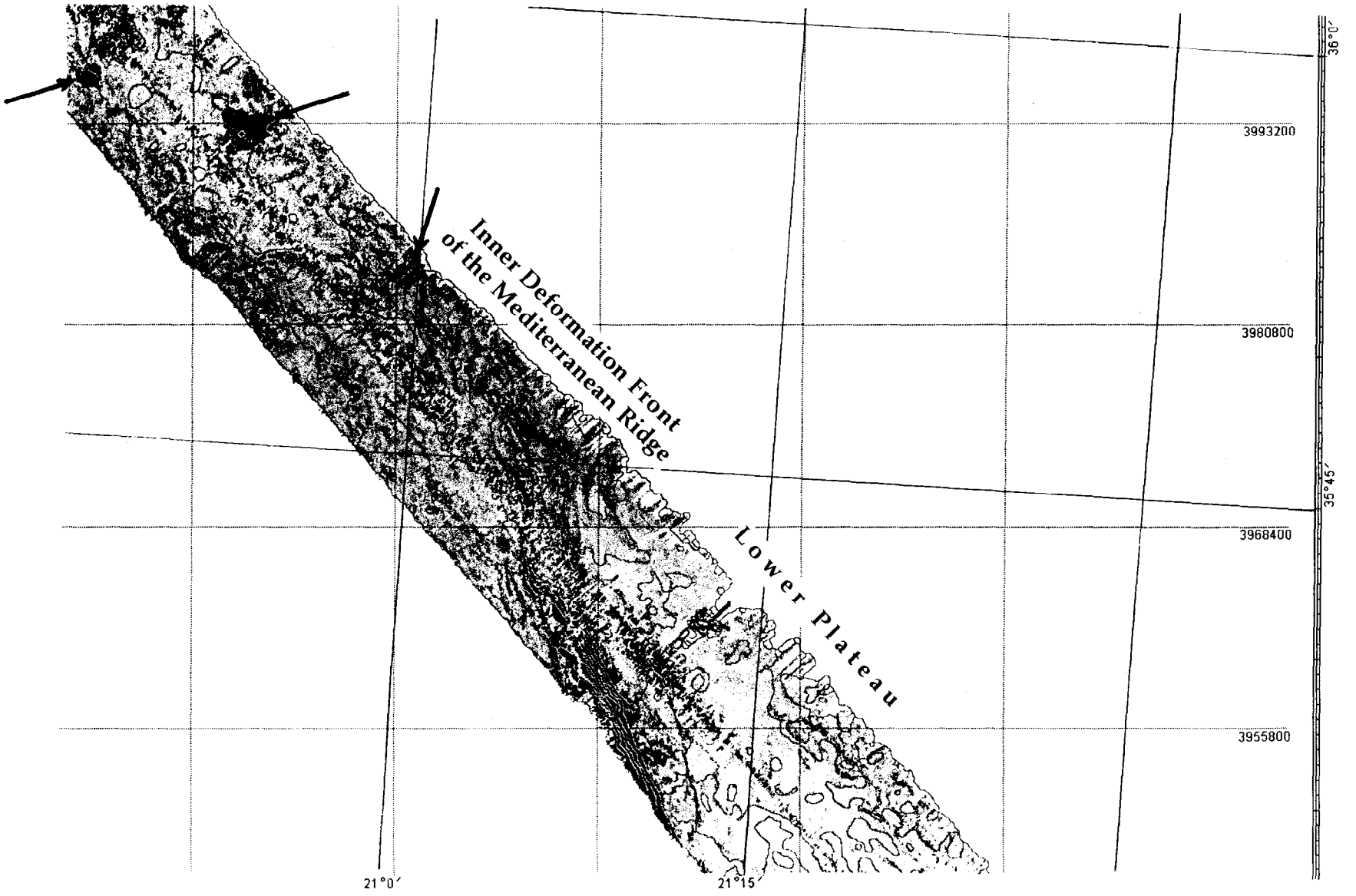

Fig. 3. The Inner Deformation Front of the Mediterranean Ridge appears as *en echelon* highly reflective linear features. Bathymetrically it is expressed as an east-northeast-facing scarp more than 750 m high. The assumed mud volcanoes are marked by arrows

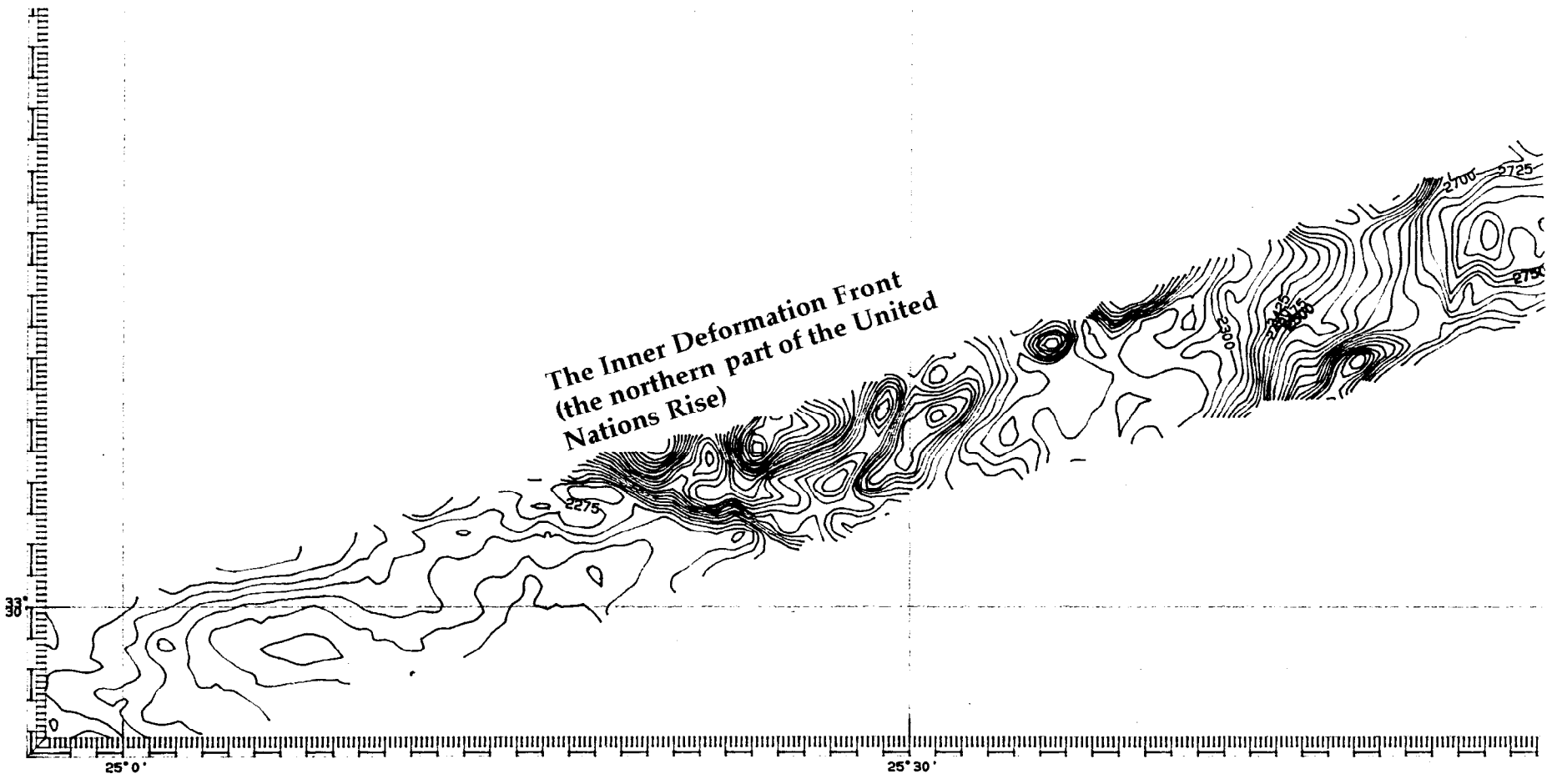

Fig. 4. The United Nations Rise is notable for steep, rather isometric seafloor highs and lows contrasting with the neighbouring parts of the Mediterranean Ridge. The rise was attributed to the Inner Deformation Front (*Ivanov et al., 1996*)

The topography sharply changes after passing the United Nations Rise. The line follows along and slightly obliquely the Strabo Trench, over the southern slope of the Mediterranean Ridge; hence the portside scan of the bathymetric swath shows consistently less waterdepth than the starboard scan. The relief is subdued and rarely exceeds 50 m. The previous OKEAN survey in this area has demonstrated that the structural trends (faults and folds) form a saw-toothed pattern here, which is consistent with the general tectonic stress distribution over the eastern Mediterranean ridge (*Limonov, in press*). Such a pattern continues to the end of the line. On the corresponding OKEAN records (*Ivanov et al., 1996a*), wide outcroppings of the Messinian evaporites were seen as a mottled acoustic signature; therefore some circular and oval depressions on the seafloor can be attributed to karst depressions.

2. Introduction to ANAXIPROBE-96 expedition

J. M. Woodside

ANAXIPROBE is a two-phased research programme funded by the Netherlands Foundation for Earth Sciences to determine the origin and evolution of the actively developing Anaximander Mountains in the eastern Mediterranean. Phase 1 of the programme was a survey completed in 1995 aboard the Research Vessel L'Atalante; and Phase 2 comprises follow-up work in 1996 aboard the Research Vessel Gelendzhik which, as part of the 1996 Training-Through-Research cruise (TTR-6), is reported here. The general scientific aims of ANAXIPROBE Project are (1) to determine the origin of the Anaximander Mountains (i.e. are they a foundered southern part of Turkey, a northward-collided part of the African lithospheric plate, or an upthrust block of the neo-Tethyan seafloor?), and (2) to determine current neotectonic deformation in order to infer the Cenozoic history and evolution of the Anaximander Mountains.

The 1995 expedition on the French research vessel l'Atalante carried out multibeam swath mapping and associated underway geophysical measurements to determine the best locations for deep-towed sidescan sonar, high-resolution subbottom profiling, and bottom sampling in the second phase of the work. Specific objectives of the ANAXIPROBE-95 expedition were (1) to complete a detailed bathymetric and reflectivity map of the region by Simrad EM-12D multibeam as a basis (a) for future submersible, sampling, and deep tow operations and (b) for mapping tectonic fabric, structural features, and sedimentary facies, (2) to make seismic reflection profiles, gravity and magnetic observations along the multibeam survey tracks to provide geological information in depth (structural, sedimentological, and deformational), and (3) using the data collected on the expedition, (a) to specify areas for detailed surveying in the second part of the cruise (in 1996) and to identify potential dive sites for the proposed submersible work, and (b) to start the analysis and interpretation of the data in support of the overall objectives. These objective were successfully attained.

Specific objectives of the ANAXIPROBE-96 expedition were (1) seafloor sampling of (a) each of the three main mountains in the group, (b) the plateau on which the mountains sit, (c) the nearby continental slope of Turkey for purposes of comparison of diagnostic characteristics of the rocks from each location which will help determine their provenance and history, (2) deep-tow MAK acoustic lines across key features identified from the previous survey to obtain detailed high-resolution sidescan sonar images and subbottom profiles, and (3) subsidiary sampling of seafloor areas where interesting targets were identified (which include mud volcanoes and active emplacement of nappes and other gravitational sedimentary deposits).

3. Onshore geological setting

J.-F. Dumont and S. Turgut

North of the area of the ANAXIPROBE cruise, the geological units are, from east to west, the Antalya nappes and the Bey Daglari and Susuz Dag Massifs. The Bey Daglari constitutes the autochthonous unit relative to the Antalya Nappes to the east. The southern end of the north-south trending Antalya Nappes intersects the coast to the east of Finike (Fig. 5; see Figure 6 for detailed position). The Susuz Dag constitutes the southwestern extension of the Bey Daglari Massif, and abuts the coast from Finike to the west. The Susuz Dag and Bey Daglari also form the autochthonous basement of the Lycian Nappes further to the west, northwest of the study area (Fig. 5). The autochthonous basement appears in the Susuz Dag and Bey Daglari Massifs as a wide anticline on the eastern margin of which stands the Antalya Nappes Complex.

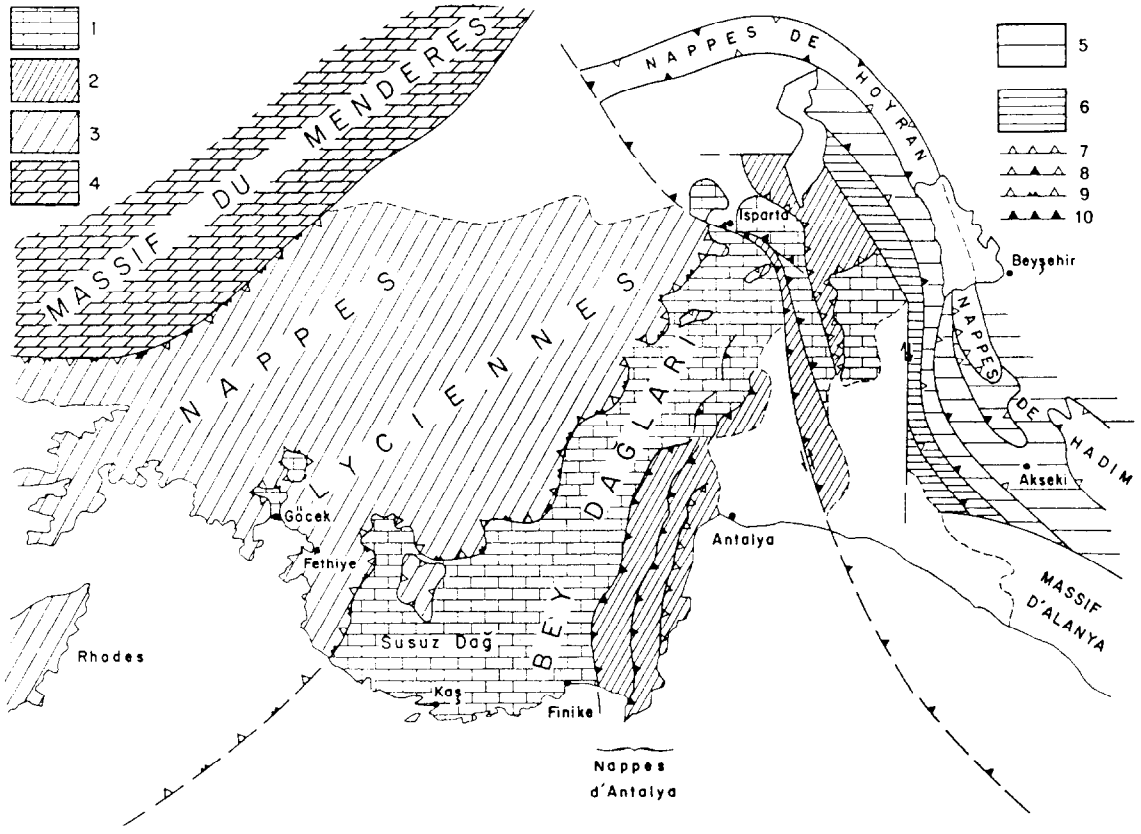

Fig. 5. Main structures around the Bey Daglari Massif, from *Gutnic et al. (1979)*. 1: Bey Daglari type platform unit. 2: Antalya Nappes Complex (Late Cretaceous-Paleocene overthrust), 3: Lycian Nappes (Middle Miocene overthrust), 4: Menderes Massif (Middle Miocene thrust), 5: Akseki- Beysehir Units (Upper Eocene overthrust), 6: Anamas-Akseki platform (parautochthonous unit, connected to the Bey Daglari), 7: Late Cretaceous overthrusts, 8: Upper Eocene tectonic phase, 9: Lycian/Aegean tectonic phase, 10: Late Miocene Aksu phase

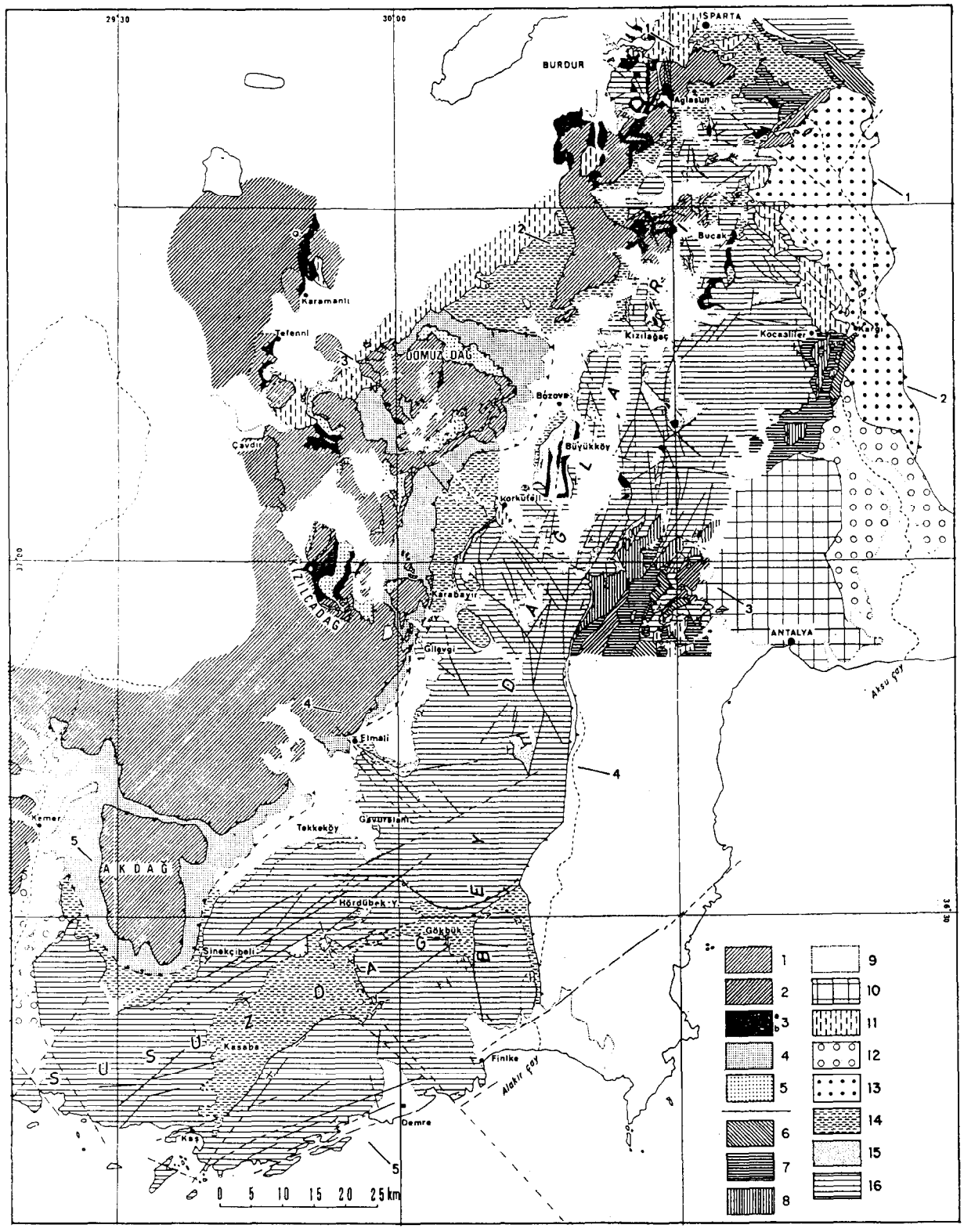

Fig. 6. Structural scheme of the Susuz Dag, Bey Daglari and surrounding areas, from *Gutnic et al. (1979)*. 1 to 5: Lycian Nappes (1: Limestone Units, 2: Ophiolite Nappe, 3: Olistostrome and ophiolite melange, 4: Eocene-Oligocene flysch, 5: other flysch units). 2 and 6 to 8: Antalya Nappes Complex (2: Ophiolite Nappe, 6: Upper Unit, 7: Middle Unit, 8: Lower Unit), 9 to 16: autochthonous, parautochthonous units, and recent formations (9: recent alluvial deposits, 10: Antalya Travertine, 11: Plio-Quaternary, lacustrine sediments and Isparta volcanics, 12: marine Pliocene, 13: Middle to Upper Miocene of Aksu Formation, 14: Aquitanian limestones and Burdigalian/Langhian Flysch, 15: Paleogene, 16: platform limestones, Trias to upper Cretaceous

Structures

The southern Susuz Dag and Bey Daglari Massifs (Fig. 6) constitute a wide anticlinal structure with relatively strongly dipping margins and a small synclinal area between the two north of Finike. The axis of this wide structure trends NNE-SSW. Miocene deposits are involved in the structure, the formation of which is attributed to the Aksu Tectonic Phase of late Miocene age. The drainage of this region is poor, without output to the sea for the water collected in the depressions of former Quaternary lakes at heights of 850 m to 1000 m in the axial part of the massif. This drainage pattern suggests an active karstic circulation between the mountain and the sea.

The main trend of faults in the southern Susuz Dag is NE-SW to ENE-WSW (Fig. 6). This trend direction is the same as that of the coast between Kas and Finike, as well as the main orientation of the Kasaba depression. The NE-SW faults cut across the Antalya Nappes Complex from Finike in the east to the sea in the southwest. They also control the position of depositional areas of the Plio-Quaternary sediments and therefore postdate the Miocene; but no more precise data are available for the age and kinematics of these faults. A secondary fault trend oriented NW- SE is observed between Finike and Demre and near the western margin of the Susuz Dag, west of Kas.

The Antalya Nappes Complex is in thrust contact with the eastern margin of the Bey Daglari Anticline. The origin of these nappes with respect to the Bey Daglari/Susuz Dag basement (from NW or from SE) is still under discussion, but this problem is unimportant with respect to the structures and the period of time considered by this study. The main thrust of the Antalya Nappes Complex predates the lower Miocene (Aquitanian). The principal contact with the eastern margin of the Bey Daglari was reactivated during the late Miocene Aksu Phase, as were most of the main structures in the area. The search for a possible offshore extension of all these units in the Mediterranean Sea area follows from the abrupt southern termination of the Susuz Dag/Bey Daglari Anticlinorium at the coast line, the large eastward dip of the contact between the Bey Daglari/Antalya Unit contact, and the near vertical position of most of the Antalya Units east of Finike to the Gulf of Antalya.

Sedimentary units

Most of the known history of the Susuz Dag/Bey Daglari dates only from the lower Cretaceous, and only some parts of the eastern Bey Daglari are exposed as outcrops as old as the upper Triassic. Paleozoic rocks are known from drilling. The Demre-1 well made by the Turkish Petroleum Company (TPAO) near Demre (Fig.6) reached a total depth of 6111 m near the apex of the southeastern flank of the Bey Daglari Anticlinorium. This well penetrated, from the bottom up, 156 m of very hard and dense Paleozoic dolomite, 590 m of thick light grey silty shale interbedded with grey marl of upper Triassic age, 2165 m of thick, very hard and dense, sugary dolomite of Upper Triassic to Jurassic age, and 3200 m of thick, hard, and dense limestone interbedded with shale and anhydrite of Jurassic to Cretaceous age. This section is very similar to other sections from the

autochthonous units of the Isparta Angle.

Elsewhere is observed a neritic facies associated with a subsiding platform of upper Triassic to Cenomanian age. After Cenomanian time, the history of the north and south parts of the Susuz Dag/Bey Daglari area shows differences related to ongoing processes of nappe emplacement. The northern platform subsided; and pelagic sedimentation is reported from Senonian to Danian time, followed by turbidite deposits with ophiolite olistostromes during the Paleocene. The southern Susuz Dag/Bey Daglari was not directly affected by these events, and pelagic sediments occur only during short periods. Moreover, these pelagic facies appear later in the western part of the Susuz Dag (Santonian-Campanian).

During the Eocene period, the platform tendency of the Susuz Dag led to the deposition of limy nummulitic deposits, with more terrigenous sedimentation toward the north. Some parts of the Susuz Dag emerged during the upper Eocene, but the sedimentation remained mainly neritic in the southern part. The Oligocene period is not well identified, but is represented by planktonic limestones and marls in the southern Susuz Dag.

The Neogene was the last important period of evolution of the Taurus Belt. Widespread facies are observed, the first of which was connected with the Aquitanian transgression with a neritic facies discordantly covering the terrains and paleogeography inherited from the Paleocene-Eocene nappe obduction. A thick flysch deposit during the Burdigalian and lower Langhian followed the Aquitanian limestone. This flysch is correlated with the last phase of overthrusting of the Lycian Nappes, and most of the detritic sandstone in the flysch is interpreted as fed by the front part of the advancing nappes.

The Taurus Belt/Mediterranean Sea connections

The structures observed on land seem to have extended, prior to the middle Miocene time, toward the area which is now occupied by the Mediterranean Sea. The Susuz Dag platform facies probably stretched far to the south. The post-Miocene period probably marks a definitive break between the Taurus units, which are uplifted and block faulted in graben basins and massifs affected by erosion/gravitational tectonics, and the development of a new orogenic system in the Hellenic and Cyprus Arcs. The connection between the post-Miocene history of the continental structures and the recent geodynamic evolution of the Mediterranean Sea cannot be deduced from the geology on land alone but requires an integrated study of the parallel neotectonic development of both the offshore and onshore areas.

4. Offshore geological setting

M. Ergün

The tectonic situation in the northeastern Mediterranean region is dominated by the interaction between the African and Eurasian plates with the Eurasian Plate here represented by the Aegean and Anatolian microplates). The African Plate currently moves north-northeastwards and northeastwards relative to the Aegean and Anatolian microplates, respectively. The boundary between these microplates and Africa is delineated by the Hellenic Arc and the Pliny/Strabo Trench in the west and the Cyprus Arc and a diffuse fault system probably associated with the Amanos Fault in the east. Only the Hellenic Arc appears to be an active subduction zone. The Cyprus Arc seems to have developed into a broader zone of deformation somewhat intermediate in nature between the eastern Turkish collision zone and the Hellenic Arc. Both the Pliny/Strabo Trench system and the East Anatolian Fault Zone are sub-parallel to the relative plate motion vector and hence are dominated by transform motion.

Direct clues as to the presence and location of subduction between the African and the Anatolian plates should exist in the distribution of earthquake epicentres. The region between the west of Cyprus and the East Anatolian Fault Zone is less seismic than both the Hellenic Arc in the west and the East Anatolian Fault System in the northeast. The seismicity is particularly low between the Pliny/Strabo Trench and Cyprus. The distribution of seismicity in this area indicates a broad zone with a generally northerly dip (*Rotstein and Kafka, 1982; Buyukasikoglu, 1979*) and having depths less than 100 km. The Anaximander Mountains/Florence Rise lie within and near the southern edge of this seismicity.

Paleomagnetic studies in Cyprus (*Clube and Robertson, 1986; Vine et al., 1973*) indicated that the Troodos ophiolite, formed during the Late Cretaceous (pre-Maestrichtian), and experienced a 90° anticlockwise rotation that occurred during the Late Cretaceous-Early Eocene initiation of the Cyprus arc. On the other hand, paleomagnetic results indicated that a 40° clockwise rotation of the Akseki-Beysehir Taurides developed during the Late Eocene-Oligocene, and that, during the Middle Miocene, the Lycian Taurides along with the Tauride platform formations situated west of the Antalya Nappes Complex (Western Bey Daglari) underwent a 30° anticlockwise rotation. Therefore the Isparta Angle seems to have resulted from the diachronous and opposite rotations of these two branches.

According to recent geodynamic analysis (*Oral, 1994; Barka et al., 1995*), the Isparta Angle currently has very little or no motion relative to Euroasia. In contrast, Central Anatolia is moving westward at about 15 mm/yr and Western Anatolia is moving southwestward at about 30 mm/yr.

According to the gravity data, the eastern Mediterranean is out of isostatic equilibrium (*Woodside, 1976, 1977; Makris and Wang, 1994*). The Eastern Mediterranean is dominated by an elongated NE-SW-trending depression known as the Herodotus Abyssal Plain with a Bouguer gravity maximum of approximately 220 mGal. To the north, broad and elongated gravity highs and

lows, lying more or less parallel to the continental areas of Turkey, coincide with bathymetric features within the Cyprus Arc system. The Rhodes Basin has a depth of approximately 4000 m and a Bouguer gravity high as great as about 180 mGal. The Antalya Basin has a 80-100 mGal Bouguer anomaly trending in a NNW direction (in apparent continuation with the approximately 240 mGal gravity anomaly of Troodos ophiolite body) and terminating abruptly against the Bey Daglari Range. On the other hand, the eastern part ot the Anaximander Mountains has a relatively low Bouguer anomaly of about 40 mGal. The Bey Daglari autochthonous platform has negative Bouguer gravity anomaly zone (about -80 mGal) trending almost N-S towards the Isparta Angle.

The magnetic field in the Eastern Mediterranean is generally characterized by a modest variation and low gradients. The Mediterranean Ridge and the Hellenic Trench provinces are generally free of any detectable magnetic anomalies. The magnetic features are associated with the main tectonic elements; for example, the Cyprus Arc is characterized by a series of dipole anomalies that delineate the known bathymetric-topographic configuration of the arc. Positive magnetic anomalies are associated with allochthonous massifs with pillow lavas and ophiolites in the Cyprus Arc both between Hatay and Cyprus in the east, and also northwest from Cyprus into the Antalya Basin. It could be argued on the basis of existing geological evidence that the Antalya Basin anomalies can be modelled by taking into account not only the effect of the ophiolitic body, but also as a localized manifestation of the brittle upper crust response to regional lithospheric stretching, without requiring it to be underlain by a very thin crust and associated zone of anomalous mantle.

5. Previous investigations

A.F. Limonov and J.M. Woodside

The northeastern part of the Mediterranean Sea has been studied for a long time primarily by geophysical methods within the framework of national and international programmes, but only two expeditions have been targeted investigations of the Anaximander Mountains proper. They are the first Training Through Research Cruise of the Russian R/V Gelendzhik in 1991 (TTR-1), and a Dutch expedition with the French R/V L'Atalante in 1995 (the ANAXIPROBE- 95 Cruise).

During the TTR-1 Cruise the whole area of the Anaximander Seamounts with the adjacent parts of the Antalya and Finike Basins and Florence Rise was mapped along a series of intersecting NE-SW and NW-SE lines. Conventional echosounder, OKEAN long-range sidescan sonar, a single-channel seismic system using a 30 kJ sparker as the seismic source, and gravity and magnetic measurements were carried out along all track lines. Several cores, some of which contained bedrock fragments, were taken as well. The results of the cruise were reported by *Ivanov et al. (1992).*

The ANAXIPROBE-95 Cruise extended the area of investigations, including a wide region from the Turkish middle continental slope in the north to the Florence Rise in the south, between the eastern part of the Rhodes Basin in the west to the western part of the Antalya Basin in the east. This area was mapped with a Simrad EM-12D multibeam system and the 'seismique rapide' system (a single-channel high resolution seismic system utilizing a 75 c.i. air-gun as a source, capable of seismic reflection profiling at a vessel speed of 10 knots). Gravity and magnetic measurements were carried out along all of the ship tracks as well. This resulted in the first detailed bathymetric map of the study area and a bottom reflectivity map which provides a way of determining the distribution of soft sediment and bedrock exposures on the seafloor (*Woodside, 1995*).

The 1991 reconnaissance survey of the Anaximander mountains (*Ivanov et al., 1992*) provided some evidence that they are a foundered part of the southern Turkish microplate (*Kuznetsov, 1992; Woodside et al., 1992*). Previous workers had proposed a variety of explanations for the formation of the mountains, for example that they are fragments of Africa which have collided with Turkey (*Rotstein and Ben-Avraham, 1985*) or upthrusted blocks of seafloor caught up in the collisional process (*Woodside, 1977*). Analysis of rock fragments taken from one of the mountains lends support to the idea that they were originally part of southern Turkey, but their lithologies and micropaleontology do not provide unequivocal proof. Gravity results from the 1991 Gelendzhik survey indicated that there is a major crustal discontinuity running directly through the middle of the mountains and that the western peaks are undercompensated crustal loads (*Ivanov et al., 1992; Woodside et al., 1992*). The hypothesized foundering must be related to transpressive wrench tectonics from the Strabo Transform zone, compression across the Florence Rise, and extension between the Turkish and Aegean microplates. Previous work indicated that the Mediterranean Ridge is overthrusting the Rhodes Basin to the north (*Jongsma*

and Mascle, 1981; Mascle et al., 1986).

The complex geomorphology of the Mediterranean Ridge and Florence Rise around the mountains makes it difficult to distinguish true neotectonic deformation resulting from the regional plate interactions (inferred from faults and folding) from local effects which may be caused by karst, mud diapirism, or halokinesis. These features can be identified in the reflectivity variations obtained during the 1995 swath bathymetry survey, in combination with the bathymetric coverage.

6. General morphology and structure of the Anaximander Mountains

J.M. Woodside and A.F. Limonov

Early bathymetric information in the region was summarized first by *Emery et al. (1966)*, who also gave the mountains their name. The morphology of the Anaximander Mountains before the TTR-1 Cruise is most widely known from the International Bathymetric Chart of the Mediterranean (*IOC-UNESCO, 1981*; also published as part of the GEBCO Digital Atlas, 1994). However excellent this data set is in most respects, lack of sufficient crossings of the Anaximander Mountains resulted in only a very general and often wrong impression of their morphology. The first attempt to construct a more reliable bathymetry map was undertaken on the basis of bathymetric data collected during the TTR-1 cruise (*Ivanov et al., 1992*); but the resulting scheme was also rather inaccurate because of a large spacing of the survey lines.

The bathymetric data acquired during the ANAXIPROBE-95 Cruise put this area in the front ranks with the best bathymetrically studied areas in the Mediterranean, like, for example, some parts of the French Mediterranean margin (see, e.g., *Bellaiche, 1993*), and sections of the Mediterranean Ridge (e.g., *Huchon et al., 1982*). The morphologic detail of the whole surveyed area can be deduced from the precise bathymetry and seafloor reflectivity maps (Figs. 7 and 8) which was constructed on the basis of multibeam surveying, with a contour interval of 10 m (*Woodside, 1995*).

The Anaximander Mountains form a group of topographically prominent features rising more than 2 km above the surrounding seafloor. They consist of three individual mountains previously referred to by *Ivanov et al. (1992)* as A-1 (the western mountain), A-2 (the south central mountain), and A-3 (the eastern mountain). It is here proposed to name the three principal mountains Anaximander (the western mountain, A-1), Anaximenes (the south central mountain, A-2), and Anaxagoras (the eastern mountain, A-3) in accordance with the naming convention already used by *Emery et al. (1966)* for eastern Mediterranean bathymetric features. The proposed new names are intended to make reference to the mountains easier in this report. With the great improvement in topographic definition of these mountains, it seems reasonable to give them individual names. The names are of three Ionian natural philosophers and scientists each of whom was born in Miletus, in the southwest corner of what is now Turkey, and who lived in the period between 610 and 428 BC. The name of the group of mountains is also the name of the largest and first-discovered one.

To the north, the mountains are bordered by a chain of relatively small but deep basins which are, from west to east, the Rhodes Basin (more than 4 km deep), the Finike Basin (3 km deep), and the Antalya Basin (about 2.5 km deep). The eastern continuation of the Strabo Trench, which is poorly expressed in the form of several shallow and gentle seafloor depressions separates the Anaximander Mountains from the eastern termination of the Mediterranean Ridge and from the Florence Rise (Fig. 9).

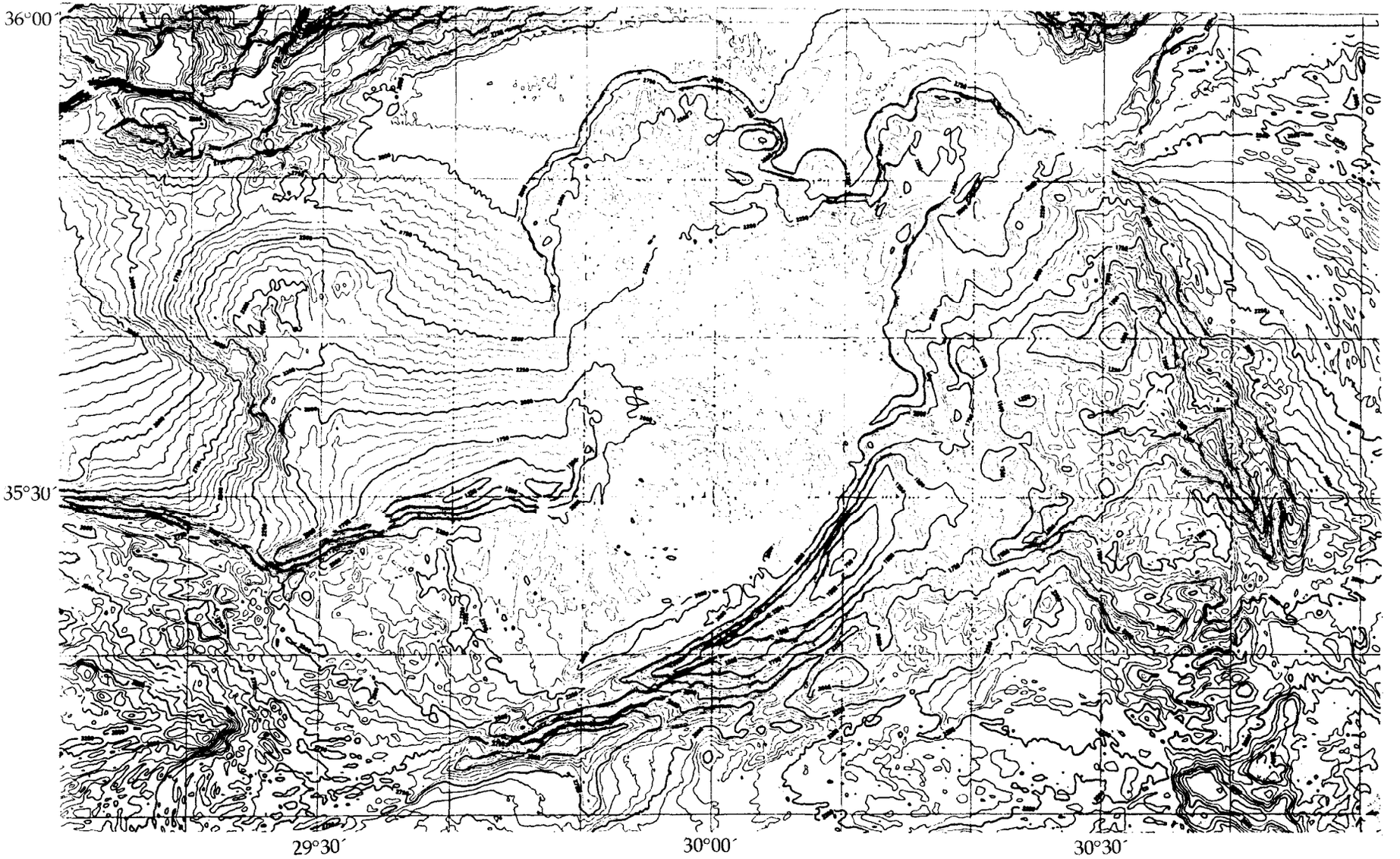

Fig. 7. Simrad EM-12D bathymetry map of the Anaximander Mountains with contour interval of 50 m (*Woodside, 1995*)

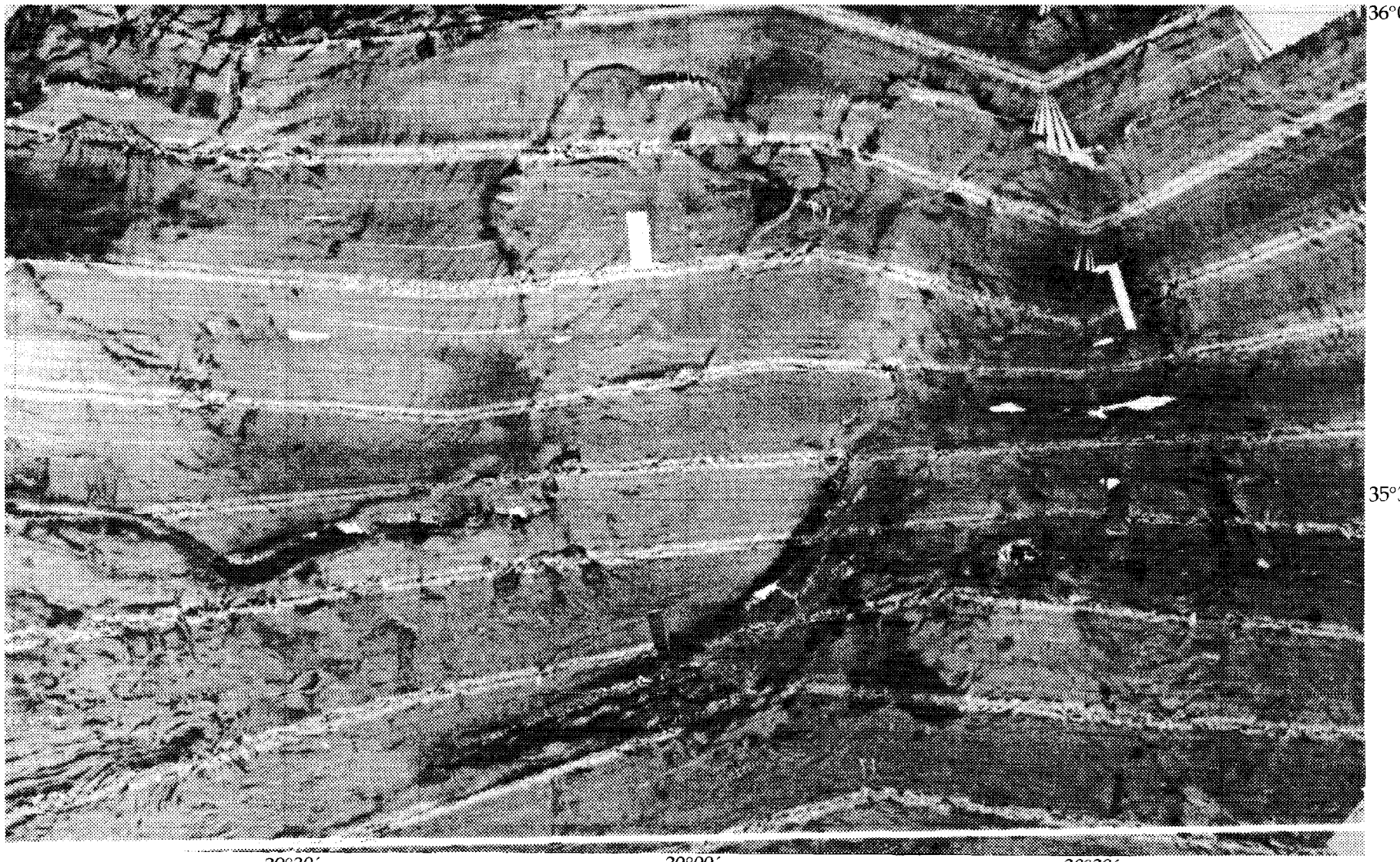

Fig. 8. Simrad EM-12D seafloor reflectivity imagery of the Anaximander Mountains (*Woodside, 1995*). Dark shades indicate high reflectivity and lighter shades lower reflectivity. The ship's track is highlighted by a lighter shaded strip in the centre of each swath of data

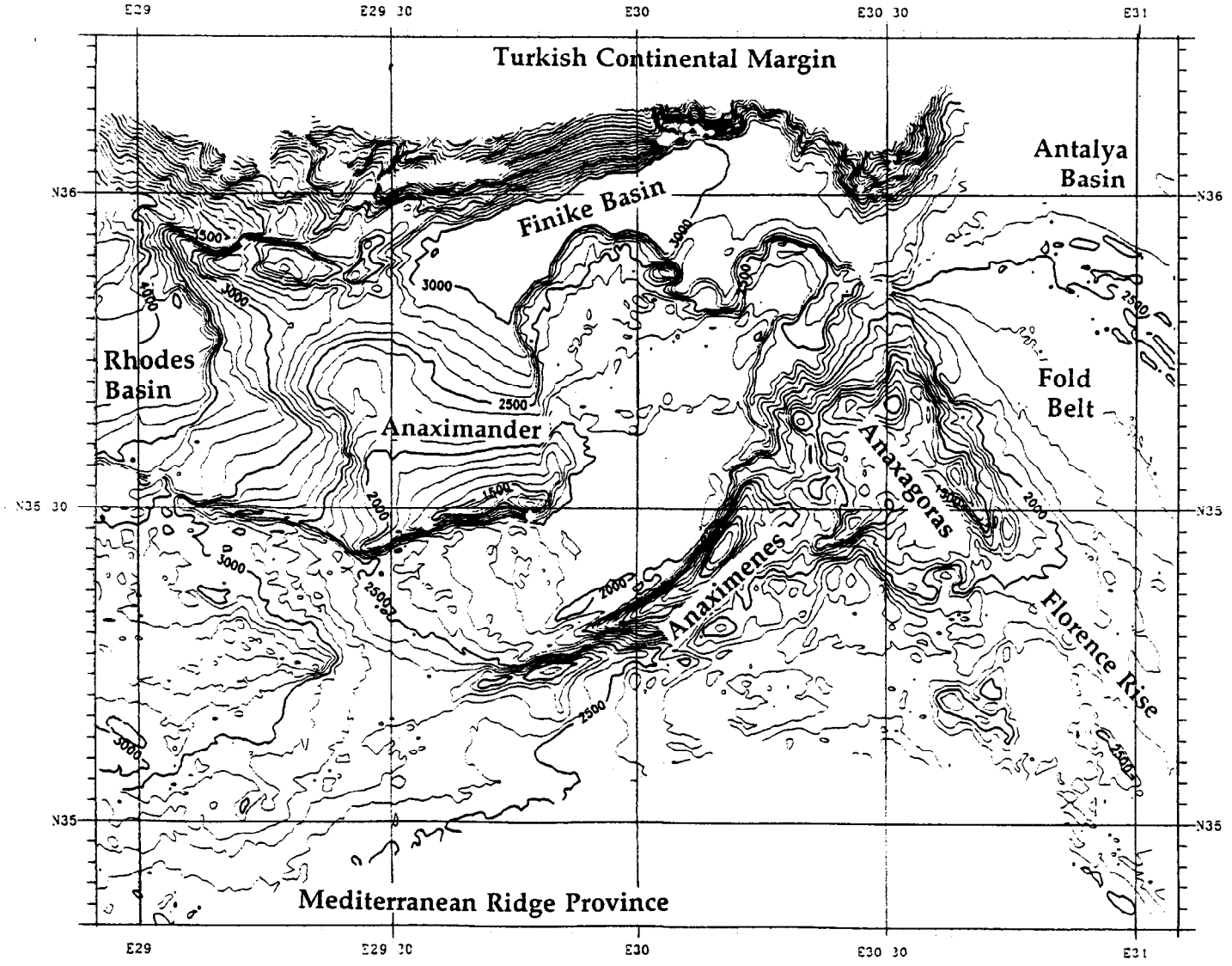

Fig. 9. Morphological provinces of the Anaximander Mountains and surrounding seafloor distinguished from Simrad EM-12D survey (*Woodside, 1995*)

Woodside (1995) distinguished five morphological provinces within the surveyed area. These provinces, which differ in morphologic aspect, are also notable for different seafloor reflectivity patterns (Fig. 9). The northernmost province embraces the steep Turkish continental slope (Turkish margin) with numerous gullies, canyons, mass flows, and cross-slope faulting. The second province includes Anaximander (the western mountain) and the threshold between the Rhodes and Finike Basins. The third province comprises the relatively flat regions of the Finike Basin and the area lying between Anaximander and Anaximenes (the southern mountain). Anaximenes and Anaxagoras (the eastern mountain) exhibit a rough and irregular topography which forms the fourth morphological province. The fifth one (southwestern province) is represented by the region to the south of Anaximander and is characterized by gentle subdued relief with highly variable trends. Additionally, a southern and an Antalya Basin province can be recognized. The southern province, including the northern slopes of the Mediterranean Ridge and the Florence Rise, is characterized by almost constant waterdepth (around 2500 m), low amplitude relief, and the absence of strong morphological trends. The Antalya Basin province within the study area is distinguished by low amplitude but well-expressed seafloor features with a NW-SE trend, representing the alternating ridges and depressions.

Anaximander, the westernmost mountain, represents a sharply asymmetrical seafloor high, with its summit (1250 m) in the form of a ridge along its southern margin. Its broad northern slope dips gently (up to 4°) toward the base of the Turkish continental slope, merging with it at a depth of 2700-3000 m or passing into the Finike Basin to the east. The western slope is also gentle, but it is complicated by two prominent fault scarps. The southeastern and particularly the southern slopes are steep escarpments (up to 15°) bounded by faults. The base of the northern slope is marked by above average reflectivity, which could be caused by clastics transported from the Turkish margin and accumulated there. The eastern part of the northern slope is striated because of the alternation of strips with enhanced and low reflectivity. The strips with enhanced reflectivity correspond to narrow and shallow erosional valleys, which are directed downslope, normal to the trend of the isobaths, and represent pathways for sediments from higher up the mountain.

Anaximenes has the smallest area and the largest relief. Its summit is outlined by a 680 metre contour. The mountain has a slightly northwestward concave appearance in plan view, with the steep (up to 24°) northwest-facing slope and the more gentle southeast-facing slope. The southwest end of the mountain terminates in the continuation of the Strabo Trench (which bends around to the east, south of the Rhodes Basin, as a northward overthrust according to *Mascle et al., 1986*). The southwestern slope of the mountain is marked by parallel strips of high reflectivity that are probably outcrops of the edges of tilted rock strata.

Anaxagoras, the easternmost mountain, is separated from Anaximenes, to the southwest, by a saddle with smooth relief except for a northeast-southwest oriented ridge which is part of a lineament across Anaxagoras (where topography and contours are displaced in a sinistral sense) and tangential to the southern

curved edge of Anaximenes. The summit area of the mountain is rather flat. The relatively steep (7 - 8°) eastern flank of the mountain is crossed by a system of faults and canyons, which are notable for high reflectivity. This flank of the mountain is rather linear, with a northwest-southeast trend, and at the top, and parallel the general trend, is a ridge with a shallowest depth of 1030 m along its southeastern extension. The shallowest part of the mountain is indicated by the 930 m contour on a plateau in the north-central part of the mountain, to the west of the ridge. The southwestern slope has a fault scarp in the upper part. Further southward this slope merges with the Florence Rise. Both northern and southern slopes of the mountain display some high reflectivity patches on the EM-12D images, two of which were proven to be mud volcanoes. In general, the whole mountain in characterized by slightly enhanced reflectivity.

The curved and generally northeast-southwest-trending valley separating Anaximander mountain from Anaximenes has a width of 20 to 40 km and a flat bottom with a depth varying from 2000 to 2250 m. Its bottom relief is dominated by low amplitude (100 to 200 m) transverse features in the southwestern and central-western parts. They are replaced by predominantly sublongitudinal features in the central-eastern part, and then again by transverse features to the north. The reflectivity level is generally low testifying to the presence of thick sediments that probably flow, being squeezed out from between the two mountains, toward the Finike Basin ('The Great Slide'; see Figure 10). These sediments form a tongue projecting into the Finike Basin, where eight almost semicircular lobes are formed at the edge of the tongue, with steep edges sloping toward the basin. One of the central lobes is complicated by a regular oval hill, about 5 km across and 800 m high, which we called 'The Anthill'. In some places, low reflectivity is disrupted by circular or curvilinear areas with high reflectivity, the latter following the contour lines.

A study of the 1991 TTR-1 seismic reflection data has demonstrated that the characteristic M-reflector at the top of the Messinian evaporites is absent on the mountains, although it appears around them, notably in the Antalya Basin, where it stops abruptly at the faulted eastern margin of Anaxagoras. Instead of the evaporites, there is inferred to be an erosional surface truncating the layers of pre-Messinian rocks. This implies that the mountains already existed as positive relief by Messinian time. There is a similarity between the western and southern peaks, but they both differ structurally from the eastern one. Part of this difference is apparent in the morphology; and it is emphasized also by gravity data (i.e. a strong westward gradient from low Bouguer values over Anaxagoras to values about 150 mGal higher over Anaximander and Anaximenes), which imply that a major discontinuity occurs west of the Eastern mountain (*Ivanov et al., 1992).* At the same time, the magnetic data suggest that the Anaximander Mountains are composed principally of sedimentary rocks, and that any ophiolites, which are wide-spread east and northeast of the mountains, are only likely to be present in the eastern part of Anaxagoras, if they are present at all.

Anaximander is considered to have been tilted north - northwestward in post-Miocene time, with the Finike Basin forming in the subsiding northern trough between it and the Turkish margin. This follows from the fact that the sediments on the northern slope of this mountain continue directly into the

Finike Basin, gradually increasing in thickness and probably passing from being more pelagic in nature to turbidites. In this aspect, this peak can be treated as a rifted part of the onshore Mesozoic carbonate Bey Daglari platform (*Woodside, 1995*). The same can be said about Anaximenes, the Southern peak, however it underwent a further rifting, and tilting associated with its neotectonic phase has proceeded much further than for Anaximander.

Anaxagoras lies on the continuation of the Florence Rise from the southeast; but it is on the expected southward geological continuation of the Antalya Nappes complex to the north. There are three morphological subdivisions of Anaxagoras from the northwest to the southeast, each apparently separated by northeast-southwest-trending faults along which there are bathymetric changes. The northern part has the greatest relief and is dominated by a plateau region in the middle. The inferred fault boundary of the northern and middle sections of Anaxagoras is a ridge extending southwestwards towards the faulted southern boundary of Anaximenes, and causes a left lateral shift in the bathymetric contours of the northeastern margin of Anaxagoras. Both the middle and northern sections share a linear northwest-southeast oriented faulted northeastern boundary. The middle section appears primarily as a southeastward narrowing ridge; however the plateau area to the southwest continues from the northwest at a slightly greater depth than in the northerly section. The southeastern section merges in the south with the Florence Rise which joins it at a slight angle from the southeast. The western boundary of Anaxagoras is roughly parallel with the eastern boundary, and roughly perpendicular to the general trend of Anaximenes. To the northeast of the northern and middle sections of Anaxagoras lies an arcuate fold belt with the general axis of shortening across the folds oriented roughly northeast- southwest.

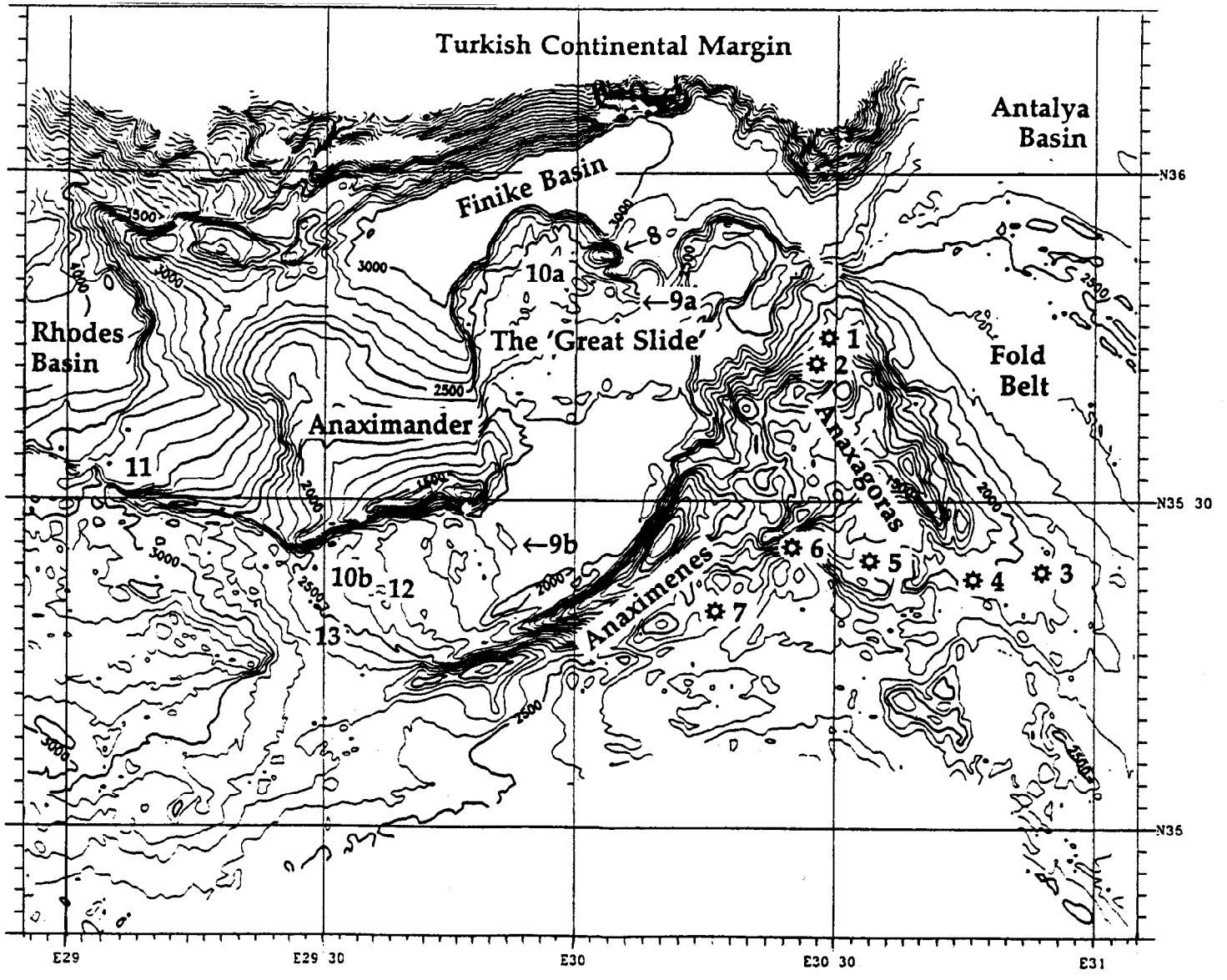

Fig. 10. Bathymetry map of Anaximander Mountains at 100 m contour interval showing locations of principal features. Mud volcanoes are numbered 1 (San Remo), 2 (Kula), 3 (St. Ouen l'Aumône), 4 (Tuzlukush), 5 (Kazan), 6 (unnamed fissure eruption), and 7 (Amsterdam). Other numbered locations refer to (8) the 'Anthill' (see text), (9a, 9b) tectonic windows, (10a, 10b) 'gas front' areas, (11) gas seeps and small mounds, (12) area of pockmarks, (13) area of slides

7. Deep-tow MAK-1 survey

J.M. Woodside, A.F. Limonov, and B. Swaak

Six MAK-1 lines were run in the Anaximander Mountains area. They cross different structural-morphological zones of these mountains (Fig. 11).

MAK line 42

Although this line was intended for testing of equipment, it was situated in an area which was of interest, in case some the tests also yielded data of reasonable quality. The line ran along the boundary between the Finike Basin and Antalya Basin. Because the line was a test there were several changes in the acquisition and playback parameters including two scale changes along the line. The scale for the bottom bathymetry was 800 m across half the Dowty thermal plotter which was used; and the scale for the sediments was 300 m between recording times 00:42 and 03:10, and 150 m between 03:10 and 06:00. The object of having one scale for the sediment and another for the bathymetry was to provide satisfactory high resolution profiles of the upper sediments but enough range for the bathymetry that there were not too many offsets where the scale was reset. These scales were used for the subbottom profiler for all the other MAK lines. The scale for the sidescan image was also changed just near the end of the line (for the last 10 minutes), from the normal 2 km swath (1 km per side) to 3 km. This was not repeated on other lines.

The level of the Antalya Basin is over 200 m shallower than the Finike Basin to the west. Moreover, there is a fold belt in the Antalya Basin whereas the Finike Basin seafloor is rather flat. The line followed a zone between the two basins where there is a mixture of topographic trends as a result of the intersection of the fold belt with an escarpment which may be fault controlled.

At the northern end, this northeast-southwest oriented line obliquely crosses a ridge of about 250 m height and a trend of about 065° (between 00:42 and 02:00). The trend of this ridge on the bathymetry map is more like 080°, and therefore appears to have the same trend as the Antalya Basin folds in this area. Downslope movement along the ridge is shown by slumps and by narrow erosional channels which may be fault-controlled and appear on the sidescan by virtue of their higher reflectivity. The end of the ridge was passed between 01:40 and 02:00. The seafloor as observed in the subbottom profiler in this area is acoustically opaque.

A second ridge is crossed between 02:10 and 02:30, and narrow valley with relatively flat floor lies between the two ridges. The second ridge has no erosional channels down its flanks, in contrast to the first ridge. Just to the south of the end of the ridge is an area (between 02:30 and 02:50) with scattered spots of high reflectivity about 25 m across.

No sedimentary layering is visible in the subbottom profile from the beginning of the line until 02:30; and between this time and 02:50 the layering is difficult to see because of relatively high acoustic opacity. At 02:50 there is a

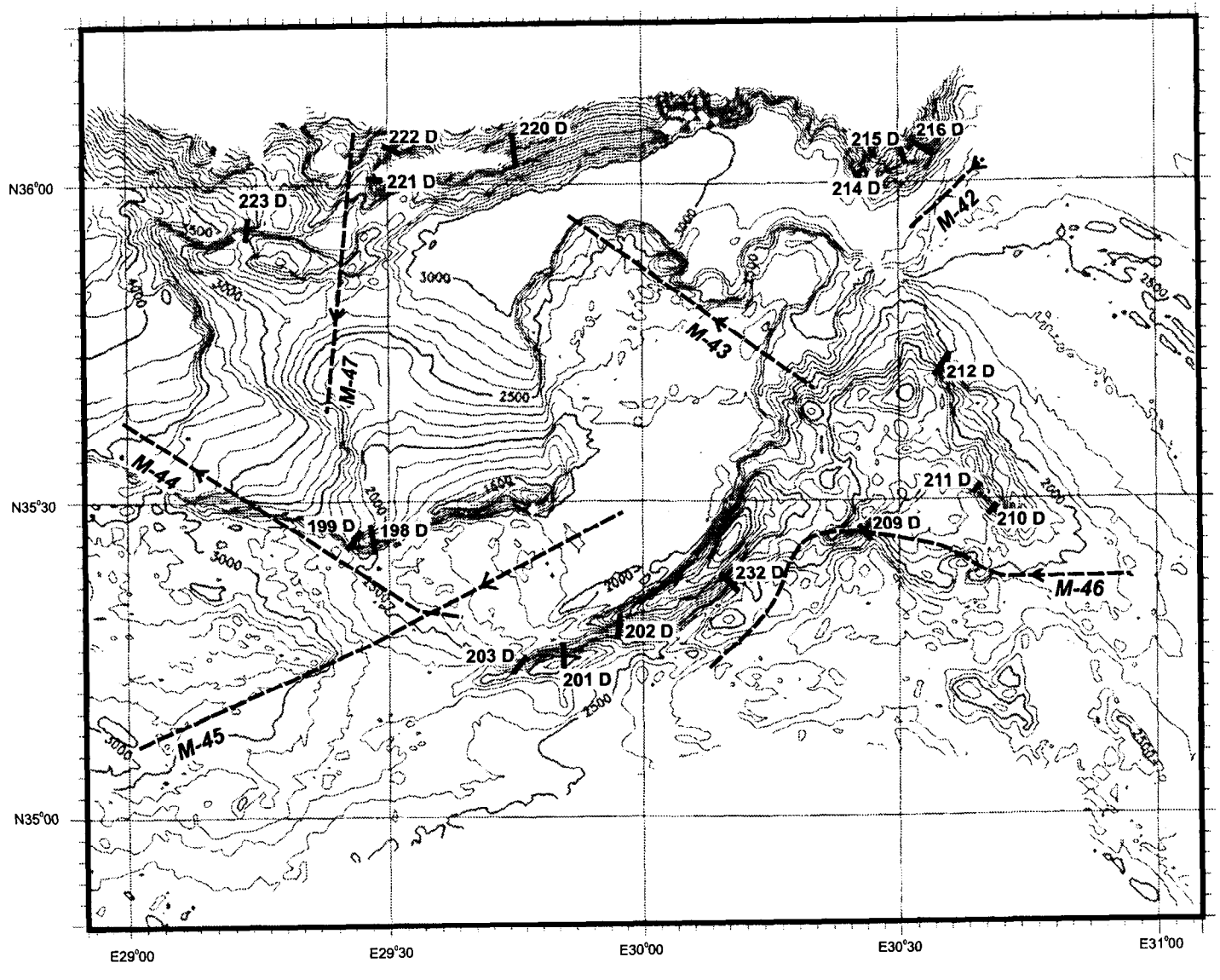

Fig. 11. Location map of MAK-1 lines (dashed lines) and dredge hauls (solid lines) in the Anaximander Mountains area

lineation trending about 150°, beyond which, to the south, are well-stratified sediments which are visible in the subbottom profile to a maximum depth of about 75 m (at 03:30). The lineation appears to mark a discontinuity in the sediments and is probably a fault. The thick sediments show some variability in layer thickness with an abrupt deepening to the south of 03:30, possible as a result of a growth fault. Interference fringes are visible in the sidescan image here (between 02:50 and 03:40) as a result of slight variations in the thickness of the sediments in this small basin. The basin is bounded on the south by an escarpment.

The escarpment at 04:00 is oriented roughly 065° and terminates near the crossing of the MAK line because of the intersection from the south-southwest (200° trend) of another escarpment. At the eastern side of the sidescan image, a large pile of slumped material lies against the north escarpment. Large surficial slides and slumps are common along the southern escarpment. Where the two escarpments intersect there is a large westward-directed slump containing well-stratified sediments which tilt upwards towards the edges of the slump.

At 05:05 another escarpment is crossed with the same 200° orientation as the previous one. Between the two west-facing escarpments the seafloor slopes gently southwestward and stratification is difficult to observe in the sediments because of acoustic opacity. Slumps and erosional gullies down the escarpment are common as on the escarpment to the east; and the gullies are observed in the sidescan image as long linear stripes of higher backscatter. The subbottom profiler shows evidence that the gullies are fault controlled because there are sedimentary discontinuities in the sediments at roughly the same locations that the high backscatter lineations cross the line. The trends of the lineations (and hence the inferred faults) is 145°.

MAK line 43

This line ran west-northwest from the northwest flank of Anaxigoras across the area of sediment lobes and ended in the Finike Basin. The purposes of the line were (a) to investigate the surficial deformation of the sediment lobes in order to understand how they are forming or moving, (b) to examine closely a local feature looking like a washout down to the top of the Miocene, (c) to look in detail at two rather enigmatic hills rising high above the lobes, and (d) to look at the upper sediment section of the Finike Basin. The enigmatic hills were not seen on the line, as it turned out, because a waypoint was missed at the centre of the line, on the flank of the hill named 'the Anthill' because of its shape and proposed origin (by extrusion of sand and mud from below under fluid pressure). Problems with both the underwater navigation system and the upward-looking echosounder resulted in erroneous geographic positions for parts of the line (as plotted in mosaic view) and generally erroneous bathymetric variations along the entire length of the subbottom profile.

The northwest flank of Anaxigoras is draped by sediments which can be observed only to about 10 m in the subbottom profile near the upper part of the slope because of a strong reflector at 5 m (gas front?) and acoustic turbidity in the record, probably caused by gas. Several reflective spots and reflective streaks can

be seen in the sidescan image; and the streaks are correlated in the subbottom profile with intersection of the seafloor by zones of acoustic turbidity. Several blocks or protuberances up to 10 or 20 m across are visible on the seafloor.

At 00:40 a canyon is crossed very obliquely. The Simrad EM-12D bathymetric chart indicates that the canyon runs down the flank in a relatively straight manner; and the sidescan image gives an orientation of about 325°-145° which suggests fault control because it is roughly parallel to the faulted eastern margin of Anaxagoras and to other faults in the area (c.f. line M-42). To the west of the valley, the depth of penetration in the upper sediments improves, increasing to about 30 m.

The base of the slope occurs at 02:15 where the penetration of the subbottom sediments increases to as much as 45 m in the basin to the west. The sediments in the basin are well-stratified, flat-lying sequences of continuous reflectors characteristic of turbiditic or hemipelagic sedimentation. At the east edge of the basin the sediments thin significantly where they onlap margin of Anaxagoras. About 6 reflective patches up to 200 m across are observed at the base of the slope over an area of acoustic turbidity and an enhanced reflector at a depth of about 8 m, again suggesting gas as the cause. The west side of the basin is marked by a large escarpment of up to 300 m. Erosional gullies and slumps are observed on the escarpment. The sediments in the basin become slightly disturbed near the escarpment suggesting slight compression; and they do not onlap the escarpment but seem to be in faulted contact with it.

Sediments at the top of the escarpment are deformed and tilted as if they had collapsed slightly basinward. Three parallel linear features on the sidescan image correspond with discontinuities in the sediment, further supporting the idea that sediments at the edge of the plateau west of the escarpment are beginning to sink into the basin along listric faults. This is confirmed also in seismic line 13 from ANAXIPROBE-95, just to the north of M-43. To the west, the sediments on the top of this eastern part of the lobes are apparently undisturbed (at least to 45 m) turbidites or hemipelagics with alternating strong and weak continuous reflectors in sequences of the order of a metre or so thick.

Between 04:50 and 06:30 there are several small hills and domes lying along what appears in the EM-12D bathymetry chart to be a curved trend bending northward to the north and westward to the south. In this area the subbottom profiler shows some disturbed and distorted sediment with intervals of acoustic turbidity. The acoustic turbidity seems to lie mostly at the base of hills but also is seen in the sidescan sonar image to correspond to lineations perpendicular to the line. Several zones of acoustic wipeout are observed as well. At 05:27 there is an offset of about 15 m in the sedimentary layers, accompanied by acoustic turbidity in the sediments on the downthrown side of the fault. One hill, between 05:40 and 06:00, appears to be diapiric, with the sediments bent up towards the hill. Penetration of the subbottom profiler is diminished over the dome. Some small erosional gullies occur on the all sides of the dome. To the west are more flat-lying sediments with several zones of very strong reflectors.

A large depression is present between 06:40 and 07:15. The east side of the depression has two steps created by blocks of sediment started to slump into the depression along listric faults. Between 06:18 and 06:30 is a tilted block which is

offset downwards with respect of sediments to the east by about 3 m. The lower step at the east margin of the depression is tilted eastward much more than the upper step; and there is slumping along the small scarp between the two steps. The floor of the depression is very rough looking with what appears to be debris from slumps into it. Some blocks on the seafloor are up to 20 m across. There is no subbottom penetration on the subbottom profiler which shows only strong diffractions and acoustic turbidity.

To the west of the depression, the same well-stratified sedimentary sequence as on the eastern side is observed, with penetration to about 25 m on the subbottom profiler. This gives way gradually westward to less penetration and more deformation in the sediments. Along the east edge of a channel crossed obliquely at 08:10 there are acoustic wipeouts and the sediments in the channel are severely distorted. The trend of the escarpment defining the channel (between 07:20 and 08:10 on the sidescan sonar image) is 267°. Small erosional gullies are present on the escarpment.

The line runs along the south flank of a long east-west oriented ridge between 08:20 and 09:30. At the base of this flank is a pile of sediments which appear to have slumped off the ridge and collected in a small basin. Along the ridge itself, is a very strong reflector at about 5 m depth below which can be seen no deeper reflectors. The reflector is very uniform in appearance all the way to the base of the hill where penetration suddenly increases to about 30 m over the east flank of an eastward tilted block.

A straight 015° trending channel between 09:55 and 10:20 is notable for its acoustic appearance. The subbottom profile shows acoustic turbidity interspersed with patches of high and low reflectivity. These zones of alternating reflectivity trend across the channel in a northerly direction. Sediments are again observed to the west of the channel in the subbottom profiler.

Reflectors in the sediments become stronger west of the channel between 10:30 and 10:50 and penetration decreases with increasing acoustic opacity. Several small diapiric structures with acoustically transparent cores can be detected in the sediments at 10:25, 10:37, and 10:42. Between 10:45 and 11:15, the sediment is acoustically very disturbed above a very strong and irregular reflector interpreted as a gas front. The strong reflector lies at a depth of about 25 m and has a roughness approaching 8 m with a wavelength of about 100 m. Sediment layers can not be seen below this high reflectivity zone. In the sidescan image the seafloor has a low to intermediate reflectivity with a north-south oriented grain and some small reflective patches. This area stops rather abruptly at about 11:15 where subbottom penetration increases to about 30 m, although there are still layers with enhanced reflectivity in the upper part of the section.

North-south ridges are present from 11:15 to 12:05. The subbottom profiler indicates many small faults in the sediments, some buried and some reaching the seafloor. It is assumed that they have the same trend as the bathymetry. Sediments in the upper part of the section have enhanced reflectivity. This zone has a very sharp boundary at 12:05 with a deepening onto another lobe to the west. At the base of the step are several pockmarks, one over 100 m across, and to the west the sediments are acoustically opaque, with a mottled appearance on the sidescan image.

The line ends in the Finike Basin (between 13:10 and 13:50). The edge of the lobe is an escarpment of about 250 m with high reflectivity and small erosional channels. Sediment in the basin is well-stratified with several thick units which may have resulted from large debris flows from the Turkish margin. One such 'grain flow' is 10 m thick. Near the escarpment the sediments appear to be gassy because there is a tendency to acoustic transparency.

MAK line 44

This MAK line ran northwest from a point directly south of Anaximander and midway between Anaximander and Anaximenes, obliquely across the southern edge of Anaximander to a point on its northern flank near the western edge of the survey area. The purpose of the line was to investigate possible karst structures both south of Anaximander and on its northern flank and to look for neotectonic activity along the ridge which forms the southern edge of Anaximander [and which appears from 1991 data (see *Ivanov et al., 1992*) to be a wrench zone].

The line starts in an area containing a number of pockmarks that were imaged on MAK line M-45, which crosses line M-44 there. The pockmarks are poorly imaged on M-44. Both lines show evidence for slop instability in the area with crumpled surficial sediment which is slowly creeping downslope, and one large slide (between 02:40 and 03:00 - also better seen on line M-45). The slump scar at 03:00 also marks the southern edge of a very distinctive reflector interpreted as a gas front which extends to time mark 05:20 in the north.

A long shadow at 02:22 indicates the presence of a hill near the line; and the edge of another hill to the southwest is defined by higher reflective zone between 02:40 and 03:20 caused by debris flows downslope and small scarps. The general character of the sidescan sonar images in this area, apart from the features mentioned, is a mottled low to intermediate backscatter; however, the subbottom profile is acoustically opaque or characterized by wipeouts except for a short section between about 02:32 and 02:38 where about 15 m of layered gassy sediments are inferred to be onlapping relief at 02:40.

In the region of inferred gas front between 02:50 and 05:20, the subbottom profiler displays no good reflectors except the gas front, and the character of the record is acoustically opaque with occasional acoustic wipeouts. The strong reflector interpreted as the gas front lies about 10 to 20 m below the seafloor and shows a rough relief of 6 to 7 m. The seafloor displays a small scale roughness caused apparently by crumpling of sediments downslope to the southwest. The roughness is gentle folds with a wavelength of about 100 m and axes parallel to the contours of the seafloor. At 05:20 the gas front reflector disappears in the subbottom record, and the seafloor roughness expressed in the sidescan image increases slightly between 05:20 and 06:00. Between 05:40 and 06:00 there is a small scale rifting of surficial sediments, probably in response to downslope gravitational transport; these cracks show up as more reflective strips of seafloor in the sidescan sonar image. The subbottom sediments are acoustically opaque throughout this region.

There is a data gap between 06:00 and 06:20.

A series of three deep, steep-sided circular depressions lies between time marks 06:20 and 07:40. The depressions range from about 300 m to about 600 m across and are up to 150 m deep. Pockmarks are observed near the southeasternmost of the three basins, and slumps are associated with all three. The inner slopes of the depressions have higher than average reflectivity. Reflectivity of the bottoms of the depressions is generally low, suggesting collapse of sediment above rather than infilling by debris from the sides (although this is occurring around the edges, as is apparent from erosional gullies on the inner slopes). Near two of the basins, at 06:40-06:45 and 07:05-07:15, tilted sediments are visible in the subbottom profile; but elsewhere the profile is acoustically opaque. A large slump up to 300 m across is observed to the southwest of the central depression, and slumping is clearly associated with the others also.

An east-west elongated hill lies between time marks 07:40 and 08:50; however, it is cut by a roughly north-south oriented valley between 08:00 and 08:20. Debris flows and slumps are associated with the southwestern side of the hill and the flank itself. The subbottom profile is acoustically opaque over part of the hill, but some sedimentary stratification is visible down the northern flank. These sediments are gently folded and there is enhanced reflectivity defining them. The seafloor displays an intermediate level of backscatter but with broad patches of lightly higher reflectivity lying parallel to the axis of the ridge (and presumably parallel to the folding observed in the sediments). From 09:00 to 09:40 the seafloor increasingly shows a mottled and higher reflectivity towards the northwest.

An east-west elongated asymmetric trough lies just south of the escarpment marking the south margin of Anaximander Mountain (between 09:40 and about 11:00). The southern side of the trough has a relatively gentle slope, at least in this oblique crossing, with several steps marked by scarps with high reflectivity cut by erosional canyons. The small basin in the centre of the trough displays well-stratified, gently folded sediments dipping northward toward the mountain. The northern side of the trough is steeper, shows high backscatter apparently from the outcropping older sediments, and has several examples of mass gravitational movement, including one apparent slump (crossed between 10:40 and 11:00) about 600 m by 600 m in size. The ridge at the southern edge of Anaximander is crossed at 11:20 where shadows on the sidescan image change to backscatter and *vice versa*.

The ridge marking the edge of Anaximander Mountain extends bathymetrically in the EM-12D chart westward to the edge of the survey area, and curves gently southeastward to the main south - southeast-facing scarp of Anaximander. It is very linear also in the sidescan image where the orientation is measured as 275°. Along the northern side of the ridge are series of steps and sloping terraces parallel to the trend of the ridge (between 11:20 and 12:00). The steps have a high backscatter, probably as a result of outcropping Pliocene sediments. The intermediate terraces appear to be covered by sediment from further up the ridge and show an intermediate reflectivity. Perpendicularly across the steps are a series of incised valleys with higher backscatter defining

their channels, probably because of coarser debris in them. In some cases the valleys appear to have developed further just below one of the steps.

Just below the steeper upper part of the ridge is an enigmatic surface feature on the northeastern side of the sidescan image. It is a very sinuous, very low reflectivity strip which meanders across the slope without apparent relation to the bathymetry. It can attain a width of about 50 m but is usually about 30 m across. Its edges are commonly defined by high reflectivity. In places some high reflectivity material seems to be 'bleeding' downslope from a short thin line of very high reflectivity. In the EM-12D image the feature forms what could be almost described as a loop which is displayed exclusively as very high backscatter, suggesting that the low backscatter part seen on the MAK is a surficial attenuation phenomenon.

No subbottom information can be seen on the subbottom profiler down the upper slope of the ridge because of strong reflection from the seafloor and acoustic opacity below; however, from the base of the upper slope at 12:10 the subbottom penetration gradually improves although the bottom remains a high backscatterer. Between 12:10 and about 13:10 is a gentle slope in which the subbottom penetration reaches about 15 m.

From 13:15 to about 14:15 is a province which can be characterized on the subbottom profiler as being generally acoustically opaque with short sections showing laminated sediments and zones of acoustic wipeouts or acoustic voids from the seafloor downward. In the sidescan sonar image the seafloor is seen as having small scale relief which is caused by randomly distributed blocks of a few tens of metres in size which cast good acoustic shadows. There are some twisted lines of high backscatter which have no apparent bottom relief. These lines are thought to represent carbonate crusts associated with seafloor gas escape along randomly oriented cracks in the sediment; and they may be associated with the acoustic wipeouts seen in the subbottom profiler record. The small topographic highs also seem to be associated with acoustic wipeouts leading to the idea that they might be carbonate mounds over gas vents.

Between 14:00 and 16:00 there is more penetration in the subbottom profiler (to a depth 30 m at most) but there remain zones of acoustic voids and acoustic turbidity, indicating the presence still of gas (Fig. 12). This continues to 18:40 with more widely separated occurrences of the same feature (e.g. acoustic voids at 17:05-17:10 and 18:14-18:17) and longer stretches of acoustic turbidity. The patchy high reflectivity on the sidescan image forms curves of higher backscatter in places. The lineations of high backscatter tend to follow the bathymetric contours; thus they may be caused by small scarps or by gas emanations along steps in the basement.

The line ends at 19:20 on a small hill. Acoustic turbidity in the subbottom profile indicates that the sediment draped on the hill is gassy. Small gullies down the sides of the hill are evidence of small scale sediment movement which would be unusual on such a feature unless the sediment were rather mobile because of lack of consolidation and possible disturbance, for example, from fluid circulation.

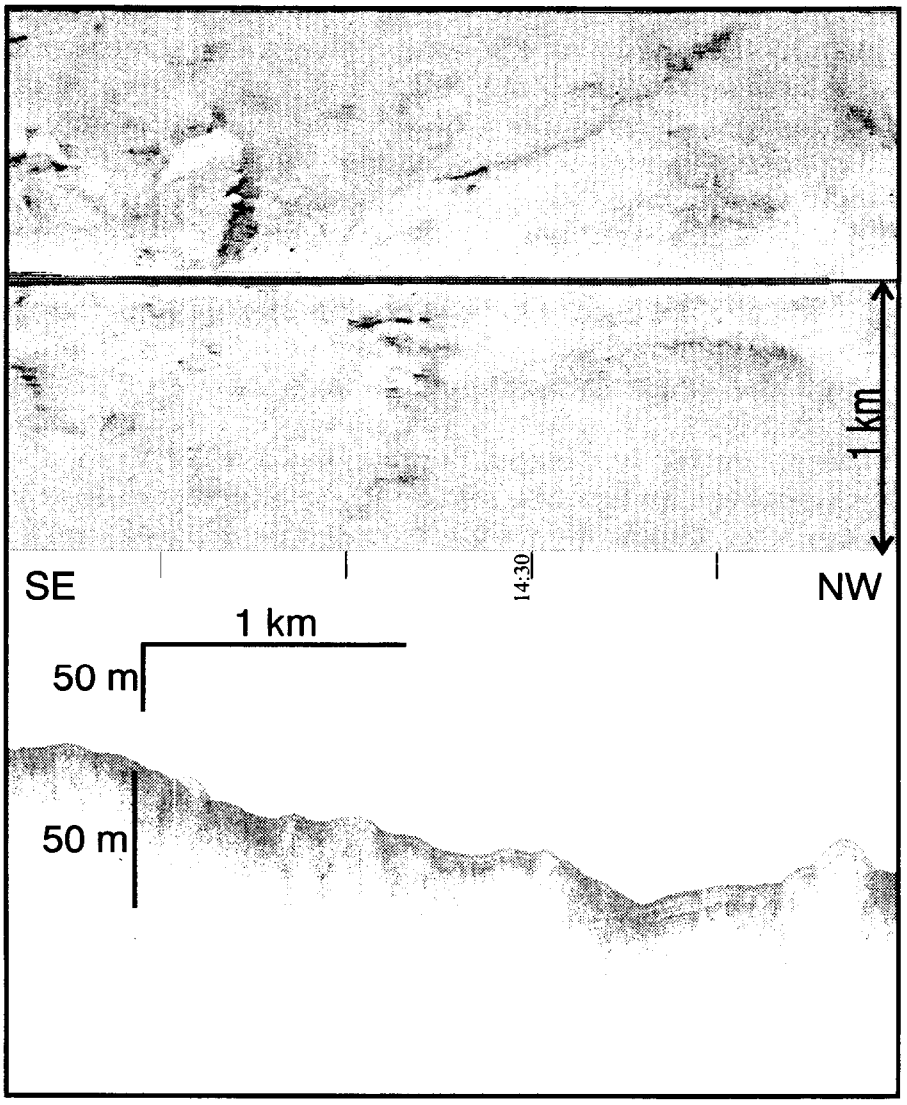

Fig. 12. MAK line-44 across area of gas seeps above which are small seafloor mounds, and an area of seafloor disturbance. The subbottom profile shows almost no penetration because of acoustic wipeouts and acoustic turbidity, suggesting gas may be responsible for the character of the seafloor

MAK line 45

MAK line M-45 was run from a point between Anaximander and Anaximenes mountains toward the southwest, ending near the southwestern corner of the study area. It ran through three areas which can be distinguished on the basis of their seafloor morphology. The area between the two mountains is characterized by relatively low relief interrupted by rectangular depressions up to 150 m deep which lie perpendicular both to the line and to the facing flanks of the two mountains. A seismic line across one of the depressions indicates that most of the Pliocene-Pleistocene section is missing there, as if a window had been opened on the deeper layers by pulling the upper sediments to the side. The southwestern half of the line runs across an area of long sinuous ridges and

troughs with a relief of about 100 m. The ridges converge at two deep depressions. In the middle of the line, between the two other provinces, is a transitional area which has some features of both provinces as well as some erosional channels. The purpose of the line was to examine especially the rectangular depressions and the ridges and troughs prior to sampling and to understand their origins.

In the plateau region between Anaximander and Anaximenes are gentle folded to flat-lying stratified sediments which are visible in the subbottom profile to a depth of about 25 m. Continuity and alternation of strong and weak reflectors suggests hemipelagic or turbiditic sedimentation. Folding is subparallel to the line. The sediments are interrupted between 11:25 and 11:55 by a depression in which the upper sediments appear to be missing. This is more apparent at a similar but larger depression from 12:45 to about 13:20. The Pliocene-Pleistocene sediments surrounding the depression are apparently unstable, and large slumps are visible on the sidescan sonar image.

It is not clear how or why the depressions formed because there does not appear to be subsidence below and there is no apparent sink for the sediments; rather it appears almost as if the upper sediments had been pulled apart. Furthermore, the depressions, once created, are then filled in by slumping from the steep sides and, in this case, by drifting sediment from the west observable between time marks 13:15 and 13:40. Between the depressions are what appear to be incipient depressions. For example, a small graben visible in the sidescan sonar image to the south of the line between 11:10 and 11:20; and the line runs also along the axis of a shallow depression between 12:00 and 12:40, as can be seen by subsidence cracks near the margin of the depression.

Three depressions between 12:45 and 15:35 appear to be in difference stages of development. The easternmost basin is the deepest and emptiest (Fig. 13) whereas the middle one is shallowest. These basins are actually connected along their northern edge by a shallow depression. Between the basins are laminated sediments which tend to slump into the basins along listric faults causing the sediments to tilt away from the basin. The westernmost of the basins has a number of pockmarks near its margins as well as one inside. The pockmarks near the west margin may be related to strong acoustic backscatter in narrow bands in the subbottom profile. To the west of the depressions lies gently folded stratified sediment with alternating strong and weak continuous reflectors visible to a depth of about 30 m but with very enhanced reflectors in the upper 10 m. The lower sediments in this folded area appear slightly diapiric as if deforming plastically.

A long slightly sinuous shallow depression roughly parallel to the others (running perpendicular to the line) lies between 16:50 and 17:15. Along the central axis of the depression are several pockmarks up to 60 m in diameter (Fig. 14). One pockmark nearly crossed by the line is at least 8 m deep. The subbottom profile across the depression is acoustically opaque. Along the rim of the depression are small spots of high reflectivity which are associated with a large acoustic void and a discontinuity in the sediments in the subbottom profile. The discontinuity looks like a fault which may correspond to a lineation across the line in the sidescan sonar image.

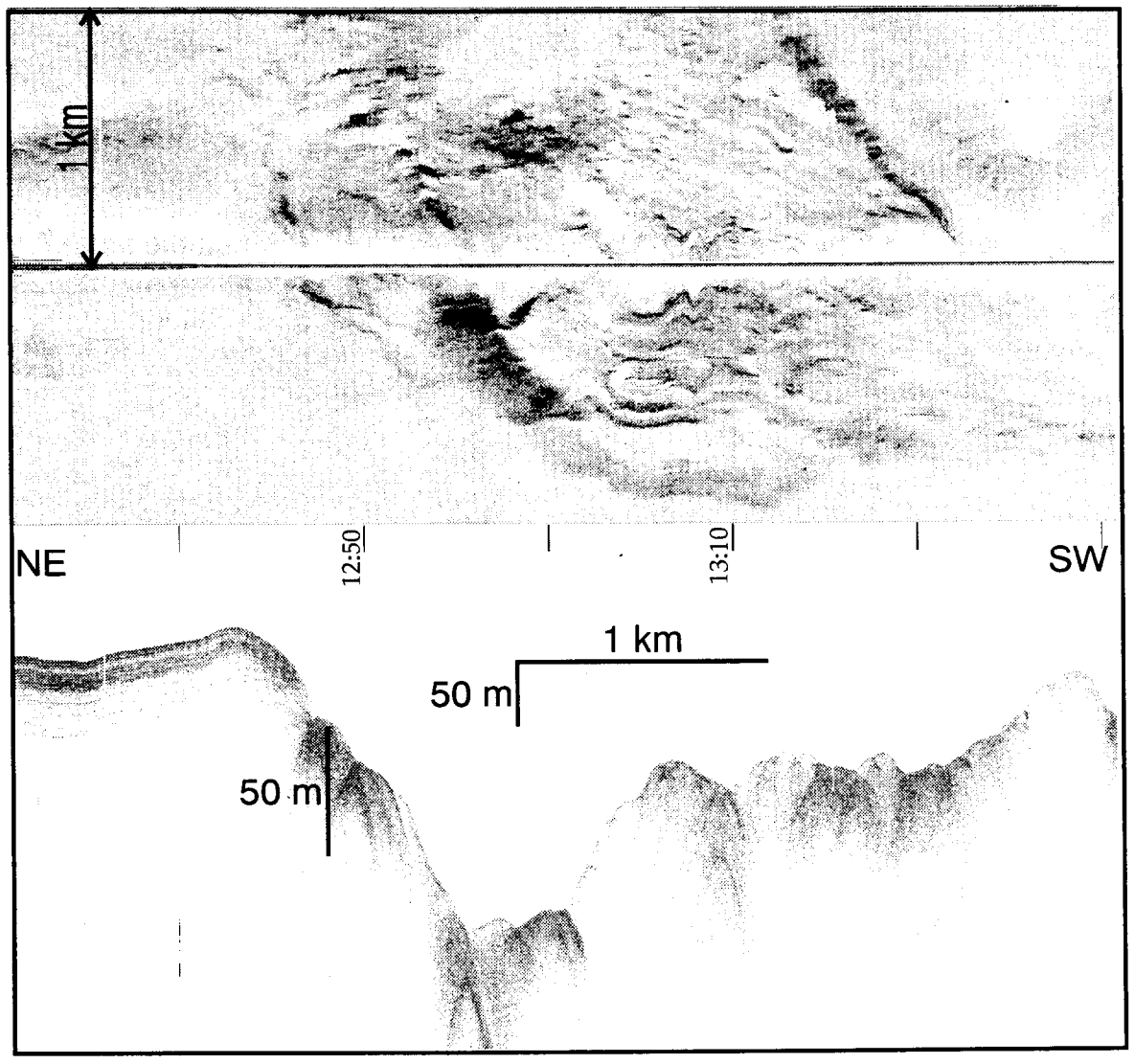

Fig. 13. MAK line 45 across a seafloor depression which is interpreted as a tectonic window. Core TTR6-231G taken from this window showed slump breccia below sapropel S1

The edge of another depression is crossed at 17:45, marked by a topographic step with slumping along it. Downslope creep seems to be occurring to the south along the depression. The subbottom profile is acoustically opaque from 17:45 to 18:40, and pockmarks up to 30 m across are grouped along the western boundary of the depression at 18:35 (Fig. 14).

Beyond a section of stratified sediment between 18:40 and 19:00 is an broad region that can be characterized as one of mass movements downslope to the south (roughly 190° to 200° as shown by seafloor fabric caused by channels debris flows, etc), pockmarks, and acoustically opaque sediment (between 19:00 and 20:25). Two large slides of different age can be observed in the sidescan sonar record. The older one (from 20:05 to 20:10; Figure 15) has been covered with more recent sediment but has left a clearly visible scar which shows up as a high

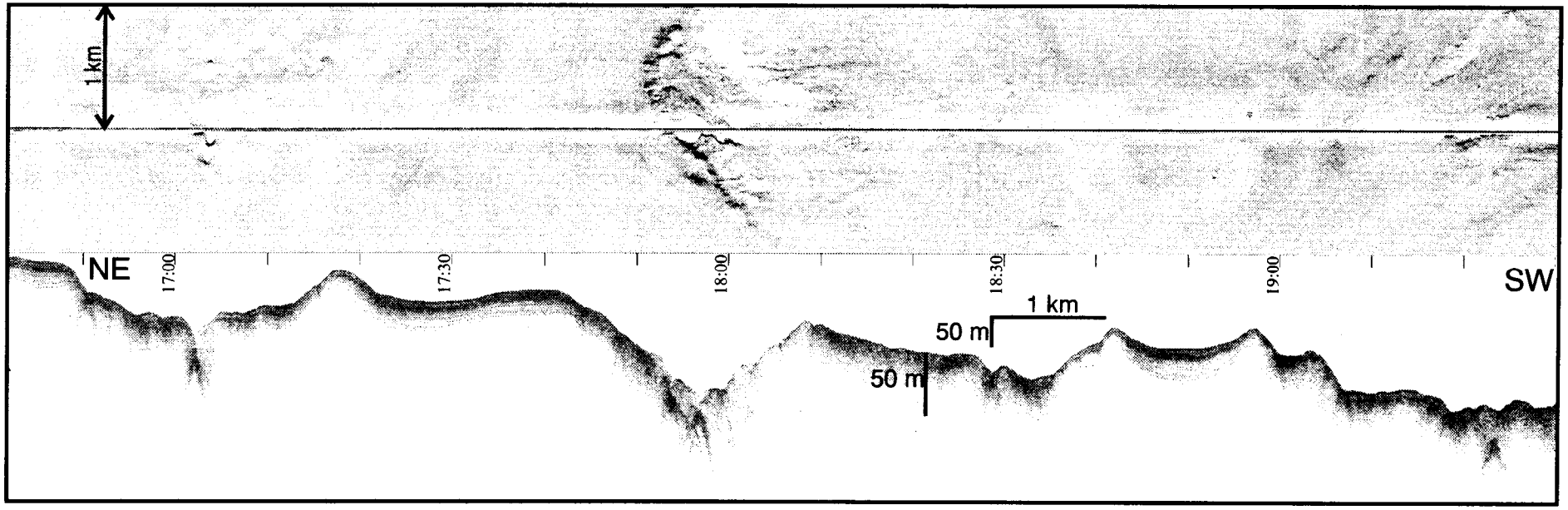

Fig. 14. MAK line running across area of gas venting and seafloor instability. In the centre is a trench which has been created by sediment slidind to the west - southwest and gas venting. To the left are several large pockmarks within another linear trench perpendicular to the line; and to the right is an area of north-south sliding of gas-filled sediments

backscatter scarp. In the more recent slide (between 20:20 and 20:25; Figure 16), a rectangular sheet of upper (about the upper 5 m) sediments has slid intact to the south (190°) about 400 m leaving a rectangular scar floored by sediment showing very high backscatter. The lower part of this slide block has disintegrated into a rather fluid-looking debris flow (seen as a sinuous patch of high backscatter with relief suggesting blocks up to 50 m across) which continues into a westward directed canyon for a total length of about 1500 m. In the slide scar, subbottom sediments show enhanced reflectivity and diminished penetration. The older slide is also imaged on the line M-44 sidescan sonar record. The hill down which the slides are occurring to the south displays fairly regular stratification of parallel enhanced reflectors with a total penetration depth on the subbottom profile of about 20 m. On the north side of the hill is a linear channel running to the west - southwest.

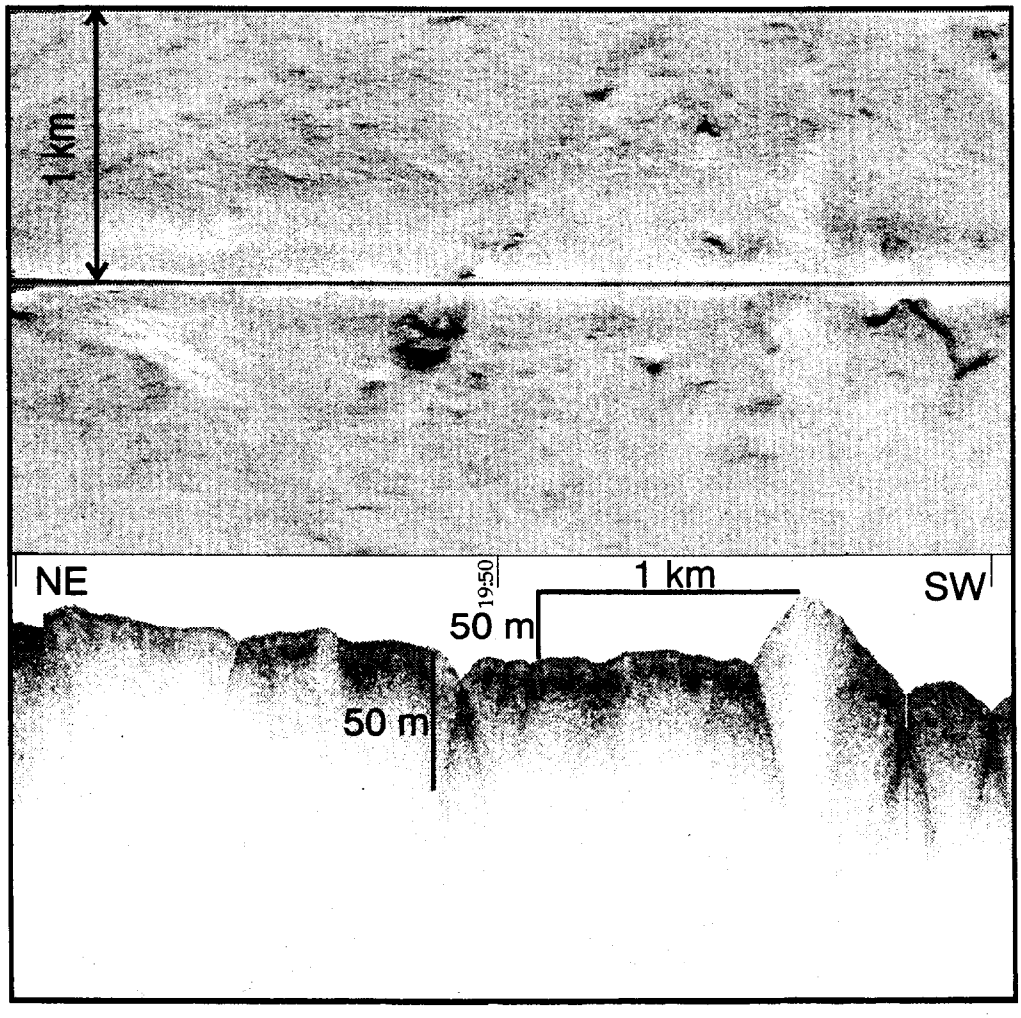

Fig. 15. MAK line over an area where seafloor sediments have been sliding to the south. Gas in the sediments may have facilitated their mobilization through lowering the shear strength. The line crosses a linear feature (centre) which is related to gas escape, and pockmarks are observed to the right of it. To the extreme right is an older slightly buried slide scar (with the head wall visible as an irregular high reflectivity line just below the centre line of the image)

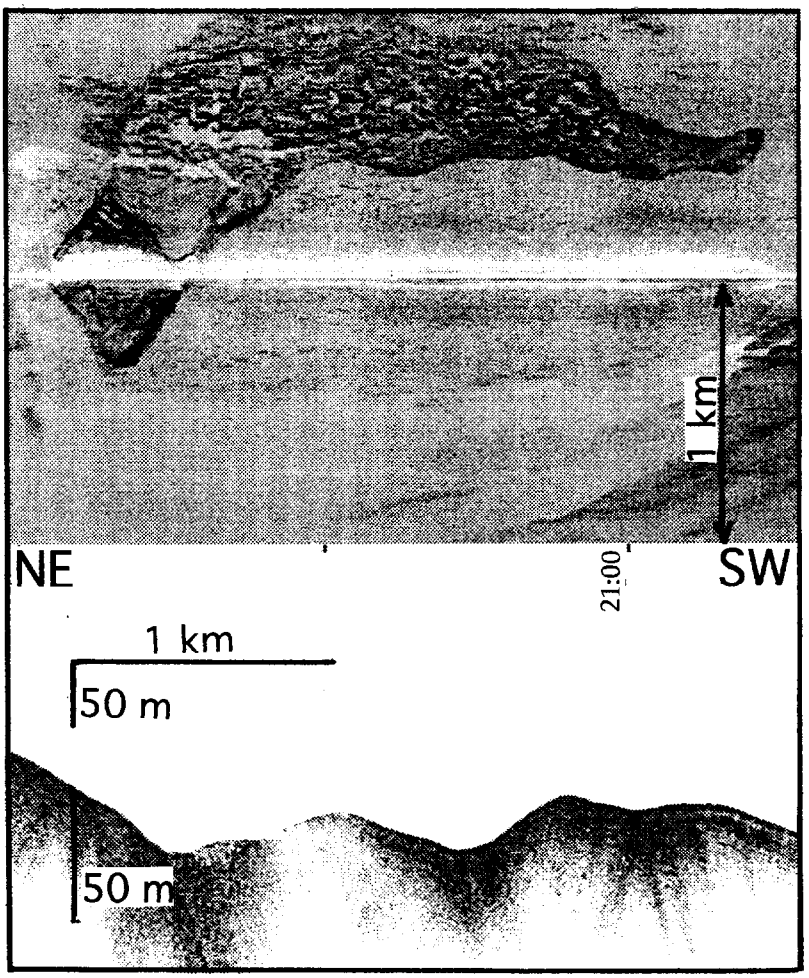

Fig. 16. This is a slide showing, at the left of the MAK image, the high reflectivity slide scar, and, to the south (above the centre line), the slide itself. The lower part of the slide (upper centre in image) has completely fluidized into a debris flow recognized by the higher backscatter from the coarse material

The line runs along a ridge between 21:15 and 22:20. On either side of the ridge can be seen evidence for small scale downslope movement. The sediments are poorly seen in the subbottom profiler over most of this section because of acoustic turbidity, but between 21:15 and 21:35 the upper sediments appear to have been deformed by small vertical faults (with throws of a couple of metres between 21:25 and 21:30) or shearing (at 21:20).

A new province is entered along the line at 22:20, with a zone of transition from 22:20 to 23:30 marked by depressions (Fig. 17). The At 22:20 there is a strong linear stripe of high reflectivity across the sidescan sonar image (NNE-SSW) which has no topographic expression where it crosses the line but evidence of gas venting from high acoustic turbidity in the subbottom profile. West of this lineation, the seafloor slopes westward, interrupted only by the three depressions. The first two depressions are circular, about 1 km across at the surface and perhaps 300 m across at the floor. At the far edges are concentric lines of high backscatter inferred to mark small scarps where subsidence is starting. On the margin of the first depression, the sediments can be seen in the subbottom profile to be tilted toward the centre of the hole. The appearance of material slumping into the depressions suggests that they are in the process of forming by

active subsidence. The centres of the holes have low backscatter and a thin layer of horizontally layered sediment is visible in the middle hole (at 23:00). Across the depressions is a subtle lineation with a 130° trend. The westernmost of the three depressions is elongated with an azimuth of 190°, is V-shaped in cross-section, and has strong backscatter along it.

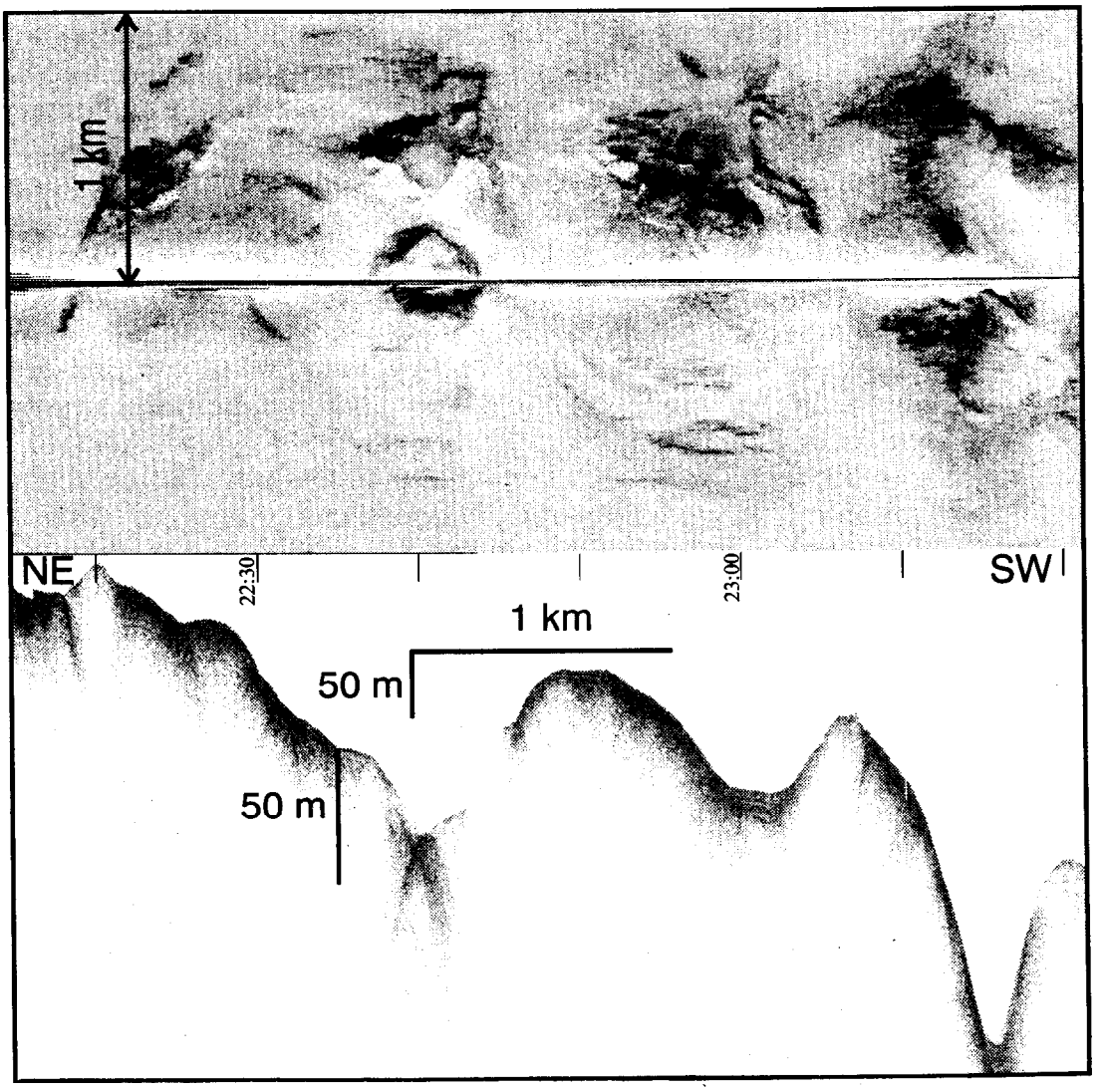

Fig. 17. MAK line 45 crosses three large circular pits. As they are in an area of elevated gas content in the sediments, it is speculated that they could be mega-pockmarks. Sediments are being tilted into or slumping into the pits as seen in the subbottom profile across the left pit

From 23:30, the seafloor deepens steadily into a deep trough with the deepest point at about 00:50. The seafloor on the margin of the trough is rough and has high backscatter in general (the exception being the upper slopes which are assumed to be draped in sediment although layering is not seen because of acoustic turbidity). Debris flows down the slope can be seen at 01:35.

To the west of the deepest part of the trough, all the structural trends change, with two predominant ones visible, roughly west - southwest and east-southeast. The structures are mainly broad ridges and troughs. Between 01:40 and 04:40 there are a couple of good examples of this type of structure. Lineations of strong backscatter crossing the line at azimuths of about 225° (e.g. between 02:40

and 04:00) and about 075°-080° (e.g. between about 04:00 and 04:30) mark the steeper sides of asymmetric ridges with sedimentary strata dipping in the direction of the less steep side. These structures are interpreted to be thrusts from both the south and north which intersect along a trough running to the west. These structural trends are clearly visible also in the EM-12D bathymetric chart. Examples of individual thrust units can be seen between time marks 01:40 and 02:15, and between 02:15 and 03:40. The sidescan sonar image displays some apparent crumpling of surficial sediments parallel to the structural trends in support of the idea of compression, and some of the sedimentary units observed in the subbottom profile are gently folded. Along steeper slopes at the edges of thrust units are debris flows and slumps (e.g. at 03:55 on the south sidescan image).

The thrust province continues to the end of the line. Between about 05:20 and about 07:40, the toe of a large thrust sheet is traversed, parallel and just to the south of the edge, across slumps, debris, and folded sediments connected with this active part of the thrust. The sediments along this part of the line are so deformed that there is little to see in the subbottom profile. Interfering structures are seen between 07:40 and the end of the line at 09:40 where most of the structures swing to the south making a sort of cusp in the fabric of the seafloor. The subbottom profiler displays sedimentary blocks tilted in opposite directions (e.g. two blocks are tilted to the east between 08:20 and 09:00, and to the west of 09:00 are at least two blocks tilted to the west). All the sediments along this part of the line are distorted slightly by faults, folds, and different stages of tilting. This province could be seen as the continuation of a region of backthrusting of the Mediterranean Ridge at the Strabo Trench, which has been seen to continue eastward south of the Anaximander Mountains; and thrusting from the north seems to be connected with the deformation of the Anaximander Mountains.

In summary, this line appears to have crossed a boundary between the Anaximander Mountains region and the Mediterranean Ridge. The Mediterranean Ridge is represented by thrusting to the north in this area. The boundary seems to follow the structural trends observed in the bathymetry to the south of Anaximenes Mountain. To the north, in the plateau region between Anaximenes and Anaximander to the north is a province of Pliocene-Pleistocene sediments which appear to be mobilized above a more consolidated basement, probably of late Miocene sediment, by excess fluid and gas and tectonic shortening between the mountains.

MAK line 46

Following the successful sampling of several mud volcanoes which had been identified in 1995 on the basis of their sonar and bathymetric characteristics in the EM-12D data (*Woodside, 1995*), a MAK line was made westward across them south of the main peak of Anaxagoras as far west as the trough south of Anaximenes. The first part of the line was fairly straight, but the last part had several turns in order to cross the location of dredge 209D and the Amsterdam mud volcano. The purpose of line was to image the mud volcanoes and their possible structural and tectonic controls. For example, the ridge on which dredge

209D was taken was hypothesized to mark a strike-slip fault zone cutting across Anaxagoras from southwest to northeast, and the mountain itself was thought to be formed by southwest-directed thrusts from which some mud volcanoes might originate.

The line began just to the east of the Saint Ouen l'Aumone mud volcano in an area of low relief. Up to 30 m of well-stratified sediment can be seen in the subbottom profile, with regular strong continuous reflector typical of hemipelagic or turbiditic sedimentation. Acoustically the bedding can be seen at the metre scale. The seafloor is slightly disturbed by several submetric scarps oriented roughly 070° on the sidescan sonar image. A cross-cutting trend (about 305° to 315°) is suggested by folds of similarly low relief near the mud volcano.

The Saint Ouen l'Aumone mud volcano is not very reflective in the MAK sidescan data (Fig. 18) although it gives a high backscatter image in the lower frequency EM-12D data, indicating that most of the mud breccia is likely buried under perhaps 50 to 100 cm of sediment. There are a few reflective spots on it, about 100 m across and lying along a line crossing the mud volcano with a strike of about 085° to the north of line. The mud volcano is roughly circular with a diameter of just over 1000 m and a height of slightly over 50 m. The subbottom profiler shows the presence of two old buried flows extending eastward from the mud volcano: one extends to about a kilometre beyond the dome at a depth of about 6 m, and a second younger one above it lies buried by about 2 m of sediment. Clearly there have been several eruptions in the past. There is a rather sharp boundary between the mud volcano and the normally stratified sediments to the west.

Beneath the roughly 8.5 km intervening seafloor between the Saint Ouen l'Aumone and the Tuzlukush mud volcanoes (see Fig. 10) lie slightly disturbed sediments. They are seen on the subbottom profiler to a penetration depth of about 20 m. The disturbance appears to be caused by small scale folding with an axial trend of 130° to 140°, a wavelength of under 100 m and an amplitude which is difficult to measure because it is so slight. At 15 to 20 m beneath the seafloor, the amplitude of the folds is about 1 m, indicating that the folding event is continuing and influences the older sediments more than the younger beds. Cutting across the folds are several lineaments with a trend of about 030°. The cross-cutting lineaments are small elevations or depressions affecting the seafloor over a width of up to 100 m and probably with relief under a metre. Also of note in this section of the line are several pockmarks to the south of the line at 08:10 and an area of disturbance between 09:10 and 09:30 which may be an incipient mud volcano. There is doming of the sediments at 09:10 and 09:25. The disturbed sediments in both locations appear to contain gas which shows up as acoustic wipeouts in the deeper (>10 m) sediments and acoustic turbidity in places within the upper sediments.

Tuzlukush mud volcano is a circular conical dome 80 m high and about 600 m across. It is surrounded by a shallow moat of the order of 10 to 20 m deep and perhaps 500 m across. The level of backscatter observed in the MAK sidescan is moderate, indicating the presence of a probably more recent flow than is inferred for Saint Ouen l'Aumone. The surrounding strata bend down slightly

toward the mud volcano, and one flow can be seen interfingering with sediments to the east. On the western side there is evidence of several overlapping flows. Across the northern slope of the mud volcano is a small (submetric?) scarp trending 075°.

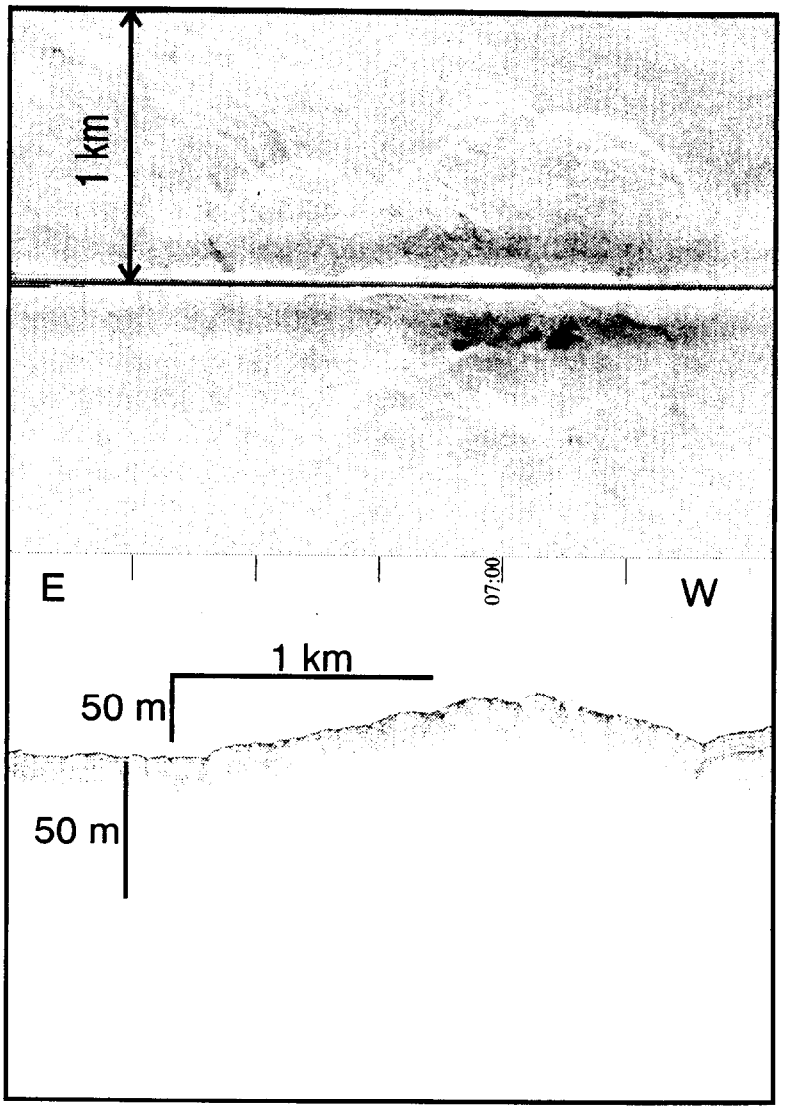

Fig. 18. MAK line crossing Saint Ouen l'Aumone mud volcano. The sidescan image shows several high reflectivity patches on this dome which are probably centres of current activity. The tongue of a buried flow can be seen to the left in the subbottom profile indicating greater activity in the past. The right side of the mud volcano is very abrupt, as if it were on a fault

West of Tuzlukush, the seafloor has small scale (tens of metres) long-wavelength relief (500 m or so). The upper 10 m of sediments appear to be well-stratified with acoustic evidence of beds around 1 to 2 m thick. Deeper in the subbottom profile, the sediments become increasingly more folded and disturbed, and the units are defined by boundaries with low reflectivity. Between

10:55 and 11:15, some acoustic wipeouts suggest the presence of gas in an area of slight doming. Downturn in the sedimentary layers deeper than 15 m to the east of this dome further suggests that there might be a buried mud volcano which is still degassing to some degree (Fig. 19).

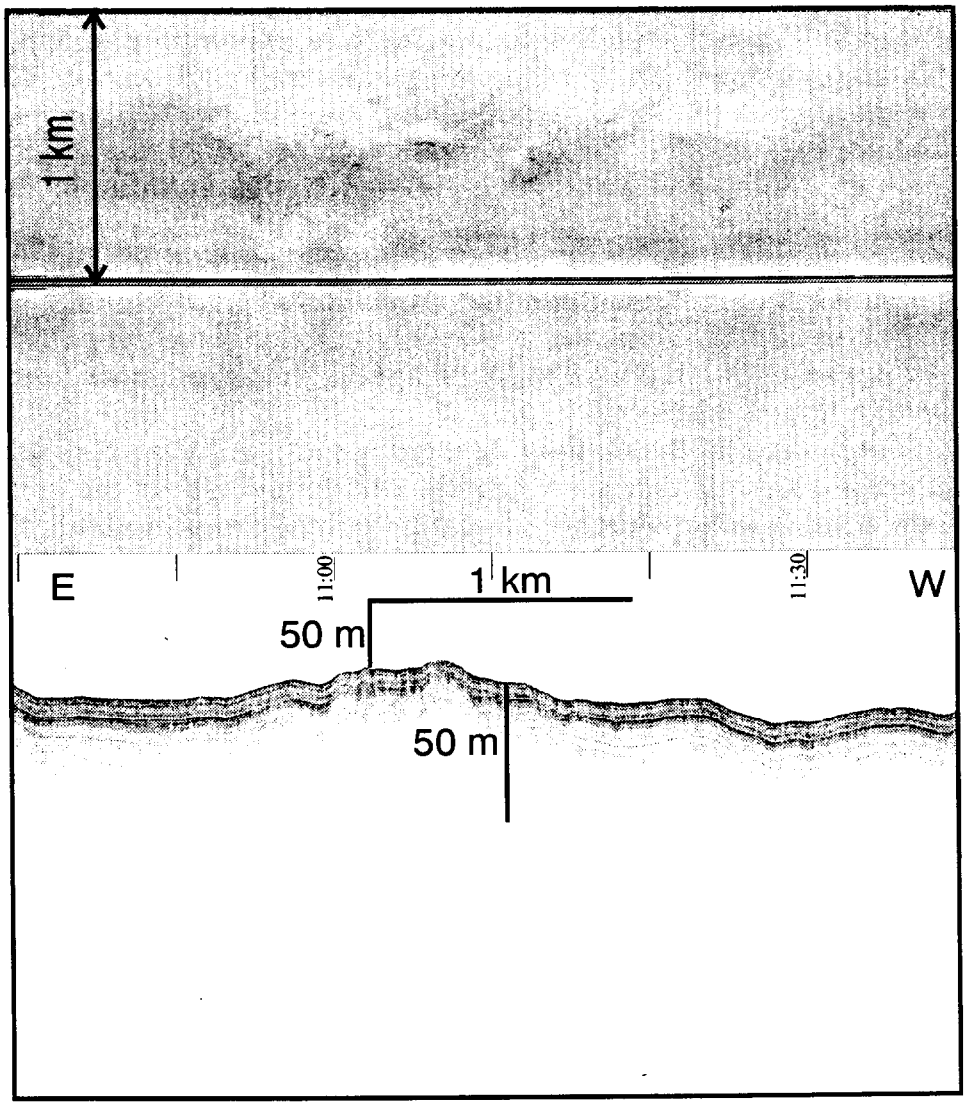

Fig. 19. MAK line 46 crosses what is possibly a very old and buried mud volcano, but pockmarks, acoustic wipeouts, and seafloor disturbances indicate gas seeps

The line bends to the northwest at about 11:10, and at 12:05 crossed from an area of well-stratified sediments to an area of rougher seafloor and no acoustic evidence of stratification. This may be a fault running south from the end of Anaxagoras Mountain to the north. The tip of the mountain lies less than 5 km to the north and there is a prominent north-south oriented valley cutting across it. West of the inferred fault, the relief increases to about 100 m and there are noticeable north-south offsets in the topography. The sidescan sonar image

shows both high and low backscatter which appears to be a function of the seafloor roughness and larger scale relief. Some sedimentary stratification is observed in places through this section of the line (e.g. in a plateau area between 30°40.8′ E and 30°40 ′E and in a more contorted form between 30°39.1′ E and 30°37.5′ E). There appears to be another fault, oriented about 020°, at 13:45 (30°38.4′ E). Between 14:00 and 15:30, the line obliquely crosses a linear (about 085° trend) slope rising about 250 m to the north - northwest. Some stratification is present in the slope sediments to the depth of penetration of the subbottom profile (in places up to 15 m), but there are some small slide scars on the slope. At the top of the slope is the Kazan mud volcano (see Fig. 10).

Kazan mud volcano sits on a small promontory at the edge of a gently northeastward sloping plateau which rises from 1750 m at Kazan to about 1500 m around 12 km to the northeast. The height of the mud volcano is about 50 m and the diameter is around 1000 m. The circumference is irregular because of flows of mud breccia which have run down the flanks of the mud volcano to the north and east. The backscatter from the flows is high, making the mud volcano clearly visible in both the EM-12D and MAK imagery. The uppermost flow is slightly less reflective than the others.

To the northwest the seafloor deepens slightly and then rises onto another promontory of the plateau area. Gullies on both sides of the ridge indicate downslope mass wasting. Further west the seafloor drops by about 100 m or so, but the MAK fish remained at the previous level to avoid difficulties at another high ridge 3.5 km further to the west which was to be crossed; thus the seafloor between 17:00 and 18:40 remained too deep to be observed well.

The ridge which comes into view at 18:40 is over 700 m high where crossed by the line, and lies on a strong lineament which cuts across Anaxagoras with an azimuth of 055°. The location of dredge 209D was chosen on the basis of strong backscatter in the EM-12D image of the side of the ridge. The strong backscatter appears in the MAK sidescan sonar image to be caused by debris flows from the top of the ridge. The debris flow is at the steepest part of the ridge which coincides also with a broad gully down the side of the ridge. Blocks on the order 10 to 20 m across can be seen on the lower part of the slope. A small linear scarp with a trend of 040° defines the top of the ridge where it is reached at 19:55.

The end of the ridge is separated from the part just crossed by a small saddle with a 040° trend. The end of the ridge has an elevation of 1360 m. Along the summit are several pockmarks and acoustic wipeouts, especially along the west side of the ridge, suggest gas is escaping (Fig. 20). Between 20:50 and 21:30, the line turns southward by about 90°.

From 21:30 to 22:00 the line runs parallel to the southeast slope of Anaximenes. There is evidence for downslope creep to the southeast in the left sidescan image, and the subbottom profile shows very vague stratification, probably as a result of sediment disturbance during sliding. At about 21:35 the line crosses narrow lineations of high reflectivity which have a 070° orientation. These are thought to mark small scarps parallel to the slope at the upslope side of a minor slump.

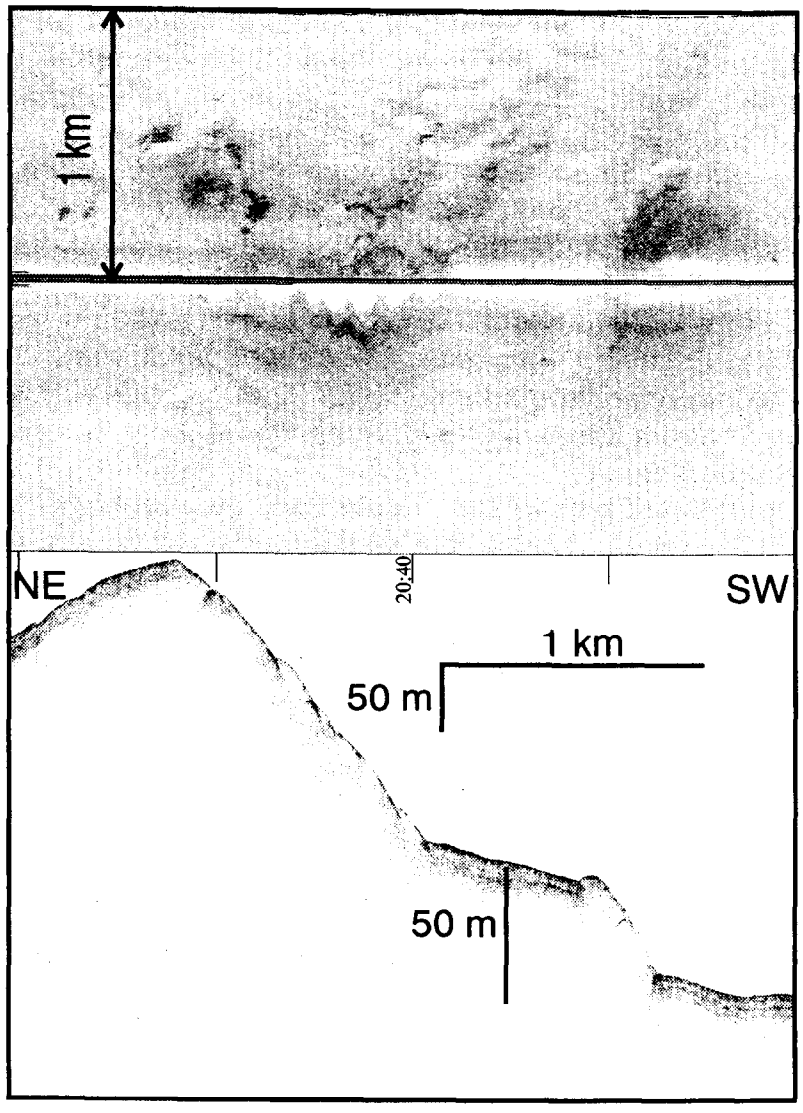

Fig. 20. MAK line 46 crosses obliquely the WSW-ENE-trendind ridge between Anaximenes and Anaxagoras along which gas seeps were sampled just to the east of this section of the line. Pockmarks are observed along the top of the ridge indicating gas escape here also. Sediments have slumped down the flank of the ridge to the west, and acoustic wipeouts are observed there in the subbottom profile

Further on, between 21:40 and 22:00 on a bathymetric step (which might be the top of slightly rotated slump block just mentioned) are several high reflectivity patches in the sidescan sonar image. They appear to have formed, possibly as a debris flow, from a local 100 m high hill to the northwest, as one long strip about 150 m wide and at least 1 km long which was subsequently broken by dextral strike-slip faulting. The dextral faulting has a strike of 040° and a cumulative offset of over 250 m since the strip was formed. The slope at the outer side of the step is covered with disturbed sediments showing only vague stratification; and near the base of the slope are pockmarks which show a rough alignment with the contours of the slope between 22:00 and 22:40. There is also evidence for downslope slumping seen in the sidescan sonar image along this section of the slope.

A small promontory crossed at 22:52 is attached via a narrow ridge to a

040° trending ridge. The latter ridge looks in the sidescan sonar image to be of partially diapiric origin, with a broad anticlinal top and steeper edges near the base. To the south of the promontory, the seafloor deepens steeply by over 300 m down a short slope with evidence of downslope sedimentary movement (between 23:00 and 23:20).

Although the line follows the edge of the small basin at the foot of the slope (between 23:20 and 23:45), it appears that the basin contains layered sediments to the maximum depth of penetration of 12 m. The east side of the basin is formed by a ridge about 800-1000 m wide and over 50 m high, trending about 030°. From 23:40 to about 00:05 can be seen a lineation trending 015° which is probably a fault cutting very obliquely across the ridge and disappearing in the basin. A small circular promontory, about 20 m high, is visible on the west side of the sidescan sonar image at 00:00. From about 00:00, the seafloor rises out of the basin by about 150 m.

The northwest half of the Amsterdam mud volcano is crossed between 00:20 and 01:40 (Fig. 21). The surface of the mud volcano is a series of concentric ridges with a relief of the order of 10 m. This is shown well on the sidescan sonar image which has a wide range of backscatter: high backscatter in general, probably as a result of the mud breccia erupted from the mud volcano, with shadow zones of low to no backscatter outlining the ridges. A local point of eruption between 01:25 and 10:35 is an elongated cone of about 30 m elevation. The roughly 020° elongation of the feature is the same trend as a lineation (probably a fault) which runs through it and continues to the southwest in the sidescan sonar record to at least 02:00. The subbottom profiles shows no penetration, only many small strong diffractors near the seafloor, which is common for most active mud volcanoes because of the acoustic scattering caused by the mud breccia.

To the southwest of the roughly circular plateau formed by Amsterdam is another vaguely circular plateau with a depth about 50 m lower than that of Amsterdam. The texture of the seafloor shown by the sidescan image and the similarity of the subbottom profile with that across Amsterdam suggests that this is an inactive mud volcano. The reflectivity is lower than for Amsterdam in the sidescan image but is slightly greater in the EM-12D image. A central elevated hill, about 30 m high, could be a former point of eruption (at 01:50). Nearby are a number of small high reflectivity spots less than 50 m across, with shadows indicating that they are raised and conical in cross-section. Lineations suggestive of faulting run roughly 055°-060° through this area between 02:10 and 02:35.

From 02:35 to 03:25, the line runs across a slope separating the inactive mud volcano from a trench trending roughly 065°. To the northwest between 02:30 and 03:05, a small scarp can be seen in the sidescan image at the base of a slope with the same trend (040°). The small scarp appears to be faulted, especially between 02:50 and 03:05, where it is well-expressed, narrow, and very linear. It is possible that the faulting and other examples to the southeast downslope (between 03:00 and 03:20) are the traces of slump scars. Throughout this region the subbottom profile shows acoustically homogeneous sediments. It is only from about 03:20 that the subbottom profile shows, with about 25 m penetration, what appear to be structureless debris flows of 5-8 m thickness.

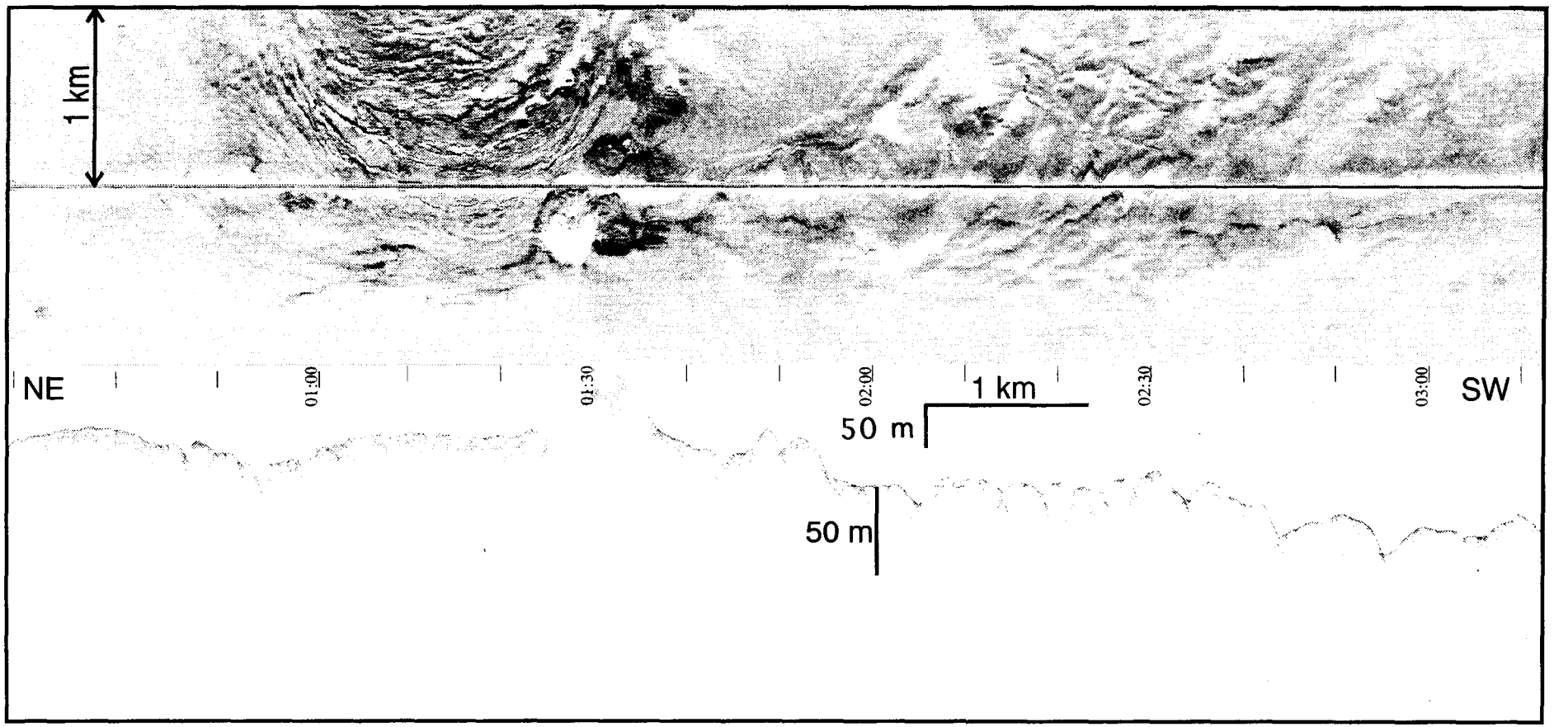

Fig. 21. MAK line 46 crosses the northwestern part of the Amsterdam mud volcano. This is a large mud volcano, with the average diameter of about 6 km, as seen from the EM-12D reflectivity chart. A local point of mud eruption is observed between 01:25 and 01:40 on the centre line of the sonograph, and an extensive mud flow is spreading southwestward from it

A narrow valley with a trend of about 060° is crossed obliquely between 03:50 and 04:10. It is well-expressed in the bathymetry at least over a distance of 10 km. Faulting through the valley is highly probable. The sidescan sonar records show long lineations that look like drainage channels running to the southwest, but this could equally be the fronts of sediment slides into the valley from the sides. The subbottom profile shows disrupted and contorted layered sediment, with greater deformation with depth, suggesting that faulting is the more likely cause of the valley. The valley seems also to mark the edge of the Anaximenes structure, with the seafloor to the southeast resembling the Mediterranean Ridge more.

The last part of the line (between 04:10 and 05:20) crosses gently upward sloping seafloor. The sidescan sonar in this part shows gentle folds trending 060°, with an amplitude of about 20 m and a wavelength of 200-300 m. The subbottom profile penetrates to 20 m and shows well-layered sediments overlying more deformed sediments. This is typical of ongoing (probably compressional) deformation. Bedding can be observed at the metre scale, and there is a particularly strong reflector at about 6 m depth.

MAK line 47

MAK line M-47 started on the south margin of Turkey and ran south-southwest over the lower slope and across a trough at the foot of the slope, and finally over the lower northern slope of Anaximander. The purpose of the line was essentially tectonic: to examine a series of faults which cut across the southern margin of Turkey and define the slope geometry. Of particular interest was the following of a conspicuous lineament running down the slope (at roughly 010°-190°) and southward across the northern flank of Anaximander Mountain to at least 35°38′ N, and to look at the nature of large structural (fault?) blocks at the base of slope. The structural relationship of the mountains to the margin of Turkey might be discernible in this way, an important element in the interpretation of the origin of the mountains.

The line starts over the northern flank of a prominent canyon on the Turkish slope and runs slightly oblique to the canyon trend. The walls of the canyon are linear (with an azimuth of about 020°) and possibly fault-controlled. The floor of the canyon is relatively flat, and there are linear steps across it with an azimuth of about 105°. Several cross-cutting faults (oriented at about 065°) intersect the canyon. The canyon is about 4 to 5 km in width.

Up to about 20 m of sediment can be seen in the subbottom profile, varying slightly in thickness, and looking like turbiditic units with strong reflectors separating beds with low to medium reflectivity. Acoustic sedimentary units are about 2 to 4 m in thickness. Two faulted steps observed at 12:00 and 12:15 probably represent the edges of blocks sliding into the canyon. The edge of the canyon is crossed between 12:20 and 12:55. There is a drop of about 400 m; however this is not observed on the subbottom profiler because of difficulties in measuring and correcting for the actual depth of tow fish. The local azimuth of the canyon wall in this area is about 040°. Near the base of the canyon wall is a

rotated slump block with internal stratification. The actual canyon floor is not reached until 13:45; between the steepest part of the canyon wall and the canyon floor is an intermediate region of gentle slope with material which may have been deposited as debris flows from the side.

A relatively flat section of canyon floor is crossed between 13:45 and 14:30. There is relief of no more than a few tens of metres over this roughly 3 km long section. The subbottom profiler exhibits almost 30 m of sediments which thicken to the north. Separation of reflectors is quite variable suggesting acoustic units of less than 1 m thickness in places (e.g. the upper sediments) and the thickest being about 7 m thick. The sediments are thinnest at the southern edge of this 'step', at about 14:30.

The step crossed between 14:30 and 14:50 descends about 350 m to the south. The step coincides with the intersection of the channel by a lineament from the east with an orientation of 065°, interpreted as a fault.

The line runs along the edge of a scarp between 14:50 and 15:25. The scarp is linear and faces east. The height of the scarp is about 150 m. Its orientation is about 025° and it lines up with other lineations further up the canyon to the north. The subbottom profile shows four rotating blocks, in which the acoustic sedimentary units fan out upslope and tilt in the same direction. The seafloor on both sides of the scarp is relatively flat. The impression is that the different levels are controlled by faults along the scarps. Between 15:30 and 16:00, the scarp can be seen in the sidescan sonar imagery as a strong linear feature with very high backscatter which trends locally at 035°.

From the edge of the scarp at 15:30 to about 17:30, a distance of about 7 km, the seafloor is again relatively flat, with a relief of less than 50 m until about 17:10 when the seafloor begins to slope up toward the south. This flat area of the canyon seafloor also shows northward thickening and dipping sediments with the acoustic appearance of turbidites. Sedimentary units are defined acoustically by strong continuous reflectors with low reflectivity between them. Thickness of the units varies from less than a metre, especially in the upper sediments and the more southerly area, to perhaps 5 or 6 m in the north. The 'step' appears to be actively tilting to the north. The penetration depth of the sediments is seen to be no more than about 30 m in this area.

From 17:45 to 18:00, the line crosses a zone of debris flows or zone of active sediment creep. The subbottom profile shows stratified but slightly disturbed sediment, and the sidescan sonar image is characterized by moderate to high backscatter and the rough relief at the metre level. The direction of the sediment movement is about 040°, and it follows a shallow valley (no more than about 20 to 30 m deep and about 8 km wide), steepening and deepening to the southwest where it begins in a saddle point between a large block to the west and a smaller block to the east. The western block rises more than 300 m and is more than 20 km long with a roughly east-west orientation and a width of 4 to 5 km. The eastern block has about the same height, but is half as wide and extends about 7 km to the northeast as two ridges, apparently fault-controlled (with the 065° orientation described for other lineaments in this area). The sediment moves along the northwest side of the eastern block. At 17:10 to 17:25 there is a small offshoot of the main flow visible on the east side of the sidescan image, curving

downslope to the northwest with a trend of about 335° for 800 m.

At 18:00 the line crosses a corner of a slide block around the west end of which the flow is diverted. The slide has moved downslope in the direction 315°, as shown by the linear northeast edge of the block in the sidescan sonar image. Another linear escarpment (azimuth about 025°) suggests that another fault crosses the region.

The saddle point mentioned above lies on a roughly east-west trending ridge which joins the two blocks to the west and the east. The ridge is covered with relatively well-stratified sediment visible in the subbottom profile to a penetration depth of less than 10 m. The sediments appear to contain gas which may wipeout deeper reflections and cause acoustic turbidity in at least one place on the top of the ridge and on the southern slope. An isolated hyperbolic reflector in the subbottom profiler is interpreted as a gas plume originating in a gas vent suggested by a highly reflective spot in a small depression of about 25 m diameter, shown approximately 200 m off line to the east in the sidescan sonar image at 18:25. The southern slope of the ridge is marked by localized patches of very high reflectivity inferred to be areas where gas is emanating with debris from below, and possibly localized outcrops of basement. The base of the slope, at 19:00, lies on a lineament with an orientation of about 060° which could be the inferred as a fault along the southern boundary of the block to the east.

From the foot of the small ridge at about 19:00 to the south, the seafloor rises gently along the northern flank of Anaximander Mountain. A small ridge, the western tip of which is crossed between 19:20 and 19:25, shows small gullies with presumably slightly coarse material moving through them downslope, as can be seen by the elevated backscatter in the sidescan image. This ridge on the lower flank of Anaximander is the westernmost part of the block seen in the bathymetry to the northeast. The ridge lies on a broader and gentle swell (between 19:00 and 20:20) and has a small escarpment on its southern side with an azimuth of approximately 110° to 120°. Sedimentation on the broad swell is well-stratified thin units with the appearance of turbidites. The deepest reflectors seen are no more than 15 m deep.

South from the swell, the flank of Anaximander continues its rise. In the gentle depression between the swell and the rise, the sidescan sonar image shows interference patterns, probably caused by very gradual variations in the thickness of the upper thin beds of sediments. Here the penetration depth is about 20 m and the beds giving rise to reflectors that are less than a metre apart.

The seafloor rises about 500 m along the flank of the mountain, crossing a prominent lineament observed on the bathymetric charts to cross the Turkish margin and continuing to about 35°37′ N in the south. The sediment here is fairly well-stratified acoustically and visible to about 15 m. The sidescan image exhibits a strip of slightly higher reflectivity with roughly the same 190-195° trend as the lineament between 21:45 and 22:10, and a series of strips and shadows with the same trend between 21:25 and 23:10, mainly on the west side of the sonograph. An area of disturbed and displaced sediment lies within this zone between 21:40 and 21:55 in the subbottom profile; and there are localized faults observed at 22:32, 22:45, 22:48, 23:06, and 23:13. A broad fault zone about 500 to 600 m wide is inferred.

To the east of the line up the flank of the mountain (i.e. upslope to the southeast), the reflectivity is generally higher, as is expected on the upslope side of a sidescan record, but it is interrupted by downslope-oriented strips of lower reflectivity. These variations are interpreted to originate mainly in small-scale relief. At a relative topographic high between 23:35 and 00:10, the relief is seen to be a low ridge oriented about 145° across the sidescan sonar image, but apparently part of a general 125° trend which is seen on the bathymetric chart to cross this area towards the Rhodes Basin to the west.

The 125° trend also characterizes the southern margin of the relative topographic high lying midway along the northern flank of Anaximander Mountain. A prominent ridge between 00:35 and 00:50, belonging to this high, shows downslope sediment transport (debris flows) both north-northeastward and southward. From 23:50 the line runs down to the base of this margin at about 02:10. Down this linear southwest-facing hill are numerous small channels with material of higher reflectivity in them. These are likely debris flows; however, the presence of gas-charged sediments inferred from the acoustic wipeouts and limited penetration depth of the subbottom profiles is considered to be a possible cause of the flows. The flows, especially those at 01:45-02:20 on the sidescan sonar image, originate at specific points or short linear strips of very high reflectivity which are similar in appearance to areas of gas seeps and fluid venting. At the base of the slope the sediments are poorly imaged because of the acoustic voids and wipeouts, but where seen, they are deformed. A fault zone is interpreted to bound the slope and to act as a conduit for fluids and mud breccia which has flowed out on the seafloor here.

The line ends at about 03:35 at a point where the slope up the flank of the mountain to the south is resumed. It was successful in providing clear information about the structures and their fault control.

8. Bottom Sampling

a. SAMPLING STRATEGY

J.M. Woodside and J.-F. Dumont

The chief aim of the bottom sampling was to obtain rocks from each of the Anaximander Mountains, the surrounding seafloor, and the margin of Turkey. To establish the nature and origin of the mountains, it would be necessary to determine differences and similarities between the geology of the mountains inferred from the samples on the one hand, and the geology of southwestern Turkey, the neo-Tethyan seafloor, and north Africa on the other hand. Comparisons would be made on the basis of diagnostic aspects of the lithologies, depositional environments, facies variations, and geologic history. For example, the geological connection or discontinuity between the mountains and the Bey Daglari and Antalya nappes of southwestern Turkey might be established by sampling transects across the Turkish margin and in the mountains.

Because the ANAXIPROBE-95 reflectivity images only indicated limited outcrops in the mountains, another strategy was followed. Sampling would be made of any likely outcrops (e.g. escarpments at the margins of the mountains), potential mud volcanoes inferred from the ANAXIPROBE-95 reflectivity images (because mud volcanic eruptions could be expected to bring to the seafloor rocks from below the Pliocene-Pleistocene sediments covering the bedrock), areas where deeper levels might be exposed by karstic collapse or removal of sediment by slides, and so on.

Sampling was done by dredging and coring (Figs. 11 and 22). Only the hard rock samples were retained from the dredge hauls. Recent sediments were sampled by coring; however, hard rock samples were also recovered from the mud volcanoes, as clast in mud breccia, and one core included hard rocks from slope deposits. Hard rocks were sampled mainly to define the stratigraphy and structure of the mountains, because of a nearly total lack of previous data from the area. The samples were processed immediately as discussed elsewhere in this report. They were classified and checked for fossils in order to get an overview of the geological units as early as possible. Core sampling was done with intention to analyse the sediments and clasts in detail later (mostly in Moscow). The cores were described in general with special attention to the sapropels, tephras, and marker beds, as well as examining different horizons and lithologies paleontologically, and sampling for later geochemical analyses.

b. DREDGING RESULTS

General description of dredged rocks

J.-F. Dumont and J.M. Woodside

The hard rock samples obtained by dredging were very variable in quantity and quality. Half of the dredging operations provided hard rock samples. Some dredges were empty or contained only a few rocks because of the specific morphology of the rock outcrops they sampled, especially on the Taurus slope. Limestones frequently have very rough outcrops anchoring the dredge, or a smooth morphology of rounded surfaces from which it is difficult to take a sample even on land. Another problem specific for the area is the development of a limy crust over rock outcrops and even some soft sediments on the sea bottom. Nevertheless, if crusts were frequently recovered, they were in most cases accompanied by hard rock samples from the underlying geological units, even if these latter rocks were few in number. In other cases only crust and recent sediments was recovered because of a location error (one case), or the need to change course due to strong bites and the anchoring of the dredge.

Hard rocks samples were processed on the ship in order quickly to obtain information about the particular geological units sampled. The first classification of the recovered rocks was made simultaneously with the first examination of the samples for fossils. Samples with fossils or specific organic remains were immediately sent to the paleontological team. Some sample collections were reviewed later for fossils and facies, and surfaces polished for better observation when necessary.

Dredge TTR6-209D (see Fig. 11) appeared to be the key for the understanding of the area located east of Anaximander mountain. The occurrence of a unit of Middle Miocene flysch was recognized with help from paleontological analysis. Considering samples from Cores TTR6-207G and TTR6-208G (see Fig. 22) and from later dredging at Sites TTR6-210D and TTR6-211D, this unit appears to be present over a large part of the area. Bathymetric distribution of these occurrences lends some support to a possible NE-SW fault as previously hypothesized. Apart from this, the rocks recovered from Core TTR6-213G in the Kula mud volcano raise the question of the possible occurrence of Antalya nappes in the northeast corner of Anaxagoras mountain, extending southward from their southernmost exposure on land.

Dredge TTR6-202D from the southern margin of Anaximenes mountain is consistent with the results from a previous cruise (*Kuznetsov, 1992*). Eocene and Middle Miocene rocks especially have been reported from the southeastern margin of the mountain.

Dredge TTR6-198D provides evidence of a cover of Pliocene-Pleistocene sediments in the area, which is in agreement with inferences from the seismic profiles.

Samples in *Dredge TTR6-222D* from the Turkish continental slope directly south of the autochthonous Bey Daglari included Mesozoic limestone.

Dredge TTR6-223D provided similar limestone (with more recrystallization) in the context of breccia deposits, partly accumulated in the sea and reworked near tidal level. East of the Bey Daglari, ophiolitic rocks were recovered (at *Dredge TTR6-214D*) in a place where they were expected on the basis of samples taken further south at Kula and San Remo mud volcanoes (Cores TTR6-213G and TTR6-239G, respectively).

Regarding evidence of tectonics, two fault planes in lithified sediments were present on sampled rocks. Both have slickensides, and also traces of rupture suggesting that the rock broke off "in place". One dredge (*TTR6-198D*) was in Plio-Pleistocene sediments, and the other (*TTR6-211D*) in similar rocks inferred to be post-Miocene flysch). Considering the possible original position of the samples according to the stratigraphic level which can be inferred for the samples, one case (TTR6-211D) suggests vertical movement, and the other (TTR6-198D) reverse movement. It is very unusual to observe slickensides near the surface in relation to extensional tectonics. Thus, the observed slickensides on sample TTR6-211D are probably also related to compressive tectonics.

Micropaleontological analyses on rock samples recovered from dredges and gravity cores

J. Henderiks, E.M. Ivanova, S.S. Gablina, and A.P. Sautkin

Preliminary dating of selected rock samples that were recovered during the first Leg of the cruise by dredging and gravity coring (mud volcano breccia) was done in the shipboard micropalaeontological laboratory. The rock assemblages of the Anaximander Mountains Region were expected to express a wide range of geological ages. Therefore, all Cenozoic and even Mesozoic (Jurassic-Cretaceous) foraminifera (benthic and planktic) and calcareous nannofossil species were considered in the biostratigraphical analyses. Smear slides were used for the study of the calcareous nannoplankton, and analyses on the washed residue were carried out to investigate planktic and benthic foraminifera. This section is a short summary of the results of these investigations. Furthermore, an attempt is made to link separate selected samples within and between the different sample locations.

Dredge TTR6-198D

Samples from Dredge TTR6-198D included clays (198D-8b, 9b, 11b, 12b), siltstone (1b) and limestones (4b, 13, 16b). The ages of the clays range from Middle Pliocene to Pleistocene and the siltstone is of Pleistocene age. The limestones did not contain any fauna, most probably due to carbonate recrystallization.

Dredge TTR6-199D

From this dredge only a sample (199D-1b) from a carbonate crust was

selected. This material was dated as Quaternary.

Dredge TTR6-201D

Three different lithologies were investigated in this dredge, including a siltstone, sandstones and a limestone. The siltstone (201D-1) was dated as Early Pliocene, the sandstones (201D-2 series) lie within the Middle Pliocene - Pleistocene range. Again, the limestone (201D-1a) was recrystallized and no fauna was found.

Dredge TTR6-202D

A large suite of samples was investigated from Dredge TTR6-202D. The lithologies include clays, siltstones, sandstones, marls, lime mudstones and grainstones. In 12 samples no fauna was found (clay samples 202D-6, 7, 12; siltstone 202D-25; sandstones 202D-3, 8, 9, 10, 11, 15, 16 and 24), and there was insufficient time on the ship to investigate 11 samples. For the rest of the selection it was found that the siltstones could be dated as Early-Middle Miocene (202D-14) and within the Late Pliocene - Pleistocene range (202D-4). The lime mudstone and marl (202D-26 and 27) seem to be of Middle Miocene (Serravalian?) age. The grainstone samples (202D-5, 19 and 32) consisted of the benthic larger foraminifera *Nummulites* sp., and were thus dated as either Paleocene or Eocene. Further refinements on this age were made by smear slide investigation of sample 202D-19, which revealed Eocene calcareous nannofossil species (provisionally identified as *Chiasmolithus* cf. *minimus* and *Helicosphaera* sp.).

Dredge TTR6-209D

One of the most prominent facies recovered in Dredge 209D is the black siltstone facies (209D-3). However, these samples seem to contain no fauna at all and thus dating was impossible. Other samples that were investigated include siltstones as well, and they could be dated. The 'flysch facies' (209D-2) has Middle Miocene age (indicated by the provisional identification of the following coccolith assemblage *Discoaster ruggii, D. exilis, D. pansus, Coccolithus pelagicus,* and *Calcidiscus macintyrei,* and by the foraminifera *G. continuosa, G. aguasayensis,* and *G. dehiscens*), whereas the rest of the siltstones are all of Pleistocene age.

Dredge TTR6-211D

A sandstone sample in this dredge (211D-9) did not contain any foraminifera and thus could not be dated. Two limestone samples (211D-3 and 4), however, reveal Middle Miocene (Serravalian) fauna (provisionally identified as *G. continuosa, G. mayeri,* and *G. aguasayensis*). These samples seem very similar to the 202D-26 and 27 limestones, at least in age.

Dredge TTR6-223D

It was very difficult to deduce any useful information regarding age from the very hard lithified limestones and limestone breccia sampled in this dredge. Besides washed residue analyses, investigations were done on polished surfaces (samples 223D-4, 5 and 11), which revealed radiolarians (5) and corals (11). No dating was possible. For the softer rocks, the conglomeratic and finer 'sandy' limestones (poorly lithified; 223D-1, 2 and 2a), analyses on the washed residue resulted in an age determination of not older than Early Pliocene (based on provisional identification of the nannofossils *Gephyrocapsa* cf. *caribbeanica*, and *Calcidiscus* sp.). The conglomeratic facies is very rich in shallow-water benthic foraminifera. For this suite of 223D samples microfacies analysis on thin sections will be necessary for obtaining more precise information.

Mud Breccia: Gravity Cores TTR6-207G, TTR6-208G (Amsterdam Mud Volcano), and TTR6-219G[1]

Preliminary smear slide (nannofossil) investigations on some of the selected mud breccia clasts from these cores reveal all Pleistocene species (*Gephyrocapsa* sp.). However, some evidence has been found for reworked Eocene and Miocene material (mainly *Discoaster* sp.).

Gravity Core TTR6-213G (Kula Mud Volcano)

No clasts from this mud volcano were suitable for micropaleontological investigations on board, either because of strong lithification and recrystallization or because the clasts were not sedimentary in origin. Nevertheless, two samples (or groups of lithologies) could be dated as Jurassic-Cretaceous by the macrofossils they contained. Sample 213G-3 revealed a compacted belemnite, and sample 213G-1 an *Inoceramus* sp. No other fauna were found during the shipboard investigations.

Interpretation

J.-F. Dumont and J.M. Woodside

Five geological provinces were identified on the basis of a preliminary analysis of hard rock and mud volcanoes samples. They are (1) the Anaximenes-Anaxagoras, (2) the Kula, (3) the South Cape Chelidonia, (4) the Anaximander, and (5) the South Bey Daglari wall provinces. Areas (3) and (4) are the seaward extensions of continental structures. The other areas do not appear to have any structural connections with continental Turkey, but rock samples from areas (1) and (2) are comparable in facies and age with geological units on the continent. In the following, these geological provinces are presented briefly, then their possible relationships with each other are discussed. Some points of

[1]See Section I.8.c for a more detailed description of the cores

discussion need to be complemented with seismic profile data which are in the process of being interpreted. For this reason, some structural interpretations remain open, but the geological data facilitate an understanding of the problem. The conclusion focuses on the interpretative geological history as deduced from the available data.

The Anaximenes-Anaxagoras area (1)

This is currently the best documented area, with four dredge hauls (TTR6-202D, TTR6-209D, TTR6-210D, and TTR6-211D), four cores in mud volcanoes (TTR6-207G, TTR6-208G, TTR6-235G, and TTR6-236G), and one core in a slope deposit (TTR6-237G), all giving coherent and consistent results. The TTR6-209D dredge was a partial key to this province because of the large number of samples which contribute to a coherent image of a flysch unit. Several layers with microfossils and nannofossils were quickly identified by paleontologists on board as Middle Miocene deposits. Most of the rocks are black claystones (massive when recovered, but which broke down into small angular blocks when they dried out), and sandstones with a flysch facies. In lesser quantities are light grey layers of carbonate mudstone. These layers commonly include an accumulation of planktonic microfossils observable with the hand-lens. A similar facies of Serravalian deposits has been identified from Core TTR6-211G.

Eocene rocks were identified in Dredge TTR6-202D. Analysis of Cores TTR6-207G and TTR6-208G from the Amsterdam mud volcano, and Core TTR6-219G suggested reworking of Eocene and Miocene material. These preliminary data suggest the occurrence of a geological province characterized by the Middle Miocene flysch probably overlying a neritic Eocene limestone. This is a classic succession in the Bey Daglari Massif, but, because it is transgressive, it does not exist everywhere. Results from gravity Core TTR6-219G, to the west of Anaxagoras Mountain in the 'lobes' area, suggest that the Eocene/Miocene units extend westward into the area between Anaximenes and Anaximander mountains. This unit probably extends farther westward below the Pliocene-Pleistocene cover.

Kula (2) and Cape Chelidonia (3) areas

The Kula mud volcano area is located at the northern end of Anaxagoras mountain just to the south of Cape Chelidonia. The two provinces are presented together because of their probable connection with the Antalya Nappes Complex. Dredge TTR6-214D at the base of the Turkish continental slope south of the Cape Chelidonia provided only a few samples but they are characteristic of ophiolites. The location and the material fit with the Antalya Nappe units described between Finike and the Gulf of Antalya. The rocks from Cores TTR6-213G and TTR6-239G at the Kula and San Remo mud volcanoes, respectively, provided various facies from sandstones and cherts, with some evidence of Jurassic-Cretaceous deposits. Similar material is not known from the Bey Daglari Massif, but it has similarities with rocks observed in the Antalya Nappes Complex, either from the lower or from the middle allochthonous units.

If there is no doubt concerning the attribution of the samples from Dredge TTR6-214D to allochthonous units, it is not so evident for the material from the Kula area. First, we must weigh the possibilities of elements being 'in place' or reworked, in some wild flysch or molassic deposits for example. There is no evidence of reworking; and the contrary seems to be the case because there are no rounded elements and there is an absence of detritic facies containing reworked material. Especially important is the lack of any evidence of Miocene flysch fragments accompanying the 'nappe' facies.

If the nappe material can be considered to be 'in place', two interpretations are suggested. In the first case the Kula unit is assumed to be covered by the Miocene flysch. Although this case is the simplest, it does not fit with the situation known in the southern Bey Daglari; and it is necessary to go far north in the Isparta area to find a place where the Antalya nappes are covered by the Middle Miocene flysch (but without Eocene). In this case, the Eocene neritic deposits that we observe in association with the Middle Miocene flysch are difficult to explain (this Eocene is a Bey Daglari facies, not a post-tectonic sediment). Furthermore, if the Middle Miocene flysch overlies the 'nappe' facies material, the possibility remains that it would be picked up during eruption of material from below to the mud volcano at the surface.

The second hypothesis is that the Antalya Nappes Complex extends southward and was thrust over the Middle Miocene flysch, as probably occurred in the Antalya area, during the late Miocene phase (Aksu tectonic phase). Seismic profiles may probably help to determine the best interpretation.

Anaximander area (4)

This area was characterized by the recovery of only Pliocene and Pleistocene sediments from two dredges (TTR6-198D and TTR6-199D) on the southern scarp and one core (TTR6-200G) on the slope of the ridge extending to the west. Similar deposits were also recovered from the Anaximenes area where they occur on the eastern slopes, along with Eocene and Miocene rocks (at dredge Station TTR6-202D), and exclusively on the western slopes (at Dredge TTR6-201D). This is in agreement with the observed distribution of sediments, and with the structure inferred from other data. Similar observations were also made from gravity Core TTR6-219G, which suggests that the history of the Anaximander and Anaximenes mountains is basically the same, but that the Plio-Pleistocene unit is more important to the west. Thus, a Miocene flysch unit could be expected from the basement of the Anaximander Mountain.

South Bey Daglari wall (5)

Two dredges from this area (TTR6-222D and TTR6-223D) provided information only about limestones. Dredge TTR6-222D provided evidence for the presence of the Mesozoic comprehensive Bey Daglari unit from a neritic facies with rudistids. The other dredge (TTR6-223D) provided three facies of

limestone: a white pelagic mudstone, a partly recrystallized light grey packstone, and a well recrystallized brown facies. Each of these elements are involved in a breccia with clast sizes varying from millimetres in length to over 40 cm. There is no indication of the age of the limestone. The pelagic facies may be related to the pelagic onlaps which are observed in some places of the southern Bey Daglari during the upper Cretaceous/Paleocene. The cement of the breccia is either sparitic or a more or less recrystallized mudstone which looks like a deep water deposit. A grainstone-microconglomeratic facies seems to be made of rounded fragments from the breccia, with some detritic elements of terrigenous origin. We have also observed a strange facies which is a thin carbonate sand made of well sorted 0.5 mm or smaller limestone clasts, with some terrigenous elements. Paleontological remains washed from the grainstone and the carbonate sand suggest an Early Pliocene or younger age.

All the observations suggest that the breccia probably formed during the Pliocene in a neritic tidal environment, in contact with terrigenous material, before reaching its present position at 2500 m depth. Hypothetically, this relationship could be explained by vertical tectonics or downward gravitational movement along the oceanic wall of the Bey Daglari massif. This phenomenon may be correlated with the higher accumulation of Plio-Pleistocene sediments in the area located northwest of the Anaximander Mountain. Movements would have taken place after the Aksu tectonic phase (post Tortonian in age), and may be correlated with the beginning of the extensional graben system observed between Isparta and the Aegean region.

c. CORING RESULTS

G.G. Akhmanov, A. M. Akhmetjanov, M.K. Ivanov, A. Mazzini, H. van der Bosch, T.P. Kleeven, A.V. Korkin, E.K. Ivanova, E.V. Kozlova, S.S. Gablina, I.Yu. Belen'kaya, E. van der Schans, A.N. Stadnitskaya, A.P. Sautkin

Introduction

A total of 28 coring sites were selected for sampling during Leg 1 of the ANAXIPROBE/TTR-6 Cruise in the Eastern Mediterranean (Fig. 22). The total recovery was 64.22 m. The longest core recovered was 484.5 cm (station TTR6-224G from a topographic high on the northernmost part of the Anaximander Mountain), whereas the shortest core was 16 cm (station TTR6-208G from one of flows of the Amsterdam mud volcano). There was no recovery at all at coring station TTR6-204G.

Sampling sites were chosen on the basis of the bathymetric and bottom reflectivity data obtained during a 1995 Simrad EM-12D multibeam echosounder survey, and of the acoustic images of the MAK-1 deep-tow sonar system obtained during the cruise. Coring was focused mainly on obtaining rock samples from the mountains and the surrounding seafloor by sampling mud volcanoes, plateaus and the slopes of the Anaximander Mountains. Initial results are summarized in this chapter.

The general coring information is provided in Table 1, and generalized core descriptions are illustrated in Figures 23 to 54.

Main coring transects of Anaximander Mountains area

For convenience, most of the cores obtained can be grouped and projected onto coring profiles across the investigated area, to compare the principal characteristics of recent sedimentation and their variability in various parts of the ANAXIPROBE-96 area.

Transect A (southwest - northeast across the investigation area)

This core transect covers an area south of Anaximander Mountain and the slopes of Anaximenes and Anaxagoras (Fig. 22). The aim of the coring was mainly to obtain clasts from the deeper lying strata. Therefore slope sites and high reflectivity spots were chosen to core because it was assumed that rock fragments from the mountains could be sampled there. This transect contained seven cores: TTR6-229G, TTR6-230G, TTR6-231G, TTR6-205G, TTR6-206G, TTR6-238G, and TTR6-237G (Fig. 23).

Core TTR6-229G taken on the flank of a deep depression in the seafloor south of the Anaximander Mountain contains a slightly slumped pelagic marl section, a carbonate hardground, sapropel S3 and tephra layers (Fig. 24). TTR6-230G was taken in another high reflectivity patch thought to be a debris flow south of the Anaximander Mountain, not far away from the TTR6-229G station. The slightly disturbed pelagic marl section of TTR6-230G contained

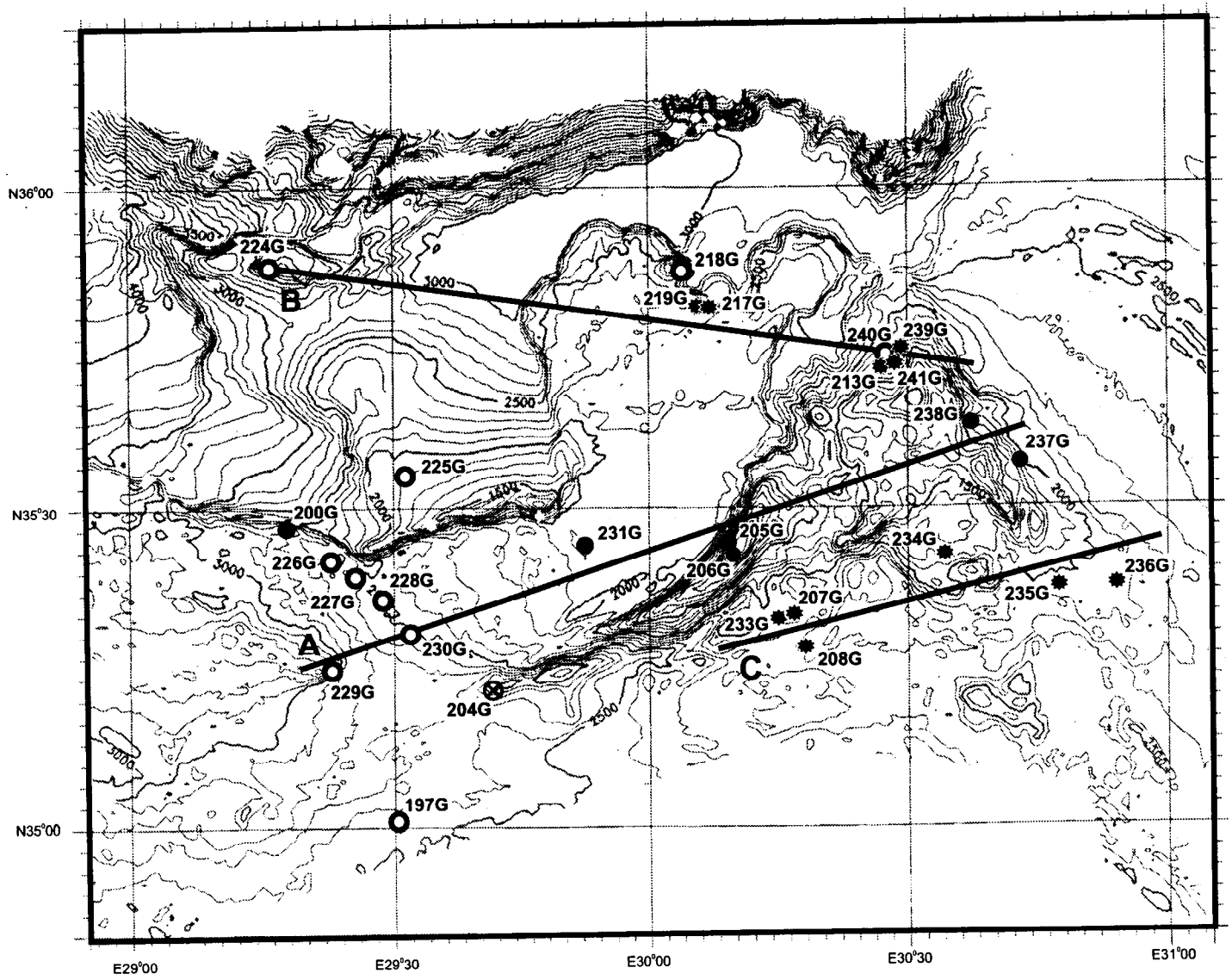

Fig. 22. Location map of coring sites and coring transects on the Anaximander Mountains

Table 1
General information on the cores sampled on the Anaximander Mountains

Core No	Date	UTC	Latitude	Longitude	Cable Length (m)	Depth (m)	Recovery (cm)
TTR6-197G	9/07/96	0:03	35°00.10	29°30.30	2650	2595	386
TTR6-200G	9/07/96	15:30	35°28.65	29°17.27	2900	2770	79
TTR6-204G	10/07/96	13:23	35°13.20	29°41.20	3200	3099	-
TTR6-205G	10/07/96	15:02	35°26.80	30°08.40		1502	177.5
TTR6-206G	10/07/96	18:32	35°25.63	30°09.08	711	682	276
TTR6-207G	10/07/96	20:31	35°20.08	30°15.97	2131	2036	48
TTR6-208G	10/07/96	22:49	35°16.93	30°17.43	2350	2329	23
TTR6-213G	12/07/96	7:35	35°43.75	30°27.51	1750	1639	186
TTR6-217G	13/07/96	12:47	35°49.11	30°05.67	2500	2380	16
TTR6-218G	13/07/96	14:51	35°52.48	30°03.37	2000	1961	320.5
TTR6-219G	13/07/96	16:27	35°49.11	30°05.72	2450	2368	177
TTR6-224G	15/07/96	13:41	35°53.21	29°15.51	2160	2040	484.5
TTR6-225G	15/07/96	17:51	35°33.39	29°31.09	2990	2250	242.5
TTR6-226G	17/07/96	1:16	35°25.50	29°22.41	2650	2624	313
TTR6-227G	17/07/96	3:12	35°23.83	29°25.30	2620	2614	269
TTR6-228G	17/07/96	5:56	35°21.82	29°28.37	2620	2490	499
TTR6-229G	18/07/96	16:02	35°15.16	29°22.48	3375	3330	153.5
TTR6-230G	18/07/96	18:14	35°18.61	29°31.54	2690	2535	288
TTR6-231G	18/07/96	21:21	35°26.73	29°51.82	2275	2197	124.5
TTR6-233G	19/07/96	12:27	35°19.79	30°14.88	2180	1982	195.5
TTR6-234G	20/07/96	15:06	35°25.73	30°33.64	1800	1709	121.5
TTR6-235G	20/07/96	17:11	35°22.65	30°46.72	2095	1972	341
TTR6-236G	20/07/96	19:26	35°22.79	30°53.49	2150	2045	367
TTR6-237G	20/07/96	21:43	35°34.40	30°42.38	1980	1870	234
TTR6-238G	20/07/96	23:32	35°38.01	30°36.80	1725	1652	403.5
TTR6-239G	21/07/96	1:49	35°45.11	30°29.04	1810	1721	339
TTR6-240G	21/07/96	3:20	35°43.80	30°27.55	1870	1639	181.5
TTR6-241G	21/07/96	4:28	35°43.74	30°27.50	1758	1638	176

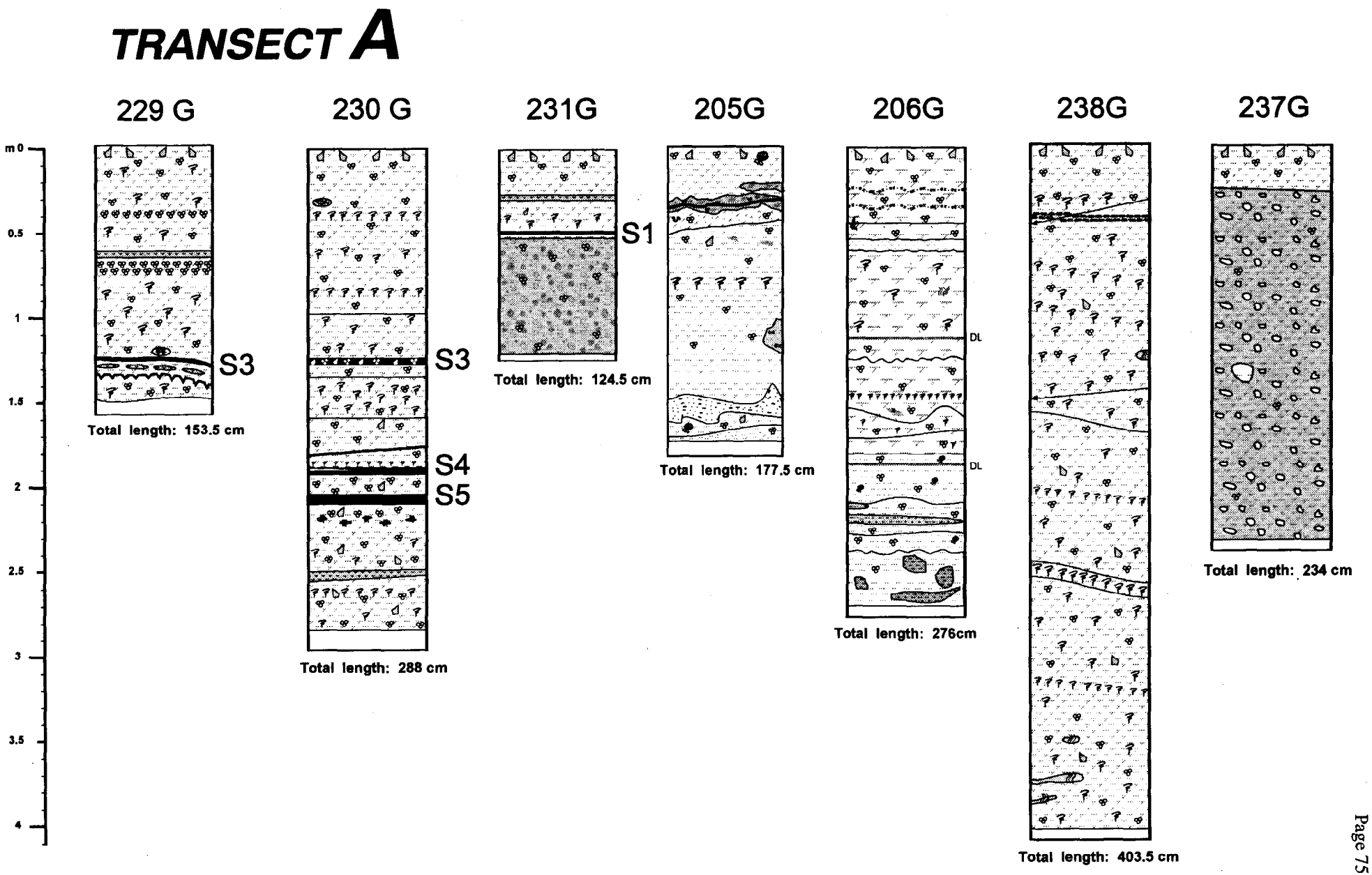

Fig. 23. Generalized core logs arranged along Transect A. (See Figure 30 for legend)

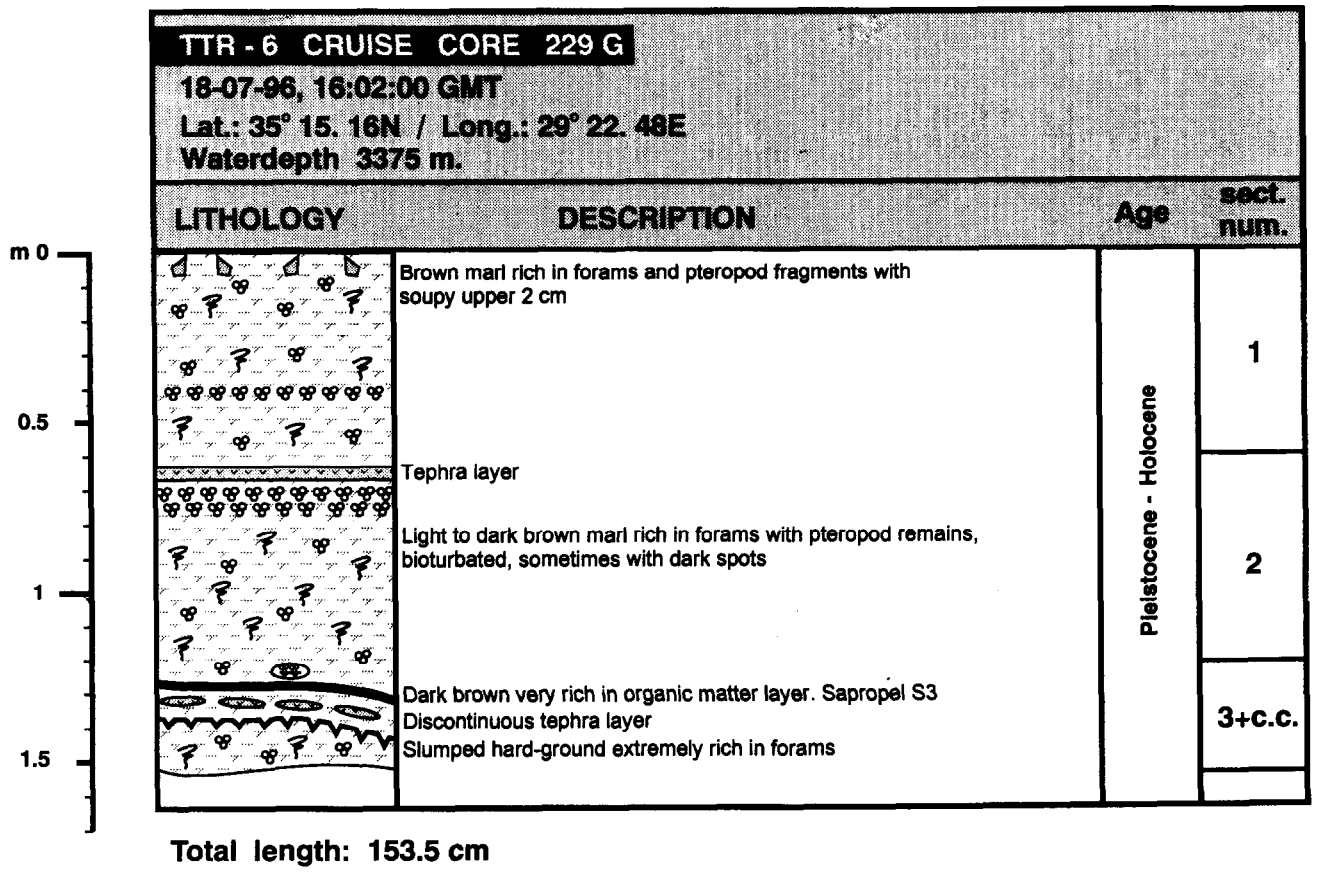

Fig. 24. Core log TTR-229G

---

sapropel S3, S4, S5 and tephra layers overlain by a slumped marl section (Fig. 25). Recoveries from both these cores characterize the same depositional environments of a weakly tilted plateau.

Lack of typical pelagic S1 and tephra layers in the uppermost parts of the cores implies, probably, an increased role of slope processes in the material input that might have marked a beginning of a new period of uplift of the Anaximander Mountain. Both of the cores sampled only unconsolidated deposits suggesting the high reflectivity target was missed.

Core TTR6-231G was taken in a high reflectivity patch on the floor of a large depression south of the Anaximander Mountain. The material cored can be interpreted as slump breccia from the inner slope of the depression, considering the lithology: grey structureless clay, rich in forams, with fragments of more consistent clayey sediments, overlain by a short pelagic section containing the sapropel S1 and tephra layers (Fig. 26).

Core TTR6-205G was taken on the western slope of the Anaximenes Mountain. This core contained only slumped sediments with marl, clay and carbonate hardground pebbles. This lithology suggests that slope processes were prevalent and have been very active until the present day (Fig. 27). TTR6-206G was taken close to the top of the Anaximenes Mountain. A slumped section was found overlain by a thin pelagic marl section (Fig. 28).

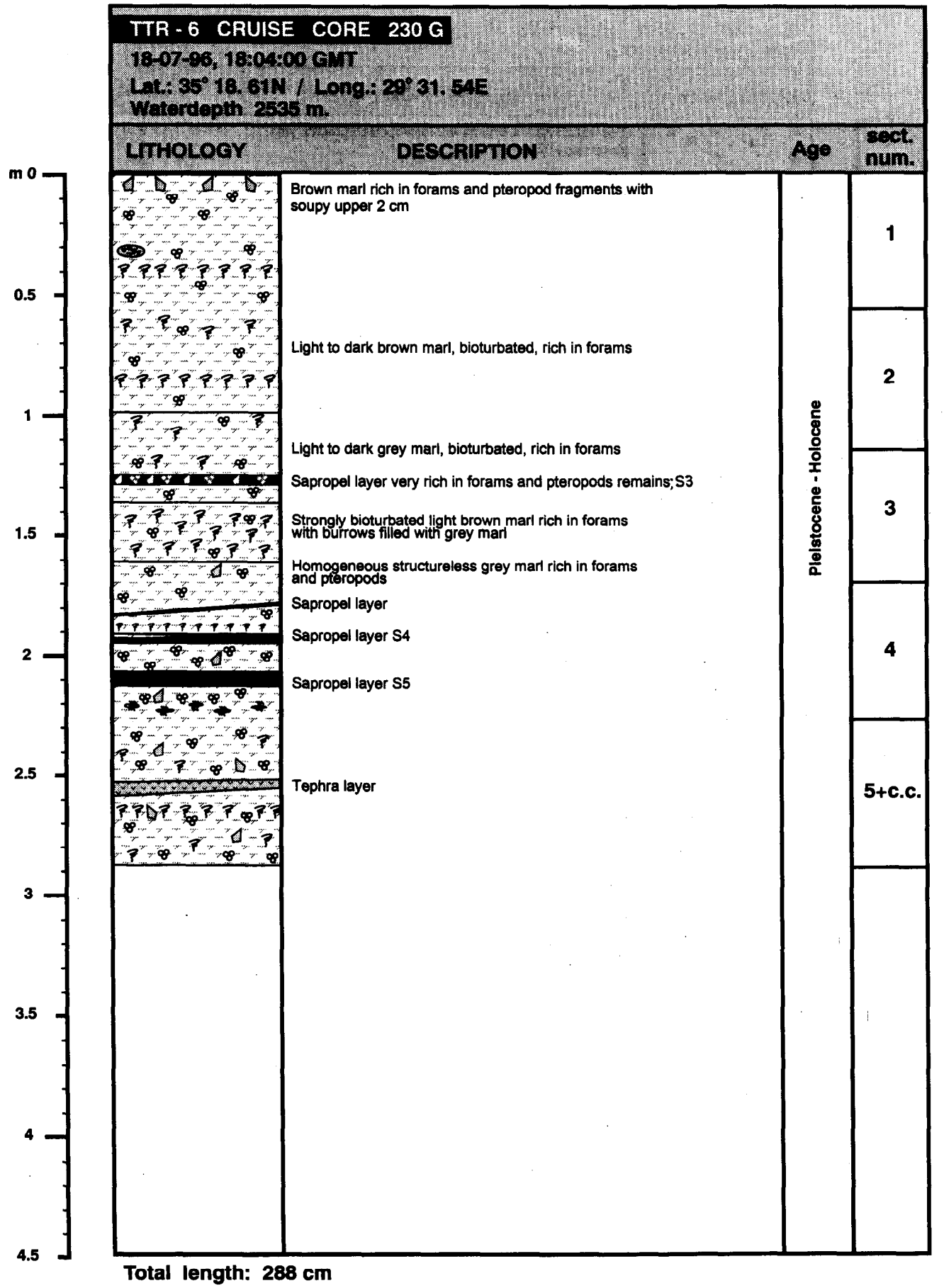

Fig. 25. Core log TTR-230G

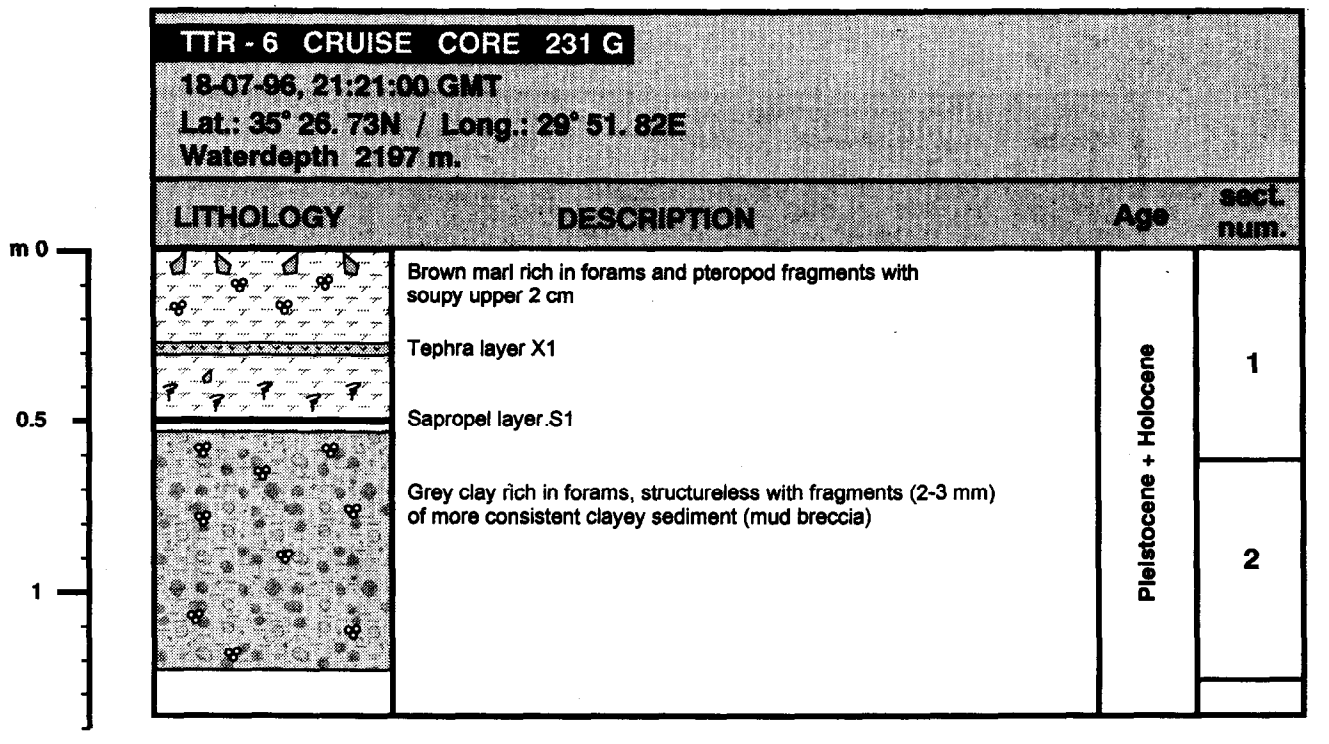

Fig. 26. Core log TTR-231G

Core TTR6-238G (Fig. 29) was taken on an upper part of the eastern slope of the Anaxagoras Mountain showing a slightly slumped marl section without pelagic sapropel and tephra layers. Some microfaults were observed in the core. The prevalent slumping of recent sediments might have been the result of neotectonic movement. TTR6-237G (Fig. 30) was taken at the base of the faulted eastern slope of Anaxagoras Mountain. The thick debris flow deposits found contain fragments of sapropel, tephra, mudstone and claystone pebbles. The uppermost thin interval is documented by a slightly disturbed pelagic section.

The lithologies found on this transect to a large degree indicate slope processes of recent activity across the whole investigation area. This is partly the result of bias in the selection of core sites in areas of either higher than normal acoustic reflectivity of the seafloor or irregular relief. The presence of different kinds of slope deposits is controlled morphologically, and can be interpreted as a record of neotectonic activity in the investigated area.

Transect B (west - east across investigation area)

This core transect contains the so-called 'lobe structure' and a few newly discovered mud volcanoes (Fig. 22). The aim of the coring was mainly to obtain clasts from the deeper lying strata, to investigate some intriguing features and to analyze the make up of the 'lobe structure'. This transect contained seven cores: TTR6-239G, TTR6-213G, TTR6-240G, TTR6-241G, TTR6-217G, TTR6-219G, TTR6-218G and TTR6-224G (Fig. 31).

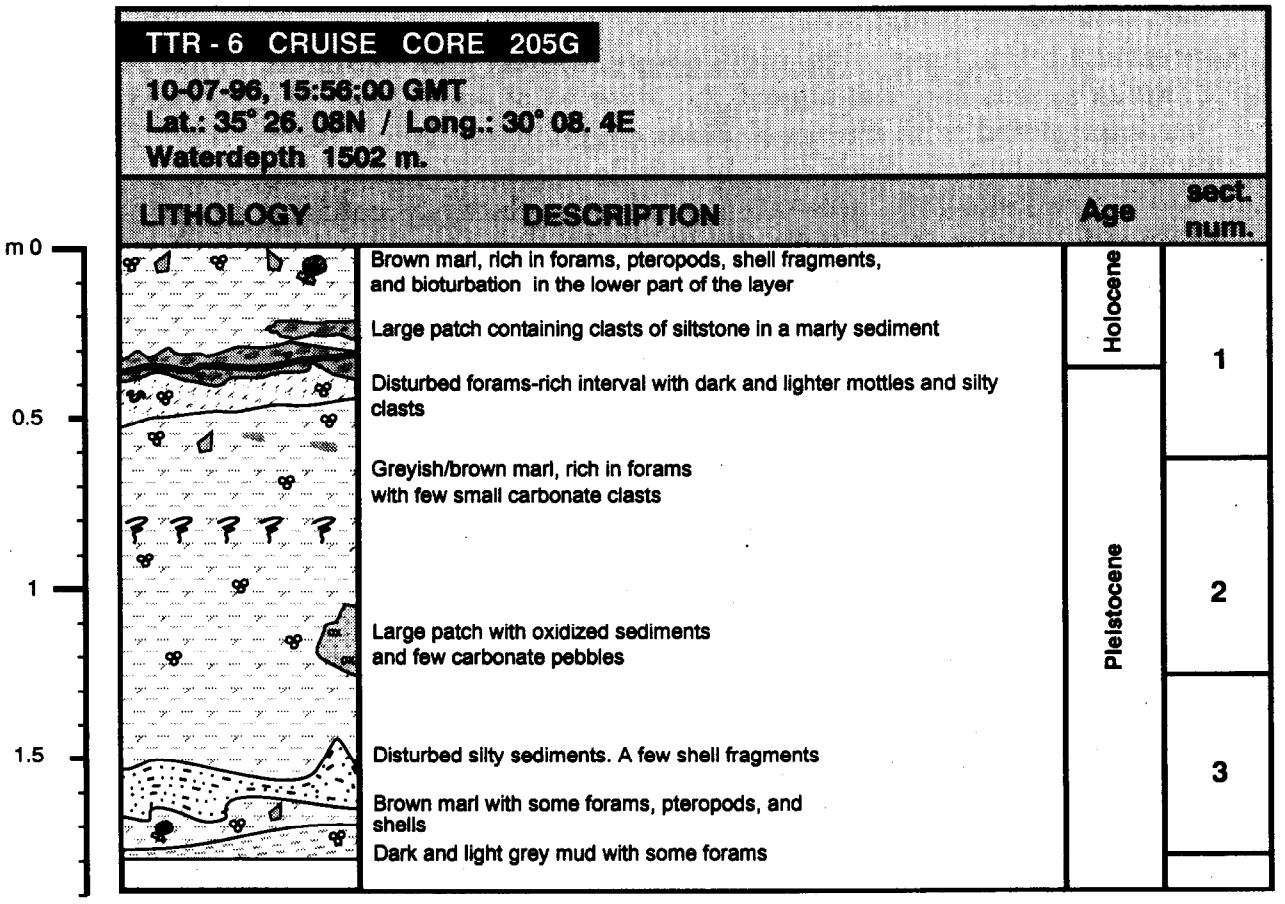

Fig. 27. Core log TTR-205G

Core TTR6-239G was taken in a suspected mud volcano which was later named the San-Remo mud volcano. The reddish-brown, poorly-sorted, matrix-supported mud breccia is overlain by a normal pelagic section containing the sapropels S1, S3, and tephra layers. The upper, rather thick, pelagic succession which started below sapropel S3 indicates that this part of the San-Remo mud volcano stopped activity about 80 kyrs ago (Fig. 32).

Core TTR6-213G was placed on a high reflectivity spot interpreted as a mud volcano and later called the Kula mud volcano. It contained, apart from a very thin layer of pelagic sediment at the top, a dark grey structureless matrix-supported mud breccia (Fig. 33). This core was of considerable importance for several reasons. The mud breccia from this core was not only intensively gas-saturated but it also contained the first gas hydrates to be recovered from the Mediterranean. The Kula mud volcano has therefore been recently active and continues as a site of intensive gas venting. Furthermore, besides various sedimentary rock fragments in the mud breccia, the core also contained samples of ophiolites and cherts which imply the continuation of the Antalya Nappes Complex south of mainland Turkey into the northeast part of the Anaximander Mountains.

Although core TTR6-240G was taken close to the newly discovered Kula

mud volcano, it contains only a normal pelagic section with sapropel S1, and an interval at the base with grey, soupy, bioturbated sediment (Fig. 34). Core TTR6-241G was taken at almost the same location. A layer of grey mud breccia was intercalated with a normal pelagic section just below sapropel S1. This is a record of a relatively distal mud breccia flow of Holocene age (Fig. 35).

Core TTR6-217G was taken in a high reflectivity patch on a depression in the northern part of the 'lobe structure'. The core contained a very thin pelagic layer overlying deposits similar in the appearance to mud breccia which contained gypsum among other clasts (Fig. 36). Core TTR6-219G was taken at almost the same site as TTR6-217G but contained a different lithology (Fig. 37). The pelagic top layer was distorted but at the base sandy and silty sediments containing a sandstone pebble were present. Such deposits might be the result of expulsion of rather thick, very water saturated, silty-sandy sediments. The site was chosen because it had been interpreted as the location of a 'wash-out' of post-Miocene sediments (into the Finike Basin to the north), leaving behind a window on the Miocene sediments below the 'lobe structure'. The core material is consistent with this because it appears to be a sort of lag deposit, and the presence of a gypsum fragment is suggestive of Messinian evaporites.

Core TTR6-218G was a long pelagic core taken on a peculiar high near the north side of the 'lobe structure'. In this three meter long core only sapropel S1 was present (Fig. 38), indicating an above average sedimentation rate for the study area. How the highest sedimentation rates observed in this cruise could be found on a hill is enigmatic, but it could be the result of mixing of pelagic sedimentation with sediment ejected from the top of the hill as a result of overpressuring of sediments below the lobes.

The longest recovery of the cruise was in core TTR6-224G taken on a hill in northernmost part of Anaximander Mountain. It consists of about five meters of mostly marly pelagic sediment, with sapropels S1, S3, and S4, and interbedded tephra layers (Fig. 39). Unusually thicker marker lithologies such as the sapropelic layers imply higher sedimentation rates which are not yet understood. Unfortunately, no core was taken in this region to obtain reference sedimentation rates for comparison. The higher productivity expected around the Rhodes Basin where upwelling of deep water occurs could contribute to the higher rates.

The cores taken on this transect show very complex environments and numerous agencies for sedimentation occurring. Numerous types of recent deposits observed along the profile reflect the complex structure of the region and its high neotectonic activity. The eastern part of the studied area is characterized by mud volcanism manifestations whereas the western part, by an at least local abnormally high sedimentation rate. It must be kept in mind that coring locations were chosen on the basis of their special characteristics rather than on their normalcy. In any case, the coring results illustrate several different sedimentation agencies occurring in different parts of the region of study, and their dependence on different kinds of tectonic activity.

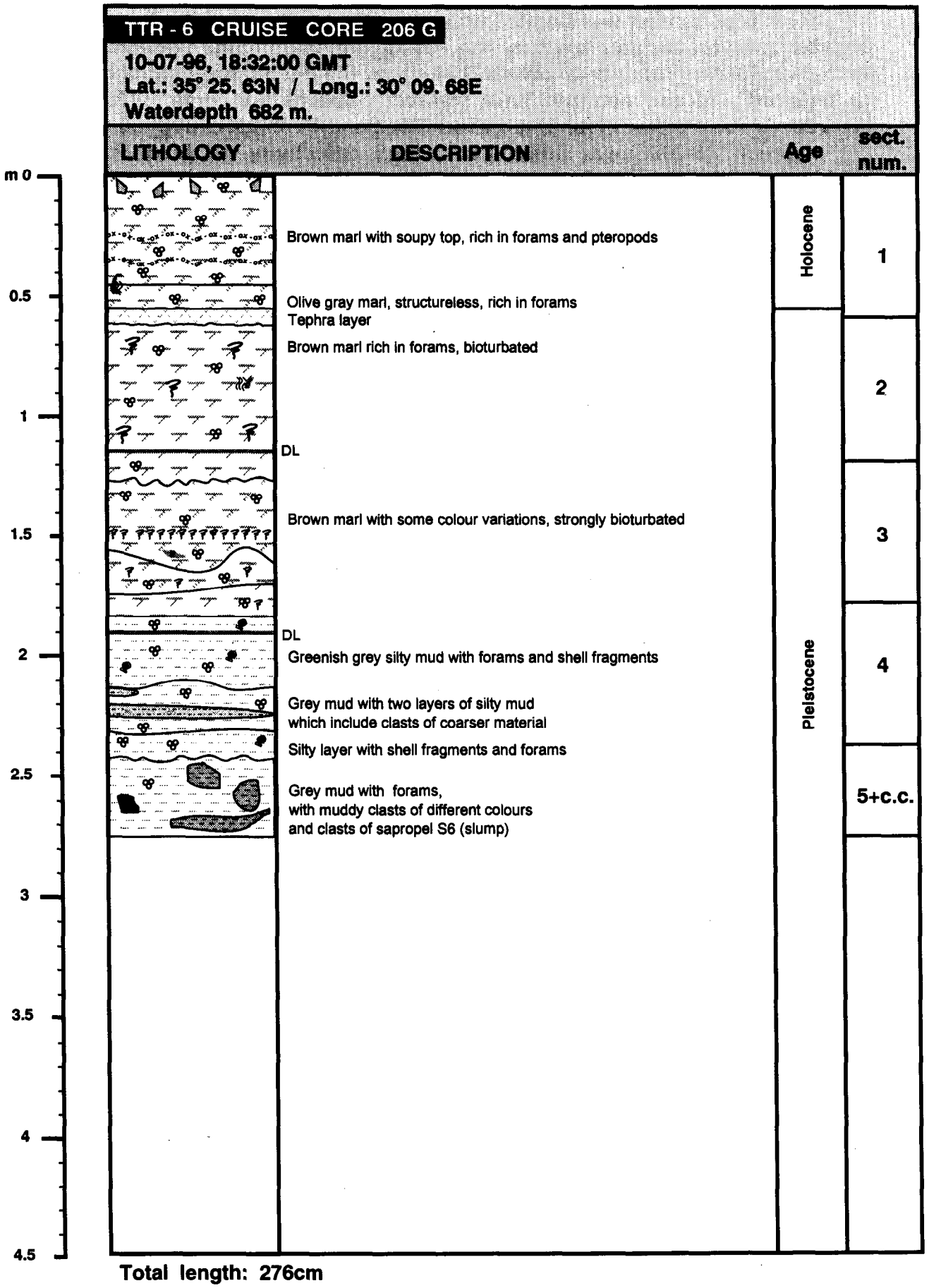

Fig. 28 . Core log TTR-206G

Transect C (along a line of mud volcanoes)

This core transect was situated roughly in the southeast of the studied area (Fig. 22). It covers an area south of the Anaxagoras Mountain. The aim of the coring was likewise mainly to obtain clasts from the deeper-lying strata brought up by mud volcano activity. This transect contains six cores: TTR6-207G, TTR6-208G, TTR6-233G, TTR6-234G, TTR6-235G, and TTR6-236G (Fig. 40).

Core TTR6-207G was situated in a high reflectivity patch south of the Anaximenes Mountain, inferred to be a mud volcano which was later named the Amsterdam mud volcano. The core contained mud breccia overlain by a thin layer of pelagic sediment (Fig. 41). The upper part of the mud breccia was oxidized. The mud breccia contained clasts of up to 9 cm long and a lot of shell fragments. Living bivalves were found in the uppermost brown part of mud breccia flow (see Section I.8.f). Core TTR6-208G was taken in an old mud flow to the southeast of the mud volcano, a few kilometres from TTR6-207G. The lithology was the same as found in core TTR6-207G, only with smaller clasts (up to 5 cm long) (Fig. 42).

Core TTR6-233G was taken near a high reflectivity spot determined to be a edge of flow from the Amsterdam mud volcano. It contained, apart from a very thin layer of pelagic sediment on the top, a greenish grey structureless, very poorly sorted mud breccia. This mud breccia was saturated with H_2S gas and contained rock fragments up to 6 cm in size, and shell fragments. The upper 10 cm of the mud breccia recovered was oxidized, olive brown in colour. An interval of carbonate crusts was also found in the upper part of the breccia (Fig. 43).

Core TTR6-234G was situated in a high reflectivity patch southeast of the Anaxagoras Mountain which was identified as a mud volcano which was named the Kazan mud volcano. Apart from a very thin layer of soupy pelagic sediments, it contained grey mud breccia. Fragments of soft sediments and hard rocks of up to 7 cm in size and numerous shell fragments were observed and collected. No upper oxidized part was found in the mud breccia flow here (Fig. 43).

TTR6-235G cored another high reflectivity patch southeast of the Anaxagoras Mountain. It was also interpreted as a mud volcano and later named the Tuzlukush mud volcano. The top 160 cm consist of a pelagic section containing sapropel S1 and tephra layers. The rest of the section consists of a dark grey mud breccia with an upper oxidized interval (Fig. 44).

Core TTR6-236G to the southeast of the Anaxagoras Mountain sampled a patch of high acoustic reflectivity caused by mud volcanic breccia from a mud volcano later named the Saint Ouen l'Aumone mud volcano. The top 225 cm consist of a pelagic section containing sapropel S1 and tephra layers. The lower section consists mostly of dark grey mud breccia with clasts of up to 4 cm in size and shell fragments. An upper oxidized interval was also observed (Fig. 45).

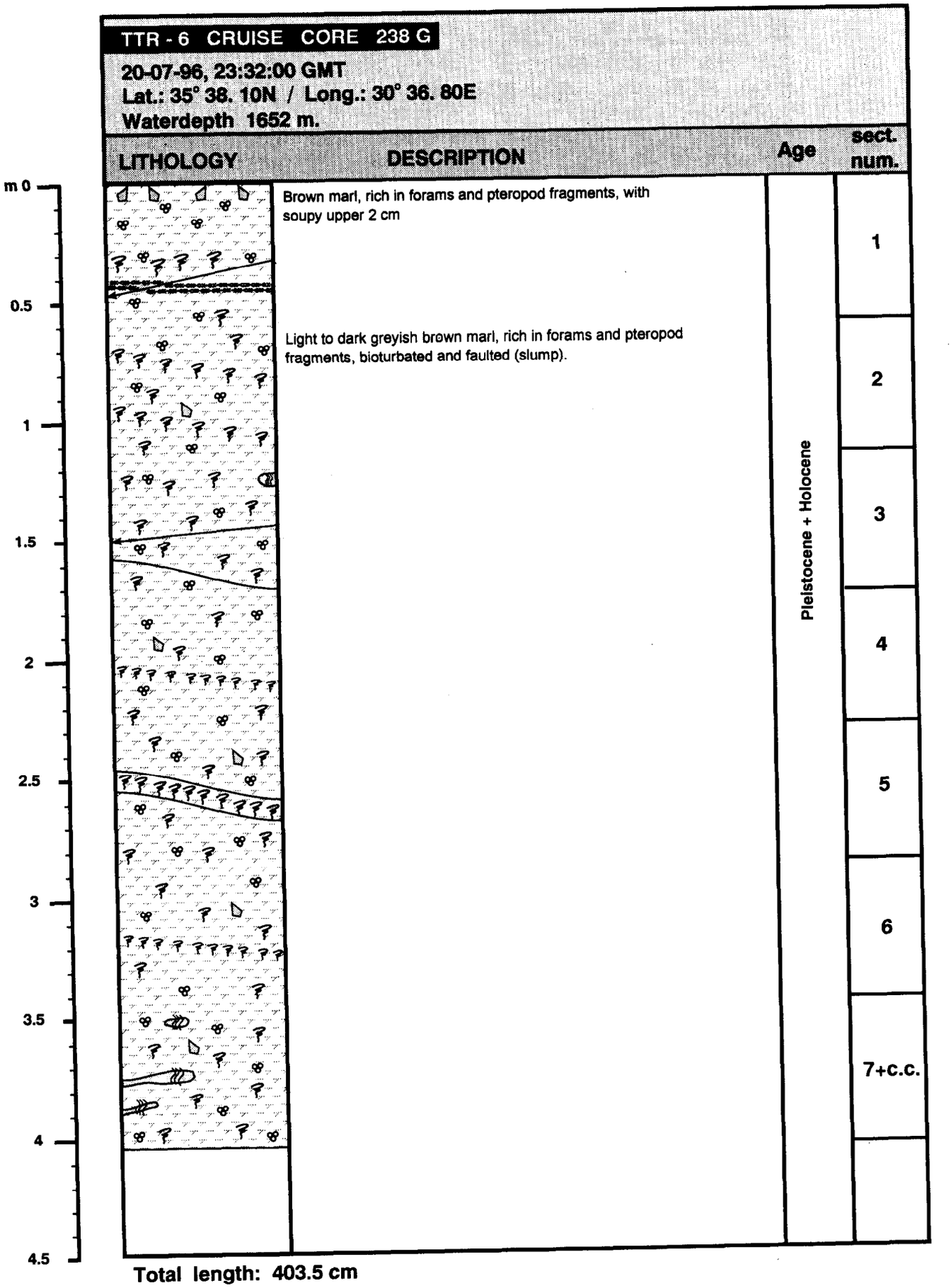

Fig. 29. Core log TTR-238G

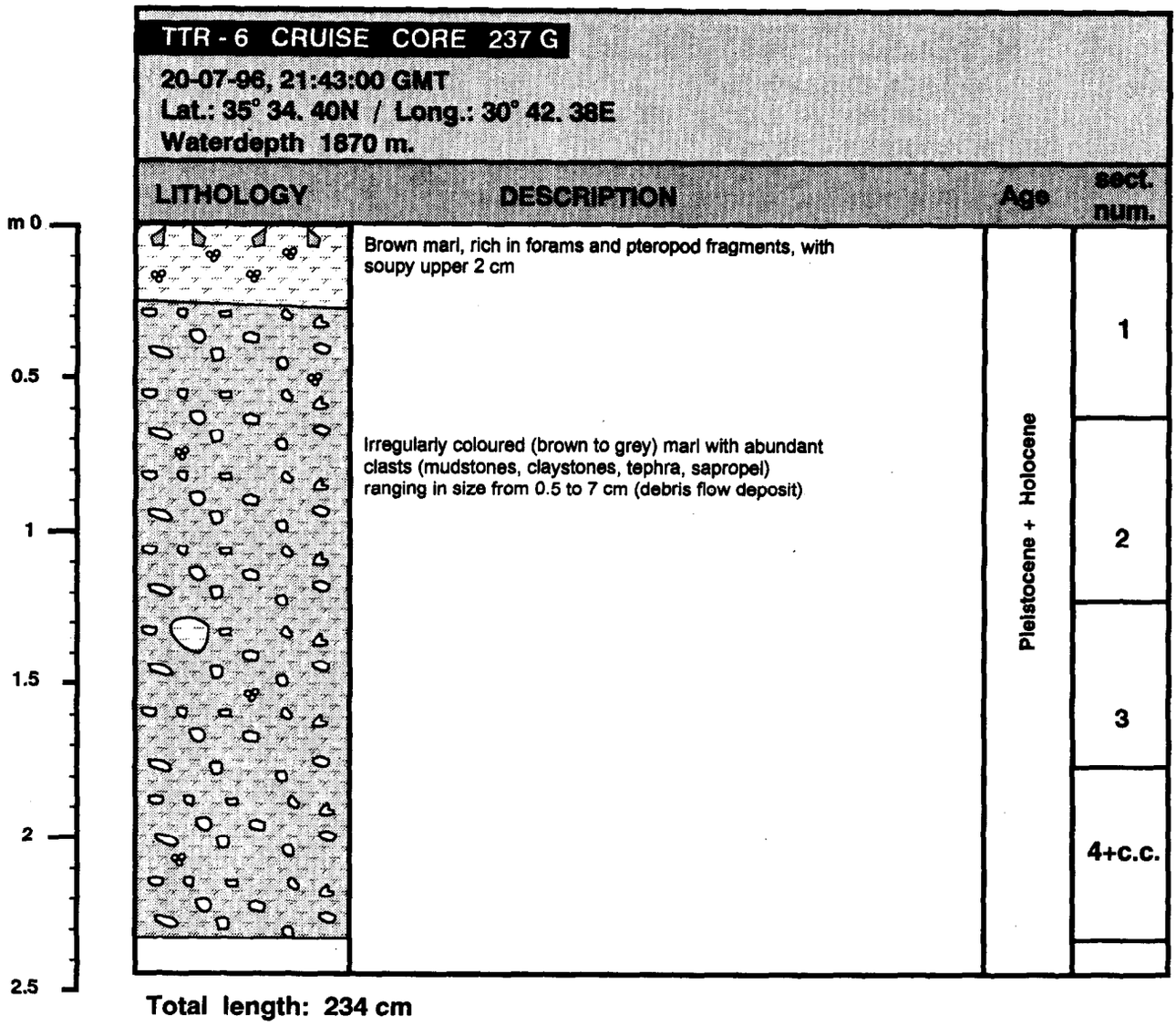

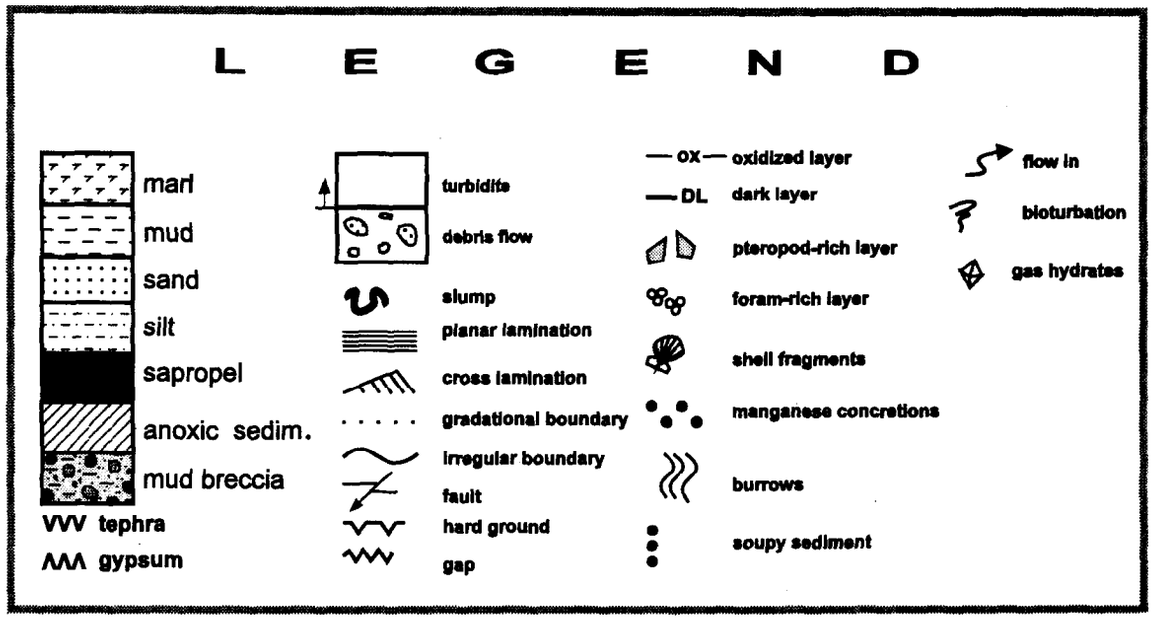

Fig. 30 . Core log TTR-237G

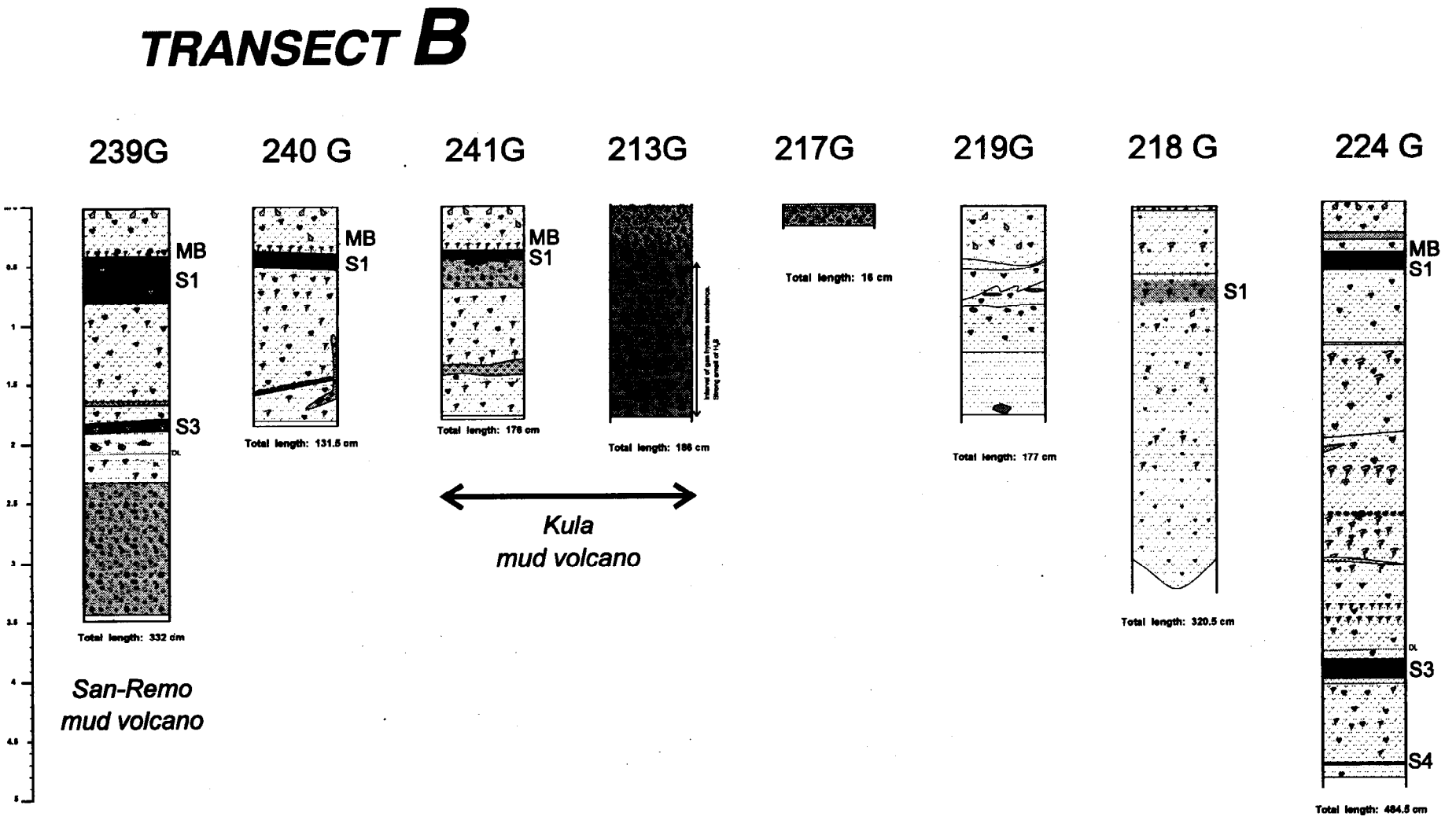

Fig. 31. Generalized core logs arranged along Transect B

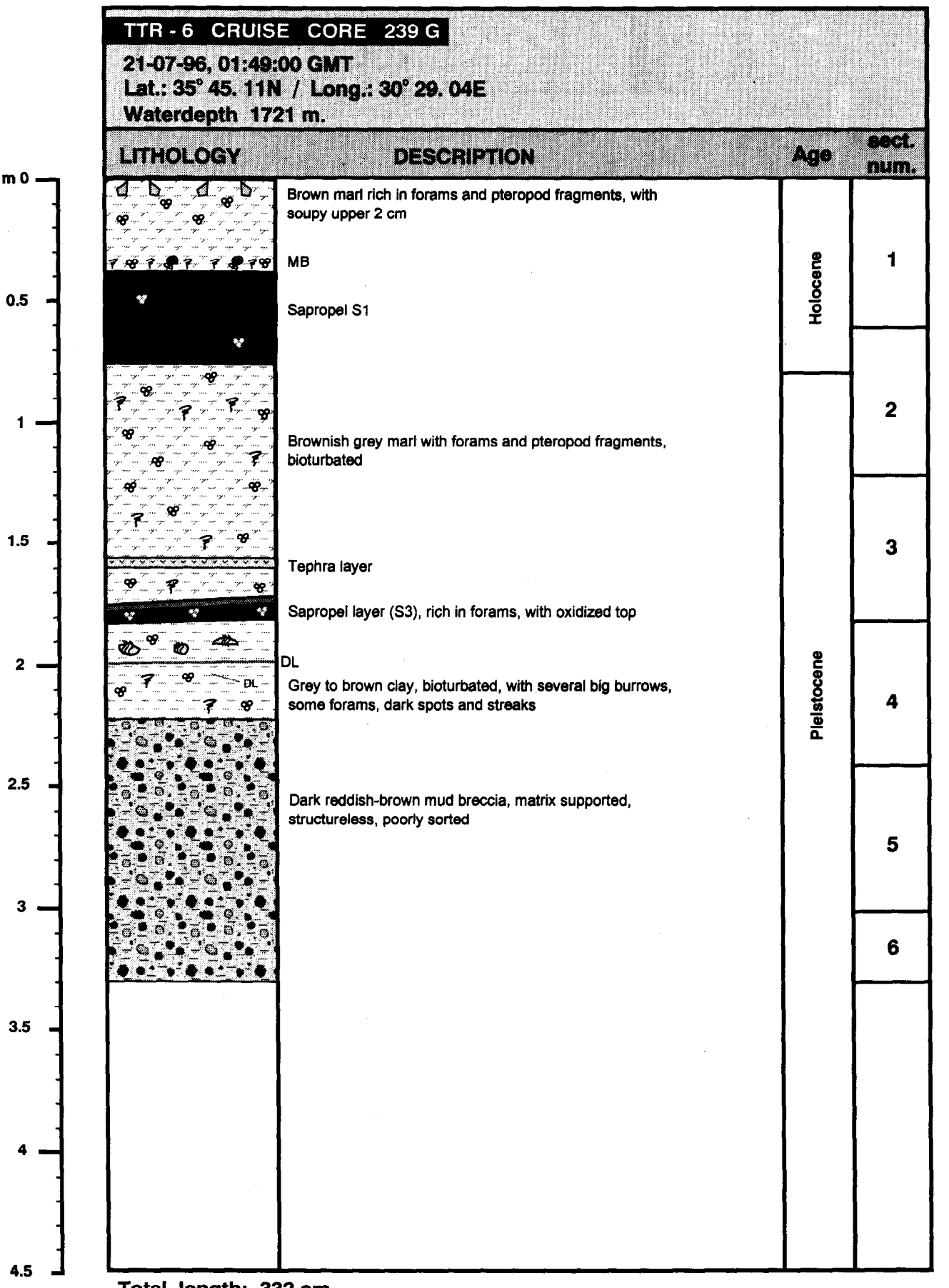

Fig. 32. Core log TTR6-239G

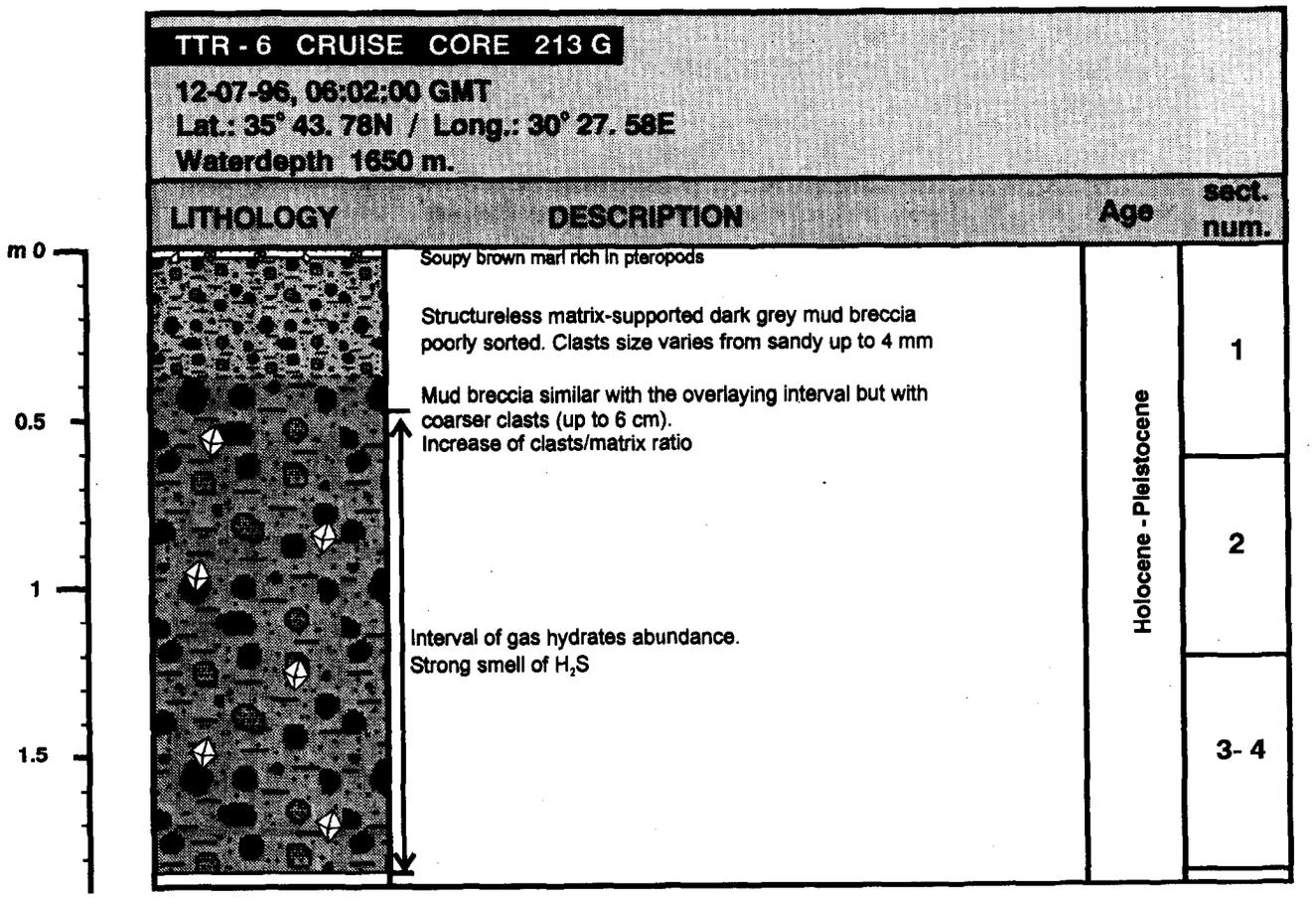

Fig. 33. Core log TTR6-213G

The cores taken on this transect show large mud volcanic activity in this area. The presence of pelagic sediments overlying mud breccia flows in all of the cores suggests a relatively short recent period of quiescence. Only thin Holocene sediments overlie the mud flows from the Amsterdam and the Kazan mud volcanoes in the cores obtained. Gas saturated deposits and carbonate crusts are evidence for recent intensive gas venting related to the mud volcano activities. Shells and shell fragments represent probably special benthic communities in gas vent areas. We might assume the longest period of quiescence (more than 40 kyrs) of activity for the Tuzlukush (Core TTR6-235G) and the Saint Ouen L'Aumone (Core TTR6-236G) mud volcanoes, where the pelagic sediments overlying the mud breccia were 1.6 m and 2.2 m thick respectively. However, this could be explained also if the corer missed recently active eruptive centres of these mud volcanoes.

Leg 1 cores can be divided into three principal groups according to their characteristic structural and lithologic peculiarities, for purposes of generalization and discussion of the main sampling results. These groups are pelagic sediments, slope deposits, and mud breccias.

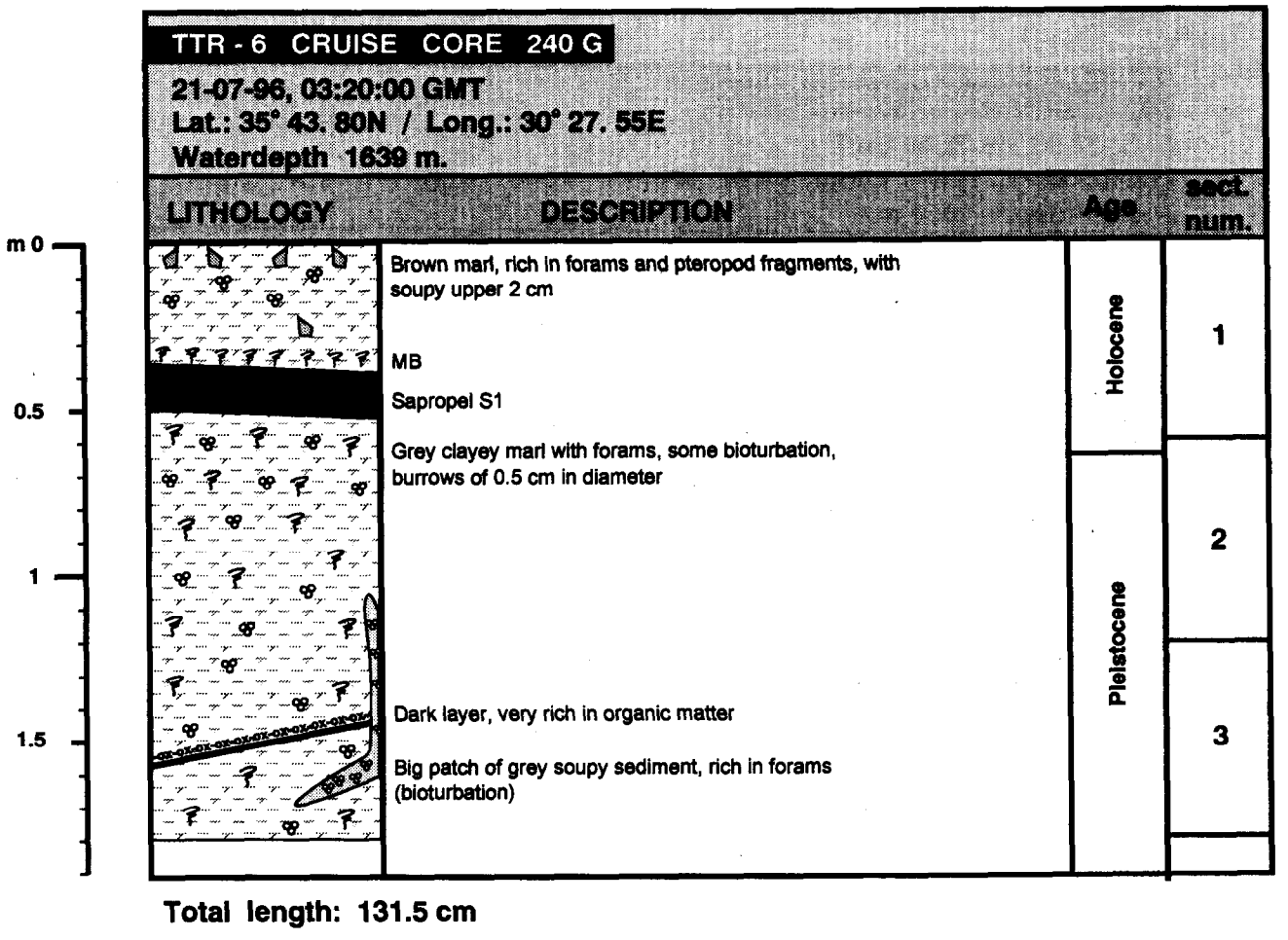

Fig. 34. Core log TTR6-240G

Discussion

Pelagic sediments

Pelagic sequences of Middle Pleistocene to Holocene age were recovered from ten coring stations. Figure 46 shows the correlation of pelagic cores based on the marker lithologies and calcareous nannofossil biostratigraphy.

The only classical Eastern Mediterranean pelagic succession was recorded in the first station of the cruise (TTR6-197G), the in southern part of the study area on a very flat part of the Mediterranean Ridge. The aim of this core was to get a reference background core. Other cores discussed here which are characterized by only slightly disturbed pelagic sections may also be considered as pelagic.

All pelagic cores observed consisted mainly of:

- marls, varying in colour, brown to grey, often with bioturbation structures but otherwise structureless, often rich in forams and pteropod remains, sometimes with a clayey or fine terrigenous admixture;
- clay (seen more often in the lower part of the sequences), grey in colour, structureless, very stiff, and sometimes with a terrigenous silty-sized admixture.

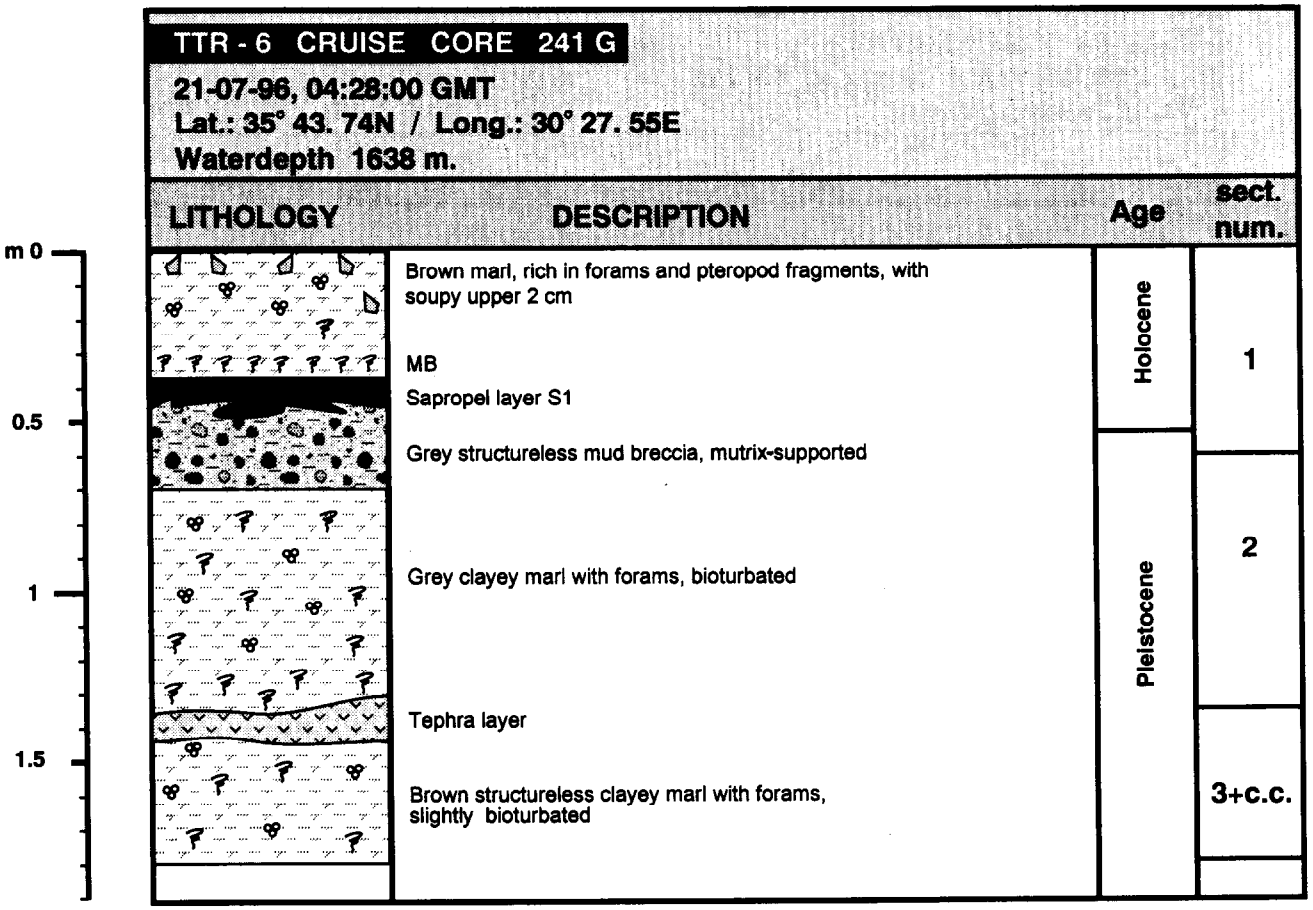

Fig. 35. Core log TTR6-241G

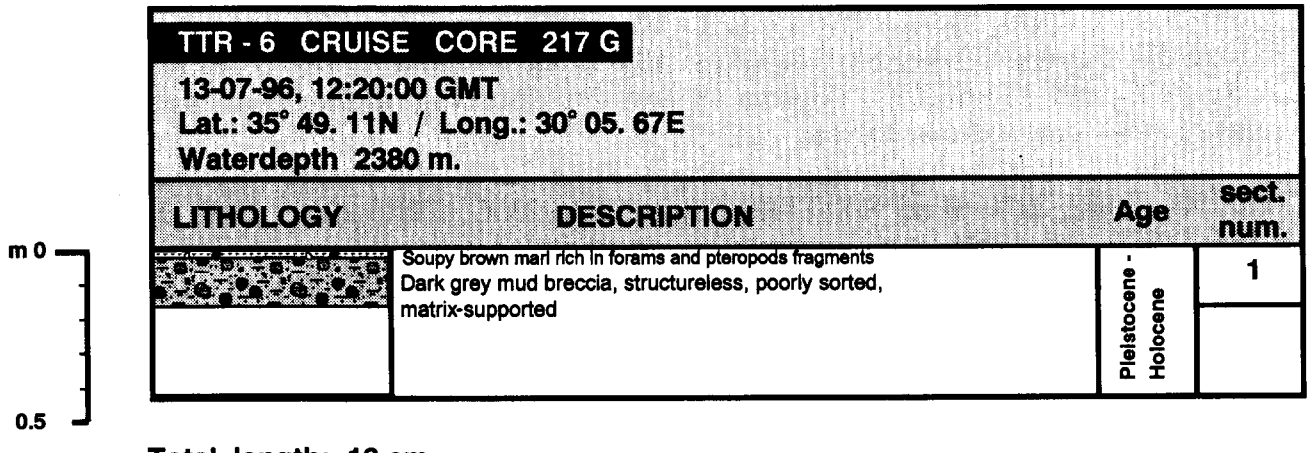

Fig. 36. Core log TTR6-217G

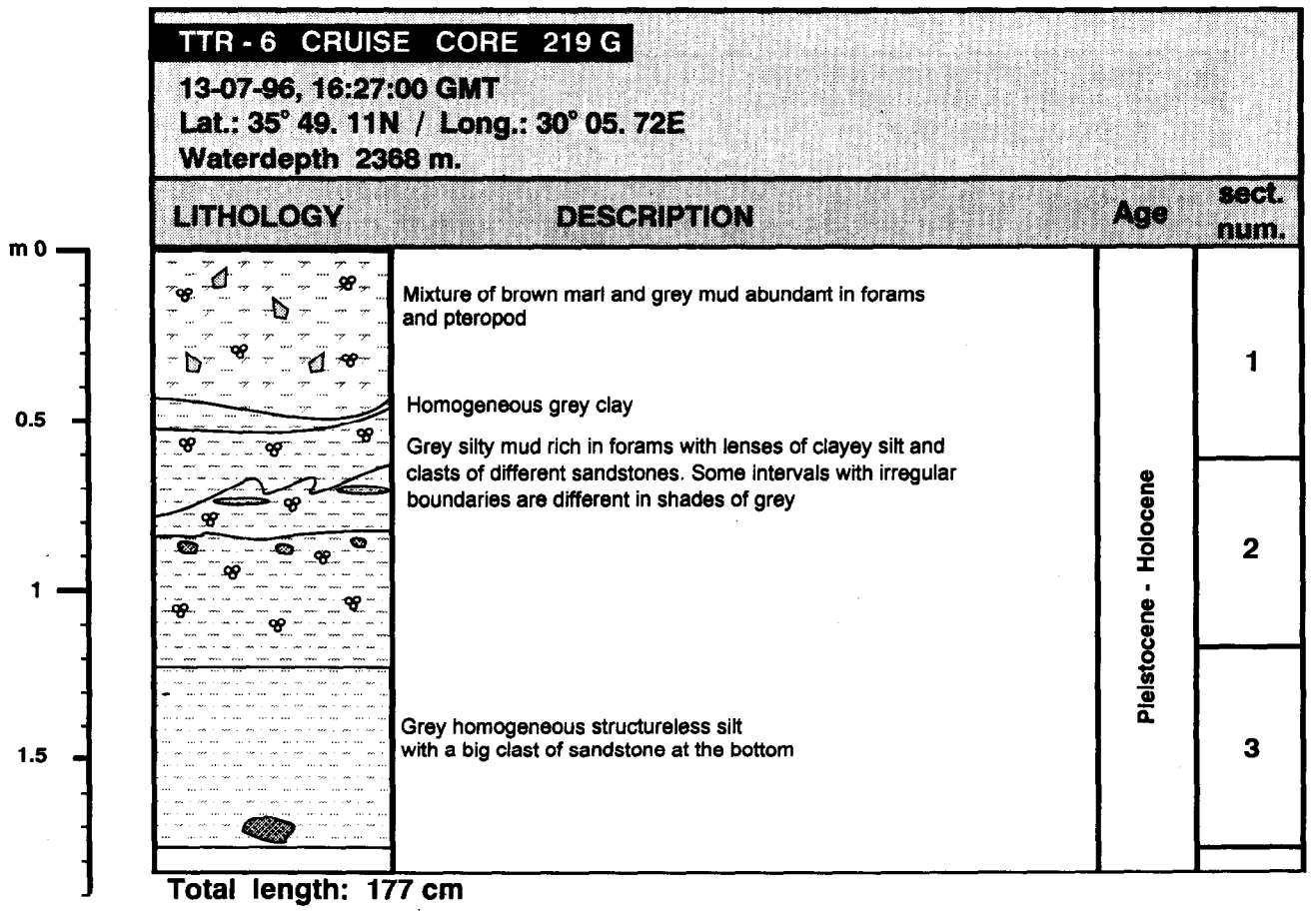

Fig. 37. Core log TTR6-219G

In addition, various sapropel (S1 and S3 to S7), tephra layers, and sometimes the Marker Bed (a peculiar layer consisting of Mn micronodules and dated as 3.5 kyrs; *De Capitani and Cita, 1996*) were observed in most of the pelagic cores. The average sedimentation rates calculated for the pelagic cores ranged between 1.7 and 2.7 cm/kyrs, but some cores notable for their higher rates were TTR6-218G (12 cm/kyrs), TTR6-224G (5 cm/kyrs), and TTR6-228G (4 cm/kyrs; Figure 47). Sapropel layer S1 was unusually thick in most of the cores (except TTR6-197G and TTR6-225G; Figures 48 and 49), implying higher than average rates of Holocene sedimentation.

The Marker Bed is present in cores TTR6-224G, TTR6-225G, TTR6-226G (Fig. 50), TTR6-227G (Fig. 51), TTR6-228G, TTR6-235G, TTR6-236G, TTR6-239G, TTR6-240G, and TTR6-241G where it is diluted to a variable extent by pelagic marls. Sapropel S3 is oxidized partially in core TTR6-227G and entirely in cores TTR6-197G and TTR6-226G.

The pelagic cores considered were obtained from different flat locations of the study area (TTR6-197G, TTR6-225G, TTR6-228G, TTR6-230G, and TTR6-240G), some isolated hills or topographic highs (TTR6-218G and TTR6-224G), a depression (TTR6-229G), and at the bottom of an escarpment (TTR6-226G and TTR6-227G).

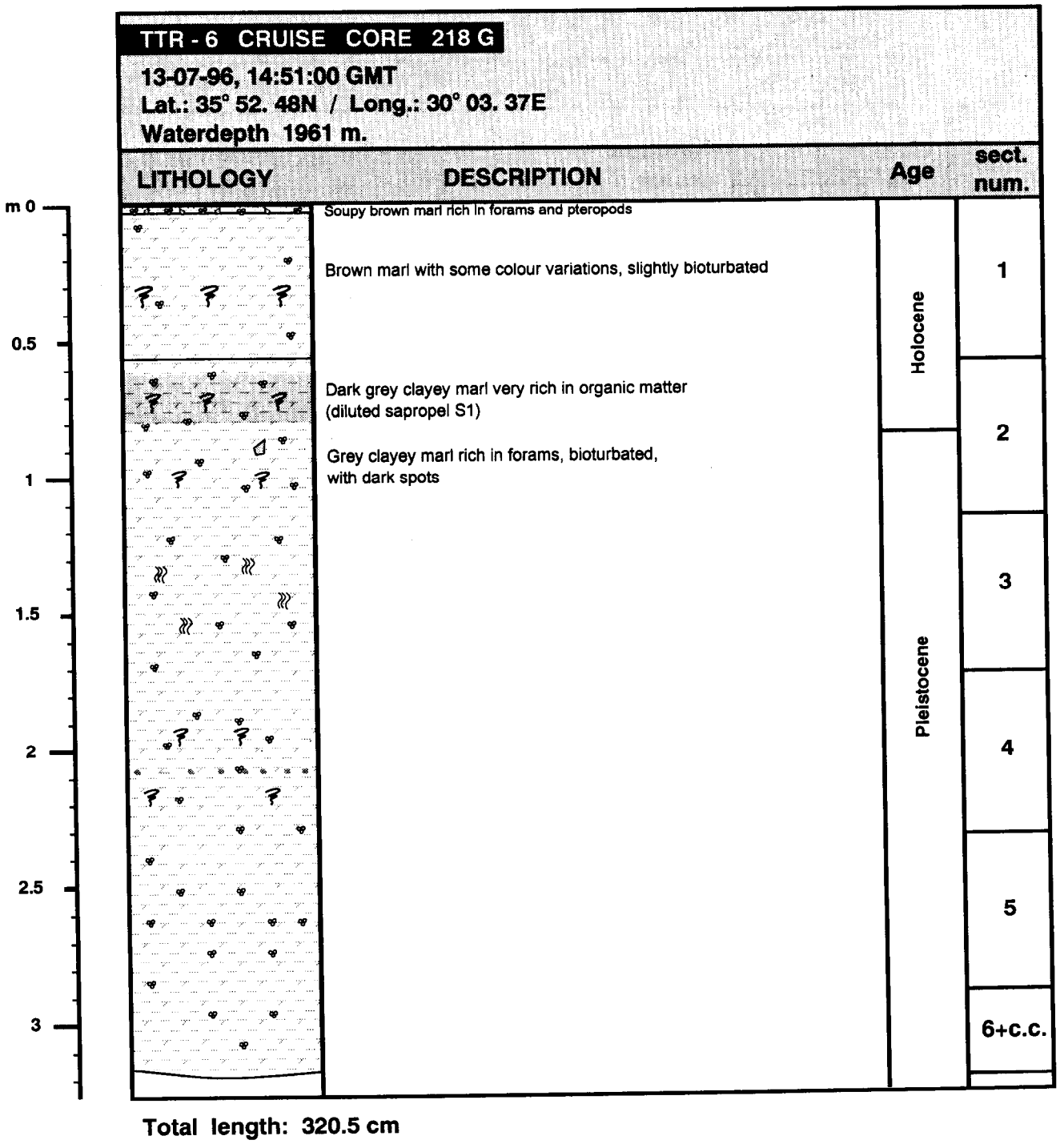

Fig. 38. Core log TTR6-218G

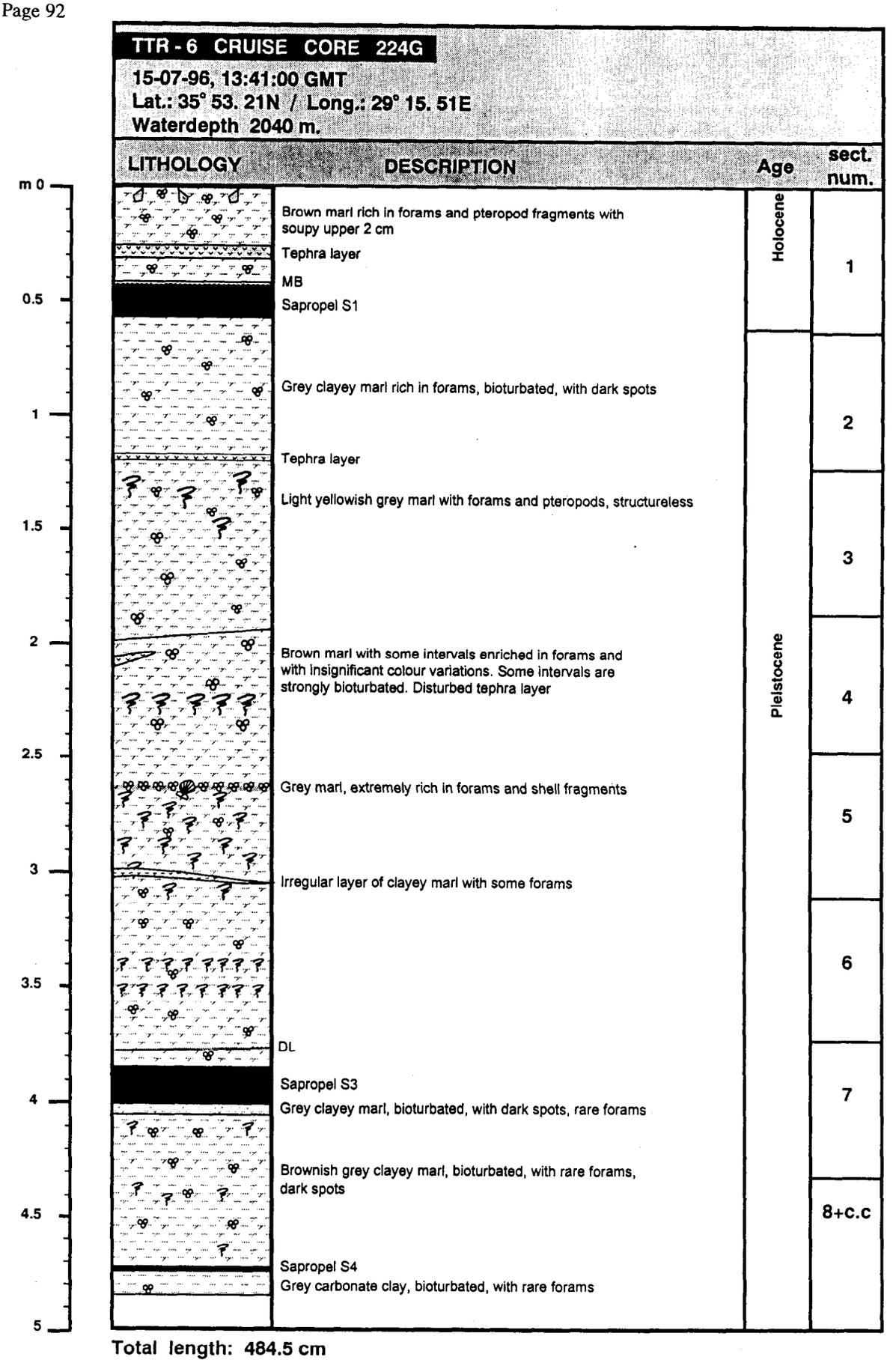

Fig. 39. Core log TTR6-224G

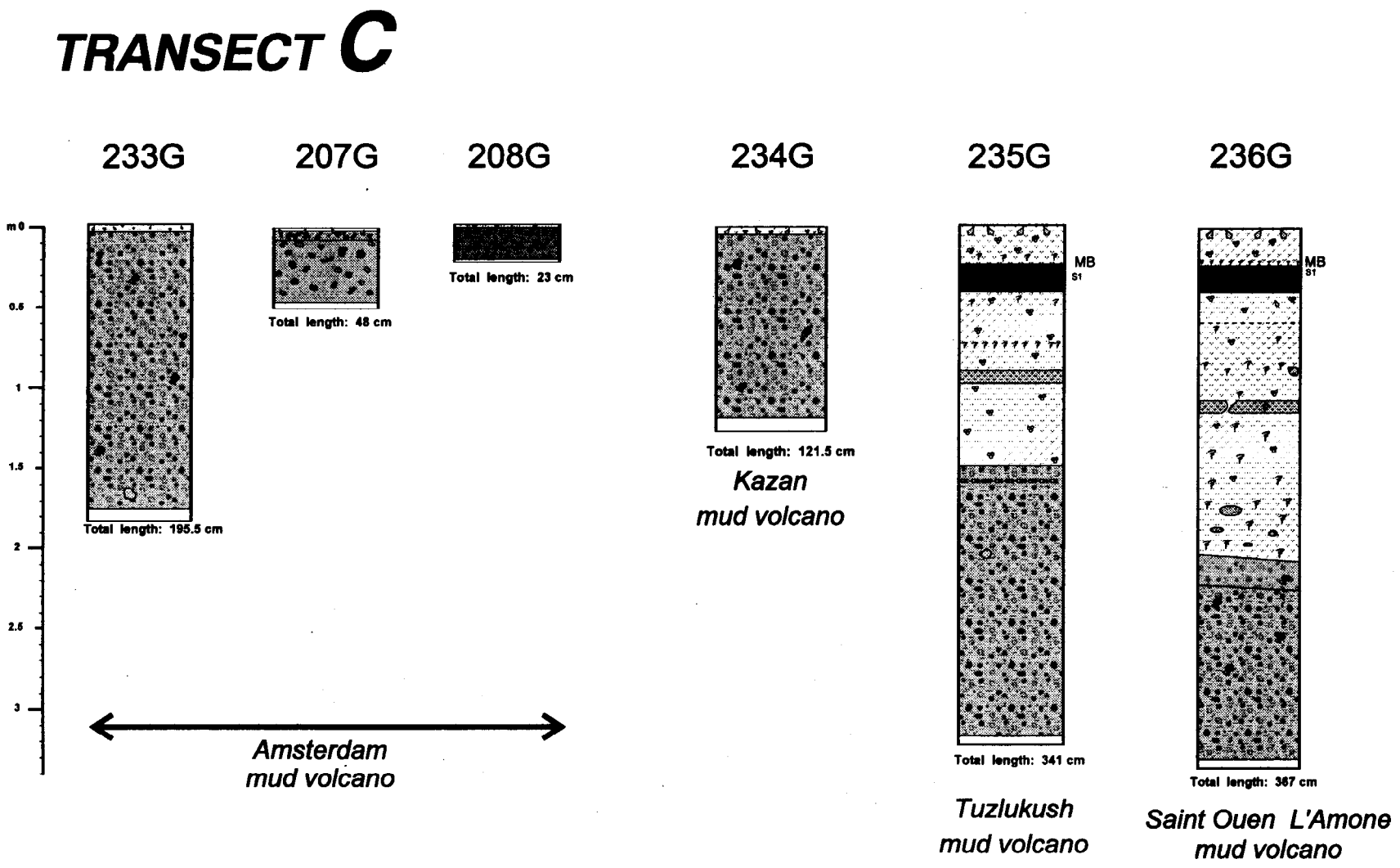

Fig. 40. Generalized core logs arranged along Transect C

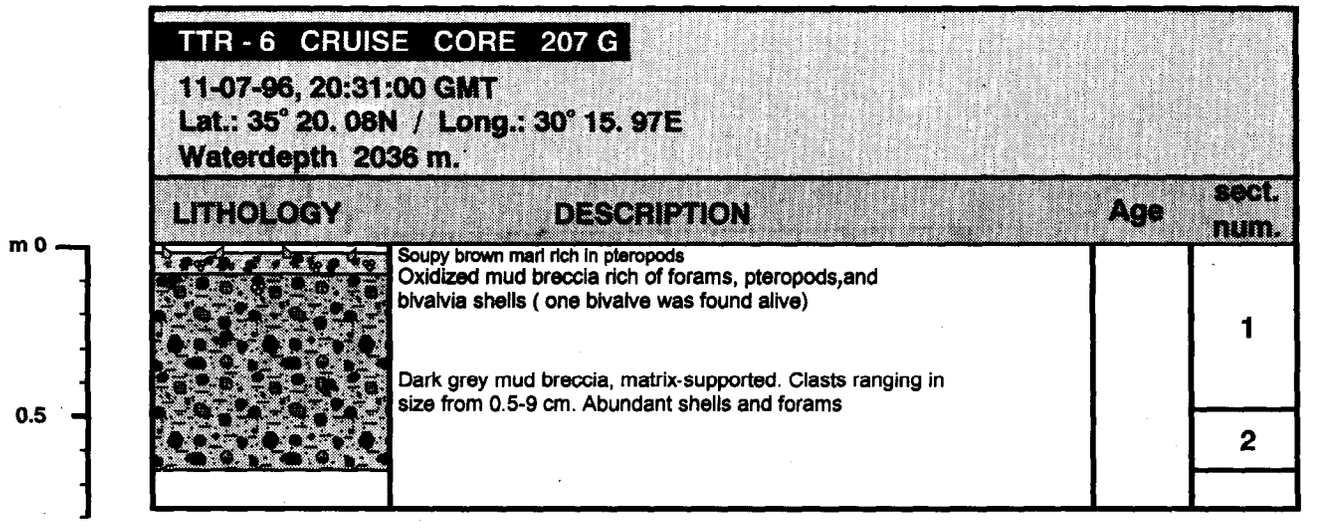

Fig. 41. Core log TTR6-207G

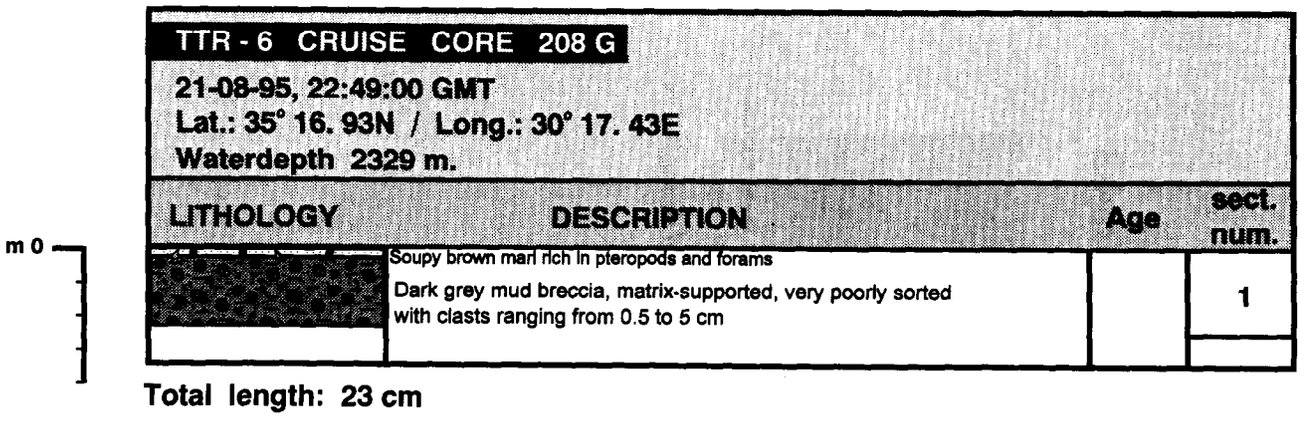

Fig. 42. Core log TTR6-208G

Some unusual features of sedimentation were recorded in several cores with mostly pelagic deposits. Although cores TTR6-218G and TTR6-224G were taken on the top of a topographic highs, they show sequences with unusually large thicknesses of sediments marking a very high accumulation rates (12 and 5 cm/kyrs respectively). Core TTR6-228G (Fig. 47) from a flat zone in the southwestern part of the lobe consists of pelagic marl interbedded with tephra layers, the Marker Bed, and sapropels S1, S3, S5, and S6. The normal pelagic succession is disturbed at least in the lower part of this core because micropaleontological analyses indicate that sapropel S5 was situated in the sequence below S6. Probably, this can be the result of slope processes. A similar situation was observed in Core TTR6-226G (Fig. 50). This core taken at the bottom of the southwestern escarpment of the Anaximander Mountain contains an abnormal alternation of sapropel S6 and S7 in addition to an upper 2.5 m long pelagic succession of marl, tephra layer, the Marker Bed, and the S1 and S3 sapropelic layers. The explanation, probably, can also be slope processes.

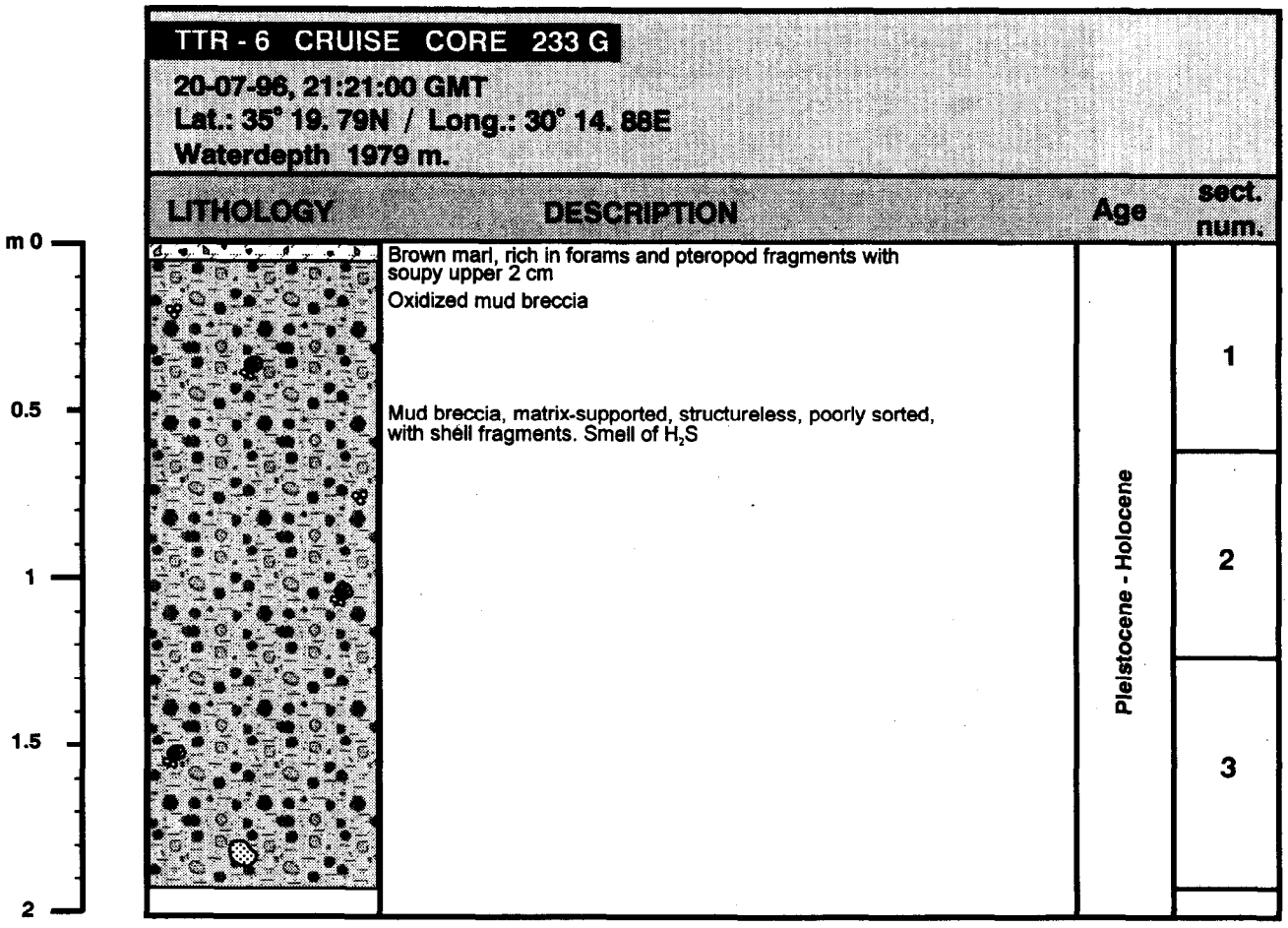

Total length: 195.5 cm

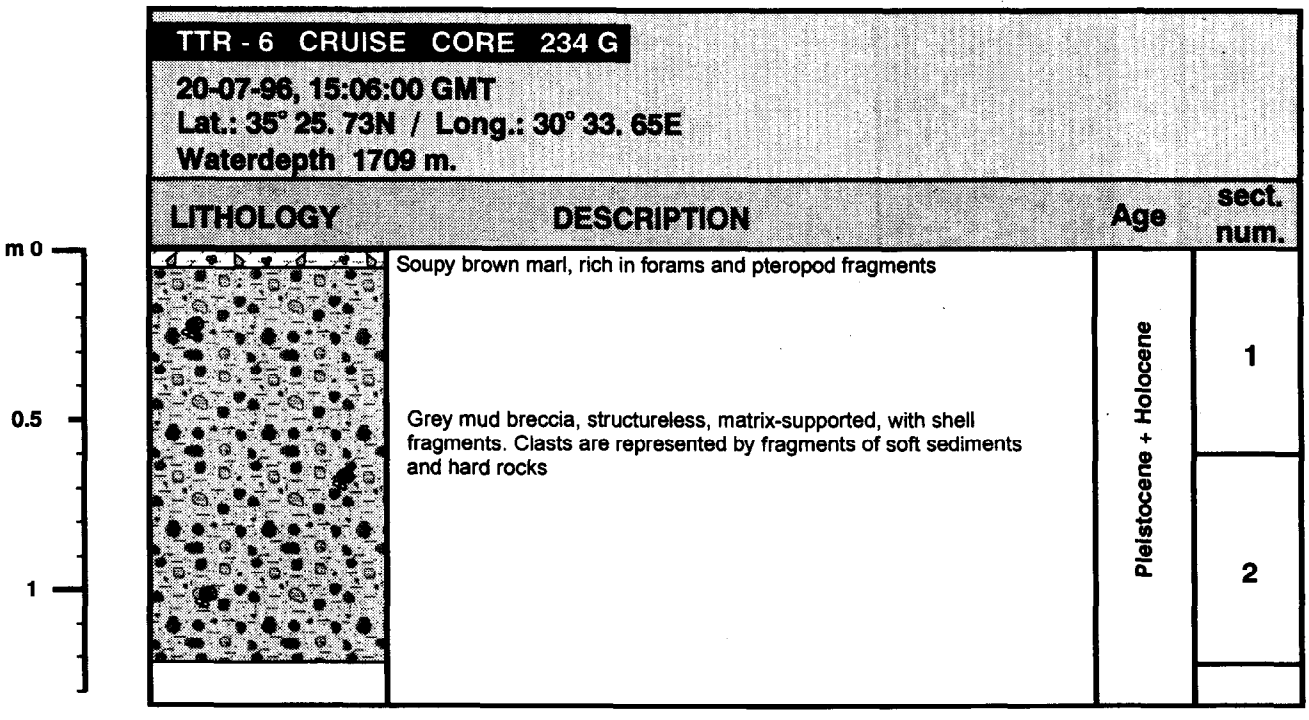

Total length: 121.5 cm

Fig. 43. Core logs TTR6-233G and TTR6-234G

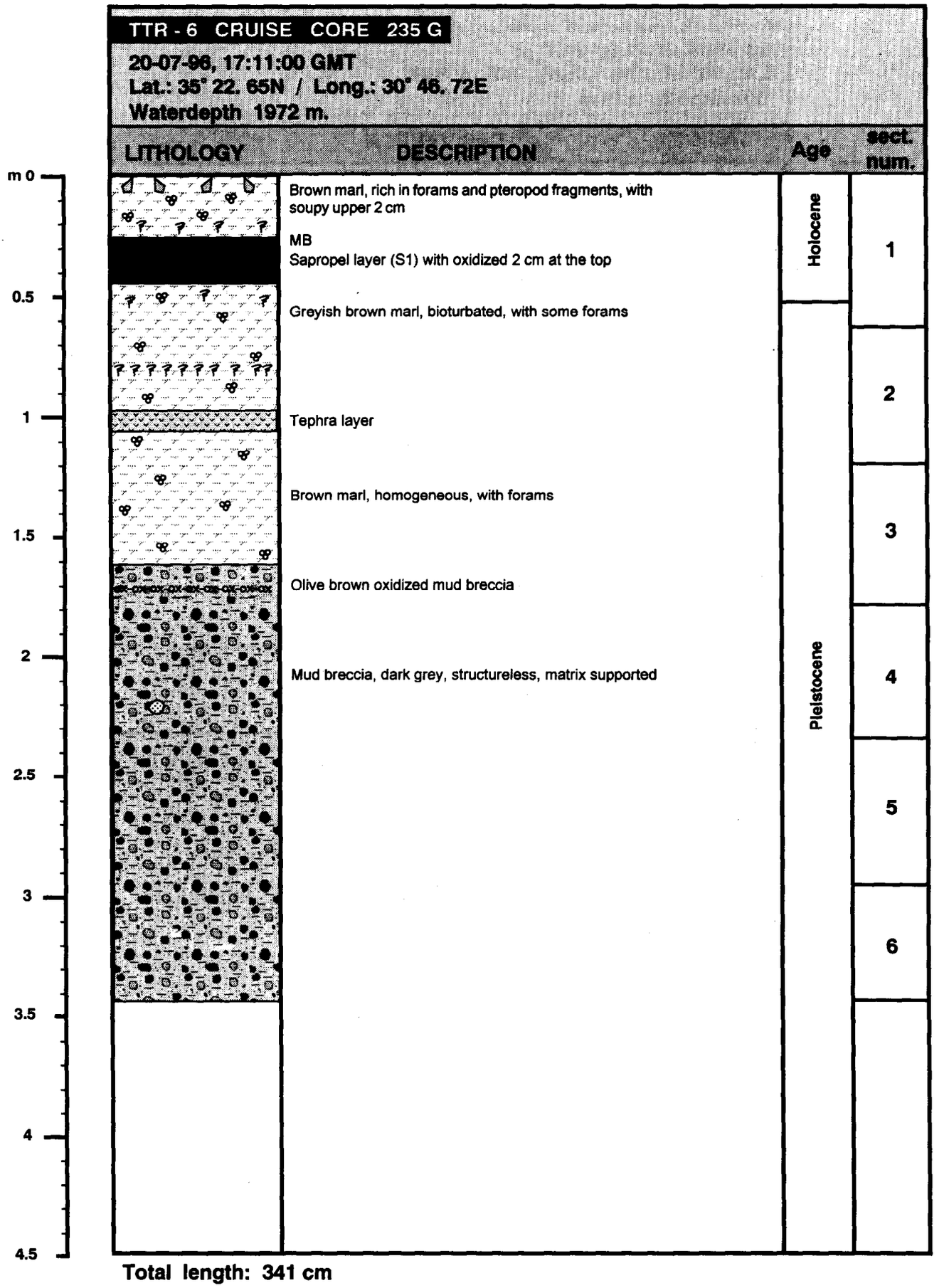

Fig. 44. Core log TTR6-235G

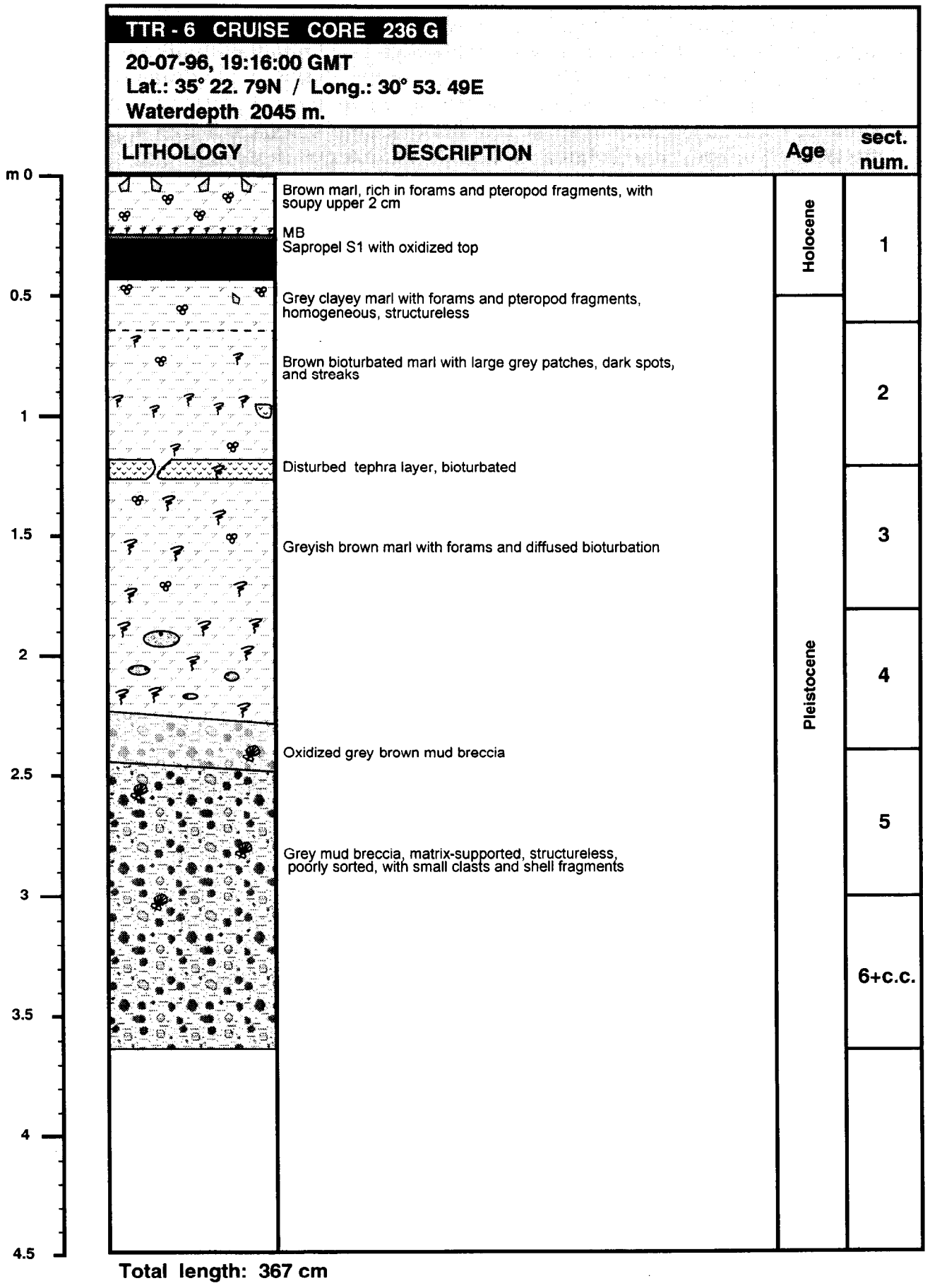

Fig. 45. Core log TTR6-236G

Slope sediments

Six of the cores recovered are reviewed in this section (Fig. 52). Most of these cores, which are situated on slopes in the Anaximander Mountains, show typical slumping structures. Different types of slope deposits were observed.

Core TTR6-200G (Fig. 53) from the southern slope of the Anaximander Mountain contained a 0.8 m thick interval of slump breccia, a matrix-supported mixture of more consolidated carbonate sediments in brown marl. These deposits usually characterize the relatively steep slopes and suggest high slumping activity. Core TTR6-231G (Fig. 26) taken on the floor of a large depression south of the Anaximander Mountain also had a interval of slope deposits represented by grey structureless clay, rich in forams, with irregularly distributed fragments of more consistent clayey sediments, foraminiferal ooze fragments, and sapropel fragments.

Core TTR6-237G (Fig. 30) contained a brown pelagic marl interval overlying a thick debrite interval at the base of a fault scarp on the east edge of Anaxagoras Mountain. Very irregularly coloured, greyish brown to olive grey debris flow deposits contained a lot of clasts ranging in size from 0.5 to 7 cm. Fragments of claystone, mudstone, marlstone and sapropel were prevalent among the clasts. Usually debrites characterize active slopes.

The entire cores TTR6-205G (Fig. 27), TTR6-238G (Fig. 29) and the lower part of the TTR6-206G succession (Fig. 28) demonstrated a variety of slump structures in sediments. Irregular inclined boundaries, microfaults, irregular thicknesses of layers, and mixtures of different types of sediment were observed, demonstrating the high activity of slope processes.

These six cores characterize different parts of the studied area and demonstrate a large variety of slope deposits: numerous slumps, slope breccias, and debrites. In addition, it needs to be mentioned that most of the pelagic cores discussed above also have slumped intervals. In part this reflects the bias in sampling areas of higher acoustic backscatter or likely to have rock fragments from the mountains; however, it also reflects various slope processes typical of the Anaximander Mountains Area, and is probably the result of active neotectonics.

Mud breccia

The eleven cores containing mud breccia provided some of the most interesting results of the cruise, and have confirmed the discovery of a previously unknown mud volcanic area in the Eastern Mediterranean (Fig. 54). The clasts from mud breccias provide important information about the composition of the deep-seated deposits and the origin of the Anaximander Mountains (Table 2).

Mud breccia from the Amsterdam mud volcano. All cores obtained from the Amsterdam mud volcano (TTR6-207G, TTR6-208G, and TTR6-233G) contained mud breccia of a similar lithology. It was a grey, structureless, very poorly sorted, matrix-supported mixture of sandy silty clay with clasts of up to 9 cm in size. The oxidized part of the mud breccia flows was noted in all these cores. Its thickness varies from 4 to 15 cm. The observation that the mud breccia

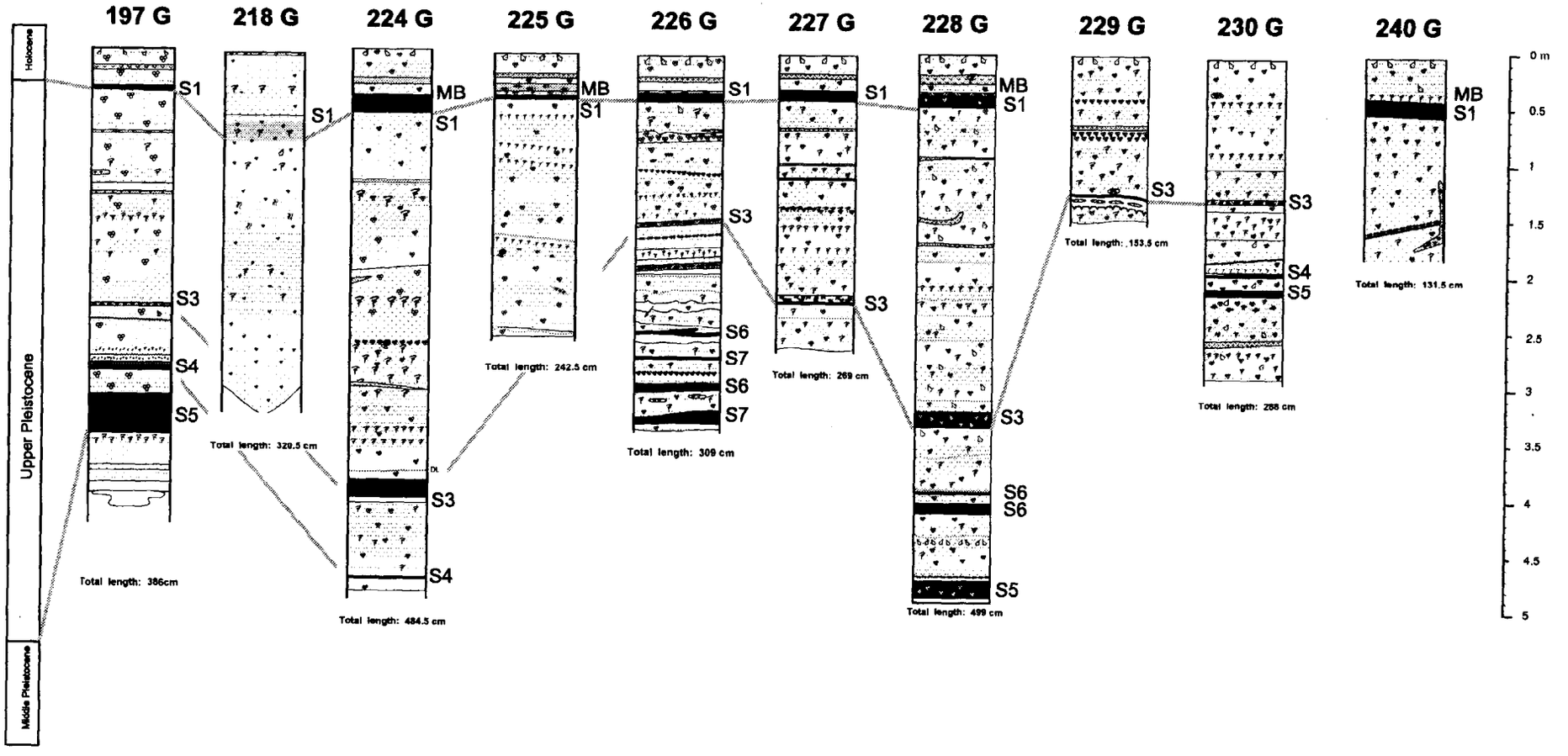

Fig. 46. Correlation of pelagic cores from the Anaximander Mountains area

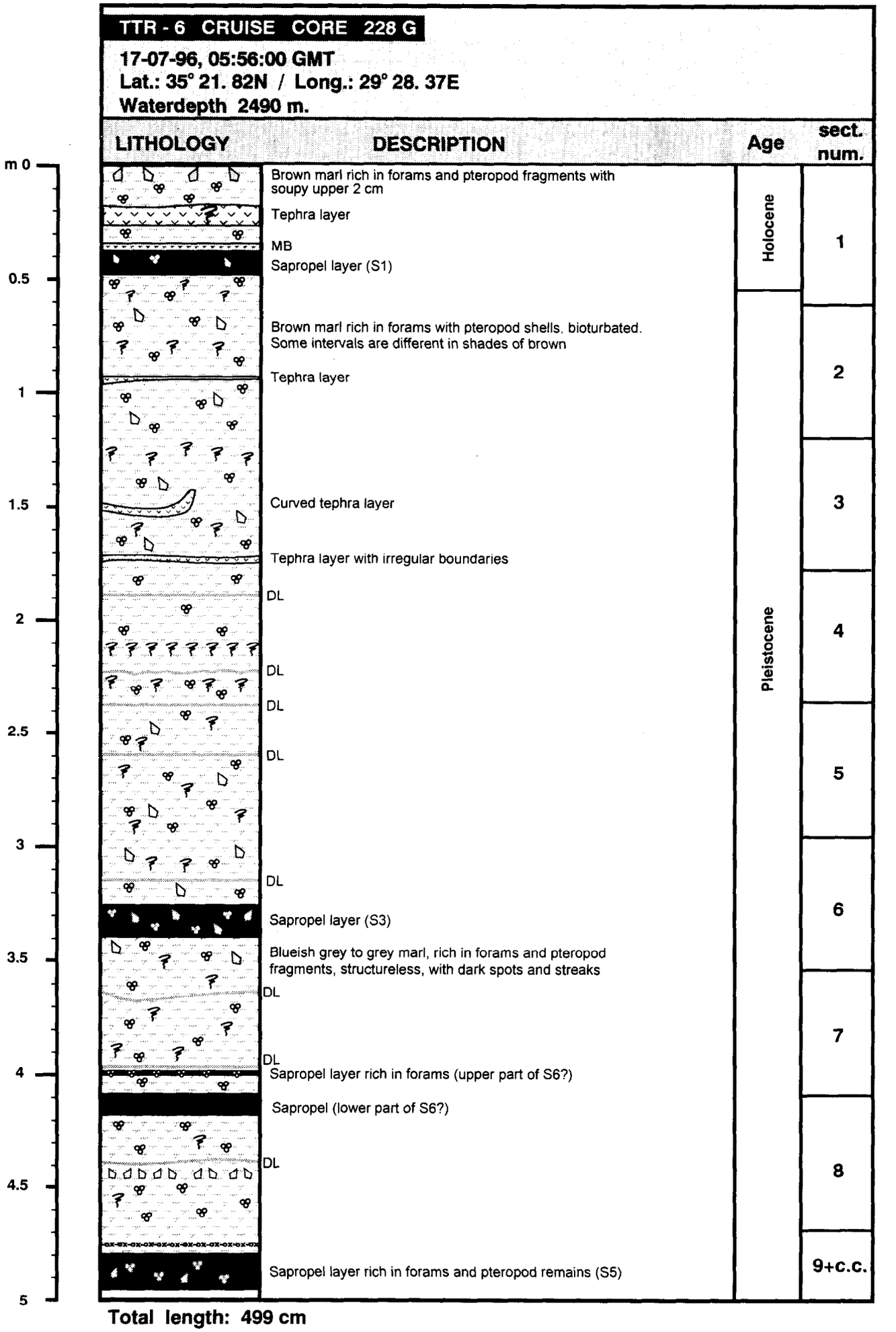

Total length: 499 cm

Fig. 47. Core log TTR6-228G

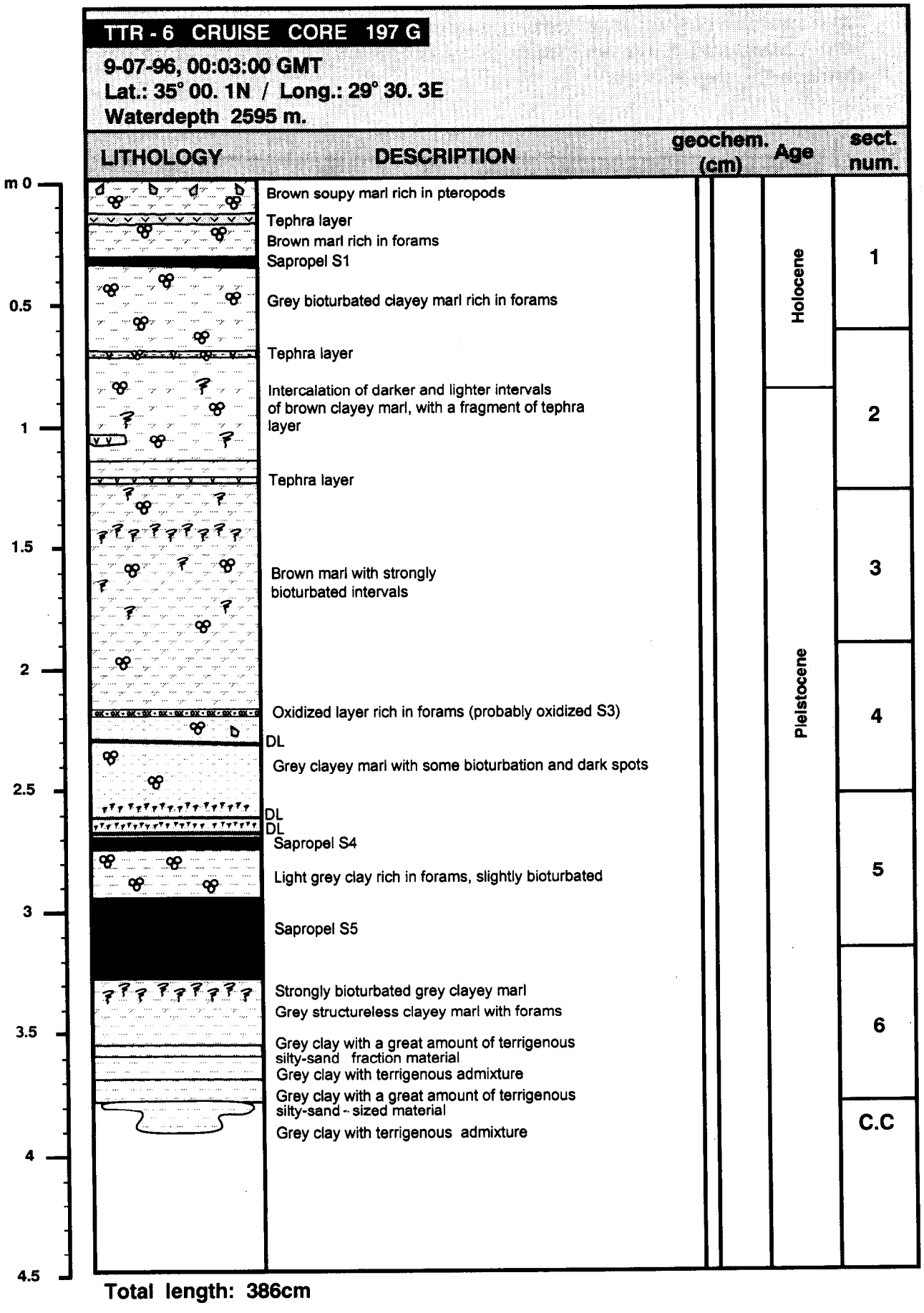

Fig. 48. Core log TTR6-197G

is overlain by only thin pelagic sediments suggests rather recent activity of the Amsterdam mud volcano. High gas saturation of the breccia, the presence of a large amount of shell fragments (remains of specific benthic communities in gas vent areas), and a live specimen (see Section I.8.f) indicate active gas venting through the deposits.

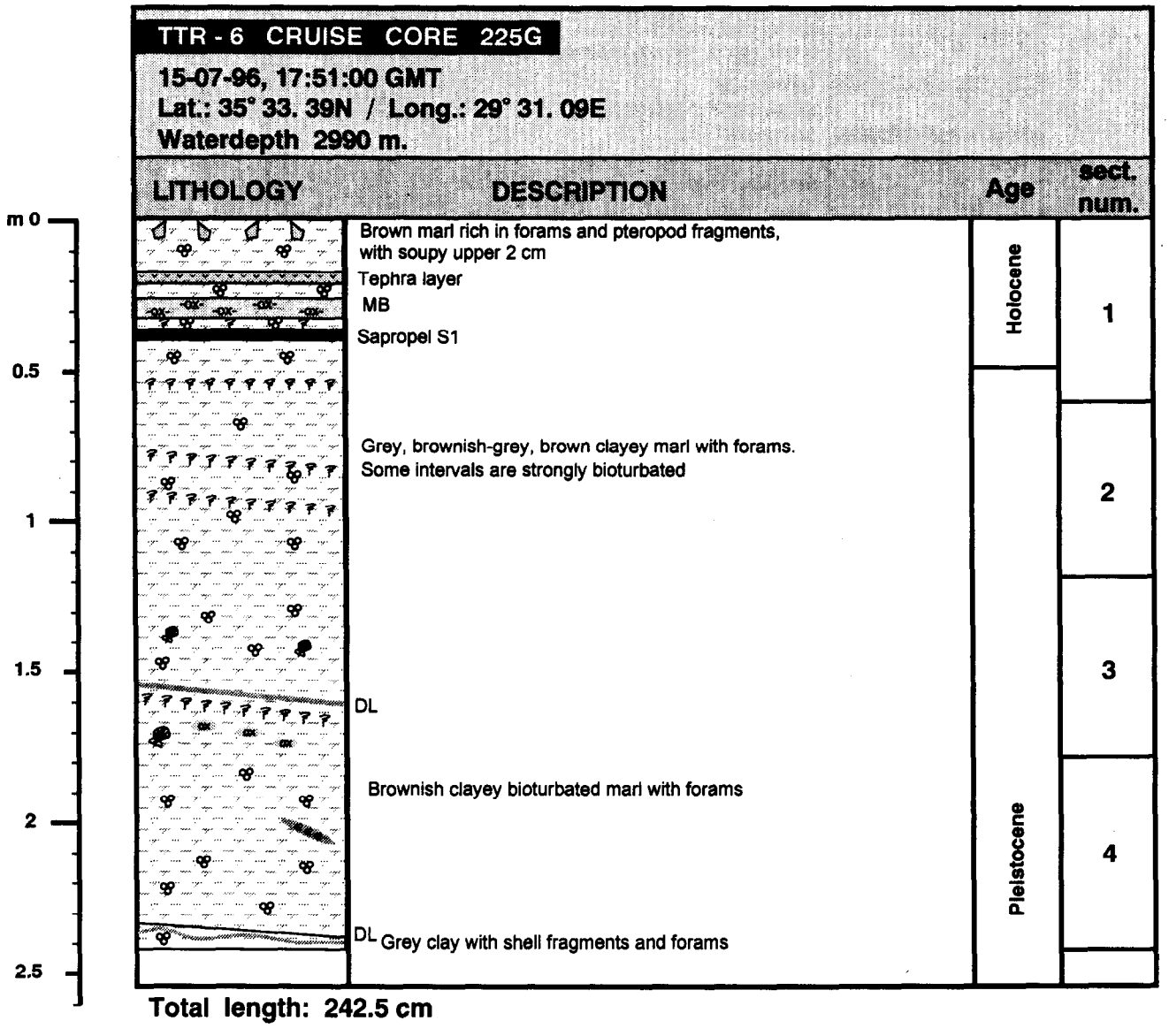

Fig. 49. Core log TTR6-225G

Mud breccia recovered from the Amsterdam mud volcano contains clasts of sedimentary rocks. Numerous fragments of detrital limestones, polymictic siltstones and sandstones, claystones and marlstones were described (Table 2). Most of these rocks may be considered as different gravity flow deposits and, with the help of paleontological analysis, ascribed to Middle Miocene flysh.

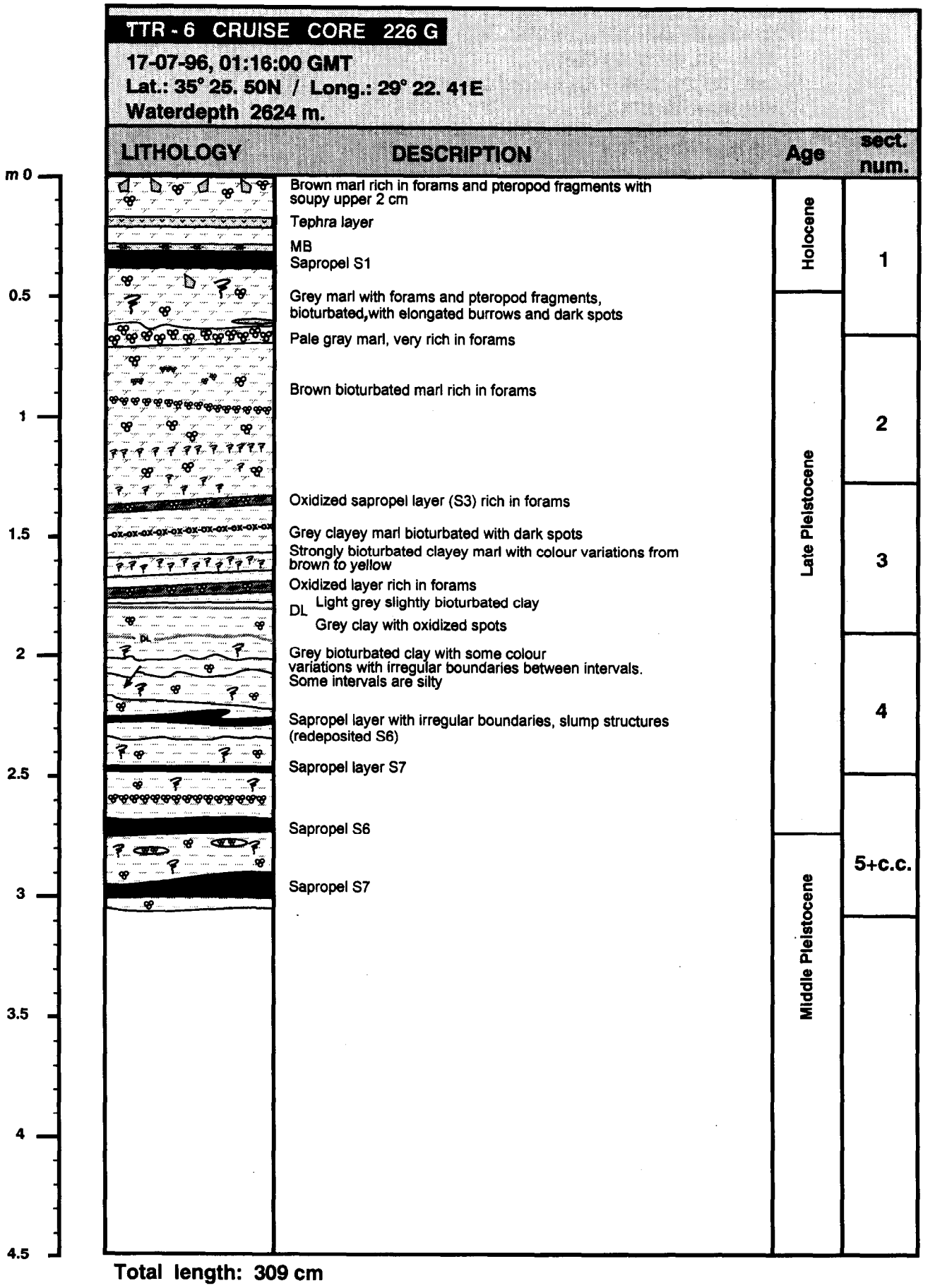

Total length: 309 cm

Fig. 50. Core log TTR6-226G

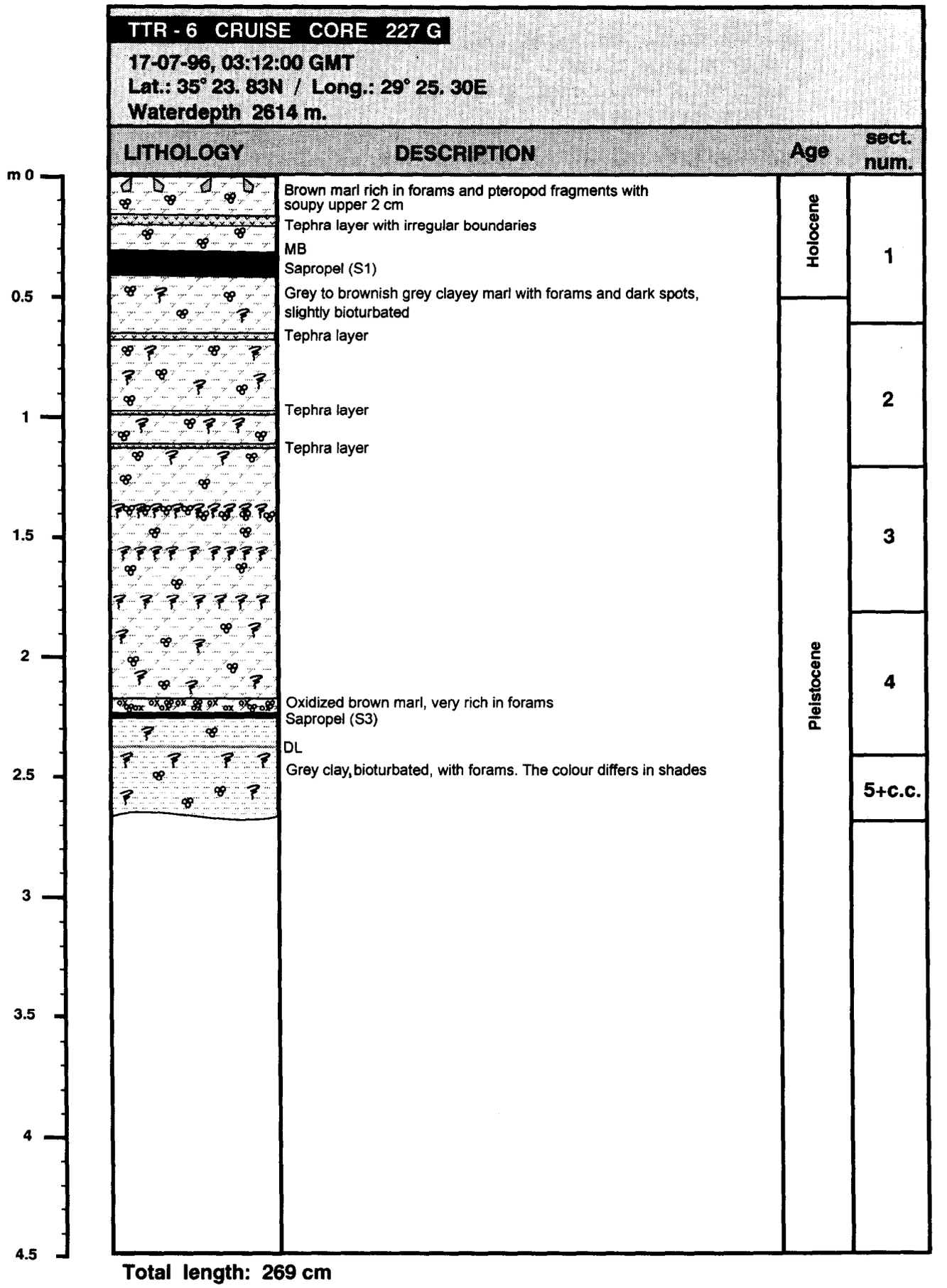

Fig. 51. Core log TTR6-227G

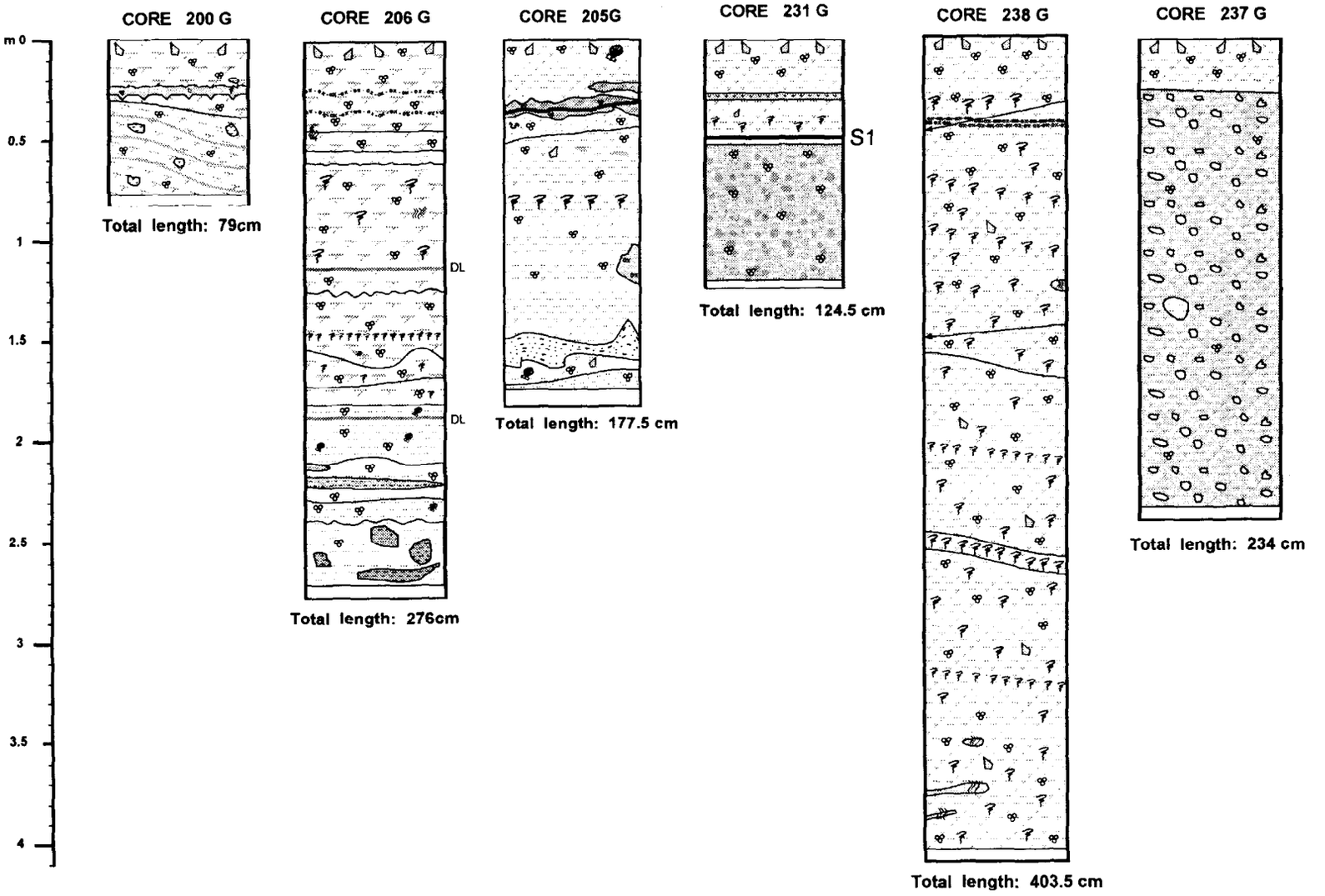

Fig. 52. Cores containing different types of slump sediments

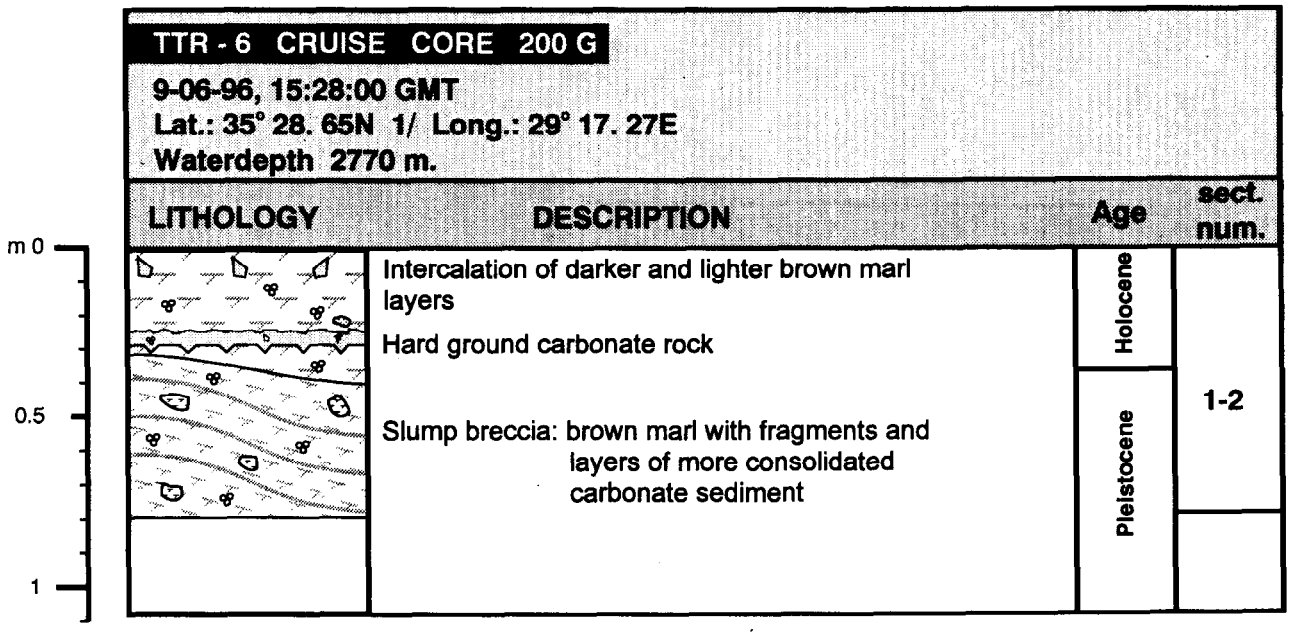

Total length: 79cm

Fig. 53. Core log TTR6-200G

Mud breccia from the Kazan mud volcano. Mud breccia from the Kazan mud volcano (TTR6-234G) was represented by deposits, very similar to that which we had found from the Amsterdam mud volcano, including the high gas saturation of the breccia and the presence of remains of a gas vent community. However, the mud flow recovered here is younger as the lack of oxidized mud breccia demonstrates.

Mud breccia clasts were represented mainly by dark grey structureless mudstones and light grey micritic limestones (Table 2). No significant indications of source formation for these rock fragments were found during onboard investigations.

Mud breccia from the Tuzlukush and Saint Ouen L'Aumone mud volcanoes. The Tuzlukush mud volcano breccia (TTR6-235G) and the Saint Ouen L'Aumone mud volcano breccia (TTR6-236G) are also grey, structureless, and matrix-supported. Flows recovered in these mud volcanoes are overlain by thick (1.7 m and 2.2 m respectively) sequences of Upper Pleistocene and Holocene pelagic sediment. An olive brown upper oxidized interval of mud breccia was 20 cm thick in both of the cores.

Rock fragments observed in mud breccia from these mud volcanoes were rather similar. They were represented mainly by limestones, sandstones, siltstones, claystones, siliceous rock fragments, fragments of ancient mud breccia flows, and specific rocks described during onboard study as volcanic rock fragments (Table 2).

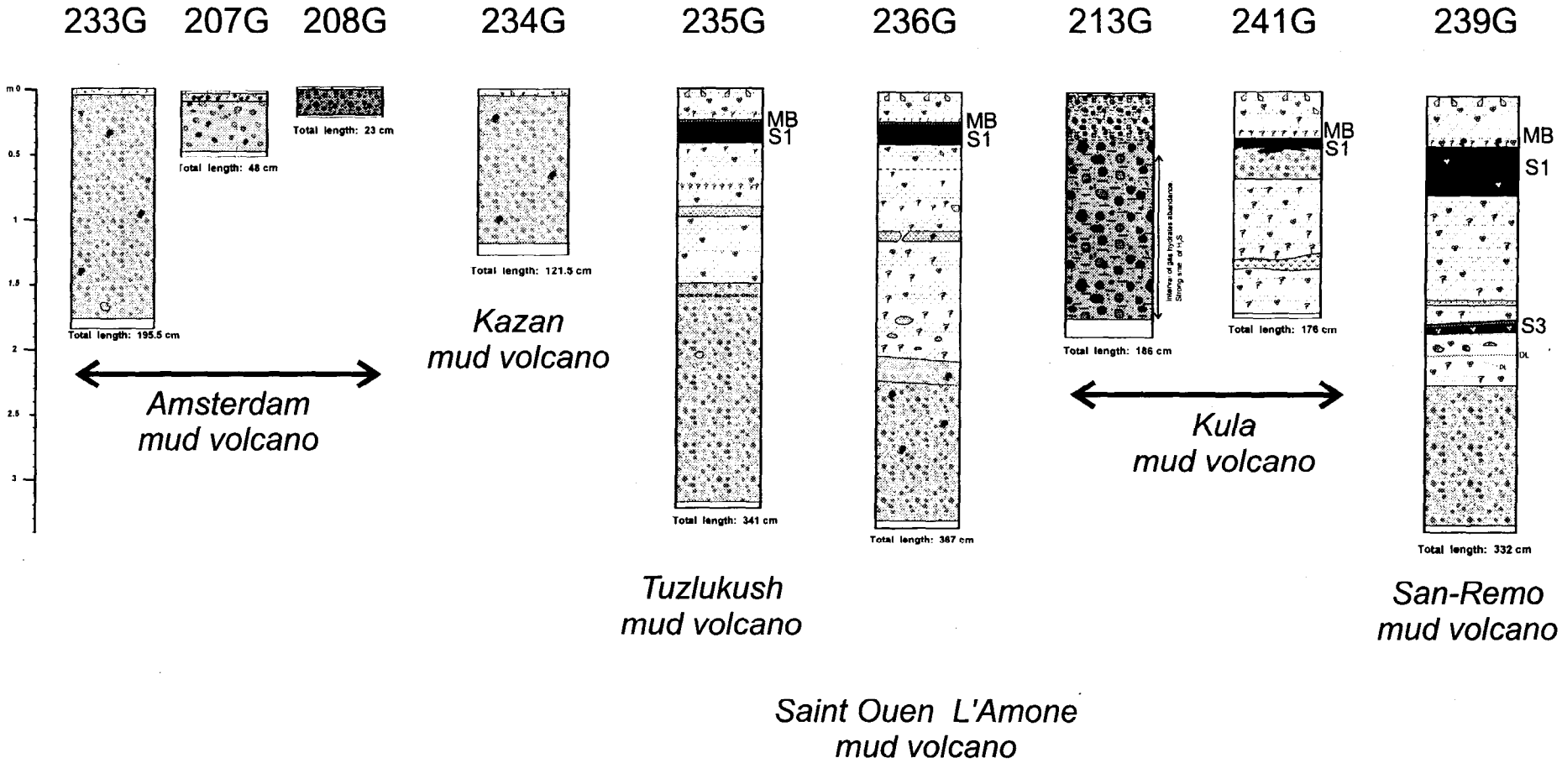

Fig. 54. Cores containing mud breccia

Mud breccia from the Kula mud volcano. Two cores (TTR6-213G and TTR6-241G) obtained from the Kula mud volcano contained a dark grey structureless matrix-supported mud breccia below a thin layer of pelagic sediment at the top. Undoubtedly, one of the most significant discoveries of the cruise consisted of a mud breccia from the core TTR6-213G. The mud breccia from this core was intensively gas-saturated and contained gas hydrates which were recovered for the first time from the Mediterranean mud volcanoes. Sedimentary rock fragments obtained from the mud breccia were represented by different sandstones, several types of cherts, limestones, clays and mudstones. Besides, volcanic rock fragments, fragments of serpentine, and serpentinized peridotite were observed among the mud breccia clasts implying that the Antalya Nappes Complex, or material derived from it, extend to the south from Turkey into the northeastern part of the Anaximander Mountains.

Mud breccia from the San Remo mud volcano. Mud breccia was obtained from core TTR6-239G on San Remo mud volcano. This breccia was represented by structureless matrix-supported mud volcanic deposits. The San Remo mud breccia was characterized by an extremely unusual reddish brown colour. This is the result of the enrichment of the extruded mud with red jasper which implies that its source formation is likely to be related to the Antalya Nappes Complex.

The mud breccia contained a large variety of clasts of different lithology: siliceous rock fragments, detrital limestones, polymictic sandstones, siltstones, claystones, fossiliferous micrites, and marlstones (Table 2). Fragments of bentonite and clast described as tuff fragment were also found among the mud breccia clasts.

Other unusual deposits, resembling mud volcanic deposits, were observed in core TTR6-219G taken in a depression on the terminal part of the lobe. They were represented by sandy silty sediments with sandstone fragments, and could be lag deposits where a large part of one of the lobes has washed out in the Finike Basin to the north.

The lithological variety of mud volcanic deposits suggests a complicated structure of the mud volcanic region studied. Different periods of activity recognized for different mud volcanoes probably reflect peculiarities of the tectonic evolution of the area.

Conclusions

The peculiarities of recent sedimentation in the area of the Anaximander Mountains reflect a complex morphology, active tectonics, and extensive fluid escape probably due to strong lateral compression. Within the relatively small study area we found numerous types of sediments of different genesis and of various depositional environments. A zonal distribution of the lithological types seems to exist in the study area, which can be explained by the different sedimentation agencies being predominant in different parts of this complicated area

Along with normal pelagic sedimentation, slope processes are taking place in the region under investigation. Tectonic activity and steep slopes cause slope

failure which results in slumping and the general mixing of sediments we observed in the cores.

The coring confirms and contributes detail to the dredging results indicating that the Anaximander Mountains are formed of rocks from the Susuz Dag - Bey Daglari and Antalya Nappes Complex of southern Turkey. Some mud volcanoes are probably still active (at least in the form of gas emanation), and the oldest period of activity of others can be dated back to 40 kyrs BP.

Table 2

Summary information on rock clasts from mud breccia

Core	Group	Number	Lithology	Colour	Shape	Texture	Structure	Composition	Admixture	Notes
207G	1	10	1) marlstone	light grey	isometric, subangular, from 0.3x0.3x0.3 to 3x3x4 cm	micritic	massive	calcite, clay	quartz (rare)	fragment of sharp, regular, planar contact between 1) and 2)
			2) siltstone	grey		fine-grained, moderately sorted	thin planar lamination	polymictic (quartz,mica,dark min.,feldspar), calcite cement	planctonic forams	
	2	1	1) marlstone	light grey	subrounded 1x1x1cm	micritic	massive	calcite, clay	quartz, mica,dark min.	fragment of sharp planar regular contact of 1) and 2)
			2) thin alternation of:							
			a) siltstone	dark grey		fine-grained		polymictic (dark min., mica, quartz, feldspar), clay matrix		
			b) claystone	dark grey					mica, dark min.	
	3	10	marlstone	light grey	isometric, subrounded, max size 0.5x1x1 cm		massive	calcite, clay	quartz, dark min.	similar to 1.1
	4	6	detrital limestone	light grey	subangular, 1x1x2 cm	silty-grained	planar lamination underlined by layers with large amount of oriented mica	calcite	quartz, dark min.	indurated
	5	4	detrital limestone	light grey	subrounded, 0.5x1.5x2 cm		thin planar laminnation underlined by irregular distribution of dark min.	calcite	quartz, dark min., clay	soft
	6	10	mudstone	dark grey	tabular, angular		massive		silty admixture	firm; fissile
	7	5	micritic limestone	white	isometric, rounded, 0.8x1x1.5cm	micritic	massive	calcite		soft, pure
	8	3	detrital limestone	grey	angular, tabular, 0.4x0.7x1cm	grained	massive	calcite	some terrigenous minerals	indurated
	9	1	detrital limestone	light grey	angular, 0.7x1.5x2cm	comformable contact between grains	massive	calcite		indurated, pure
	10	1	micritic limestone	white	angular, 0.7x1x1 cm	micritic	massive	calcite	small amount of fine terrigenous admixture	indurated
	11	1	crystalline limestone	light grey	angular, 0.7x1x1 cm	very fine-crystalline	massive	calcite	some terrigenous admixture	indurated
	12	1	detrital limestone	light grey	angular, 1x1x1cm	silty-grained	massive	calcite	rare quartz grains	indurated
	13	1	siltstone	dark grey	0.5x0.5x0.5cm	moderatly sorted	planar lamination	quatz, feldspar?, dark min. in carbonate cement		active reaction with HCl
	14	2	detritic rock	very light grey	0.3x0.5x1cm	very poorly sorted (0.05-2 mm)	massive	clasts of different composition in carbonate micritic matrix		not very indurated
	15	3	1) siltstone	dark grey	tabular, subangular,	fine-grained		polymictic with clayey matrix		fragment of very thin alternation of

Table 2 (continued)

Core	Group	Number	Lithology	Colour	Shape	Texture	Structure	Composition	Admixture	Notes
			2) claystone	dark grey	1x2x0.3 cm					1) and 2)
208G	1	16	1) marlstone	light grey	isometric, subangular, from 0.3x0.4x0.4 to 2x3x4 cm		very thin laminated	calcite, clay		fragment of sharp planar contact between 1) and 2). Lithology is similar to the group #2 described for core 207G
			2) very thin alternation of dark grey clay and fine-grained polymictic siltstone	dark grey						
	2	3	detrital limestone	yellowish grey	isometric, angular, 1x1x1 cm	fine sand-grained, moderately sorted	planar laminated	calcite grains in calcite cement	mica, dark min., quartz	indurated
	3	4	sandstone	grey	angular, planar, 0.4x2x3 cm	fine-grained, moderately sorted	massive	polymictic (quartz, feldspar, mica, rocks fragments) with calcite cement		indurated
	4	6	detrital limestone	grey	indurated, subangular, 1x1x2 cm	silty-grained	thin lamination	calcite	some terrigenous minerals	similar to group 6 (see below)
	5	3	micritic limestone	light yellowish white	rounded, 0.5x0.7x0.3cm	micritic, with some spots of recrystallization	massive	calcite	clayey, and rare terrigenous admixture	soft, pure
	6	3	detritic limestone	grey	sabungular, 0.7x0.7x0.5 cm	silty-grained	thin lamination	calcite	big amount of different terrigenous minerals	indurated
	7	2	claystone	grey	subrounded, 0.5x0.5x0.5 cm		massive	clay min., calcite	big amount of carbonate admixture	soft
	8	1	mudstone	grey	angular, tabular, 0.3x0.7x0.7 cm		thin planar lamination	clay min., calcite	carbonate admixture	soft; partially oxidized across lamination
	9	2	claystone	dark grey	subangular, 0.5x0.7x1cm		massive	clay min.		soft, no reaction with HCl
213G	1a	6	chert	light grey	angular, 1x1x1 cm	pelitomorphic	massive	siliceous		indurated, no reaction with HCl
	1b	9	crystalline limestone	light grey	angular, tabular, 0.5x2x3 cm	fine-crystalline (recrystallized micrite)	thin planar laminated	calcite		pure, indurated
	1c	13	crystalline limestone	light grey	angular, tabular, 0.3x3x4 cm	fine-crystalline (recrystallized micrite)	thin planar laminated	calcite		pure, similar to 1b but with calcite cracks
	1d	1	crystalline limestone	grey	angular, tabular, 1x3x4 cm	fine-crystalline (recrystallized micrite)	cross laminated	limestone	some terrigenous minerals	thin calcite cracks
Uncomplete description. Most of clasts from this core were sorted out by groups and sent to further analytic processing										
234G	1	7	shells							
	2	a lot	mudstone	dark grey	rounded		massive	clay min.		soft
	3	a lot	micritic limestone	very light grey	rounded	micritic	massive	calcite		soft, pure
	4	a lot	micritic limestone	white	rounded	micritic	massive	calcite		soft, very pure
	5	3	micritic limestone	light brownish grey	isometric, rounded, 1.5x2x3 cm	micritic	massive	calcite	clayey admixture	soft

Table 2 (continued)

Core	Group	Number	Lithology	Colour	Shape	Texture	Structure	Composition	Admixture	Notes
234G	6	10	micritic limestone	light grey	subrounded, tabular, 0.5x1.5x2.5cm	micritic	massive	calcite	fine terrigenous admixture	soft
	7	4	micritic limestone	very light grey	subangular, 0.5x1.5x3 cm	micritic	massive	calcite	terrigenous (less amount then in group 6)	soft
	8	1	crystalline limestone	light grey	isometric, angular, 0.4x0.5x0.7 cm	fine-crystalline	thin planar lamination underlined by irregulary distribution of admixture	calcite	terrigenous	firm
Uncomplete description. Some clasts from this core were sorted out by groups and sent to further analytic processing without preliminary description										
235G	1	a lot	claystone	brownish grey	isometric, subrounded, 1x1.5x1.5 cm		thin lamination	clay min.	quartz, dark min.	soft, no reaction with HCl
	2	a lot	claystone	grey	subrounded, isometric, 1x1x1.5 cm		thin lamination	clay min.	quartz, dark min.	soft, fissile, no reaction with HCl
	3	1	1)chert	dark grey	angular, 1.5x2x4 cm		massive	siliceous		fragment of planar contact of 1) and 2).
			2)claystone	olive grey			massive	clay min.		No reaction with HCl, firm
	4	10	thin alternation of clayey siltstones of different colours	light to dark grey	angular, tabular, max size: 0.7x3x3.5cm	silty-grained	planar alternation with sharp contacts	dark min., quartz, mica		hard, no reaction with HCl, there is orientation of flat minerals
	5	6	sandstone	grey	tabular, 0.4/0.7/1.2cm	very fine-grained, moderately sorted	planar or low wave lamination	quartz, feldspar, dark min., with chalcedone cement		hard, no reaction with HCl, 1 clast with pyritized surface
	6	2	1) limestone	grey	tabular, 0.5x0.5x1cm	medium sandy-grained	massive	sandy-sized calcite graines in micritic matrix	terrigenous (dark min.)	fragment of transitional boundary between 1) and 2)
			2) limestone	light grey		fine sandy-grained	massive	sandy-sized calcite grains in micritic matrix		
	7	2	thin alternation of light grey and grey silicious rocks (cherts?)	grey	isometric, angular, 0.7x1x1 cm	fine-crystalline		opal?	some terrigenous admixture	very hard, no reaction with HCl
	8	6	siltstone	grey	angular, 2x2.5x3cm	fine-grained	planar lamination	polymictic (quartz, feldspar, dark min., mica) with clayey cement	carbonate	hard, weak reaction with HCl, crust of well crystallized calcite on the surface
	9	3	carbonate rock	light grey	isometric, subangular, 1x2x3cm	matrix supported, with very poorly sorted, fine silty to coarse sandy sized clasts	massive	fine silty-sized dark minerals and mica; coarse sandy-sized rounded fragments of clayrocks and other rock fragments in micritic carbanate, sligthly recrystallized matrix		firm

Table 2 (continued)

Core	Group	Number	Lithology	Colour	Shape	Texture	Structure	Composition	Admixture	Notes
235G	10	1	crystalline limestone	white	angular, 0.7x0.7x1.4 cm	no grains can be observed	massive	calcite	rare dark min. and pyrite	very indurated, intensive reaction with HCl, pyritization
	11	1	1) fossiliferous limestone	white	subangular, 0.3x0.5x1 cm	fine-crystalline	massive	calcite, forams	some terrigeneous minerals	fragment of sharp planar boundary between 1) and 2); firm
			2) crystalline limestone	light grey		very fine-crystalline or micritic recrystallized	massive	calcite, rare forams		
	12	1 big, a lot of small	micritic limestone	white	rounded, 3x3x5 cm	micritic	massive	calcite		pure, soft; sharp planar contacts with mudstone and siltstone
	13	2	micritic limestone	light grey	subangular, 1.5x2x5 cm	micritic	thin planar lamination	calcite	clayey admixture, rare forams	pure, soft
	14	3	breccia	grey	subrounded, isometric, 1x1.5x2cm	matrix supported, with poorly sorted, fine sandy to gravel sized clasts	massive	mixture of rounded fine to coarse sandy sized fragments of mudrocks, siltstones, gravel sized fregments of thin laminated white soft micritic limestones, fine sandy sized quartz grains in high carbonate matrix with clayey admixture	clay	soft; sligthly similar to group 9; looks like a fragment of mud breccia flow
	15	2	breccia	brown	subrounded, 2x4x5 cm	matrix supported, with poorly sorted, fine sandy to gravel sized clasts	massive	similar to group 14 composition	clay	soft; looks like a fragment of mud breccia flow
	16	6	micritic limestone	grey	angular, isometric, from 0.5x0.5x0.5 to 2x2.5x4 cm	micritic or very fine-crystalline	massive	calcite		very hard; pure; with pyritization on the surface
	17	4	micritic limestone	grey	angular, 2x1.5x1.5 cm	micritic or very fine-crystalline	planar lamination underlined by different amount of clayey admixture	calcite	clay	hard
	18	6	chert (?)	light grey	angular, 0.7x1x1.5 cm	fine-crystalline	thin planar lamination	siliceous	irregulary distributed dark min.	hard; no reaction with HCl
	19	1	sandstone	grey	subrounded, 1.5x2.5x3 cm	medium-grained, moderately sorted	massive	polymictic (quartz, feldspar, rock fragments, dark min.) with calcite cement	clay	hard; pyritization; reaction with HCl
	20	1	fossiliferous limestone	grey	subangular, 1x1x1.5 cm		planar lamination	planctonic forams (60%) in micritic calcite	rare terrigenous admixture	hard

Table 2 (continued)

Core	Group	Number	Lithology	Colour	Shape	Texture	Structure	Composition	Admixture	Notes
235G	21	2	chert (?)	grey and slightly brownish grey	angular, 2x2.5x5 cm	fine-crystalline	planar or low wave laminated	siliceous	dark min.	hard, no reaction with HCl
	22	3	chert (?)	brownish grey	angular, 2.5x2x4 cm	fine-crystalline	massive	siliceous		hard
	23	2	micritic limestone	grey	subangular, 0.7x0.8x1 cm	micritic	massive	calcite	clay; dark min.	firm, brownish spots on the surface due to oxidization
	24	3	chert (?)	light bronish grey	subangular, 0.2x0.8x1 cm	fine-crystalline or micritic	massive	siliceous	rare dark min.	firm; no reaction with HCl
	25	2	1) chert (?)	dark brownish grey	angular, 1x1.5x2.5 cm	micritic	thin laminated	siliceous		fragment of contact of 1) and 2); hard; slikensides
			2) chert (?)	dark brownish grey		micritic	massive	siliceous		
	26	2	calcarenite	light grey	tabular, subangular, 0.4x1.2x1.5 cm	poorly sorted, fine to medium sandy-grained	thin planar lamination	angular to subrounded graines of limestone, calcite grains in micritic calcite matrix	rare forams	firm, pure
	27	4	sandstone	light grey	tabular, subangular, 0.5x0.7x0.8cm	fine-grained, moderately sorted	thin planar or wave lamination (underlined by distribution of dark min.)	subrounded quartz grains, mica, dark min. in calcite cement		firm, pyritization on the surface
	28	1	argillite	dark grey	angular, 0.4x0.8x1 cm	pelitomorphic	thin planar lamination	clay min.		very indurated
	29	1	crystalline carbonate rock	dark grey	angular, 0.4x0.7x1 cm	comformable grains contact	massive	calcite		indurated
	30	1	calcarenite	light yellowish grey	angular, 0.4x0.5x0.5cm	very fine sandy-grained	massive	calcite graines with micritic matrix	dark min.	firm
	31	3	basaltoid (?)	dark grey	subrounded, 1.2x1.3x1.5 cm	porphiric; matrix - very fine-crystalline	massive			hard
	32	3	basaltoid (?)	dark grey	subrounded, 1x1.3x1.5 cm	porphiric; matrix - very fine-crystalline	massive			soft, slightly carbonatized, altered
	33	1	volcanic rock (?)	light greenish grey	angular, 0.4x1.5x1.5cm	porphiric; matrix - very fine-crystalline	massive			soft similar to group 32 but intensively altered
	34	1	volcanic rock (?)	grey	angular, 0.5x0.5x0.7cm		massive			hard; intensively secondary pyritized
	35	1	volcanic rock (?)	light grey	angular, 0.3x0.7x1.2cm		massive	secondary zeolites (?)		soft
	36	a lot	fragments of calcite viens		angular, 0.8x1x2 cm			calcite		indurated,

Table 2 (continued)

Core	Group	Number	Lithology	Colour	Shape	Texture	Structure	Composition	Admixture	Notes
236G	1	4	volcanic rock (?)	dark green	subrounded, 0.9x1.2x1.5cm			chlorite, biotite, quartz with secondary carbonate cementation		very weak reaction with HCl
	2	1	siltstone	light grey	angular, 0.8x2.5x3 cm	coarse silty-grained	cross lamination			moderate reaction with HCl
	3	1	siltstone	light-dark grey	angular, 1.2x1.8x3.3cm	grained	cross lamination		mica, dark min.	no reaction with HCl
	4	8	micritic limestone	white	subangular, max size 0.6x0.7x1 cm	micritic	massive	calcite		soft; intensive reaction with HCl
	5	1	sandstone	grey	subangular, 0.8x1.5x3 cm	very fine-grained	cross lamination		mica	no reaction with HCl; sligthly brecciated
	6		claystone	dark grey	angular, 0.9x1.4x1.6cm	pelitomorphic	massive	clay min.		no reaction with HCl
	7	1	claystone	light grey	angular, 0.6x0.6x0.7cm	pelitomorphic	massive	clay min.		with ironoxide coating; no reaction with HCl
	8	2	calcarenite	light grey	subangular, 1x1x2 cm	grained	massive	calcite	pyrite	with greenish coating
	9	4	volcanic rock (?)	dark grey	subangular, 1.5x2x4.2 cm	very fine silty sized	massive	altered, with carbonate cementation (secondary)		moderate reaction with HCl
	10	4	marlstone	grey	angular, max size 0.4x0.9x1.3 cm	micritic	massive	calcite, clay	mica	intensive reaction with HCL
	11	5	sandstone	grey	angular, 0.5x0.7x0.8cm	very fine-grained	massive	subrounded quartz grains	mica, dark min	
	12	5	siltstone	grey	angular, 0.3x0.7x1 cm	very fine silty-grained	thin planar lamination		mica, dark min.	no reaction with HCl
	13	2	carbonate microbreccia	light grey	angular, 0.3x0.9x1cm	matrix supported, with sandy sized clasts	massive	fragments of clayrock in carbonate micrite matrix		
	14	1	detrital limestone	light grey	subangular, 0.6x0.6x0.6cm	medium to fine sandy-grained, poorly sorted	massive	calcite	mica, dark min., rock fragments	firm
	15	1	shale (?)	grey	subangular, 0.7x0.5x1 cm					firm; orientation of bladed grains
	16	1	crystalline limestone	light grey	angular, 0.8x1.2x2 cm	fine-crystalline	planar lamination	calcite	mica and dark min.	reaction with HCl
	17	1	crystalline limestone	light brown	subangular, 0.6x0.9x1.3cm	crystalline	massive	calcite		intensive reaction with HCl
	18	1	siltstone		angular, 0.4x0.7x0.8cm	fine silty-grained	planar lamination	grains in carbonate cement	mica	reaction with HCl
	19	1	chert (?)	light brown	angular, 0.4x0.5x0.6cm	very fine-crystalline	massive	siliceous		no reaction with HCl

Table 2 (continued)

Core	Group	Number	Lithology	Colour	Shape	Texture	Structure	Composition	Admixture	Notes
236G	20	1	fossiliferous micrite	yellowish white	angular, 0.4x0.6x0.4cm	micritic matrix	massive	calcite, forams	quartz grains, dark min.	firm
	21	1	marlstone	grey	subangular, 0.7x1.2x0.4cm	micritic	thin planar lamination	calcite, clay min.	dark. min	firm
	22	1	chert (?)	light grey	angular, 0.5x0.5x0.5cm	fine-crystalline or micritic	massive	siliceous		hard; no reaction with HCl; pyritization on the surface
239G	1	1	bentonite	greyish brown	subangular, 3x3x5 cm	porphiric, spherical fine to medium sandy sized inclusions in pelithomorphic mass	thin planar and low wave lamination	clay minerals, volcanic glass, zeolite, dark minerals, chalcedony		firm
	2	a lot	chert (?)	light greenish grey	subangular, max size 6x2x3.5 cm	micritic	lerise and flaser lamination	siliceous		rare well-crystallized pyrite inclusions
	3	2	chert (?)	grey	subangular, 2x1.5x2 cm	micritic or very fine-crystalline	irregulare wave lamination	siliceous	rare quartz	hard; well-crystallized pyrite inclusions
	4	2	calcarenite	grey	subangular, 2x3x1,5 cm	sandy-grained. moderately sorted	thin lamination	calcite	dark minerals, quartz grains, clay	hard
	5	12	calcilutite	grey	tabular, 0.5x2x3 to 0.1x0.6x0.7 cm	silty-grained	thin planar and low- wave lamination	calcite	big amount of clayey admixture, small mica fragmentes, dark min. and quartz graines,	hard; contact with calcarenite (carbonate turbidite ?)
	6	2	polymictic sandstone	light grey	subrounded, 0.5x0.5x0.8 cm	medium grained, poorly sorted	massive	angular and subangular quartz graines, big amount of angular dark min. and different (sedimentary and metamorphic) rock fragments in micritic calcite cement		soft, poorly cemented
	7		sand			fine to coarse grained, poorly sorted		quartz graines, dark min., rock fragmentes	some hard clasts of gravel size	loose
	8	4	polimicnic sandstone	grey with light yelloish grey surface due to oxidization	subangular and angular, 2.5x2.5x3 cm	fine-grained, moderately sorted	massive	angular and subangular quartz graines, dark min., rock fragments in micritic calcite cement		some orientation of tabular graines are observed

Table 2 (continued)

Core	Group	Number	Lithology	Colour	Shape	Texture	Structure	Composition	Admixture	Notes
239G	9a	3	chert (?)	white	subangular, 0.4x0.5x0.8 cm	micritic	massive	siliceous	rare terrigenous admixture of fine silty sized graines of quatrz and dark min.	porous, pyritized
	9b	2	claystone	grey	subangular, 0.5x1x1.5 cm	pelitomorphic	massive	clay min.	carbonate	rather pure, firm, weak reaction with HCl, with "metal- like" slickenslide on the surface
	9c	1	claystone	light yelloish grey	subangular, 0.5x1x1.5 cm	pelitomorphic	massive	clay min.	carbonate	slickenslide on the surface; similar to 9b
	10	2	flint	black	0.7x0.7x1.3cm		massive	siliceous		schistous
	11	4	rectangular cracked crystal	creamy-brown	angular, 0.3x0.5x0.8cm					no reaction with HCl, even with heating
	12	1	chert	very dark grey	angular, 0.7x1x1.5 cm		massive	chalcedony and microquartz		very hard; intensively cracked; with calcite vien
	13	3	fossiliferous limestone	light grey	subangular, 0.3x0.5x0.8cm		thin planar lamination	calcite, forams	some terrigenous silty sized admixture	porous; good reaction with HCl; pyritization
	14	3	fragment of thin planar alternation of grey claystone and light grey claystone		angular, max. 0.7x1x1.5x cm			clay min.		firm; no reaction with HCl; thickness of laminae varies from 0.5 to 2 mm, contacts are sharp
	15	1	micritic limestone	light grey	subangular, 0.5x1x1 cm	micritic	massive	calcite	clayey and rare fine silty sized terrigenous admixture	firm
	16	2	micritic limestone	light grey	angular, 0.5x0.7x0.7 cm	micritic	massive	calcite		firm, pure, sureface pyritization, close to 15 group but more indurated
	17	1	tuff (?)	olive grey	subrounded, 2.5x2x1.5 cm	0.01-2 mm sized, very poorly sorted	massive	volcanoclastic material cemented by crystalline calcite		

Table 2 (continued)

Core	Group	Number	Lithology	Colour	Shape	Texture	Structure	Composition	Admixture	Notes
239G	18	1	fine-crystalline limestone	grey	angular, tabular, 0.4x0.5x0.7cm	fine-crystalline	irregular wave lamination	calcite	silty sized terrigenous admixture	hard; a lot of calcite vien
	19	4	marlstone	brownish grey	angular to subangular, 0.6x0.7x2 cm	micritic	massive	calcite, clay min.		firm; fissile; reaction with HCl
	20	1	fragment of chert concrection (nodular chert)	outer part-light grey, inner part-grey	subangular, partialy rounded, 1x1.5x1.8 cm	micritic	zonal concentritic radial structure	chalcedony		hard, intensively cracked, outer part is more cracked
	21	2	clayrock	grey	angular, 0.7x1x2 cm	pelitomorphic	massive	clay min.	carbanate and rare silty sized terrigenous admixture	firm; pyritization; weak reaction with HCl
	22	1	alternation of cherts	grey and dark grey	angular, 1x1.2x1.3 cm	micritic	thin planar lamination	siliceous	some very small mica fragments and fine terrigenous admixture	no reaction with HCl
	23	15	claystone	light grey	subangular-angular, max. 1x1.5x2.5 cm	pelitomorphic	massive	clay min.		firm; fissile; rather pure; no reaction with HCl
	24	1	siltstone	grey	subangular, 0.5x1x1.2 cm	coarse silty-grained	thin planar lamination	quartz, dark min., muscovite		reaction with HCl; muscovite and black min. are oriented parallel to the bedding on one side
	25	1	claystone	light brown	subangular, 0.7x1x1.5 cm	pelitomorphic	planar lamination	clay min.		soft; fissile; pure; no reaction with HCl
	26	2	claystone	grey	subangular, 0.5x0.5x0.7cm	pelitomorphic	massive	clay min.		firm; very pure; no reaction with HCl
	27	1	1) micritic limestone	light grey	subrounded, 1x1x2 cm	micritic	massive	calcite		fragment of sharp, very irregular contact (risolite ?); hard
			2) claystone	grey		pelitomorphic	massive	clay min.,	carbonate	
	28	2	polymictic siltstone	greyish brown	subangular, 0.4x1x1.5 cm	silty-grained	massive	polymictic, with clayey- carbonate cement		weak reaction with HCl
	29	1	calcarenite	olive grey	angular, 2x2.5x4 cm	silty - fine sandy-grained; moderately sorted	massive	carbonate grains in carbonate cement	dark min.	hard; reaction with HCl

Table 2 (continued)

Core	Group	Number	Lithology	Colour	Shape	Texture	Structure	Composition	Admixture	Notes
239G	30	5	micritic limestone	white	subangular to angular, 0.4x0.5x0.7cm	micritic	massive	calcite	clayey and very fine silty sized terrigenous admixture	soft, reaction with HCl
	31	1	calcarenite	light grey	subangular, 0.4x0.7x1.4cm	fine sandy-grained; grains are subrounded to subangular	planar lamination	carbonate grains in carbonate cement	silty and sandy sized terrigenous admixture	hard
	32	1	chert (?)	brownish grey	angular, 2x2.5x4.5 cm	very fine-crystalline	lense- like lamination	siliceous	rare admixture of dark min.	very hard; no reaction with HCl
	33	4	clayrock	greish brown	subangular, max size 2x2x3 cm	pelitomorphic	massive	clay min.		firm; rather pure; no reaction with HCl; fissile; some clasts are with slickenside
	34	6	1) clayrocks	brownish grey	subangular, max size 0.7x1.5x2 cm	pelitomorphic	massive	clay min.		hard; fragment of alternation of 1) and 2); thickness of laminae varies from 0.1 to 7 mm; boundaries are sharp planar or low wavely
			2) clayrocks	light grey		pelitomorphic	thin lamination	clay min.	with small amount of silty sized terrigenous admixture	
	35	9	clayrock	brownish grey	subangular, max size 0.8x1.2x2 cm	pelitomorphic	massive	clay min.	small amount of silty sized terrigenous admixture	firm; fissile; no reaction with HCl
	36	2	fragment of small lense or concrection	inner part - grey; outer part - white	angular, 0.4x0.9x2 cm	micritic		siliceous		hard; pure
	37	2	crystalline limestone	very light grey	angular, 1x1.5x1.5 cm	fine-crystalline	massive	calcite		pure; a few well crystallized pyrite inclusions on the surface
	38	7	fragment of calcite vein	milky white	angular, max size 1.5x2.5x3cm			calcite		very hard; fragments of limestone (37 group) are sometimes on the surface of the vein in large fragments

Table 2 (continued)

Core	Group	Number	Lithology	Colour	Shape	Texture	Structure	Composition	Admixture	Notes
239G	39	9	siliceous rock	white and greyish white, with irregular lenses of darker material	angular, max size 0.7x1.5x2 cm	fine-crystalline	massive	siliceous	rather big amount of inclusions of rounded fine sandy- sized quartz fragments and rare inclusions of well crystalline pyrite	hard; no reaction with HCl

d. PALEONTOLOGICAL INVESTIGATIONS OF BOTTOM SEDIMENTS

E.M. Ivanova, S.S. Gablina, A.P. Sautkin, and J. Henderiks

During this leg, 10 pelagic cores, 5 cores with slump sediments, 9 mud volcano cores, 3 cores from tectonic windows, and 17 dredges were taken. Preliminary stratigraphic interpretation of sediments and rocks was made on board. The age determinations were based primarily on a quick preliminary examination of planktic foraminifera (an 'express-analysis'), as well as on some study of diatoms and coccoliths.

Express-analysis on the basis of planktic foraminifera was used in order to establish stratigraphic subdivision and correlation of the pelagic cores. Most of the recovered pelagic sediments are Quaternary in age. Thus the general stratigraphic zonation can not be used because all of the sediments can be assigned to the *Globorotalia truncatulinoides* Total-Range-Zone. However a paleoceanographic record of the Quaternary, known for its climatic fluctuations, and some knowledge on the ecology of planktic foraminifera allows the age of the sediments to be determined. The express-analysis is done semi-quantitatively on the washed residues of the samples. The fraction larger than 125 μm was checked and analyzed. Most of the planktic foraminifera are known for their preference for certain oceanographic conditions (temperature, salinity, etc.).

The Eastern Mediterranean is characterized by repeated stagnant anoxic episodes resulting in the deposition of sapropels that correlate from core to core (isochronous lithologies) (*Parisi, 1987*). The age and conditions under which these sapropel layers were formed are relatively well known and listed below, with the ages of the sapropels after *Parisi (1987)*. Only those sapropels which were recovered during the cruise are described. The deepest was sapropel S7. Sapropel S2 was not found in the recovered cores, probably because it is the result of a local anoxic event, which confines its distribution in the Eastern Mediterranean to a certain area. Generally accepted environmental indicators are as follows:

warm-water species: *Globigerinoides ruber, Globigerinoides sacculifer, Orbulina universa, Globorotalia aequilateralis* (= *Hastigerina siphonifera*), *Globorotalia truncatulinoides* (*Violanti et al., 1991; Cita et. al., 1977*);

cold-water species: *Neogloboquadrina pachyderma, Globigerina bulloides, Globorotalia scitula, Turborotalia quinqueloba* (*Violanti et al., 1991; Cita et. al., 1977*);

low-salinity indicator: *Neogloboquadrina dutertrei* (= *N. eggeri*) (*Cita et al., 1977; Thunell et al., 1984*).

The pelagic cores were subdivided into Holocene and Upper Pleistocene sediments (Fig. 46). Each core contains from one to six sapropel layers, among which S1, S3, S4, S5, S6, and S7 were determined. They are identified by different assemblages of planktic foraminifera. Benthic organisms are mostly absent in sapropels (*Cita et al., 1991*) due to bottom-water anoxia during sapropel deposition.

Sapropel S1 (9-8 kyrs B.P.) is the only sapropel which accumulated during

the Holocene and is widely distributed over the whole deep-water Eastern Mediterranean basin. It has sharp boundaries. Its thickness range is 5-15 cm, but it is normally about 10 cm thick. Sometimes the upper part of the sapropel is oxidized. The faunal composition of sapropel S1 is characterized by an abundance of pteropods. Their fragments compose up to 30-40% of the total faunal assemblage in the studied residue. The foraminiferal assemblage is represented mainly by *G. ruber*, up to 65-75% (its pink morphotype is very abundant), *Gl. aequilateralis*, up to 10-20%, *O. universa*, *G. sacculifer*, and some other species.

Sapropel S1 was recovered in all the pelagic cores with the exception of Core TTR6-230G. Core TTR6-218G has only the diluted S1 sapropel. This layer is characterized by a warm-water assemblage of foraminifera, the main feature of which is an abundance of *Globigerinoides ruber* (pink form) and the presence of *G. sacculifer*, *Globigerina bulloides*, *G. calida*, *G. trilobus*, *Orbulina universa*, and *Hastigerina siphonifera*.

Sapropel S3 (84-80 kyrs B.P) and S4 (100-95 kyrs B.P.) are very similar in their faunal composition; however S3 accumulated during a warmer period in comparison with S4. The planktic foraminifera assemblage is therefore enriched in warm-water species, in particular *O. universa*. The percentage of *O. universa* is in general lower than 10%, but in S3 sapropel they commonly can reach 19%. Sapropel S3 is often found to have been oxidized. It is usually thicker on the average than S4.

Sapropel S3 was found in Cores TTR6-197G, TTR6-224G, TTR6-226G, TTR6-227G, TTR6-228G, and TTR6-230G. It is usually rich in forams and contains the following species: very abundant *Neogloboquadrina eggeri/duttertrei*, *G. ruber*, *O. universa*, rare *G. bulloides*, *G. tenellus*, *Globorotalia scitula*, and some *G. calida* and *H. siphonifera*. Such an assemblage is typical of rather warm-water conditions.

Sapropel S4 was observed in three cores (TTR6-197G, TTR6-224G, and TTR6-230G). It was identified by the abundance of cold-water species, such as *G. bulloides*, *G. scitula*, *N. eggeri/duttertrei*, *O. universa*, the occurrence of *Turborotalia quinqueloba*, and by the rare presence of *H. siphonifera*, *Globorotalia inflata*, and *G. calida*.

Sapropel S5 (126-116 kyrs B.P.) corresponds to isotopic stage 5e that is the warmest interval in the Pleistocene. Together with sapropel S6, sapropel S5 is one of the best expressed sapropels in the sediments of the deep Eastern Mediterranean basin. Both S5 and S6 can reach 30-40 cm in thickness, and sometimes even more. S5 is characterized by warm planktic foraminifera assemblages dominated by *G. ruber* (*Parisi, 1987*). *G. ruber* can reach up to 70% at the base of S5, and both *G. sacculifer* and *G. aequilateralis* are particularly common. *G. aequelateralis* reaches its maximum abundance of 12% in S5. The extremely warm-water foraminifera assemblage in S5 can be compared only to the S1 sapropel, but differs from it mainly by a very low quantity of pteropods, and by the absence or scarcity of pink-coloured *G. ruber*. Furthermore, S5 is also much thicker than S1 and darker in colour. In some areas of the Eastern Mediterranean basin, S5 contains abundant biogenic silica material, such as diatoms and radiolaria, which is explained by some authors by the occurrence of local upwelling conditions during the deposition of the sapropel. The base of S5,

which coincides with the base of isotopic stage 5 (Termination II) at approximately 125 kyrs B.P., is considered by INQUA 1982 Congress (informal recommendation) to be the Late/Middle Pleistocene boundary (*Parisi, 1987*).

Sapropel S5 occurs in Cores TTR6-197G, TTR6-228G, and TTR6-230G, being better expressed in the first one. The rich warm-water fauna, which distinguishes this sapropel, is represented by planktic foraminifera *G. ruber, N. eggeri/duttertrei, H. siphonifera, G. glutinata,* and *O. universa.* Some other species (*G. bulloides, G. tenellus, G. inflata,* and *G. sacculifer*) were found quite rarely. Samples of this sapropel were also enriched in pteropods and diatoms, the latter in Core TTR6-197G.

Sapropel S6 (about 185 kyrs) represents an exceptional event, differing from all other sapropels in many aspects. It is a cold sapropel that formed during a period of increased primary productivity and severe water density stratification, while the other ones developed during warm climatic conditions and normal biomass productivity (*Cita et al., 1977*). As a result the faunal composition of S6 is easy to distinguish. Its main features are low species diversity, high foraminiferal number (number of specimens per gram of dry weight), and the absence or extreme scarcity of *Globigerinoides* spp. The bulk of the assemblage is represented by cold-water species *G. bulloides, T. quinqueloba, G. scitula,* and *N. pachyderma,* and by a low salinity indicator (*N. dutertrei*). Sometimes S6 consists of two sapropel layers, with the main lower part being 30-40 cm thick and the upper part 2-5 cm thick.

Sapropel S6 was recovered in Cores TTR6-226G and TTR6-228G. In Core TTR6-228G, it is located above the S5 layer; but it is distinguished from S4 because of its abundant *G. bulloides, N. eggeri/duttertrei, G. ruber, G. quinqueloba, G. inflata,* and *G. scitula,* and because of its low numbers of *O. universa.* This anomaly can be explained probably as a result of slope processes. A similar explanation can be used for Core TTR6-226G where the sequence of S6 and S7 layers was observed to be repeated twice. Sapropel S6 in Core TTR6-226G contains the same assemblage of rather cold-water species as in Core TTR6-228G.

Sapropel S7 (about 200 kyrs B.P.; *Parisi et al., 1987*) formed during a relatively warm interval. Its foraminiferal assemblage has a high diversity and a high abundance of *Globigerinoides* spp. and other warm-water species. It is characterized by the appearance of deformed *Globorotalia truncatulinoides* (*G.* cf. *truncatulinoides*), with laterally strongly inflated chambers. This unusual morphotype of this mesopelagic taxon probably arose under unusual stress conditions (*Cita et al., 1977*).

As already mentioned, the S7 sapropel was found only in Core TTR6-226G. It was identified by the abundance of keeled *G.* cf. *truncatulinoides,* which is typical of S7. Some other warm-water and temperate forams observed, such as *G. trilobus, N. eggeri/duttertrei, G. ruber, G. inflata,* and *O. universa,* are characteristic of these conditions.

An examination of the coccolith distribution in the cores revealed the following features: (a) a large number of different species of *Gephyrocapsa* and a small number of *Emiliania huxleyi* were in the Pleistocene deposits; (b) a typical Holocene assemblage of coccoliths was observed, in which *E. huxleyi*

predominates, especially in S1, and numerous *Gephyrocapsa* (*G. caribbeanica* and *G. muellerea*) and *Cycloccolithus leptoporus*, *Umbellosphaera* spp., *Umbillicosphaera* spp., *Helicosphaera carteri*, *Coccolithus pelagicus*, *Scyphosphaera apsteini*, and *Syracosphaera* spp. occur.

On the whole, a Pleistocene age was established for the cores recovering slope sediments (Fig. 52). Moreover, an assemblage of planktic foraminifera similar to that observed in sapropel S6 was found at the bottom of Core TTR6-206G. It was noted that these cores, as well as the pelagic ones, particularly in their lower parts, contain a lot of different discoasters of Miocene-Pliocene age.

Preliminary dating of the selected rock samples that were recovered by dredging and gravity coring (i.e. mud volcano breccia) was done and is reported in some detail in Section I.8.b of this report.

e. GEOCHEMICAL SAMPLING

A.N. Stadnitskaya

The main aim of the geochemical programme on board was to collect samples in order to identify the origin of hydrocarbon gases in seabed sediments and to reveal whether they are related to a deep source. The intention was to achieve this by post-cruise study of the composition of these gases, organic matter in sediments and rock clasts, and carbonate crust and nodules included in sediments.

The principal tasks of the geochemical team were:

(1) to estimate the general level of gas present in the study area;

(2) to identify anomalous zones of high gas content;

(3) to define the location of these zones in relation to different geological features, such as faults, mud volcanoes, pockmarks, etc.;

(4) to extract gas from the samples and save it for further investigation;

(5) to collect clasts from rocks that could be a potential source of hydrocarbon fluids, for further investigation;

(6) to collect carbonate crust and nodules from sediments for carbon isotope and mineralogical analyses.

During the ANAXIPROBE leg, a total of 468 samples of seabed sediments and rock clasts were sub-sampled from 16 cores and 4 dredges.

The further onshore analyses envisaged are:

(1) gas chromatography for defining molecular composition of extractable organic matter (EOM) and concentration of methane and its homologues up to C_5;

(2) fluorescence analysis of EOM;

(3) determination of total organic carbon (TOC);

(4) bituminological investigation (solvent extraction);

(5) carbon isotope analysis from CH_4 and carbonates;

(6) pore water study;

(7) X-ray powder diffraction;

(8) thin section study.

The standard sub-sampling and degassing procedures of the sampled sediments were applied, as described in *Ivanov et al. (1996).*

For TOC and fluorescence analyses, about 0.2 kg of wet sediment was sub-sampled from the same core intervals as for gas analysis and dried at a temperature of 60°C.

For bituminological study, about 1 kg of wet sediment was sub-sampled from the upper, middle, and lower parts of cores. The sediment had also been dried at a temperature of 60°C.

About 0.5 kg of sediment was taken from different parts of some cores for pore water analysis (3 to 5 sub-samples per each core). The sub-samples were stored in hermetically-sealed plastic bags, and stored in a cool room at a temperature of - 17°C.

All the cores sampled for geochemical study can be divided into two main groups: pelagic and mud volcano cores. In turn, the pelagic cores were subdivided into two groups: cores which recovered normal, undisturbed basinal sediments with some lithological markers, such as tephra and sapropel layers (TTR6-197G and TTR6-224G); and cores taken from slumped sedimentary sequences (TTR6-200G, TTR6-205G, TTR6-206G, TTR6-219G, and TTR6-229G). From the pelagic cores, all the different lithologies were sub-sampled. The cores TTR6-197G and TTR6-224G were used as reference for all further investigations.

Among the cores with mud breccia, two types can be also distinguished. The first represents cores with a single mud breccia interval overlain by a thin pelagic layer or outcropping at the seafloor (TTR6-207G, TTR6-208G, TTR6-213G, TTR6-233G, and TTR6-234G). The other includes cores with several mud breccia layers separated by hemipelagic intervals (TTR6-235G, TTR6-236G, and TTR6-241G). All the cores containing mud breccia are characterized by a strong H_2S smell, particularly Core TTR6-213G in which gas hydrates were found.

The preliminary results of the geochemical study suggest that the general level of gas content in the sediments from the Anaximander Mountains area is rather low beyond the mud volcanoes. At the same time, the mud volcano cores are notable for high gas concentration. Considering also the presence in Dredge TTR6-209D of a rock samples showing clear evidence for gas escape through the seafloor, one may conclude that the fluid venting takes place only locally, probably through faults, implying a deep source for these fluids.

f. CHEMOSYNTHETIC BENTHIC COMMUNITIES

J.M. Woodside

Samples from several sites included bivalves and tube worms. Fragments of molluscan shells were observed in a number of cores (TTR6-207G, TTR6-208G, TTR6-233G, TTR6-234G, TTR6-235G, TTR6-236G, TTR6-TTR6-239G, and TTR6-240G) and one dredge (TTR6-209D), all mud volcanoes; and live specimens were obtained at Sites TTR6-209D and TTR6-234G. The bivalves were preserved in formalin and were analyzed at the Paris Museum of Natural History where they were identified as probably a new species of Lucinidae (*C. Salas, pers. comm.,1997*). The tube worms from Site TTR6-209D were identified as vestimentiferan worms of the genus *Lamellibrachia* (*E. Southward, pers. comm.,1996*). Both these types of organisms are found in areas of cold seeps where there is a supply of sulphide or methane to support the chemoautotrophic symbiotic bacteria on which they depend.

The bivalves resemble *Lucinoma borealis* but their hinges differ enough to suggest that they are a new species of Lucinidae (*C. Salas, per. comm.,1997*), which would be an important discovery. Previously, known species of both Lucinidae (*Myrtea* sp.) and Vesicomydae (*Vesicomya* sp.) had been obtained in a box core from Napoli mud volcano (*Corselli and Basso, 1996*). These specimens were probably living in symbiosis with chemosynthetic bacteria.

The vestimentiferan worms have not been documented in the Mediterranean before, making this an important discovery also. They may have been seen on a video recording made across the Napoli mud volcano using a deep-towed camera; but the first samples were obtained during the ANAXIPROBE expedition. The vestimentiferans contain chemosynthetic symbiotic bacteria which enable them to make efficient use of bacterial carbon fixation, with the oxidation of sulphide or single-carbon compounds like methane as an energy source (*Southward et al., 1996*). They are therefore restricted to environments where both oxygen and dissolved sulphide or methane are available, such as at hot and cold seeps/vents. Vestimentiferans are assumed to disperse in a planktonic larval stage although none of the larvae have yet been captured, and colonization may be quite rapid (*Young et al., 1996; Southward et al., 1996*). The source of the Mediterranean colonies will require further in-depth studies, for example, examining genetic data and comparing them with data from colonies in the Atlantic.

The large volume of vestimentifera worms obtained in Dredge TTR6-209D were attached to a large piece of rock with irregular holes running through it (see description of sample 209D-8). The rock, which incorporated fragments of mollusc shells was assumed to have been a methane-derived carbonate crust at the location of active gas venting. The worms were attached at one end to the walls of the holes, and the other end projected about 20 cm beyond the holes. Diagenetic pyrite was present in siltstone clasts from Dredge TTR6-209D and there was also a smell of hydrogen sulphide gas from the mud and clasts.

9. Conclusions

J.M. Woodside and M.K. Ivanov

(1) Samples from the Anaximander Mountains show direct affinity with rocks from the Taurus Mountains to the north. In particular, Anaxagoras Mountain is shown to be a part of the Antalya Nappes Complex, at least as far south as a fault zone inferred to cross it at roughly 35.5° N, and the Susuz Dag - Bey Daglari continues through the Anaximander and Anaximenes Mountains to at least 35.2° N.

(2) The strategy of sampling mud volcanoes, tectonic windows, and fault scarps was successful and instrumental in revealing the basement geology of the Anaximander Mountains.

(3) The seven new mud volcanoes sampled (including an unnamed fissure eruption) extend the occurrence of Mediterranean mud volcanoes into a completely new area where only the compressional tectonics is common with previously investigated mud volcanoes on the Mediterranean Ridge. The mud volcanoes in the Anaximander Mountains seem to erupt along faults from gassy, overpressured formations otherwise sealed by overthrusts.

(4) Gas is much in evidence both in the sediments sampled from the mud volcanoes and in a large area between the mountains where sediments are moving *en masse* as a slide. Gas hydrates were sampled for the first time in the Mediterranean Sea at Kula mud volcano, on Anaxagoras Mountain. Chemosynthetic benthic communities were in evidence at several mud volcanoes; and the first Lamellibrachia (vestimentiferan worms) and a new species of Lucinid were sampled from two other mud volcanoes.

Intergovernmental Oceanographic Commission
technical series

48

Neotectonics and fluid flow through seafloor sediments in the Eastern Mediterranean and Black Seas

Part II: Black Sea

Preliminary results of geological and geophysical investigations during the ANAXIPROBE/TTR-6 cruise of R/V Gelendzhik, July-August 1996

Editors: J.M. Woodside
M.K. Ivanov
A.F. Limonov

SC-97/WS/67 Part II

UNESCO 1997

For bibliographic purposes, this document should be cited as follows:
Neotectonics and fluid flow through seafloor sediments in the Eastern Mediterranean and Black Seas - Parts I and II.
IOC Technical Series No. 48, UNESCO 1997
(English)

Published in 1997
by the United Nations Educational,
Scientific and Cultural Organization
7, place de Fontenoy, 75352 Paris 07 SP

Printed in UNESCO's Workshops

TABLE OF CONTENTS

Page

II. BLACK SEA LEG

1. Introduction

A.F. Limonov

The study on the Black Sea Leg was carried out in several areas: (i) in the central part of this deep-water basin; (ii) in the Sorokin Trough on the Crimean continental margin; (iii) in the Pallas Uplift area south of the Kerch Strait; and (iv) on the Caucasian margin, within the Russian economic zone (Fig. 55). This study pursued different objectives for each discrete area. In the central Black Sea, the aim of the investigation was to bathymetrically map with a multibeam echosounder a field of mud volcanoes known from the previous TTR cruises (*Ivanov et al., 1992; Limonov et al., 1994*). In the Sorokin Trough, where gas hydrates were earlier obtained from sea bottom sediments by *Ginsburg et al. (1990)*, the primary goals concerned the elucidation of the structure of clay diapiric folds and the searching for mud volcanoes and other evidence for fluid flux through the seafloor. The task of looking for the seafloor manifestation of deep fluid emanation was set in the Pallas Uplift area. The multibeam echosounder surveying on the Caucasian margin was aimed at the construction of the first detailed bathymetric map of this area.

Investigations in the two last areas were undertaken in cooperation with ROSKOMNEDRA, whose financial support was an important contribution to the cost of the Black Sea leg of the cruise.

The same set of the methods as on the Mediterranean Leg was applied in the Black Sea (except for dredging).

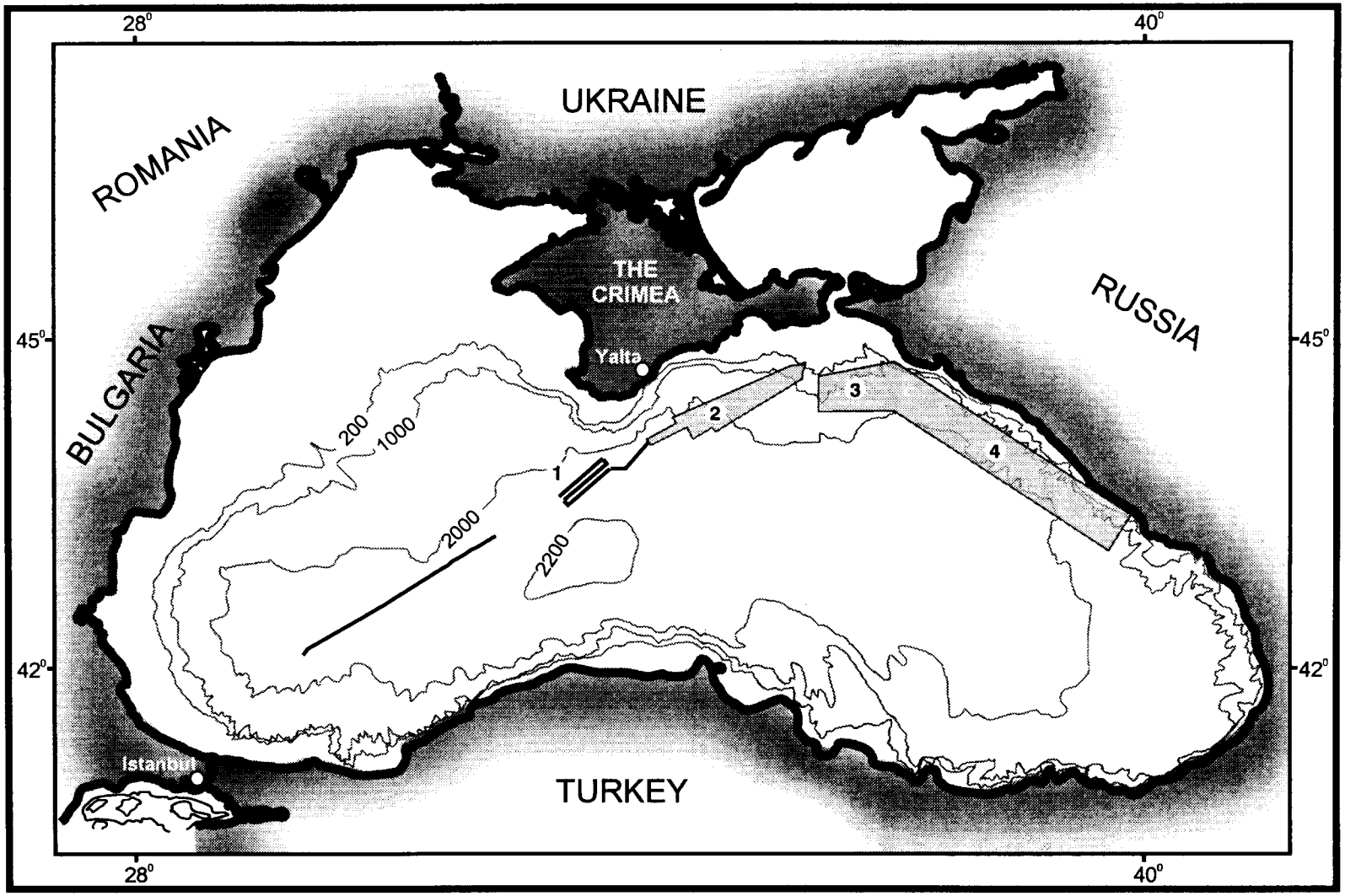

Fig. 55. Study areas in the Black Sea (ANAXIPROBE/TTR-6 Cruise):
1 - the central Black Sea mud volcano field; 2 - the Sorokin Trough; 3 - the Pallas Uplift area; 4 - the Caucasian margin

2. Bathymetric mapping in the central Black Sea mud volcano area

O.V. Krylov

Bathymetric mapping with the use of the Simrad EM-12S multibeam echosounder in the central Black Sea was an underway investigation during a transit from Istanbul to the Sorokin Trough south of the Crimea. It was aimed on obtaining a detailed bathymetric map of this area of mud volcanism that was studied on two previous TTR cruises in 1991 and 1993 (*Ivanov et al., 1992; Limonov et al., 1994*). Despite the rather dense system of seismic and echosounder profiles, the real relative elevations of many of the mud volcanoes discovered there remained unknown because profiles often crossed only their slopes. In addition to mud volcanism, the area is notable for a large-scale sliding of bottom sediments towards the southwest (*Limonov et al., 1997*).

Three echosounder lines oriented from southwest to northeast were run (Fig. 55) allowing us to cover an area with five mud volcanoes (MSU, Yuzhmorgeologiya, Kornev, Malyshev, and Goncharov). The map obtained (Fig. 56) shows that the waterdepth within the coverage (not taking into consideration the rising mud volcanoes) varies from 2060 to 2190 m, gradually increasing southwestward. Hence, the overall average inclination of the seafloor is only 1 : 186, nevertheless even such negligible inclination is capable of producing a regional sliding of gas-saturated bottom sediments. The main data on the surveyed mud volcanoes are summarized in Table 3.

Table 3
Main characteristics of the mud volcanoes in the central Black Sea

Name	Coordinates of centre		Diameter at the base (km)	Elevation above the seafloor (m)	Waterdepth over the top (m)	Width of flat top (km)
	N lat.	E long.				
MSU	43°31.92′	33°06.89′	4.2	60	2110	2.2
Yuzhmorgeologiya	43°31.21′	33°11.88′	4.0	110	2070	0.8
Malyshev	43°37.66′	33°22.34′	3.8	100	2020	0.5
Kornev	43°43.64′	33°28.93′	1.8	90	2010	0.3
Goncharov	43°42.05′	33°38.78′	1.7	100	2030	0.2

From the above table it is seen that some data on these mud volcanoes cited in recent publications (*Ivanov and Limonov, 1996; Ivanov et al., 1996b*), particularly those on their elevations, are not precise because they were obtained by means of interpolation between conventional echosounder records. Surprisingly enough is the low elevation of the MSU mud volcano (60 m *vs* 100-120 m) and the much higher elevation of the Malyshev mud volcano (100 m *vs* 60-70 m). At the same time, the diameters of the MSU and Yuzhmorgeologiya mud volcanoes turned out to be larger than defined before.

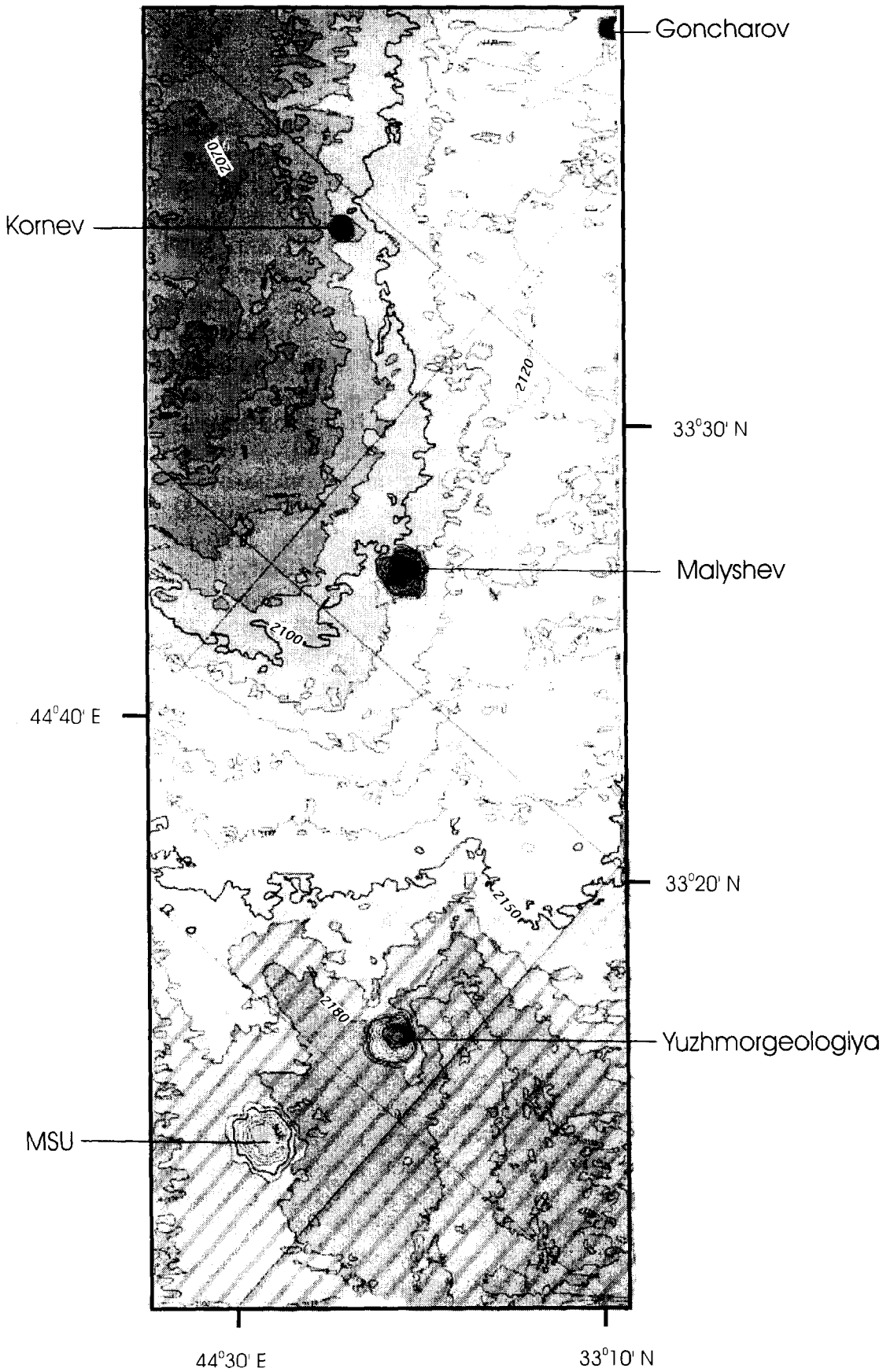

Fig. 56. Simrad EM-12S bathymetry map of the central Black Sea mud volcano area

3. The Sorokin Trough area

a. SEISMIC REFLECTION PROFILING

A.F. Limonov, L.B. Meisner, M.K. Ivanov, O.V. Krylov, E.V. Kozlova, G. Çifçi, S. V. Bouriak, A.L. Volkonskaya, S. Wagner, and V.G. Gainanov

The Sorokin Trough is located on the southeastern Crimean continental margin, at waterdepths of 600 to 2100 m. It extends for about 150 km from southwest to northeast and has a width of 50-60 km. The trough is considered to be the Crimean Alpine foredeep. This depocentre is filled mainly with the Maikopian (Oligocene-Lower Miocene) deposits that make up numerous clay diapirs. The thickness of this clay member reaches 5 km. The thickness of Quaternary sediments in the trough is also large, reaching 2 km. This thickness increases progressively to 3 km toward the paleo-Don/paleo-Kuban Pleistocene fan in the northeast (*Tugolesov et al., 1985*).

High resolution seismic reflection profiling was carried out along five lines oriented from WSW to ENE (PS-256 to PS-260) on the Crimean continental margin at waterdepths of 800 to 2100 m (Fig. 57). The profiling was accompanied by bathymetric swath surveying with the Simrad EM-12S multibeam system. Because the waterdepth decreases towards the northeast, the lines converge slightly in this direction to provide complete overlap of the bathymetric swaths.

Seismic members

Two principal seismic members can be distinguished throughout the seismic section.

Lower seismic member

The lower member was observed on profiles PS-256 to PS-258 and probably over a limited distance on profile PS-260. This member is inferred to have a rather broad age range, from the Upper Maikopian (Lower Miocene) to the Pliocene (*Tugolesov et al., 1985*). The upper surface of this member is difficult to correlate along and between the profiles because it represents a discontinuous group of reflectors often having a 'dispersed' pattern. The member is acoustically transparent, sometimes semitransparent, and is notable for the presence of numerous diffractions and side reflections from very rough topography. This produces a complex seismic pattern, which can be interpreted only in qualitative aspect. Short, high amplitude reflections are seen only in some places.

The thickness of this member is impossible to define from the seismic data obtained, but the available published data (*Tugolesov et al., 1985*) shows that it is in excess of 5 km.

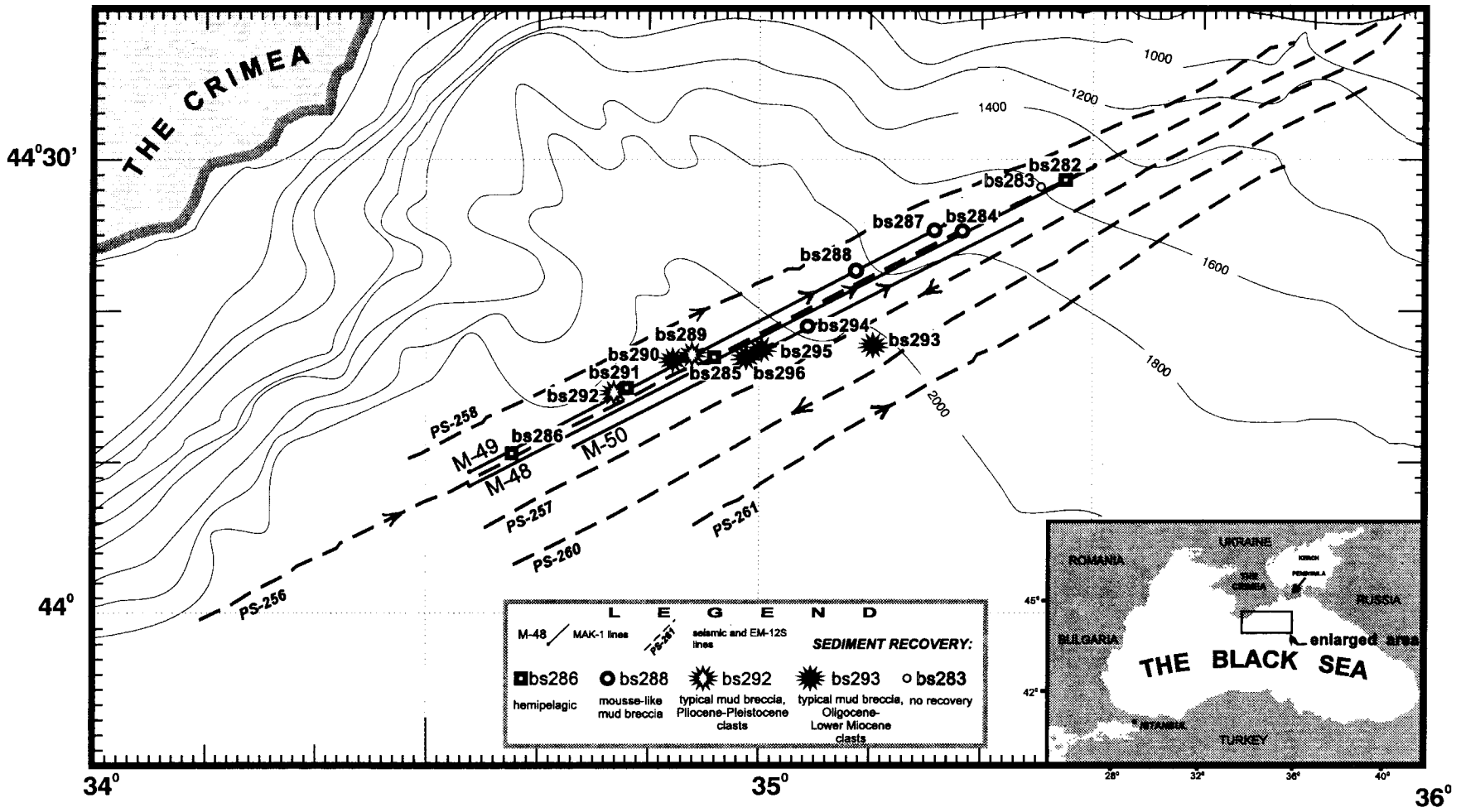

Fig. 57. Location map of seismic (including Simrad EM-12S) and MAK-1 lines and sampling sites south of the Crimean Peninsula (Sorokin Trough). The sampling sites are subdivided according to the types of the recovered sediments

Upper seismic member

The upper member was inferred to be Quaternary in age (*Tugolesov et al., 1985*). In turn, it can be laterally subdivided into fan deposits of the paleo-Don and paleo-Kuban Rivers and basinal deposits consisting of hemipelagic sediments and turbidites which were supplied from the Crimean Mountains. The lateral boundary between them is rather provisional. The fan sediments are traced from the northeastern part of the study area to the west, till approximately 35°E in profile PS-261 and 35°10′ in profile PS-258, where they merge with turbidites from the Yalta Canyon. The whole seismic section in profile PS-257 seems to be composed of the fan sediments. The maximum observed thickness of these sediments reaches slightly less than 2 s TWTT at the northeastern end of profile PS-261.

The fan sediments have an appearance typical of such deposits and are represented by the alternation of layered and acoustically transparent units. The abundance of the layered units and the amplitudes of their interior reflectors consistently decrease with distance from the shore, suggesting that this sequence gradually becomes more homogeneous in composition. The transparent units have a thickness of up to 500 ms. The stratified units, with a thickness of 50 to 200 ms, are characterized by a discontinuous layering. They are more wide-spread in the upper part of the Quaternary sequence. In profile PS-261 (from 05:40 to 06:30), at a depth of 300 ms bsf, there is a reflector marked by small irregularities which produce numerous diffractions. It is underlain by an acoustically transparent unit. The same feature is observed in less pronounced form in profile PS-260 between 17:15 and 17:40. This reflector is thought to correspond to the surface of slump deposits or grain flow.

The hemipelagic and turbiditic sediments, which are well-defined in the first halves of profiles PS-256 and PS-258, are distinguished by plane-parallel, continuous, and high amplitude reflections.

The upper member is characterized by the extensive development of bright spots that are normally observed above the tops and slopes of the diapiric structures developed in the lower seismic member. They probably testify to the presence of shallow accumulations of hydrocarbon gases. These negative-polarity, high amplitude, and relatively short reflections are distributed within the 250-800 ms interval bsf, and typical examples of them are shown in Figure 58.

Structure

The structure of the sedimentary cover is complex in the study area. It is almost completely governed by the deformation pattern of the lower seismic member. The tectonic disturbances in the upper member are also a reflection of the behaviour of the lower member.

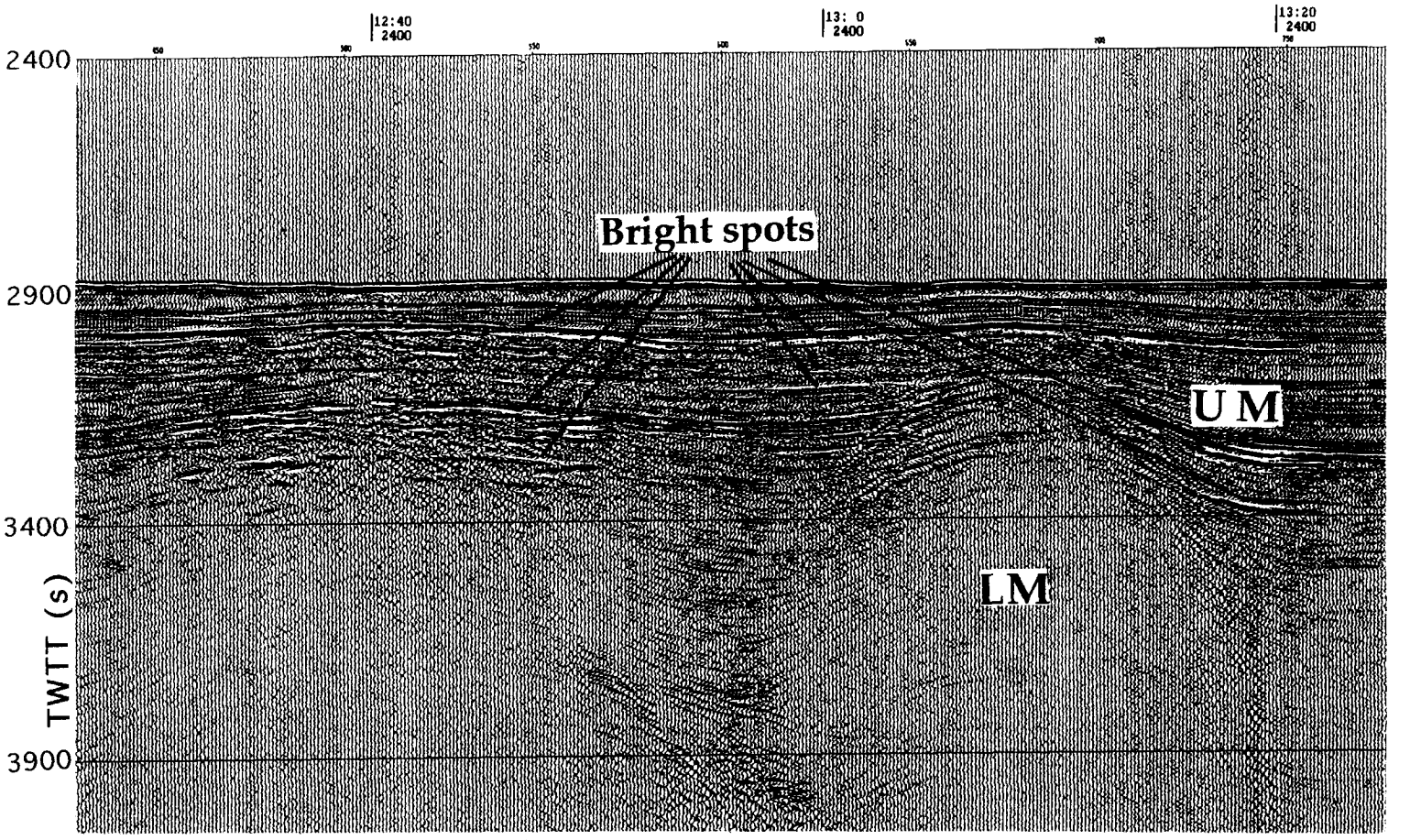

Fig. 58. Bright spots observed within the upper seismic member in seismic profile PS-256

Lower seismic member

This member is disrupted by numerous folds, complicated by faults. From previous studies (*Morgunov et al., 1976; Tugolesov et al., 1985*) it is known that folds in the Maikopian deposits are of diapiric nature; they have no roots, and the Maikopian structural pattern differs from that of the underlying Cretaceous-Eocene rocks. The available seismic data show that these folds pierce the overlying sediments, sometimes almost reaching the seafloor. The sediments included in the upper seismic member onlap the walls of these diapirs. The diapirs, in general, become more deeply buried northeastwards.

The frontal (seawards) diapiric folds have a southward vergence. This vergence is demonstrated by some folds in profile PS-258 (23:40-00:10) and PS-256 (11:35-12:00; 18:35-19:20). In other places, this is not so evident because the folds change their trends and they were crossed mostly obliquely.

In profile PS-258, from 00:20 to 02:20, one can clearly see that a large diapiric dome, with a visible height of 1.2 s, is complicated by secondary, small diapirs on its top. Both the dome itself and the secondary diapirs are well-expressed in the seafloor topography. The secondary diapirs have a diameter of 300-500 m and a height of up to 200 m.

Mud volcanoes have developed on the large diapiric bodies as well as on the secondary diapirs. Most of these occur on the slopes of the larger structures, probably because upward fluid migration is most active between the diapiric walls and surrounding sediments. When the parent diapirs are deeply buried, the mud volcanoes, which develop from them, are seen as narrow columnar disturbances on seismic sections. This disturbances terminate at the seafloor as positive topographic features. An example is shown in profile PS-257 (Fig. 59). Large diapirs which approach the seafloor closely are also often crowned with mud volcanoes, but these cases are not clearly imaged in the seismic sections. For instance, a large diapiric fold in profile PS-256 (16:20-16:40), and also recorded in the neighbouring seismic sections, corresponds to a wide, gentle seafloor dome on which a zone of mud volcanoes has developed, as observed on the MAK sonograph and profile (M-50; 05:00-09:00). The same is valid for a large diapir located further to the northeast along the same seismic line (PS-256). The presence of a mud volcano was first inferred on this line between 19:05 and 19:15 (Fig. 60), further indicated by the strong backscatter signature on the M-48 sonograph, and then confirmed by coring at Site BS-284.

An intricate positive structure can be traced near the northeastern ends of profiles PS-256 to PS-261. In profile PS-260-261, it plunges to a large subbottom depth (about 1 s TWTT) and can be poorly seen only as a broad, low amplitude anticline with an undulating top. In profiles PS-256 to PS-258, it has a very characteristic appearance, facilitating its reliable identification and correlation between the seismic lines. The structure is expressed in the sea bottom relief, but the corresponding seafloor high is shifted to the east with respect to its top at deeper levels. The structure is sharply asymmetrical in cross-section. Its eastern flank is gentle and long, while the western one is steep. Both flanks are complicated by faults, and the top is faulted as well. These faults are interpreted as listric, and they produce at least three individual anticlines. This structure

does not appear to be diapiric, and seems to have been formed by tension in a direction perpendicular to the general compressional stress vector (Fig. 61).

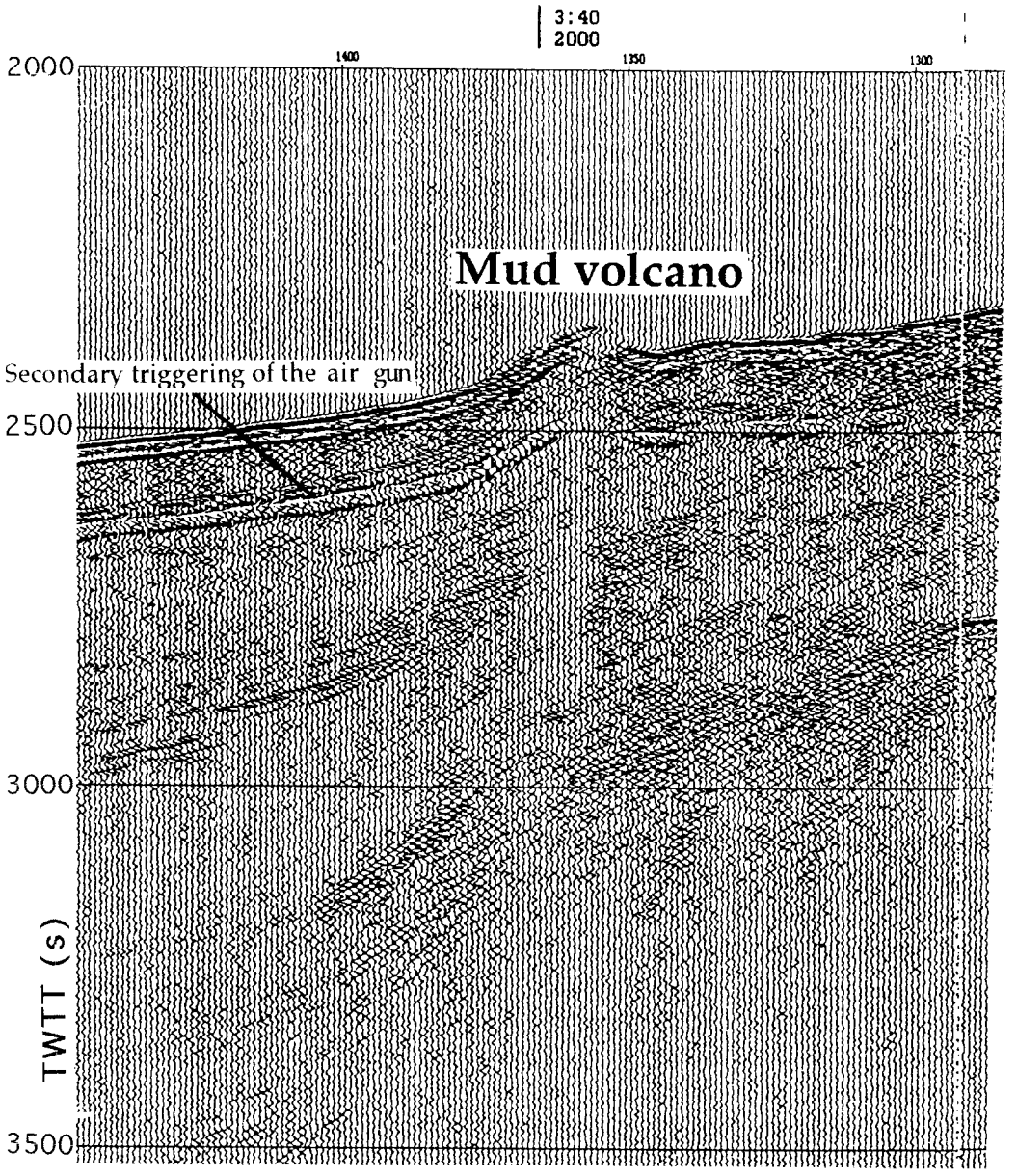

Fig. 59. Mud volcano rising from a wall of a deeply buried clay diapir. The mud volcano is situated slightly apart from seismic line PS-257

Upper seismic member

The upper member is generally weakly deformed, being slightly affected by the deformations in the lower member. Rare normal faults with offsets of a few tens of metres do not reach the seafloor. Beds in the upper member form gentle synclines between diapiric structures and bend up, onlapping margins of diapirs.

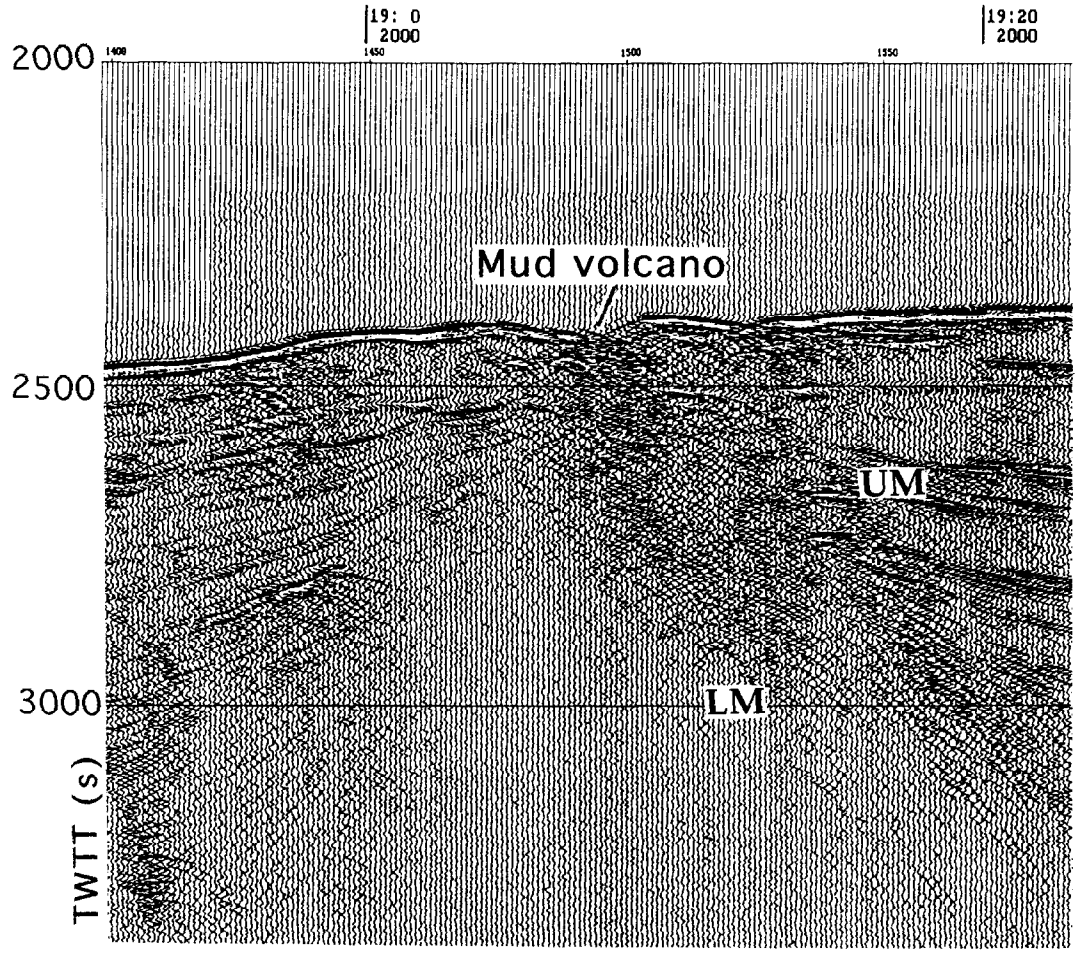

Fig. 60. Mud volcano on the top of a shallow buried mud diapir. Seismic line PS-256

Of particular interest is the structure of the upper seismic member in the extreme northeast of the study area. This region is notable for a dismembered relief consisting of a number of gentle ridges and valleys that in general form a fan-like feature widening upslope, towards the Gulf of Feodosiya, as is evident from the corresponding Simrad EM-12S bathymetric map (Fig. 62). This feature is mostly made up of sediments of the upper third of the upper seismic member, and the relief of the underlying sediments does not correspond to the relief of the seafloor (Fig. 61). The origin of this feature is believed to be largely depositional, and only little evidence for erosion is seen along the valleys walls. The ridges display a thin-bedded acoustic facies, whereas a chaotic seismic facies is observed below the valleys. The feature probably represents a system of submarine channels and levees and may belong to one of the youngest, previously unknown, branches of the paleo-Don/paleo-Kuban composite Pleistocene fan. Its unusual plan shape, narrowing toward the basin within the mapped area, can be explained by a tectonic control exerted by the growing folds in the lower seismic member, because these folds have trends concordant with that of the channels and levees (see below).

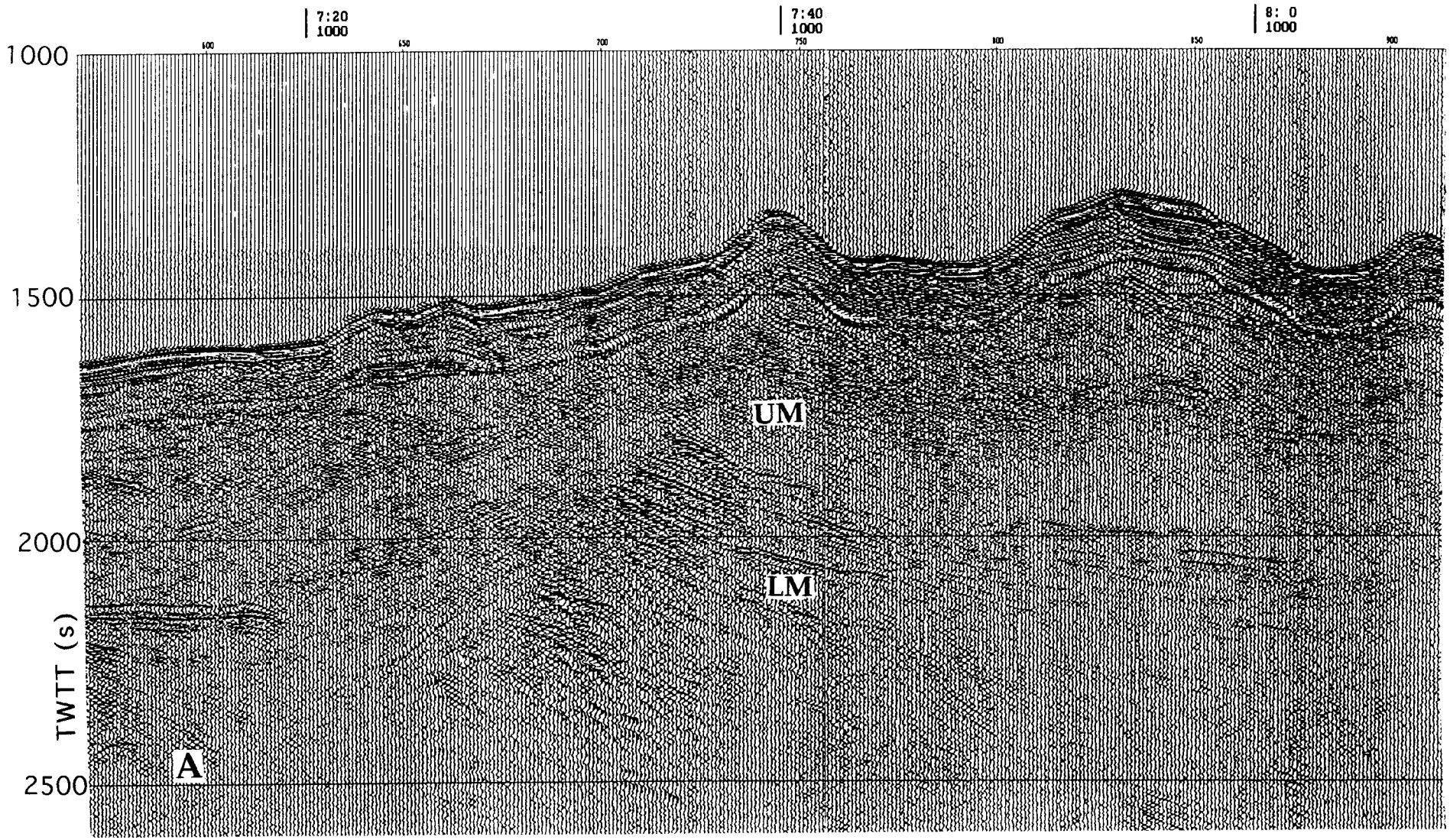

Fig. 61. See the next page

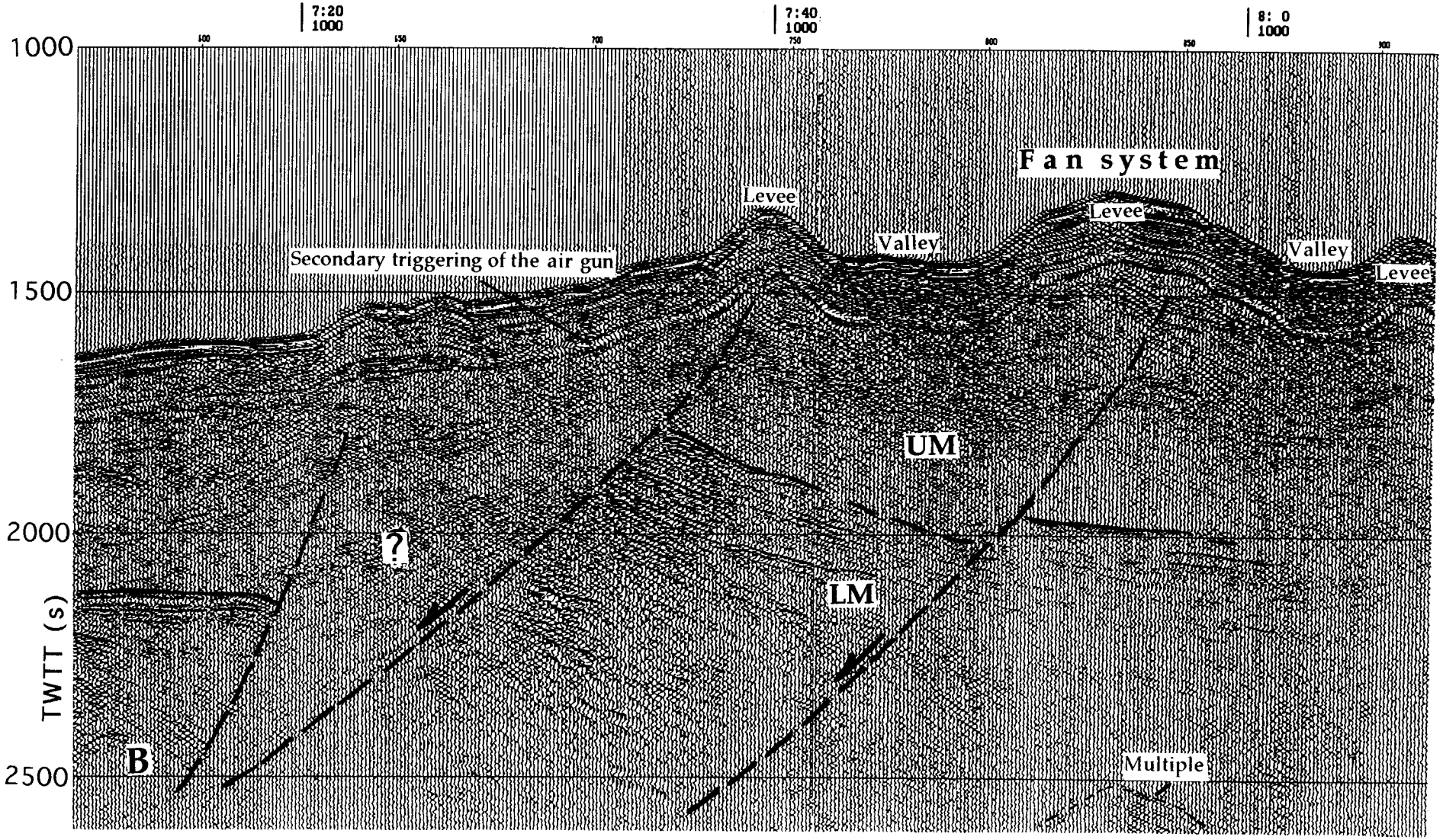

Fig. 61. An example of the tensional structure developing under conditions of compressional stress. **A**- original seismic section; **B**- its interpretation. **UM**- upper seismic member; **LM**- lower seismic member. (Seismic profile PS-258)

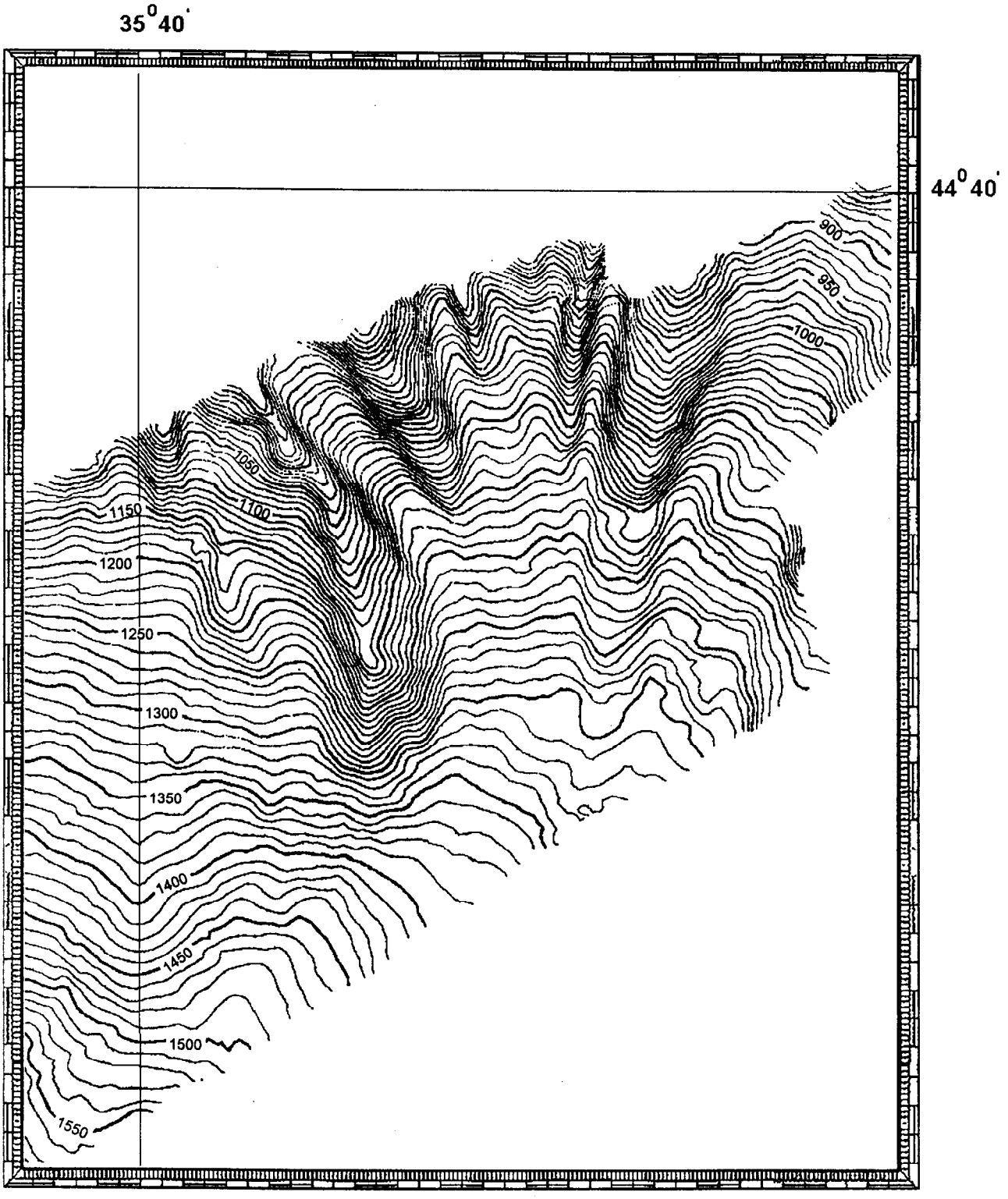

Fig. 62. Detail of the Simrad EM-12S bathymetry map south of the Gulf of Feodosia showing a fan-like feature of a depositional origin

Structural trends

Previous multichannel seismic reflection surveying along a system of lines oriented in S-N and NNW-SSE directions (*Tugolesov et al., 1985*) led to the conclusion that the diapiric folds in the Sorokin Trough have trends roughly parallel to the Crimean shoreline, and that further to the east they merge with the SW-NE-trending diapiric belt of the Kerch and Taman Peninsulas. This idea has been widely accepted for over 10 years. However, the investigation carried out during the TTR-6 Cruise revealed a much more complex pattern of the relationships of the diapiric folds. It turned out that their trends are to a great extent controlled by larger and deeper structures in the underlying Cretaceous-Eocene deposits (Fig. 63).

In the western part of the study area (around 34°30′E), the folds trend N25°-30° (zones 1 and 2), but to the east, between 34°40′ and 35°30′, they are characterized by sublatitudinal trends (zones 3 - 5). These easterly folds have curved shapes in a plan view, following the slopes of the buried Tetyaev Rise and Shatskii Ridge. From longitude 35°30′E to the east, the trends of the folds (zones 6 - 9) gradually change, first to NW-SE (N320°), then longitudinal, and finally to a N10° trend. The latter trend was defined on the basis of the seafloor morphology because the easternmost anticline was recorded only in profile PS-258. It should be noted that most of these structural trends fit well with the topographic trends derived from the multibeam echosounder map.

The observed trends of the clay diapirs are evidence of approximately south-north lateral tectonic compression. The rigid blocks of the Tetyaev Rise and the Shatskii Ridge, moving northwards (or northwestwards, in line with the scheme proposed by *Robinson et al., 1996*), make an impact on the northerly structures. The easternmost group of folds (zones 6 - 9), whose trend is roughly perpendicular to the direction of the assumed compression, was produced perhaps by listric faulting with block rotation, which also agrees with the proposed tectonic stress pattern (Fig. 64). Such an interpretation may imply that the Maikopian clay becomes more competent northeastwards, e.g., due to its stronger compaction or higher coarse clastic content.

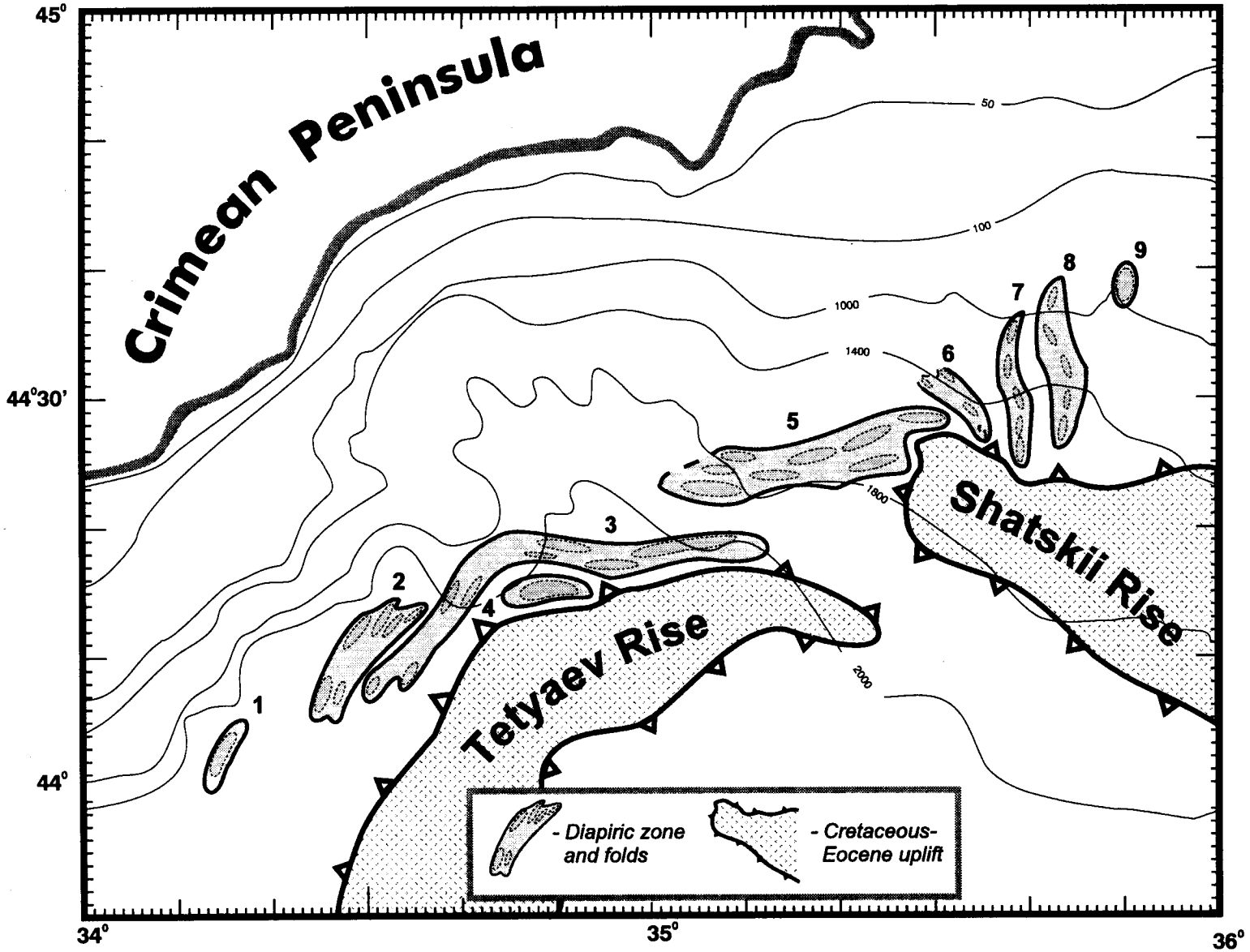

Fig. 63. Map of the structural trends of the diapiric zones and individual anticlines as recorded in the seismic profiles. The zones and folds are numbered (1 - 5 and 6 - 9 respectively) for the sake of convenience of the further description

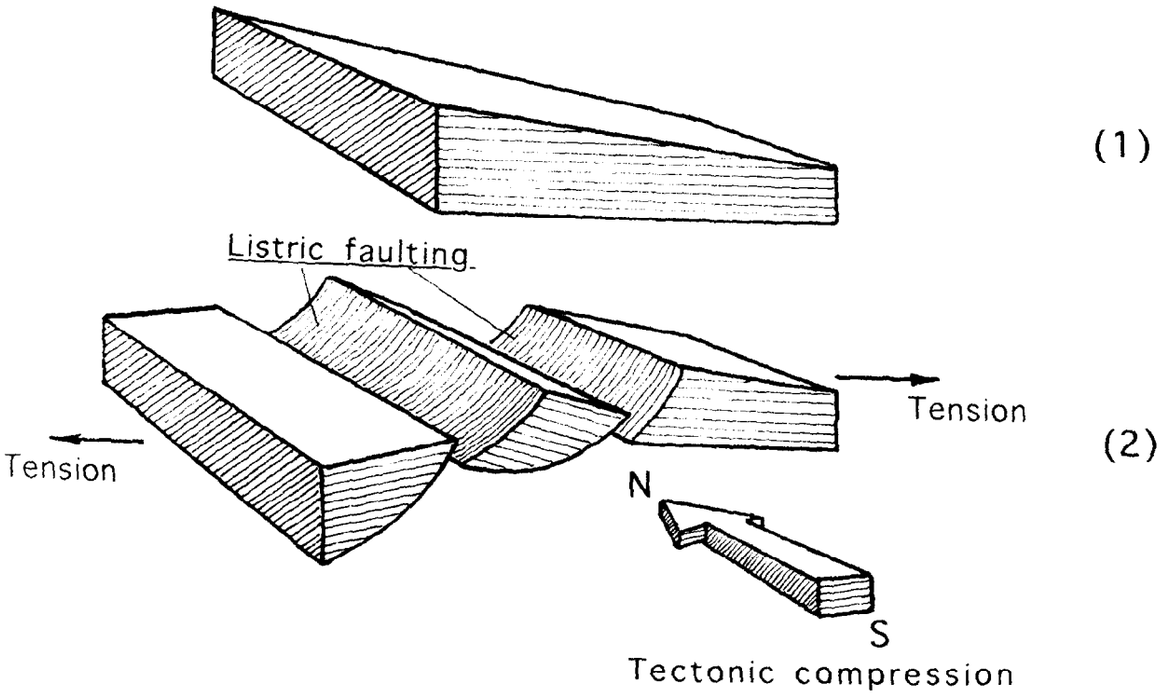

Fig. 64. Model of the formation of faulted extensional folds in compressional tectonic setting as applied to the anticlines observed in the Sorokin Trough east of 35°30´ E

b. DEEP-TOW MAK-1 SURVEY

J.-P. Foucher, A.F. Limonov, M.K. Ivanov, S. Wagner, J.M. Woodside, B. Swaak, B. Alpar Saban, and M. Lüdde

Lines M- 48 to 50 were run along the lower slope of the Crimean margin at water depths of about 1450 to 2100 m (Fig. 57). They are parallel to and are placed between seismic lines PS-256 and PS-258 in order to provide the possibility for the comparison of deep and shallow structures and seafloor features.

Line M-48

From the beginning of the record, at 13:50 on July 29th, to 15:50, the profiler data showed a flat seafloor with subparallel thin layers of sediments down to the maximum penetration depth of the profiler which in this area is about 40 m. A fault was crossed at 15:50 which is associated with a band of enhanced backscatter on the sidescan sonar image. The enhanced backscatter image suggests fluid seepage, but there is no evidence in the profiler data for gas escape, such as anomalously strong acoustic attenuation with depth. A particular feature on the MAK image from 13:50 to 15:50 is the presence of numerous sinuous lines of stronger backscatter. These lines are several metres to several tens of metres wide and some of them can be followed over distances of up to one kilometre. There is no apparent relief associated with them. It was noted that the distribution of these lines looks like the distribution of fissures produced by gas expansion in the recovered cores of gas-charged sediments. One possible interpretation of these features is therefore that they represent locations of fluids and gas escape through the seafloor; but this interpretation is not supported by the profiler data. The alternative interpretation is that these sinuous lines are initial tension fractures developed in the uppermost sediment before it starts to slide downslope. The sliding and slumping may be related to sediment instability due to shallow gas occurrence. An enhanced reflector is observed within the upper 10 m of subbottom sediments; and there is a clear indication later in the profiler data (from 16:00-16:02) for acoustic attenuation, probably due to gas escape, where there is an obvious acoustic void but surprisingly no associated response in the MAK image (Fig. 65).

The fault at 15:50 marks the beginning of an area extending to 20:10, with a series of faults (e.g. at 16:38) or flexures affecting the subbottom sediment. Typical spacings or wavelengths of the faults and flexures respectively are a few hundred metres. Flexures in the sediment are most pronounced from 19:00 to 20:10. The tension fractures facies on the MAK image extends with less numerous sinuous lines to 19:30. Lines with long linear segments trending generally N110-120° were observed at 19:38, 19:50, 20:10, and 20:18. Like the sinuous lines previously described, these linear features have no expression on the profiler record and their origin is assumed to be the same. From 19:00 to 20:50, the layering of subbottom sediments forms a typical 'migrating wave' pattern. The southern margin of a mud volcano, which is wholly seen on Line M-49, was viewed at 16:50 on the portside scan as an area of very high backscatter.

At 20:10 Line M-48 entered a broad area of active sediment deformation, mud intrusion or extrusion, and fluid seepage. This area extends to 02:00 (July 28th), over a distance of about 20 km. MAK profiler data and sonograph are complex throughout this area. Truncated stratified sedimentary sequences indicate active erosion at least at 21:22 and 21:55. This erosion is thought to be produced by turbidity currents from upslope, whose pathways are seen as fine seafloor striations between 20:40 and 22:30, crossing almost perpendicularly the well-developed tension fractures aligned along the continental slope. A highly reflective thick (10 to 20 m) sedimentary unit with obscured layering that could represent gas-charged sediments follows from 20:30 to 00:00. This unit is at a shallow depth (less than 15 m) and the sediments deeper than this unit are poorly penetrated by the subbottom profiler. After 22:00, the unit disappears, and a probable gas front is seen on the profile. Several plumes of enhanced reflectivity, which are observed between this gas front and the seafloor, could represent pathways for fluid or gas escape (Fig. 66).

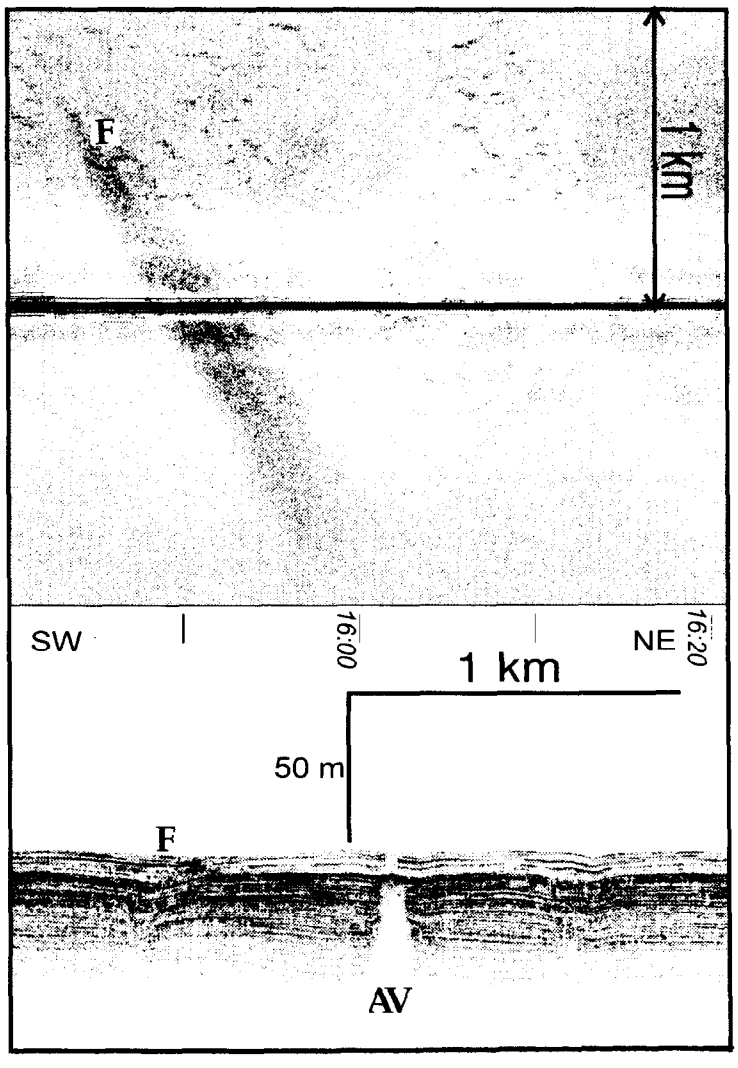

Fig. 65. A fault (F) which is probably accompanied by fluid escape through the seafloor (high backscatter band on the sonograph) and a distinct acoustic void (AV) northeast of it. MAK line 48

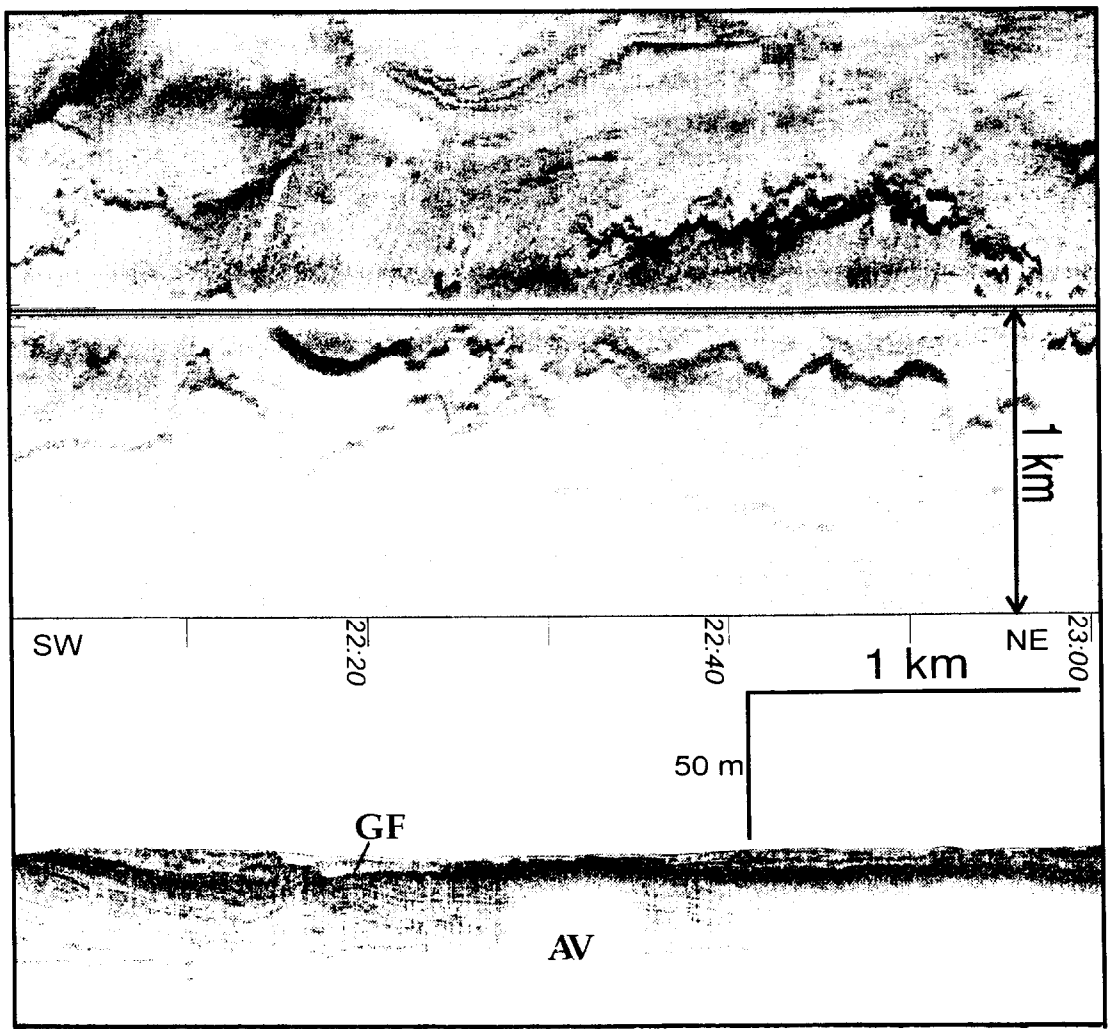

Fig. 66. Gas front (GF) and some acoustic voids (AV) in the subbottom profiler record. The sonograph shows well-developed tension fractures crossed at 22:20 by fine striations due to probable turbidity current action. MAK line 48

A prominent feature observed in this complex area between 23:40 and 01:00 is a band, about 3.5 km wide, with a highly variable backscatter strength. The gas front reaches the seafloor on the margin of this feature, at 23:52, but deepens until 01:00 which is as far as it can be traced. The gas front has a very rough relief which reaches the seafloor in places in the form of plumes. These plumes are marked by stronger backscatter on the sonograph. A band with highly variable backscatter is closely associated with rough seafloor topography (in general displaying a dome-like feature) and a weak seafloor reflection. The general orientation of the band is WNW-ESE. The northern part of a mud flow is then imaged on the right (south) side of the sonograph, from 01:00 to 02:00; and on the left (north) side, from 01:05 to 01:35, the southern termination of mud flows from a mud volcano is more completely seen on Line M-49. Both structures have a moderate backscatter, but their edges show a contrasting strong backscatter. Within the mud flow on the right side, a conical mound,

approximately 150 m in diameter, was clearly recognized at 01:10. It could represent one of the centres of mud extrusion. The profiler record, which did not cross the two mud flows described above, displayed strongly deformed sediments, truncated series, and recent infilling (by mud flows?) of some of the seafloor depressions created by the deformation.

From 02:00 to 06:00 the sonograph showed three principal acoustic facies: bands of enhanced acoustic backscatter trending NW-SE (02:00 to 03:30); a field of tension fractures (03:30 to 04:15), and streaks with contrasting backscatter (04:15 to 06:00).

The bands of enhanced backscatter have a width of 200 to 300 m and a visible length of about 1.5 km. They are clearly related to the subbottom sediment deformation, i.e. to the axes of gentle anticlinal folds in a layered sedimentary sequence which is 15-20 m thick. The bands are accompanied by continuous tension fractures. The field of tension fractures is characterized by thin, discontinuous, and curvilinear features, which have already been described above. They are aligned almost perpendicular to the MAK line direction and parallel to the local trend of the depth contours.

From this field and further along the line, up to 06:20, the profiler record showed that the subbottom sediments form two units: the lower one, about 5-8 m thick, is notable for a migrating wave acoustic pattern; and the upper unit, which lies on an erosional surface and has the same thickness, is distinctly less folded.

The streaks with contrasting backscatter are thought to be small amplitude sedimentary waves. There are some acoustic disturbances in the profiler data, such as intervals of enhanced attenuation (e.g. 05:15 to 05:35).

From 06:20 to 06:50, the stratified sedimentary sequence lies on an acoustically turbid layer (gas-charged sediments?) that becomes exposed on the seafloor at 06:50. An enhanced reflector is seen to underlie it, gradually rising from 20 to 12 m below the seafloor from 06:30 to 07:30. The acoustically turbid layer can be traced from 06:50 to 09:20 beneath the seafloor, never deeper than 7 m. Associated with the exposure of this layer on the seafloor, from 06:40 to 07:05, is a band of enhanced backscatter on the MAK image that indicates a flow of mud breccia from faults recorded in sonograph M-49 (see below). Two other centres of mud expulsion (about 400 by 200 m) are also observed at 07:20 and 07:40 (Fig. 67). Both of them have tails of enhanced backscatter that indicate the presence of debris flows. Sinuous lines with high backscatter were observed from 08:00 to 09:00.

The profiler did not penetrate the sediments from 09:10 to 10:25, whereas the seafloor is detected as a moderately strong reflector. Two large highly backscattering structures are imaged at 09:20 and 09:50-10:20. They are also interpreted as sites where mud breccia is exposed at the seafloor. The latter structure could be a collapsed mud volcano. It has a very irregular plan shape, and the profiler showed a rough but generally negative seafloor relief there.

From 10:20 to 11:30, the MAK image displayed a few sinuous lines (tension fractures) and a thin line with high backscatter that probably represents a telephone cable. This NE-SW oriented line is clearly observed from the time it enters the field of the sonograph, at about 11:20, until it disappears in the centre

of the sonograph near the structure recorded between time marks 09:50 and 10:20. One may suppose that the cable is buried by mud breccia to the southwest.

From 10:30 to 11:50, the seafloor is remarkably smooth, and the profiler record showed a strong subbottom reflector, undulating between the seafloor and a depth of 5-7 m, with a wavelength of 200-400 m. Stripes of high backscatter occur where this reflector intersects the seafloor at 11:30 to 11:40. This strong reflector was interpreted as a gas front.

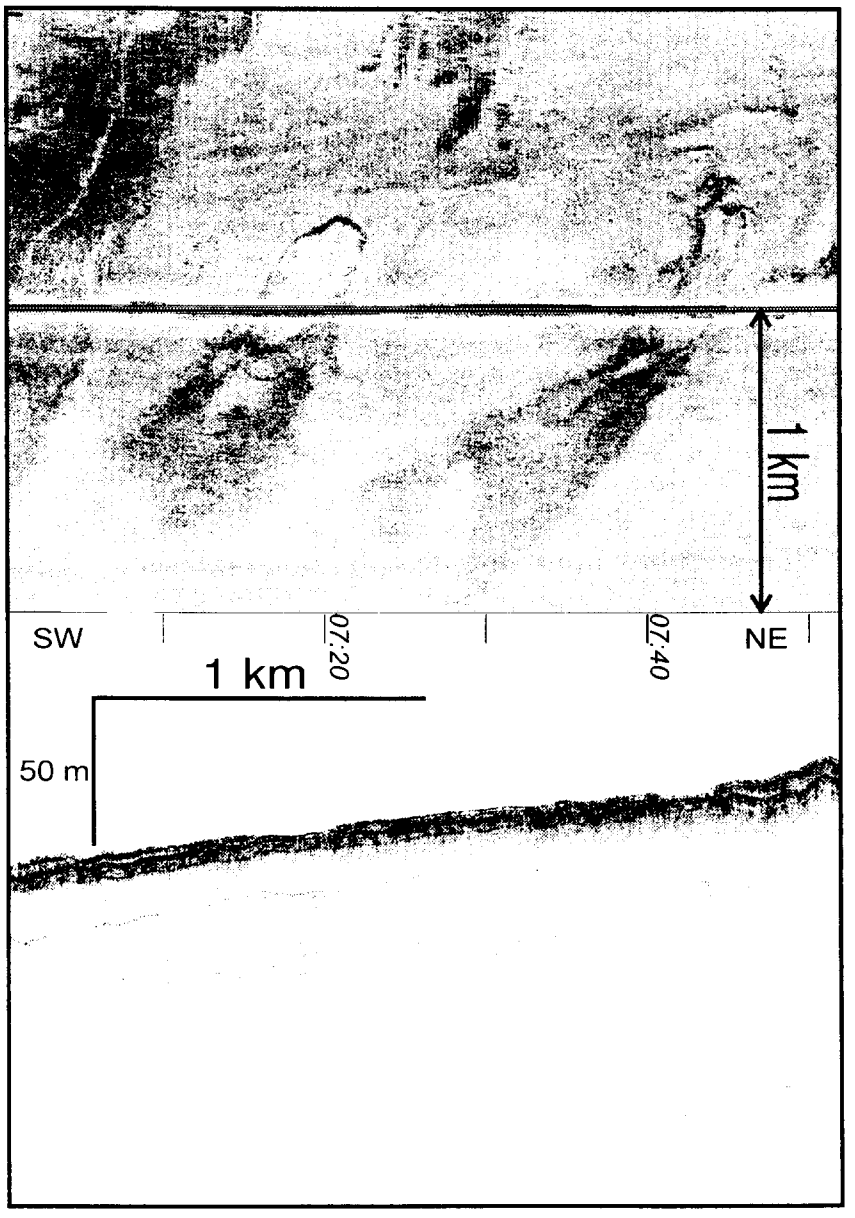

Fig. 67. Small centres of mud eruption with downslope flows of mud breccia. At the head of the right one there is a cone-shaped feature with a stronger backscatter. The profile shows acoustic turbidity in subbottom sediments. MAK line 48

From 11:50 to 13:45, both the sonograph and subbottom profile showed a complex seafloor pattern. The whole area appears to be affected by large-scale

sediment transport. The gas front is virtually exposed on the seafloor, and only rare reflectors are observed vaguely in a few places below the seafloor. The seafloor, whose slope steadily increases, is cut by two valleys, 200-400 m wide and 5-10 m deep, at 12:45 and 13:30. The general trend of these valleys is roughly N-S. The western valley bends around a circular, positive relief feature, about 400 m across, which has a rough, high backscattering surface. Its nature remains uncertain. This could be an accumulation of slumped sediments or a small gas dome. The eastern valley curves to the west down the regional slope. At the very end of the sonograph, from 13:45 to 14:20, some dispersed subbottom reflectors appear. The gas front dips beneath these reflectors down to a depth of 20 m from the eastern bank of the second valley. Numerous gas plumes extend to the seafloor from the gas front. The seafloor itself shows a fine striation directed downslope. It seems to have been caused by turbidity currents.

Line M-49

Line M-49 is subparallel to Line M-48 and about 1600 m to the north. Because of the short distance between Lines M-49 and M-48, most of the acoustic facies observed on Line M-48 are also found on Line M-49. Line M-49 began in the flat basin at the foot of the Crimean continental slope, with layered sediments observed to a penetration depth of about 30 m. The seafloor topography recorded by the profiler displayed, however, a broad arch of small amplitude (20-30 m) from 12:30 to 13:10. The arch is bordered by faults. Also, the stratified sediments are deformed by gentle folds with wavelengths of several hundreds of metres. These observations suggest that active compressional deformation is taking place at the base of the Crimean margin. Fluid and gas escape through the seafloor, probably triggered by the sediment deformation, is indicated by the presence of acoustic anomalies in the profiler data (e.g. from 12:10 to 12:20) and enhanced backscatter on the MAK image (e.g. at 12:20). The fault at 13:15, which bounds the gentle arch to the east, is also clearly associated with a 150 m wide stripe of enhanced backscatter, trending NW-SE. This fault is a continuation of that described in line M-48 at 15:50. Sinuous lines with high backscatter are common in the area and could represent initial tension fractures (see Line M-48).

Two mud volcanoes were imaged at 13:50 (on the left side) and 14:15 (on the right side) (Fig. 68). The first volcano is circular, about 600 m across, and has a dome-shaped morphology. A massive mud flow or a secondary centre of mud expulsion lies to southeast of it. The second volcano is a circular, conical mound about 800 m across. The profiler crossed its northern margin and showed prominent acoustic wipe-outs in the subbottom record. The two volcanoes probably lie on a NW-SE trending fault, associated with extensive gas seepage.

From 14:30 to 15:40, the seafloor is textured by alternating NNW-SSE bands of low and moderate backscatter. In the subbottom record, they correspond to low-amplitude folds which are expressed in the seafloor relief. The bands with enhanced backscatter coincide with anticlines whose tops also have an enhanced reflectivity on the profile. The bands are overprinted by almost transverse, smaller relief features aligned along the profile. They represent sedimentary

waves. The subbottom sequence demonstrates frequent local acoustic anomalies.

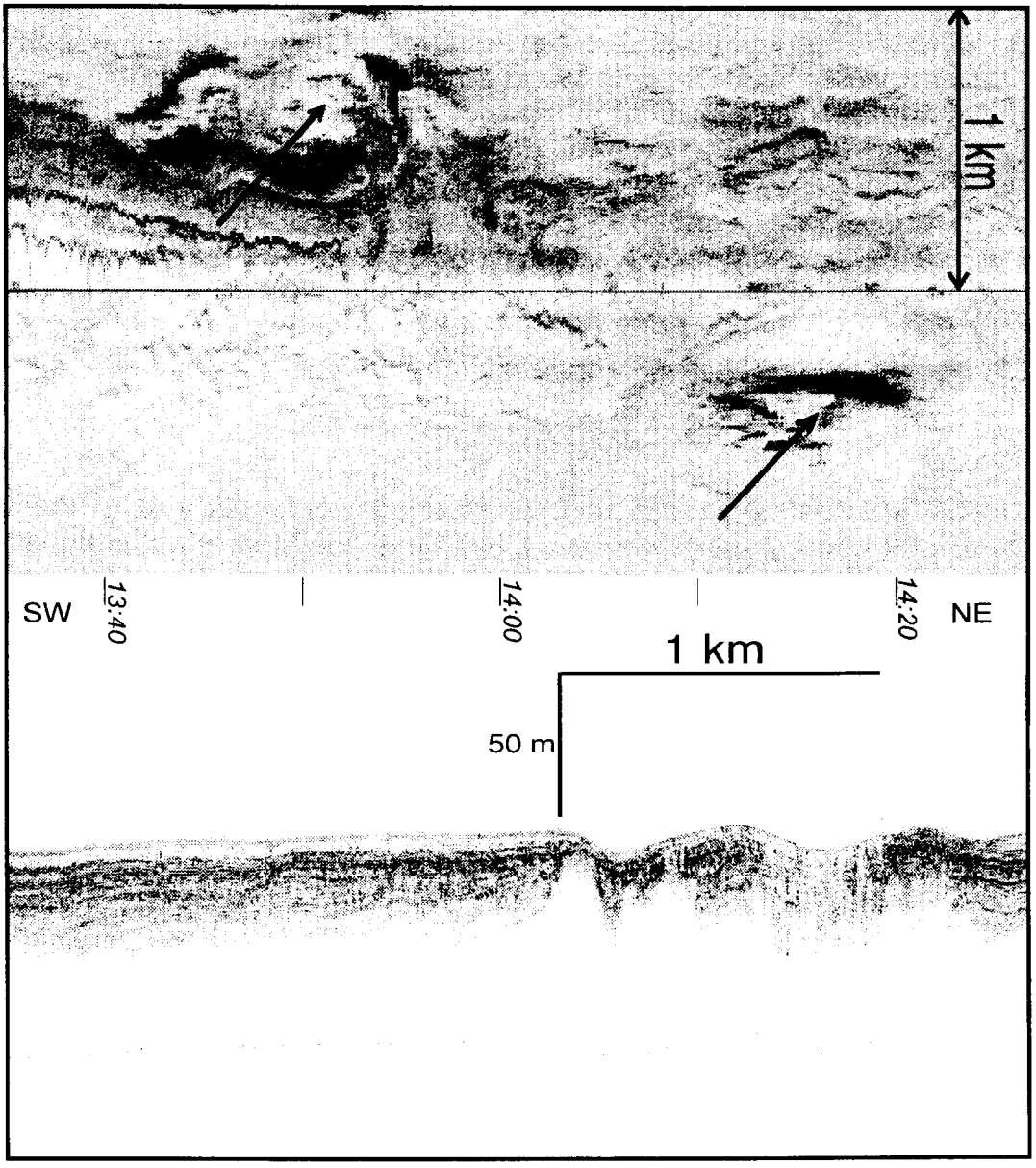

Fig. 68. Two similar mud volcanoes spaced about 1 km apart (arrows). Prominent acoustic wipe-outs and acoustic turbidity in subbottom sediments are associated with them. MAK line 49

At 15:45, a tongue of enhanced backscatter enters the MAK image from the north and approaches the central part of the record. The high backscatter could indicate gas seepage along a fault whose presence is suggested by the profiler record at 15:45.

From 16:00 to 18:20, a series of structures with several common characteristics can be observed on the MAK image. These structures are circular, 300 to 1000 m across, they show enhanced backscatter in their inner part and shadow or weak backscatter in their outer parts, and all display bright outer rims.

The most clearly imaged ones are observed at 16:05, 17:05, 17:40, and 18:02. The latter two structures, crossed by the profiler, clearly demonstrate that they are situated on a single dome with rough relief (Fig. 69). The dome is surrounded by a moat, especially well-expressed on its western side, where some collapse may have occurred. Acoustic wipe-outs occur below this dome. One interpretation of all these circular features is that they are collapsed mud volcanoes; and the coring results from the structures at 17:40 and 18:02 confirm this. All the circular structures appear to be located on a large structural high trending in an roughly east-west direction, and the dome at 17:35-18:10 marks its summit.

A strong reflector at the top of an acoustically turbid layer rises to the seafloor west of this summit area and is exposed on the outer moat wall. Then this reflector appears again beneath the seabottom on the other (eastern) side of the dome described above. It can be traced over short intervals across an area of complex deformation, erosion, mud extrusion, and probably fluid and gas seepage which is observed from 18:40 to 20:40. The MAK image showed a complicated pattern of irregular high and low backscatter features. Lineations of alternating high and low reflective stripes between 20:20 and 21:00 indicate a WNW-ESE structural direction which becomes west-east at the northern edge of the sonograph.

From 20:45 to 22:30, the profiler data showed a thin transparent cover (less than 7 m thick) of recent deposits on top of deformed, poorly stratified sediments. The horizon on top of the stratified sediments is highly reflective (enhanced reflector), and patches of acoustic turbidity stretching from it to the seafloor through the transparent layer (e.g. at 21:35) suggest gas escape at these locations. Gas escape probably accounts for the broad areas of enhanced backscatter observed on the MAK image, in particular near time mark 21:35.

From 22:30 to 01:20, profiler data showed deformed sediments with a migrating wave reflection pattern and young faults (e.g. at 22:50 and 23:21). The whole area exhibits moderate backscatter but with lineations of high backscatter that are clearly associated with faulting activity and gas seepage. Between 00:20 and 01:00, there are numerous sinuous lines of enhanced backscatter (tension fractures?).

From 03:00 to 04:35, MAK line 49 crossed a series of faults trending roughly east-west. Downslope-facing scarps of these faults can be seen from lines of high backscatter. Shorter lines also of high backscatter, several tens of metres long, could represent scars produced by slope failure. Mud extrusion along these faults has been proven by the recovery of mud breccia with gas hydrates at site BS-288. Gas escape, shown by a few big acoustic wipe-outs at, for example, 03:05 and 04:14, and the presence of mud flow on the seafloor are the most probable reasons for the high backscatter on the MAK image between 03:00 and 03:20 and between 03:40 and 04:35 (Fig. 70) The downslope continuation of the mud flow has been described above (MAK line 48, 06:40-07:05).

The rest of the line (04:35-05:50) is characterized by the absence of any notable features.

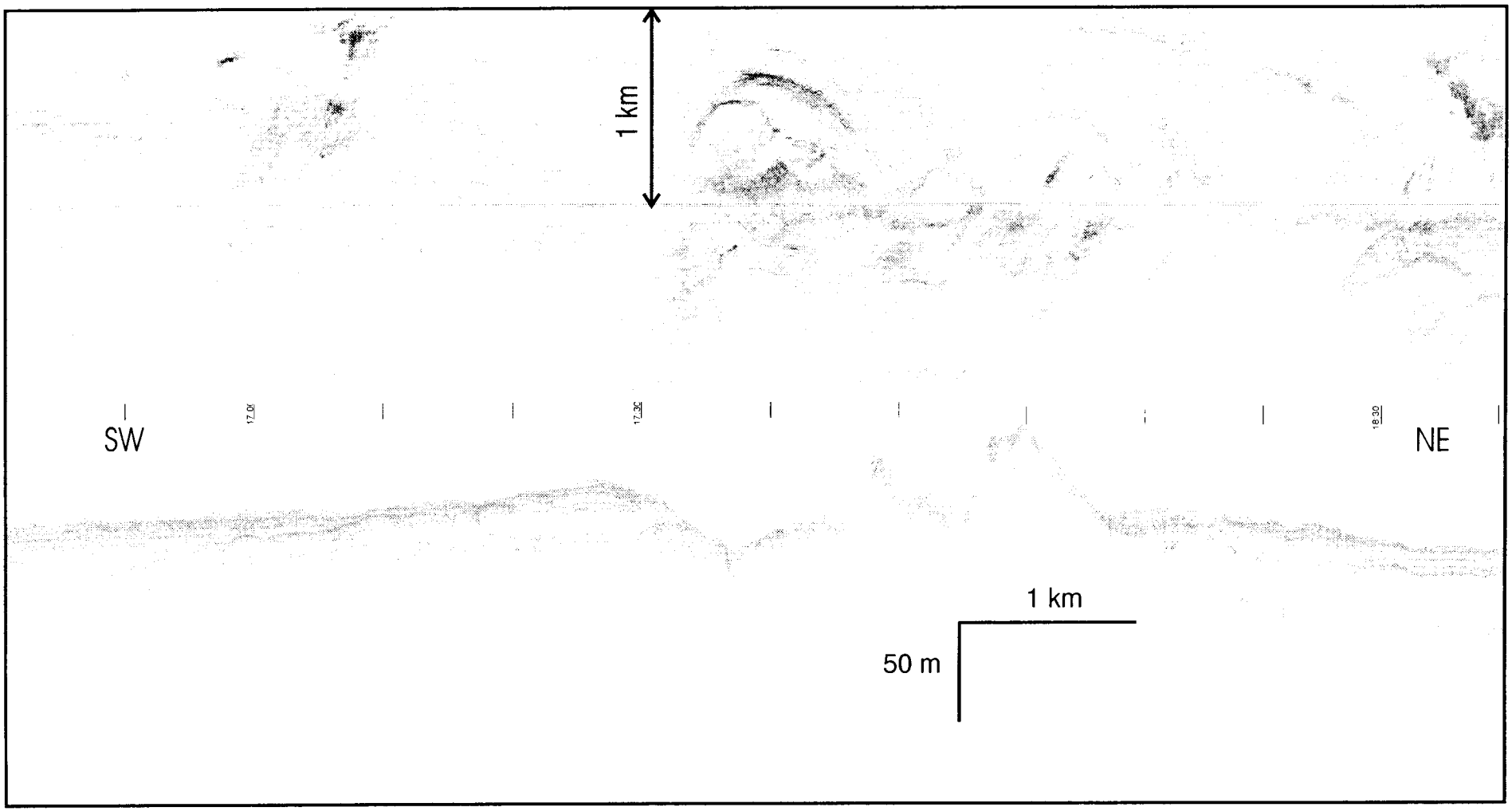

Fig. 69. Two merged, partially collapsed mud volcanoes. MAK line 49

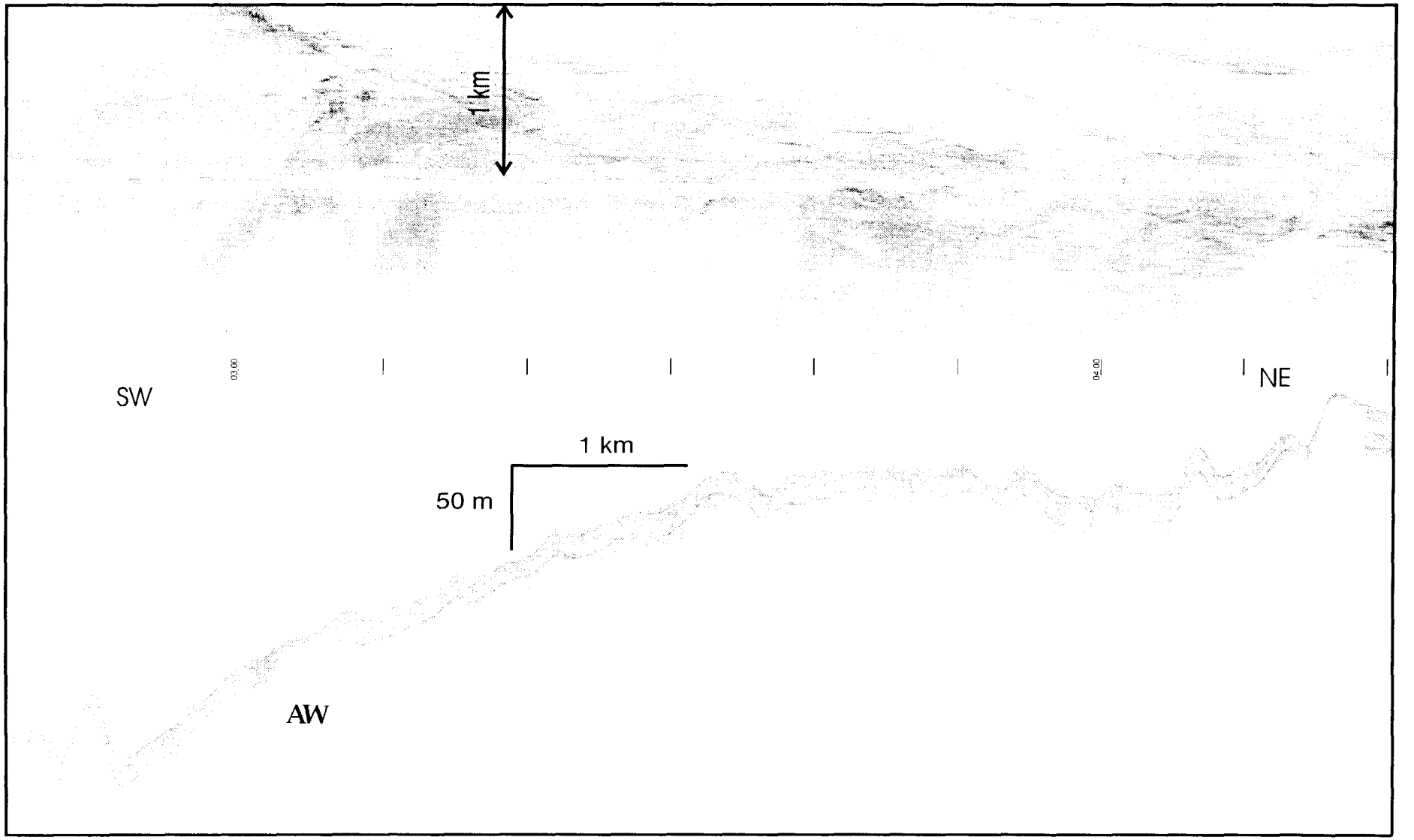

Fig. 70. Eruption of mud breccia from a system of parallel faults. An acoustic wipe-out (AW) is seen on the intersection of the mud flow and the fish track. MAK line 49

Line M-50

This line was run south of and parallel to line M-48. From the beginning of the sonograph to time mark 03:20, there is a field of tension fractures which have the same appearance as those described above, although some of them are wider and not so sinuous. A large dark spot recorded along track from 00:20 to 00:28 and the corresponding 'acoustic anomaly' on the subbottom profile are artifacts caused by the fish being towed too high above the sea bottom as a result of a winch problem. The subbottom profile showed a flat seafloor and a well-stratified sedimentary sequence, up to 40 m thick, until 02:20. A migrating wave acoustic pattern is observed on the profile from 23:20 to 01:40 (Fig. 71). The depressions between the ridges of these 'migrating wave' are filled with poorly stratified or semitransparent sediments of up to 15 m thick. Between 02:00 and 02:25, the sequence demonstrates a complex onlap pattern, which is conditioned by the presence of at least two strong reflectors related to erosional surfaces. Some faulting seems to be present as well.

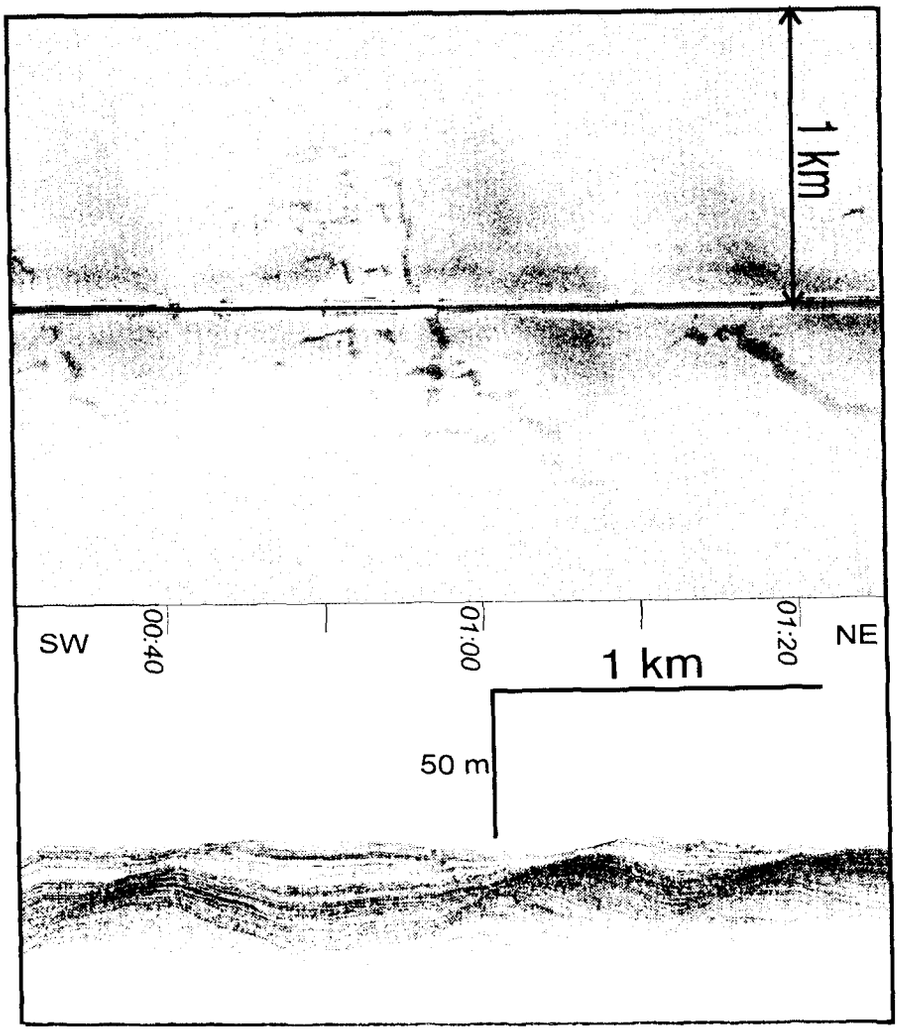

Fig. 71. Migrating wave acoustic pattern (contourites?) in the subbottom profiler record. The sonograph shows some tension fractures which are wider and not so sinuous as those described above. MAK line 50

A mottled pattern of acoustic backscatter can be seen between 03:20 and 06:20. Irregular dark patches (often sinuous lines) with strong backscattering are chaotically distributed on the generally low-backscattering seafloor. Between 05:20 and 06:20, these patches merge with each other, marking a wide area of possible fluid expulsion and mud extrusion. Some acoustic anomalies and probable faults are observed in this area on the profile. The thickness of the stratified subsurface sediments progressively decreases from the area with tension fractures toward the 'mottled area'. The lower part of this stratified sequence disappears on the transition to the 'mottled area', and the upper, poorly stratified, part pinches out at 06:05.

The next portion of the sonograph between 06:20 and 09:05 is notable for the presence of several mud volcanoes, three of which were crossed by the profiler and cored. The first mud volcano (between 06:45 and 07:05) which is about 1 km across and is slightly elongated in a W-E direction. It can be classified as 'a mud pie' (*Le Pichon et al., 1990*), because it has a very flat top and clearly-defined outer walls (Fig. 72). The top of the volcano has a very strong and uniform backscatter without any features. The subbottom profile suggests that the mud breccia is not covered by hemipelagic sediments, but its exposure on the seafloor is accompanied by a relatively low reflectivity. Some reflectors dip toward this mud volcano from the ENE. We named this structure 'the Dvurechenskii mud volcano'.

The second mud volcano, between 07:20 and 07:30, has a diameter of 800 m and irregular relief. Its eastern part rises 20 m above the western one. The backscatter is enhanced only in the central part of the mud volcano. The volcano is bounded by a system of concentric faults, some of which were recorded on the profile. A peculiarity of this mud volcano is a gas spout that is clearly visible on the unprocessed sonograph. The spout is about 50 m high.

Below the mud volcano, no reflectors were recorded, but they are present on both sides of it, showing numerous dislocations. The profiler penetration outside the mud volcano reached 35 m, and the upper part of the subbottom sequence is marked by a strong reflectivity with some acoustic voids.

Surprisingly, the core raised from this mud volcano contained relatively little gas. Thus, the gas venting, if it really takes place, occurs in a very restricted area of this mud volcano.

Two small, assumed mud volcanoes were observed on the right part of the sonograph from 08:00 to 08:15. They have an ellipsoidal shape in plan view and a probably conical cross-section. The available Simrad EM-12S bathymetric swath data suggests that the height of the two volcanoes does not exceed 10 m.

The last mud volcano found on this MAK line (08:51-09:02) has a height of about 20 m and a diameter of 850 m. Its northwestern boundary is not clearly outlined, and it is likely to be overlain by hemipelagic sediments that pinch out toward the top of the volcano. Two strong acoustic shadows suggest the presence of deep depressions on the southern slope. No subbottom reflectors can be observed below the mud volcano.

All of the mud volcanoes described above for MAK line 50 are situated within the same large structural high whose summital part was noted in Line M-49 between 17:35 and 18:10.

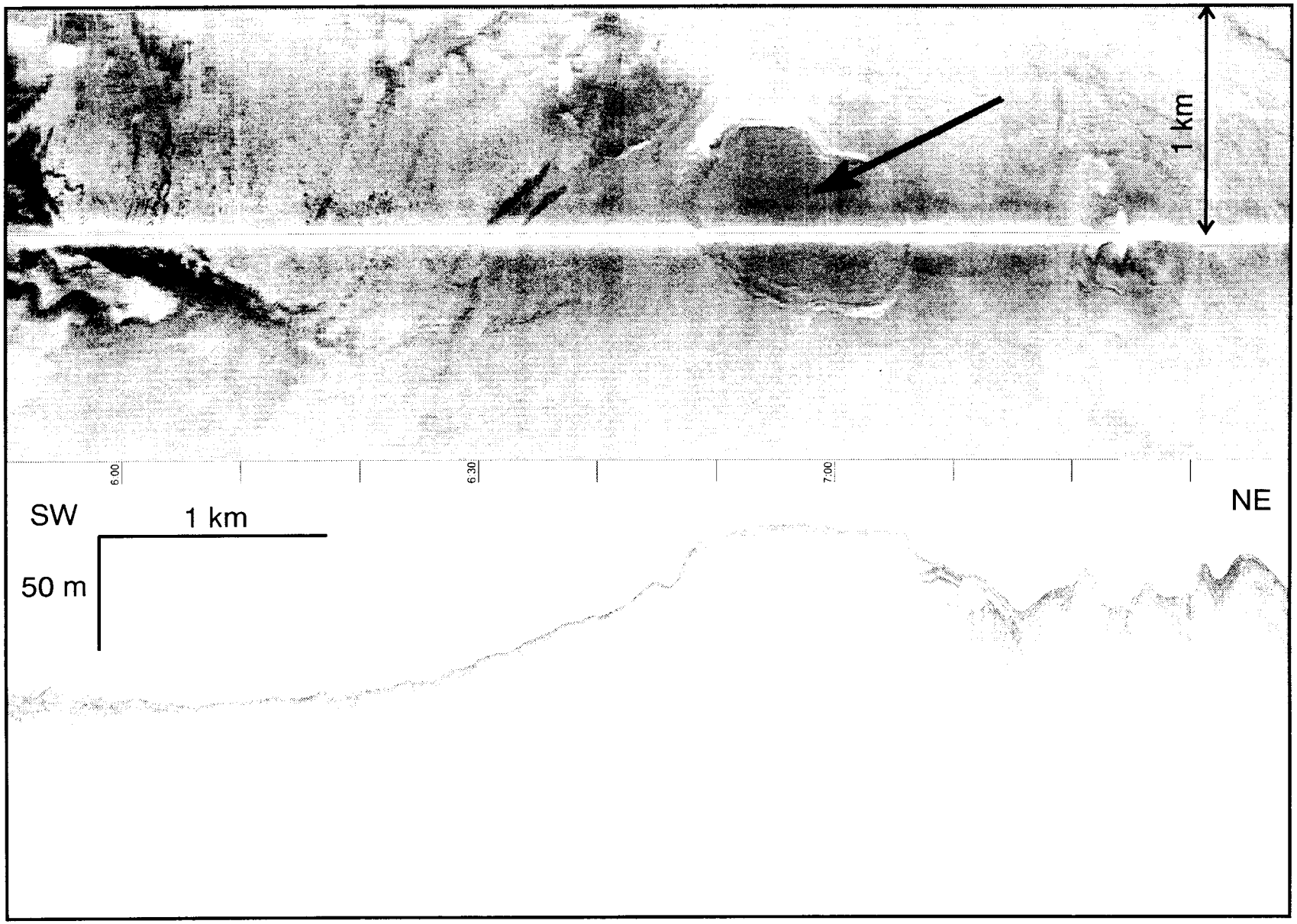

Fig. 72. Dvurechenskii mud volcano (arrow) which is morphologically similar to some 'mud pies' from the Barbados Ridge accretionary prism. MAK line 39

From 09:02 to 11:00, the seafloor is marked by an alternation of curvilinear features with low and moderate backscatter, about 150 to 200 m wide and up to 1.5 km long. They trend NNW-SSE. They are poorly expressed in the seafloor relief, but on the subbottom profile it is clearly seen that the light backscatter corresponds to the synclines of gentle folds in the subsurface sediments. Dark tones on the sonograph are inferred in this case to be caused by turbiditic accumulations trapped in grooves on the seafloor which were created by folding. The observed thickness of the sedimentary sequence is 15-20 m, and the lower part of it is marked by acoustic turbidity (gas occurrence?). Some small faults are also present in this area.

From 10:50 to 11:35, the sedimentary sequence thins progressively, and after the 11:35 time mark until the end of the line, no subbottom reflectors were recorded. The seafloor topography is dominated by gentle undulations with relief of 10-20 m. Between 11:00 and 11:20, the MAK image showed a large area, about 1 km wide, with strong backscatter. A tongue of this high-backscattering seafloor was crossed by the profiler between 11:00 and 11:07. The record showed a layer, about 5 m thick, of transparent sediment, which could correspond to a debris flow.

The final portion of line M-50, from 12:00, is characterized by mottled acoustic backscatter, which is caused by seafloor features having two trends. Discontinuous streaks on the seafloor with widths of a few tens of metres and lengths of more than one kilometre could indicate pathways for turbidity currents from the upper slope. They have NE-SW trends. They are onlapped by more isometric features with variable but generally stronger backscatter and a flow-like appearance. These features are thought to be slumps.

c. CORING RESULTS

A.M. Akhmetjanov, M.K. Ivanov, A.J. Doets, G.G. Akhmanov, A.V. Korkin, E.V. Kozlova, S.S. Gablina, A.P. Sautkin, S. Woodside, I.Yu. Belen'kaya, and A.N. Stadnitskaya

Introduction

A total of 15 core sites were selected for sampling during Leg 2 of the ANAXIPROBE/TTR-6 Cruise in the Black Sea on the Crimean continental slope and rise. In general 14 attempts were quite successful, and at Site BS-283G we failed to take bottom sediments except for a handful of fine sandy sediment in the core catcher. Total recovery was about 33.5 m, with the longest core being 602 cm and the shortest one of 28 cm. All the cores were collected using a gravity corer with a length of 6.6 m.

Fourteen core stations have been planned after the preliminary interpretation of the MAK-1 sonographs and profiles, and one coring site was selected on the basis of the EM-12S and seismic data from previous years. The main purpose of the coring was to calibrate MAK-1 acoustic facies and to confirm the existence of mud volcanoes and fluid flow.

The location of each coring site along the MAK-1 lines is shown in Figure 57, and the coring sites coordinates, together with technical details, are given in Table 4. Core description sheets were generalized as shown in Figures 73 to 86.

Further information on the cores, such as brief sedimentological data, sonar acoustic facies at the coring sites, and geological/geographical setting is shown in Table 5.

General Core Description

According to the general coring strategy, the core descriptions are arranged with respect to the MAK-1 or EM-12S lines they belong to.

MAK-1 line M-48

Totally 5 gravity cores were taken along this line and they are described below.

Core BS-282G. The first core was taken on the Crimean Peninsula slope with a general inclination toward the southwest, in an area of a high acoustic backscatter seen on M-48 sonograph and with a penetration of a few metres on subbottom profiler record. The core was hemipelagic (Fig. 73), and 2.89 m was recovered. The core contained the typical Black Sea sedimentary units, such as recent soupy upper horizon of fine alternation of sapropel, dark grey mud, and a coccolith ooze laminae; a sapropel layer (at 2.1 m); and a grey clay layer with a hydrotroilite admixture. Both sapropel and grey clay layer lying below revealed well-expressed features of slumping.

Table 4
General information on the cores sampled in the Sorokin Trough

Core No	Date	GMT	Latitude	Longitude	Cable Length (m)	Depth (m)	Recovery (cm)
BS-282G	30/07/96	19:38	44°28.58	35° 27.49	1740	1630	289.5
BS-283G	30/07/96	21:31	44°28.18	35° 25.38	1710	1629	15
BS-284G	30/07/96	23:23	44°25.27	35° 18.35	1840	1768	307
BS-285G	31/07/96	2:47	44°16.93	34° 56.05	2200	2100	139
BS-286G	31/07/96	7:49	44°10.59	34° 37.81	2267	2095	586
BS-287G	1/08/96	10:38	44°25.33	35° 15.86	1790	1701	245
BS-288G	1/08/96	12:20	44°22.64	35° 08.81	1980	1847	240
BS-289G	1/08/96	14:57	44°17.07	34° 54.06	2240	2119	57
BS-290G	1/08/96	16:29	44°16.87	34° 52.36	2200	2017	28
BS-291G	1/08/96	17:48	44°14.81	34° 48.07	2210	2067	602
BS-292G	1/08/96	19:10	44°14.58	34° 47.15	2280	2100	60
BS-293G	3/08/96	20:03	44°17.71	35° 10.42	2040	1950	102
BS-294G	3/08/96	22:06	44°18.95	35° 04.44	2080	2024	160
BS-295G	3/08/96	0:40	44°17.35	35° 00.05	2170	2090	216
BS-296G	3/08/96	2:30	44°16.92	34° 58.93	2162	2062	322

Table 5
Brief sedimentological data and sonar acoustic facies at the coring sites

Core No	General Sedimentological Information	Sidescan Acoustic Facies
BS 282 G	Hemipelagic section with sapropel layer and grey Pleistocene clay at the bottom	Mottled enhanced backscatter on MAK line M-48
BS 283 G	No recovery, terrigenous sand in core catcher	High backscatter patch on MAK line M-48
BS 284 G	Mousse-like mud breccia with three layers of typical breccia;clast with Pleistocene bivalves	High backscatter patch on MAK line M-48
BS 285 G	Hemipelagic section consisting of Pleistocene clay, disturbed by microfaults	Bands of high backscatter on MAK line M-48
BS 286 G	Hemipelagic section , gas-saturated crumbly clay, interbedd. with sapropel layers	High backscatter patch(+low bs.spots)on MAK line M-49
BS 287 G	Mousse-like mud breccia with typical clasts;e.g. limestone containing Pliocene ostracod	Low to moderate backscattering on MAK line M-49
BS 288 G	Mousse-like mud breccia with 20 cm sapropel layer with clasts. Gas hydrates at bottom	Elongated patch of high backscatter; MAK line M-49
BS 289 G	Mud breccia topped by a few mm of recent sediment. Gas hydrates in lowest part of core	Generally strong, sharply variable backscatter on MAK line M-49
BS 290 G	Mud breccia with fragments of Oligocene - L.Miocene Maikopian clays. Gas hydrates (lost)	High backscatter patch (300m) on MAK line M-49
BS 291 G	Hemipelagic section,top - gas-sat.clay & sapropel alternation; bottom - grey clay with silt	Low to moderate backscatter on MAK line M-49
BS 292 G	Mud breccia, gas-saturated, matrix supported, H_2S. Gas hydrates in lowest 60 cm.	High backscatter on MAK line M-49
BS 293 G	Mud breccia, gas-saturated with Maikopian claystone clasts, topped by thin recent sediment.	High reflectivity on Simrad EM-12S record
BS 294 G	Mousse-like mud breccia;two sapropel layers;carb.crust with microbial mats;gas hydrate	High backscatter patch (500m) on MAK line M-50
BS 295 G	Mud breccia, matrix supported with clasts of Maikopian claystones	Enhanced backscatter on MAK line M-50
BS 296 G	Soupy mud breccia, strongly gas-saturated with clasts of Maikopian claystones	High backscatter on MAK line M-50

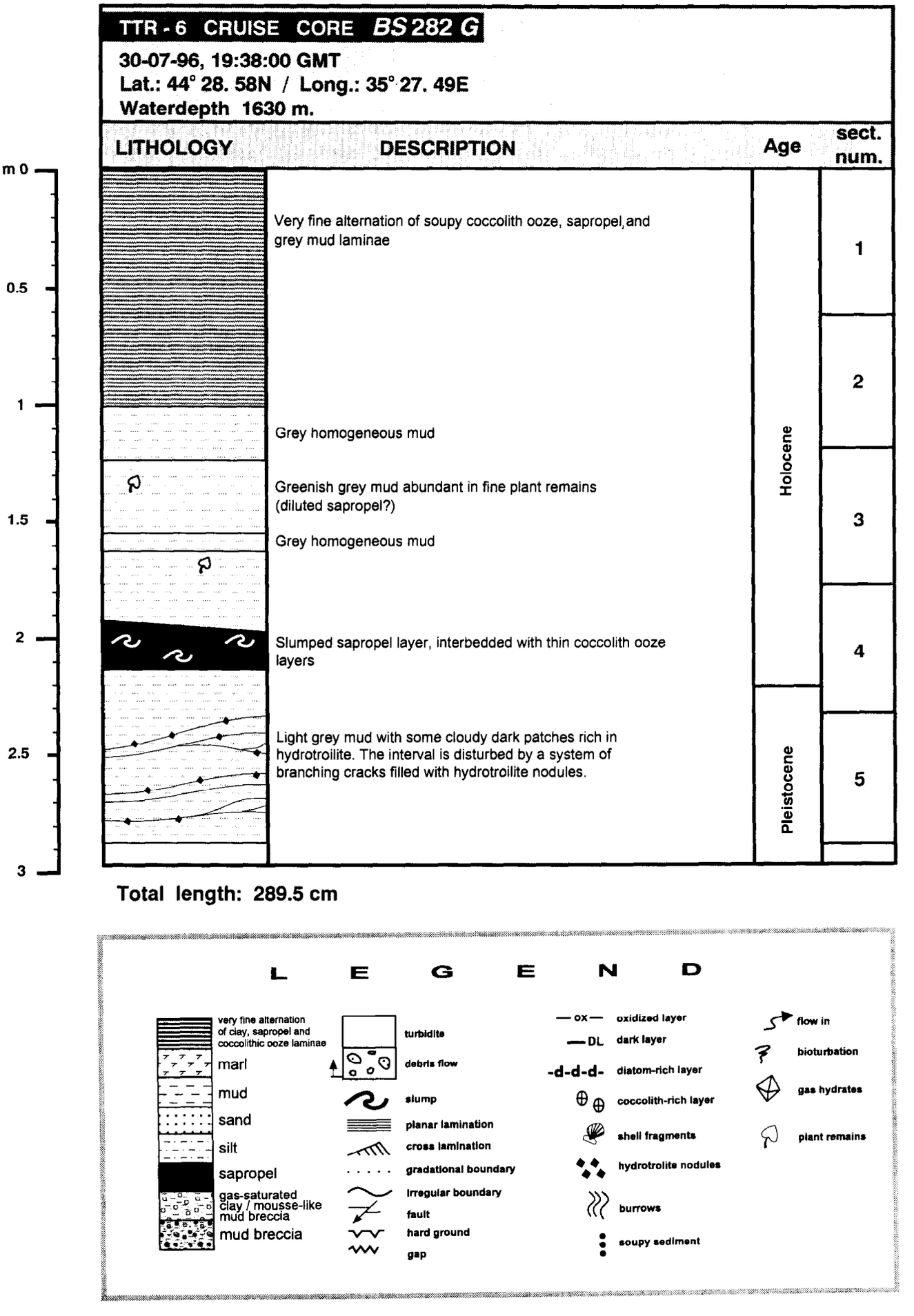

Fig. 73. Core log BS-282G and legend

Core BS-283G. The core was taken on the Crimean Peninsula slope to the southwest of BS-282G from a patch of a high acoustic backscatter with a diameter of about 500 m as seen on the MAK sonograph. The core revealed a small amount of fine to medium sand with bivalve shell fragments.

Core BS-284G. The core was taken on the Crimean Peninsula slope, 10 km to the southwest of BS-283G, in an area of high acoustic backscatter and with no penetration on the subbottom profiler record. The recovered sequence was 3.07 m in length (Fig. 74) and contained a layer of dark grey matrix-supported mud breccia in the upper 50 cm. A layer of the same lithology was found also at 1.5 m. Below this layer, a clast of limestone of a variable consistency and with a large number of the typical Pleistocene bivalve shells was found. The rest of the core was mainly composed of grey, gas-saturated clay with a crumply structure interpreted as a mousse-like mud breccia. A layer of breccia with carbonate rock clasts (up to 3 cm in size) produced by a downslope movement was recognised at 2.5 m. The whole core had a smell of H_2S.

Core BS-285G. The core was sampled on the Crimean continental rise, where the seafloor is generally gently sloped toward southeast in an area with a rather complex acoustic backscatter pattern (dark and light ragged bands with no penetration on the subbottom profiler record). The core was hemipelagic (Fig. 75), and 1.4 m was recovered. The bulk of the sequence was represented by grey clay overlain by a thin layer of recent soupy sediment. The grey clay was Pleistocene in age, according to the defined coccolith assemblage. Microfaulting was observed along the Pleistocene interval.

Core BS-286G. This core was taken on the Crimean continental rise, from the seafloor area generally gently sloping southwestward. On the sonograph, the area is marked by several highly backscattering spots within a positive seafloor feature about 0.7 km in diameter. The subbottom profiler recorded a well-stratified sequence with a penetration of up to 50 m, although the sampling site was at a significant distance from the profile. The core was hemipelagic (Fig. 76), and 5.9 m of sediment was recovered. The upper 70 cm was represented by a typical alternation of sapropel, dark grey mud, and coccolith ooze laminae. The rest of the core was a sequence of grey crumply clay, gas-saturated, and interbedded with numerous sapropelic layers of different thicknesses. The boundaries between the grey clay and sapropelic layers were mainly transitional, although sometimes showed a sharp base of the clay layers and an eroded top of the sapropel layers.

Micropaleontological study revealed the abundance of Pleistocene coccolith species from the grey clay layers and established a Holocene age for the sapropelic layers. The entire core had a smell of H_2S.

MAK-1 line M-49

A total of 7 cores were taken along this line (see below).

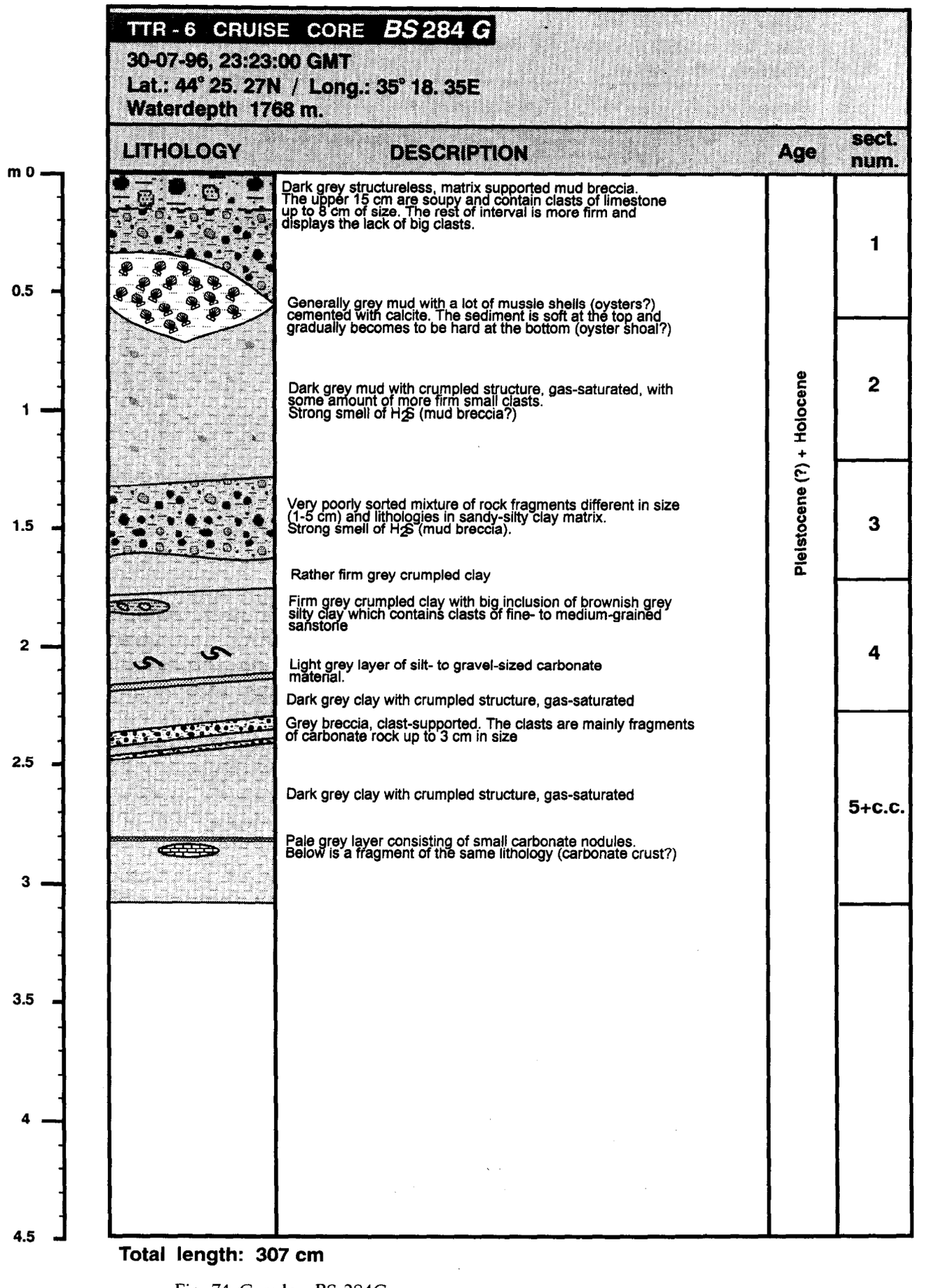

Fig. 74. Core log BS-284G

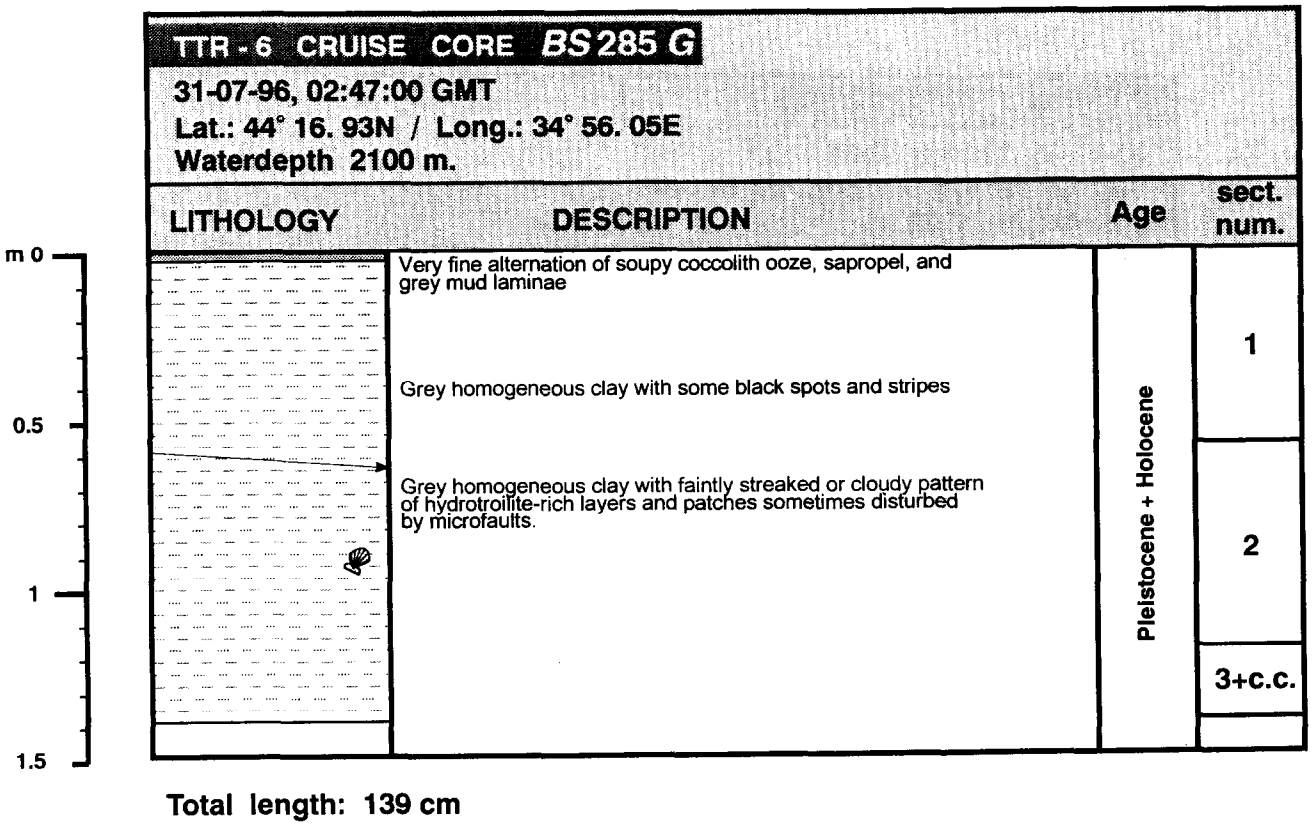

Fig. 75. Core log BS-285G

Core BS-287G. The core was raised from the lower Crimean slope, from an area of a low to moderate acoustic backscatter seen on the MAK-1 sonograph, and with no penetration on the subbottom profiler record. The site was interpreted as a mud volcano with a diameter of about 800 m. The core recovered mainly mousse-like mud breccia overlain by a recent fine laminated horizon with a thickness of 20 cm (Fig. 77). The total recovery was 2.45 m. The mousse-like mud breccia interval included a layer of mud breccia enriched with clasts of different lithologies at 0.7 m. One of the clasts was represented by limestone, containing an ostracod shell dated as Pliocene in age. The entire core revealed a smell of H_2S.

Core BS-288G. The core was taken on the lower Crimean slope, approximately 11 km to the southwest along the MAK line from core BS-287G. An elongated patch of a high acoustic backscatter interpreted as mud flows spreading down the slope was sampled. The subbottom profiler record displayed a prominent acoustic wipe-out in the intersection with the mud flow. The core recovered mainly a mousse-like, gas-saturated mud breccia interval (Fig. 78), which was overlain by a sapropel layer with a thickness of 20 cm, and a finely laminated interval of recent sediment at the top of the section. The total recovery was 2.4 m. Some fragments of detrital limestones with plant imprints were found within the sapropel layer. Other carbonate nodules showed the presence of bacterial colonies (Fig. 79). Abundant gas hydrates were found in the lower 60 cm of the core. One fragment of gas hydrate was also found in the sapropel layer, but it probably was displaced during the core extraction from the plastic liner. The entire section revealed a smell of H_2S.

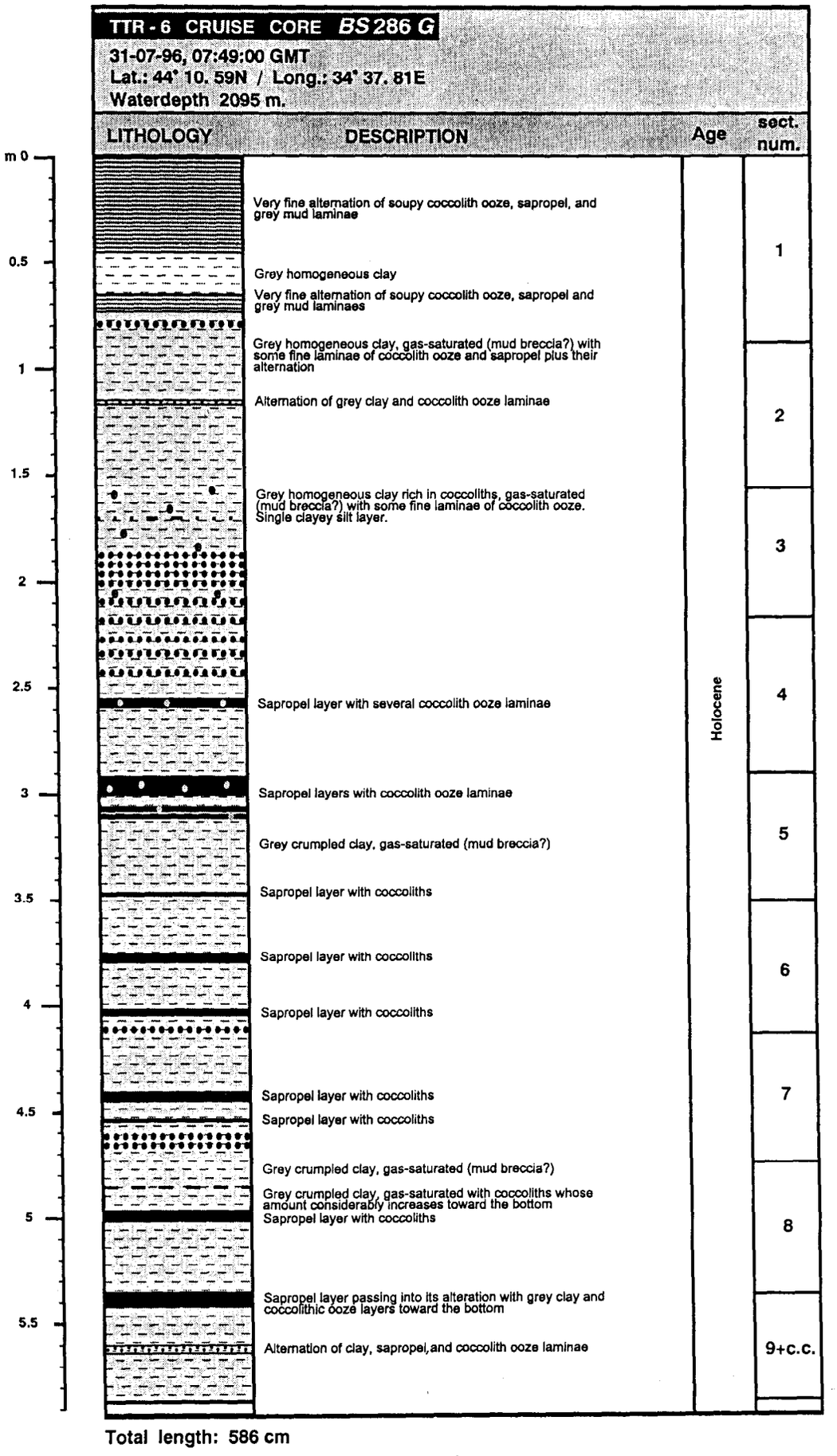

Fig. 76. Core log BS-286G

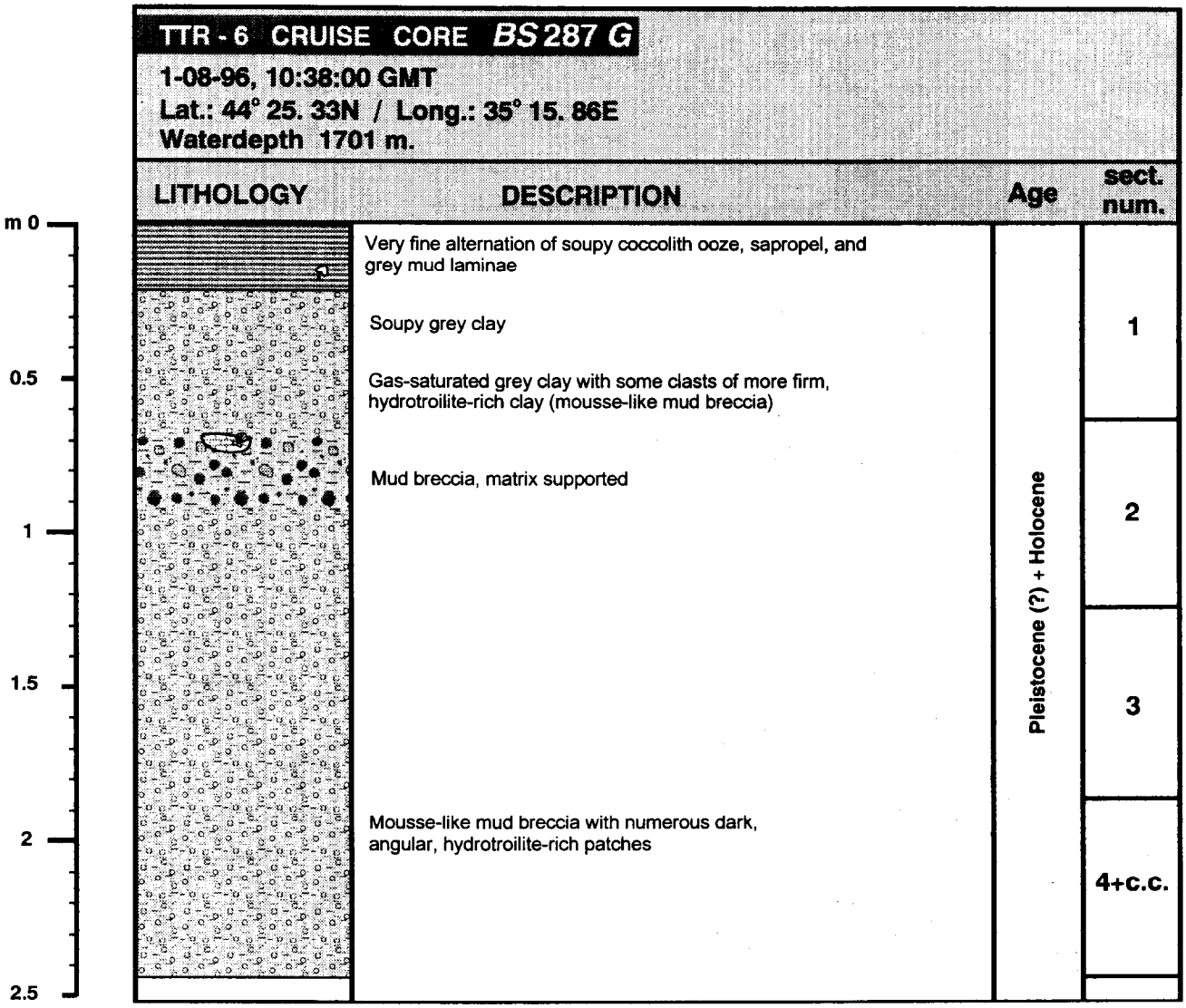

Fig. 77. Core log BS-287G

Core BS-289G. The core was taken from the Crimean continental rise, in an area of a very complicated acoustic backscatter pattern, with discontinuous probable gas front-type reflections seen on the subbottom profiler record. An interval of mud breccia with a thickness of 0.6 m was recovered (Fig. 80). Only a few millimetres of recent sediment overlay the mud breccia. Rare gas hydrates were recognized at the bottom of the core. The entire section smelled of H_2S .

Core BS-290G. The core was obtained close to BS-289G from a patch with a very high acoustic backscatter, about 300 m across, and with the similar acoustic signature on the subbottom profile record. Only a mud breccia interval (Fig. 81) with a thickness of 0.28 m was recovered. The clasts from the mud breccia were recognized as fragments of Oligocene-Lower Miocene clays (the Maikopian). Some gas hydrates were evidently initially present in the core catcher, but they had fallen out near the sea surface in the process of bringing the core on the deck.

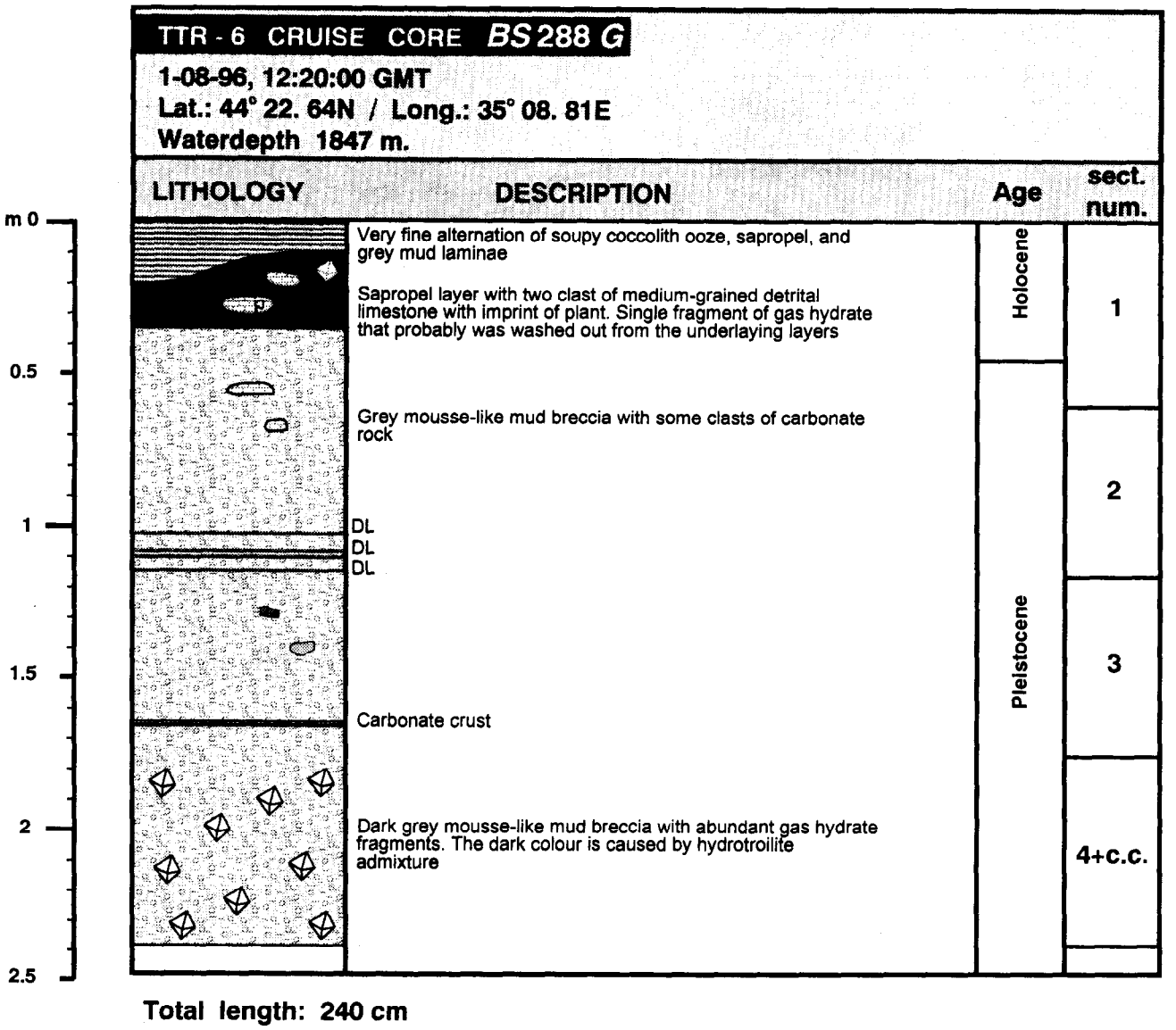

Fig. 78. Core log BS-288G

Core BS-291G. This core was taken about 7.5 km to the southwest along the profile from BS-290G from a seafloor feature with a low to moderate acoustic backscatter and an opaque acoustic pattern on the subbottom profiler record, which was interpreted as a collapsed structure. The core was hemipelagic (Fig. 82), and 6.02 m of sediment was recovered. The upper 20 cm are represented by typical recent, finely laminated sediments. The rest of the core can be divided into two parts. The upper one showed a sequence of alternating sapropel and grey, gas-saturated clay layers where more than 60 sapropel layers were counted. The boundaries between the sapropelic and grey clay layers were sharp. Some fine laminae of diatom ooze were also found. The lower part of the core is mainly represented by grey homogeneous clays without sapropel but with several silty layers of different thicknesses. Micropaleontological study established the prevalence of Pleistocene coccolith species in the grey clay from both core parts, while the sapropel layers were found to be of Holocene age. The entire section was gas-saturated, with the characteristic smell of H_2S.

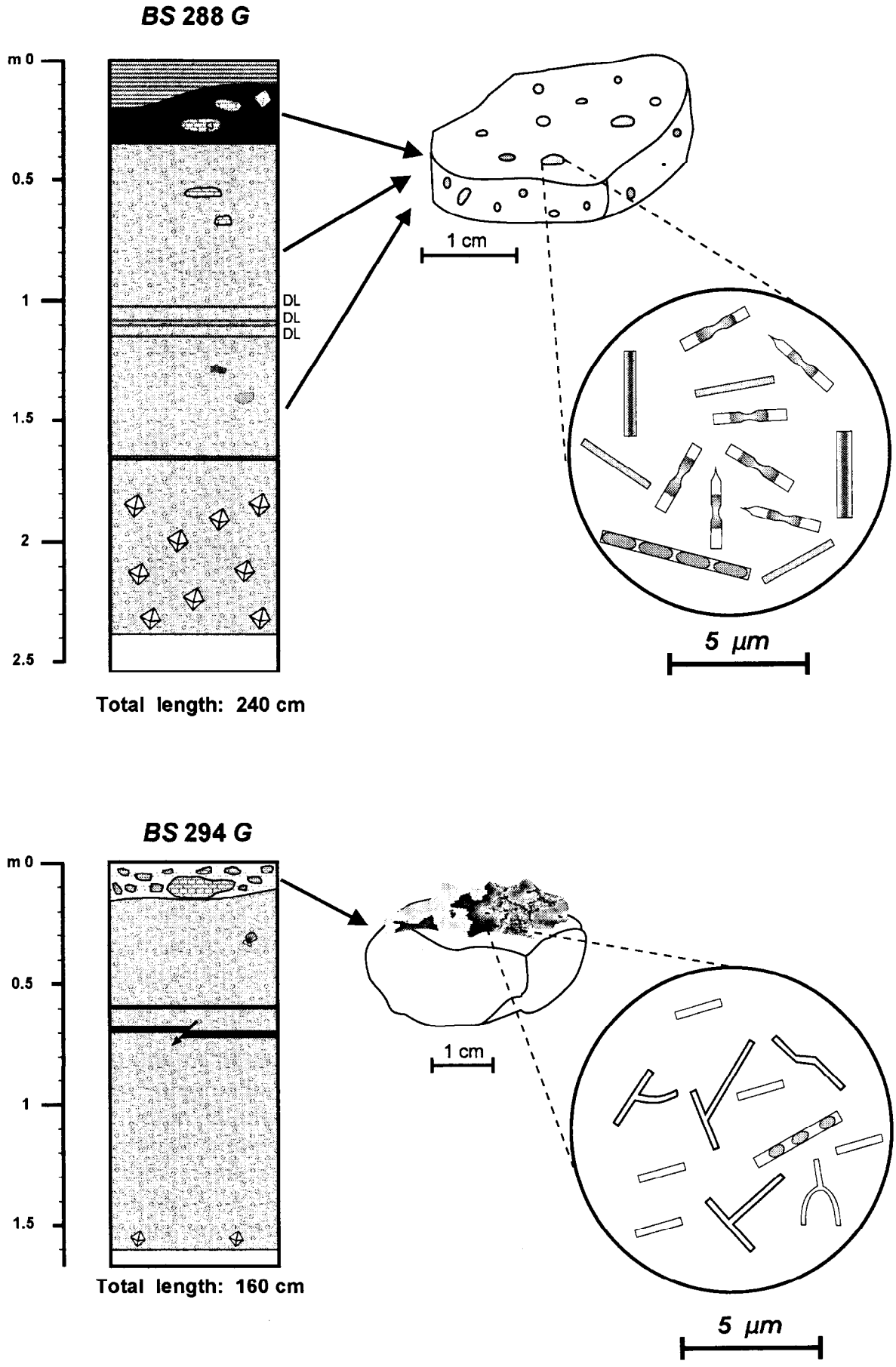

Fig . 79. Sketch of the occurrence of the bacterial mats associated with carbonate crust in the mudbreccia and the appearance of bacteria at X1000 magnification

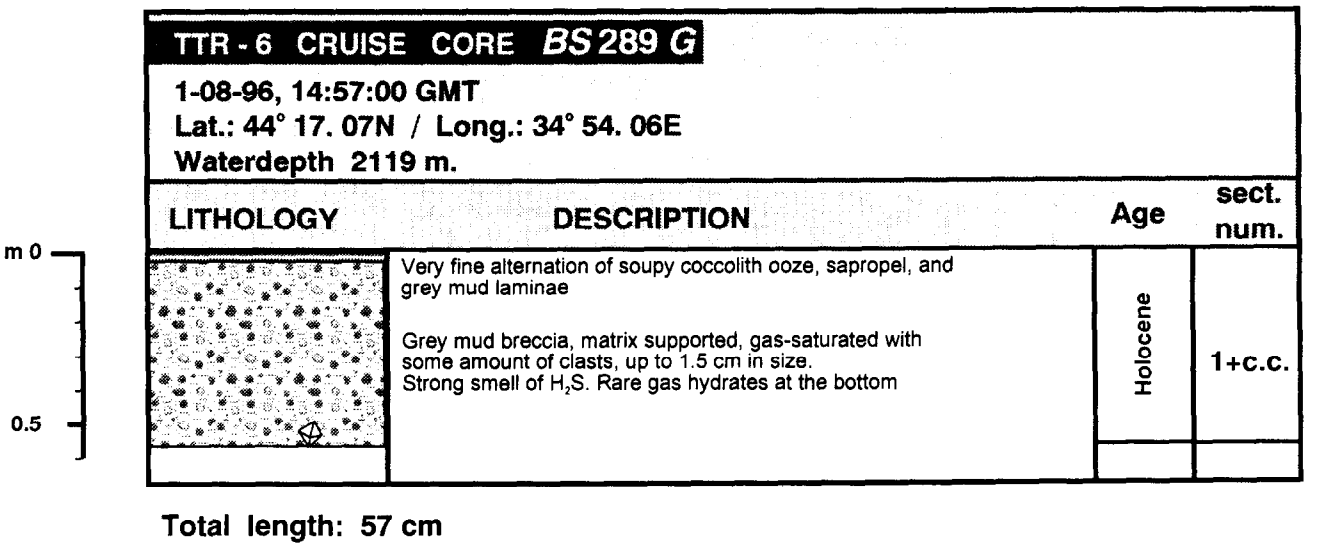

Fig. 80. Core log BS-289G

Core BS-292G. This core was raised nearby to BS-291G approximately 1.5 km to the southwest along the profile, from the same feature as BS-291G. A 0.6 m interval of the gas-saturated, matrix-supported mud breccia was recovered (Fig. 83). Some carbonate clasts contained bacterial mats. Much gas hydrates were found in the lower 20 cm of the core. The entire section smelled of H_2S .

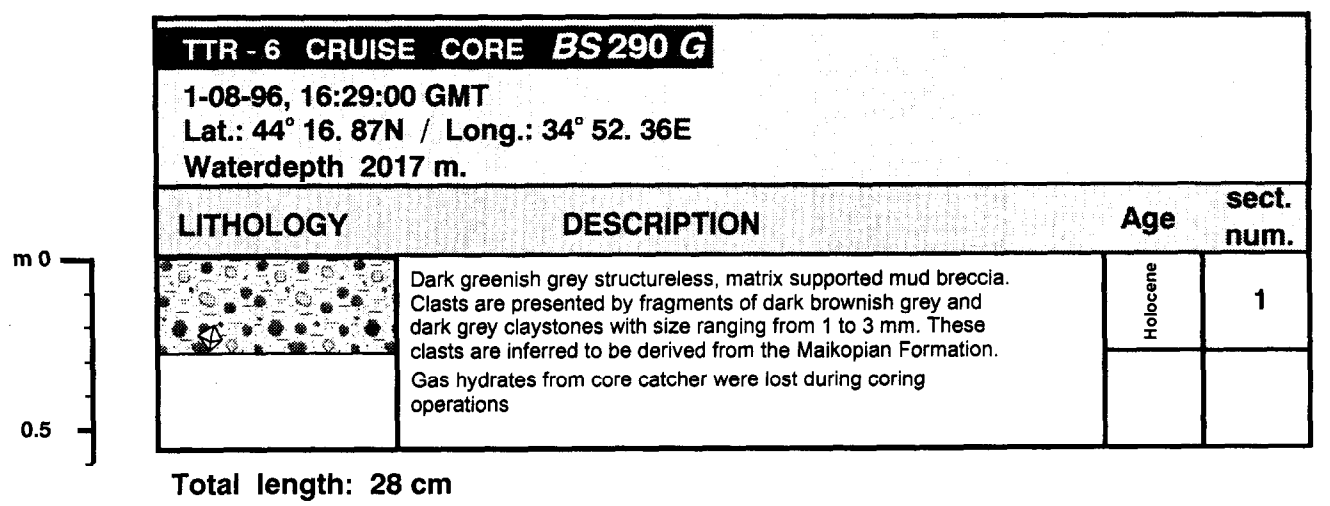

Fig. 81. Core log BS-290G

MAK-1 line M-50

A total of 3 cores were taken along the profile and they are described below.

Core BS-294G. This core was taken from the Crimean continental rise, in an area of a highly backscattering patch with a diameter of about 800 m and with no penetration on the subbottom profiler record. The core recovered an interval with a thickness of 1.6 m of mousse-like mud breccia, gas-saturated, interrupted by two sapropel layers at 0.7 m (Fig. 84). The mud breccia interval was overlain by a horizon consisting of soupy grey clay, with fragments of carbonate crust

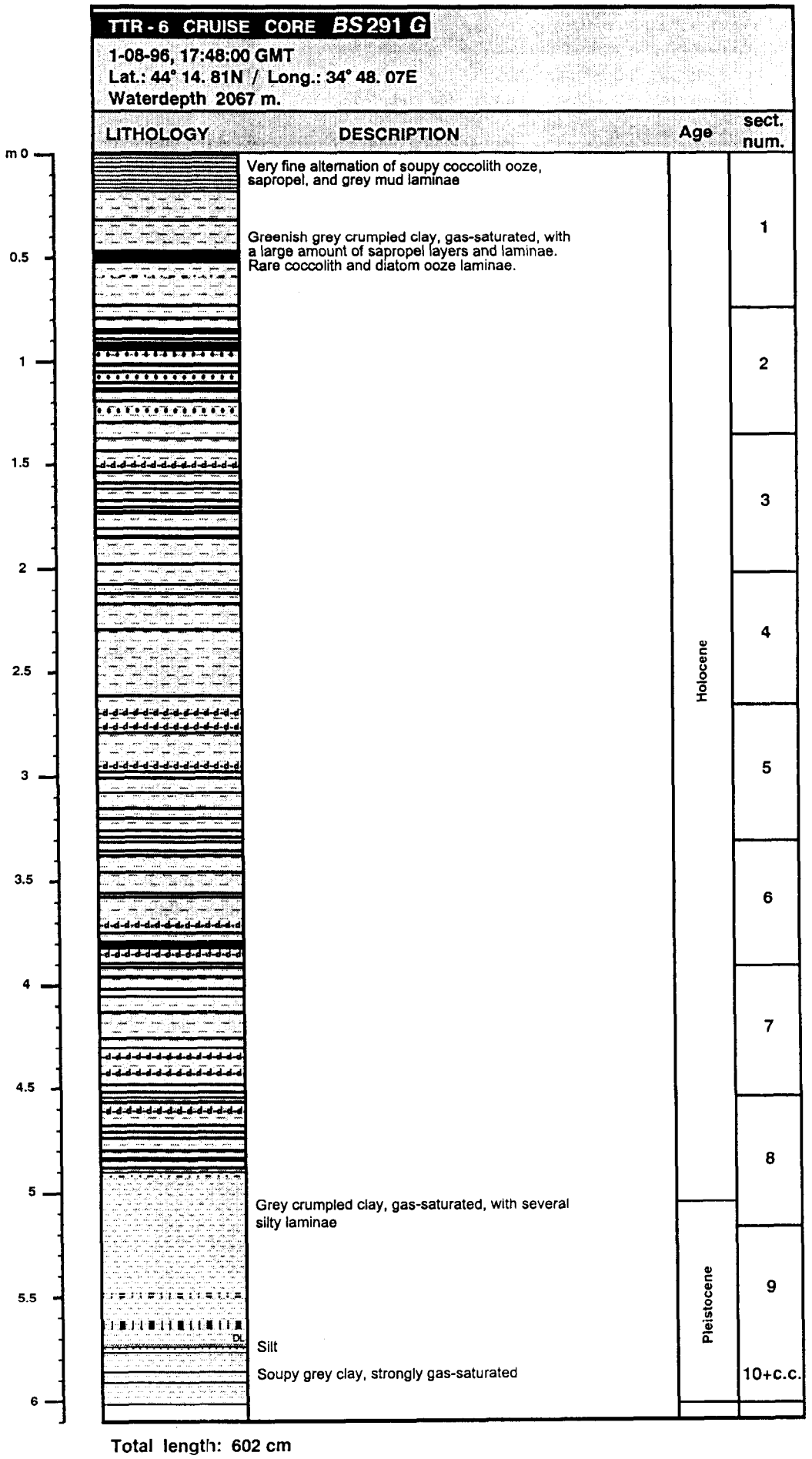

Total length: 602 cm

Fig. 82. Core log BS-291G

covered by well-developed multicoloured bacterial mats (Fig. 79). Some gas hydrates were found at the bottom of the section. The entire section revealed a smell of H_2S.

Core BS-295G. The core was taken on the continental rise, approximately 6.5 km from BS-294G to the southwest along the profile, on the top of an assumed mud volcano. A high acoustic backscatter and no penetration on subbottom profiler record were observed.

The core recovered 2.16 m of mud breccia, matrix-supported, with clasts represented by fragments of Maikopian claystones (Fig. 85). The upper 20 cm differed in colour from the rest of the core.

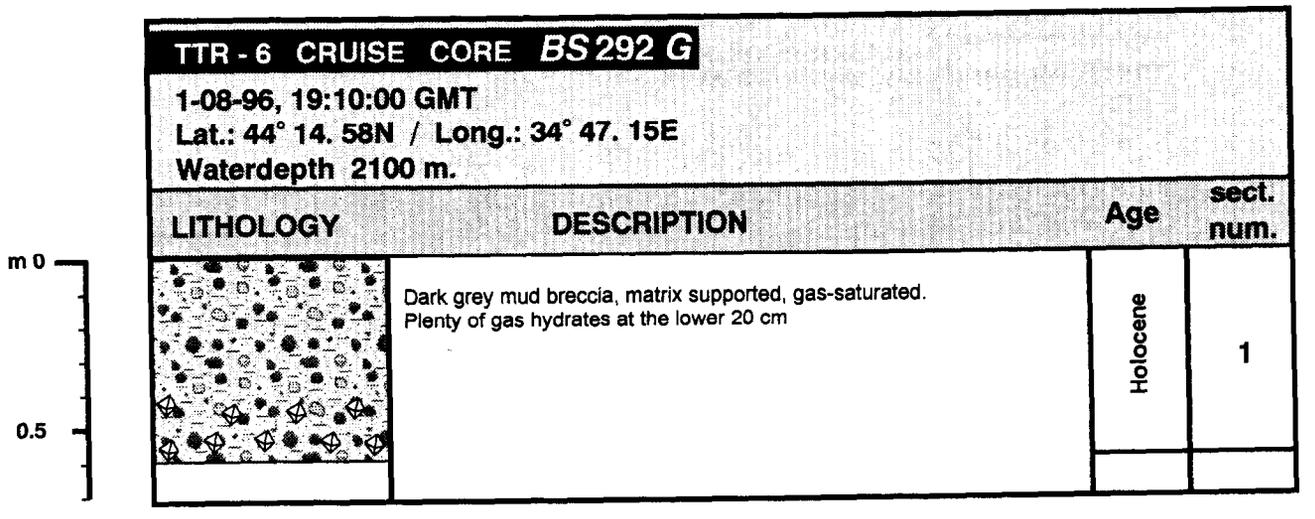

Fig. 83. Core log BS-292G

Core BS-296G. This core was obtained near BS-295G, approximately 2 km to the southwest along the profile, from a well-expressed crater of the newly discovered Dvurechenskii mud volcano. About 3.2 m of very soupy, strongly gas-saturated mud breccia was recovered (Fig. 86). Clasts, reaching in size 2.5 cm, were represented by fragments of the typical Maikopian claystones.

EM-12 imagery

Core BS-293G. The core was sampled from the Kazakov mud volcano, the existence of which was only inferred from seismic data from previous years. The position of this structure was clarified on the basis of the EM-12S multibeam echosounder data. The sampling site was situated about 8.3 km to the southeast of BS-294G. The core recovered 1.02 m of mud breccia, matrix-supported, gas-saturated, with clasts represented by fragments of Maikopian claystones overlain by a rather thin layer of recent soupy sediment (Fig. 87). The matrix of

this particular core was of dark grey colour with a brownish shade.

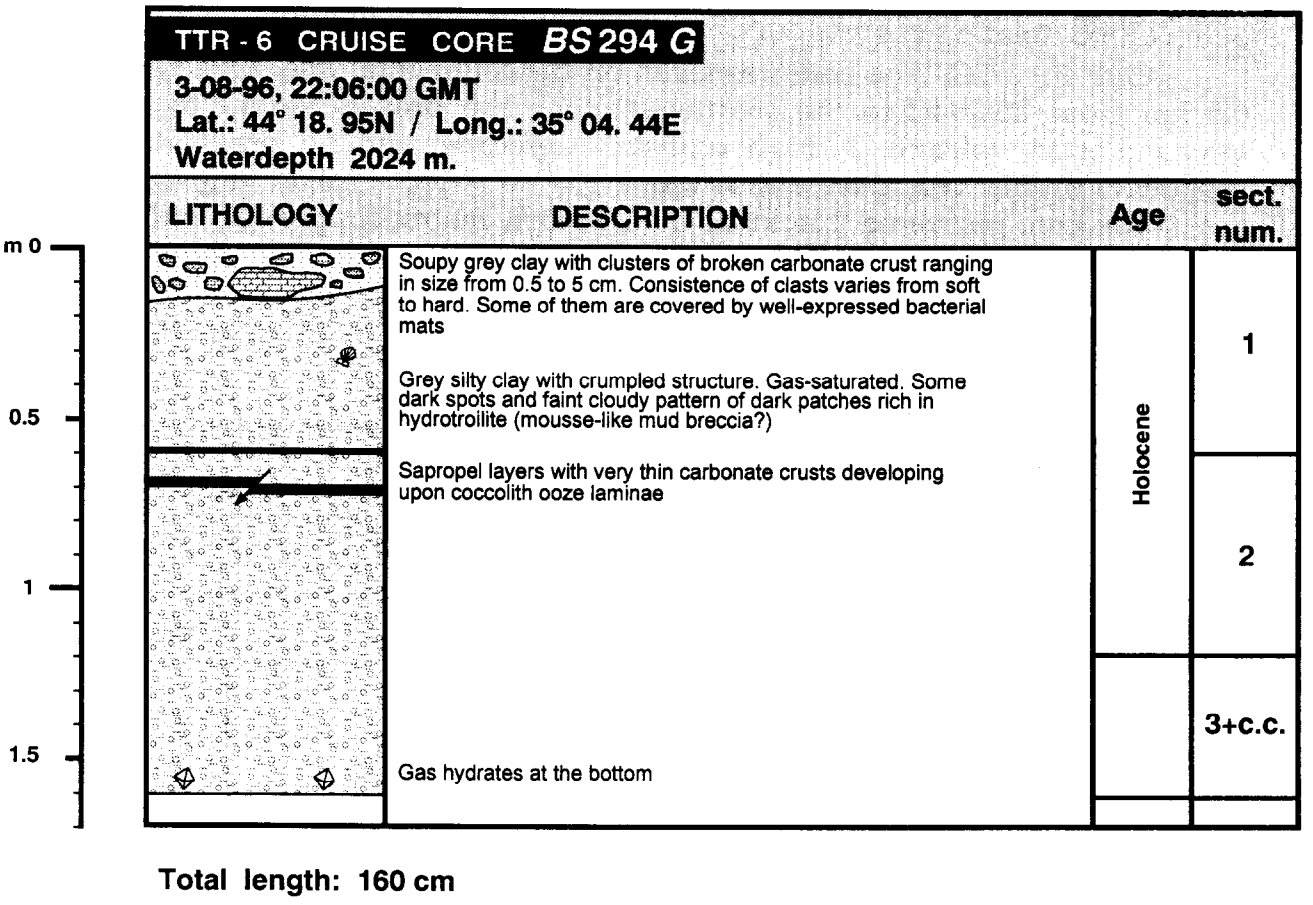

Fig. 84. Core log BS-294G

Preliminary study of rock clasts from the mud breccia

Data analysis

Of all the cores recovered during Leg 2, Cores BS-284G, BS-287G, BS-288G, BS-289G, BS-290G, BS-292G, BS-293G, BS-295G, and BS-296G contained rock clasts. Cores BS-284G, BS-287G, BS-288G, BS-292G, and BS-294G contained carbonate crust fragments and nodules, probably formed *in situ* under the influence of methane flux. The mud breccia consisted of a structureless mixture of matrix-supported, poorly-sorted clasts of different lithologies. In most cores the matrix had a mousse-like appearance associated with gas-saturation of the matrix.

After description of the cores by shipboard sedimentologists, the clasts were washed and dried. In the sedimentological laboratory, detailed clast examination was carried out using a binocular microscope. All clasts were examined and grouped, according to the following criteria: colour, lithology, texture, structure, composition, admixture, sphericity, reaction with HCl, and the presence of special unique features (such as bivalve embryonic capsules). Clasts

containing bacterial mats were separated, in order to be frozen for study at Moscow; some carbonate crust clasts were also taken separately for mineralogical and carbon isotope analyses. The size of each clast was measured and the frequency of similar rock clasts noted.

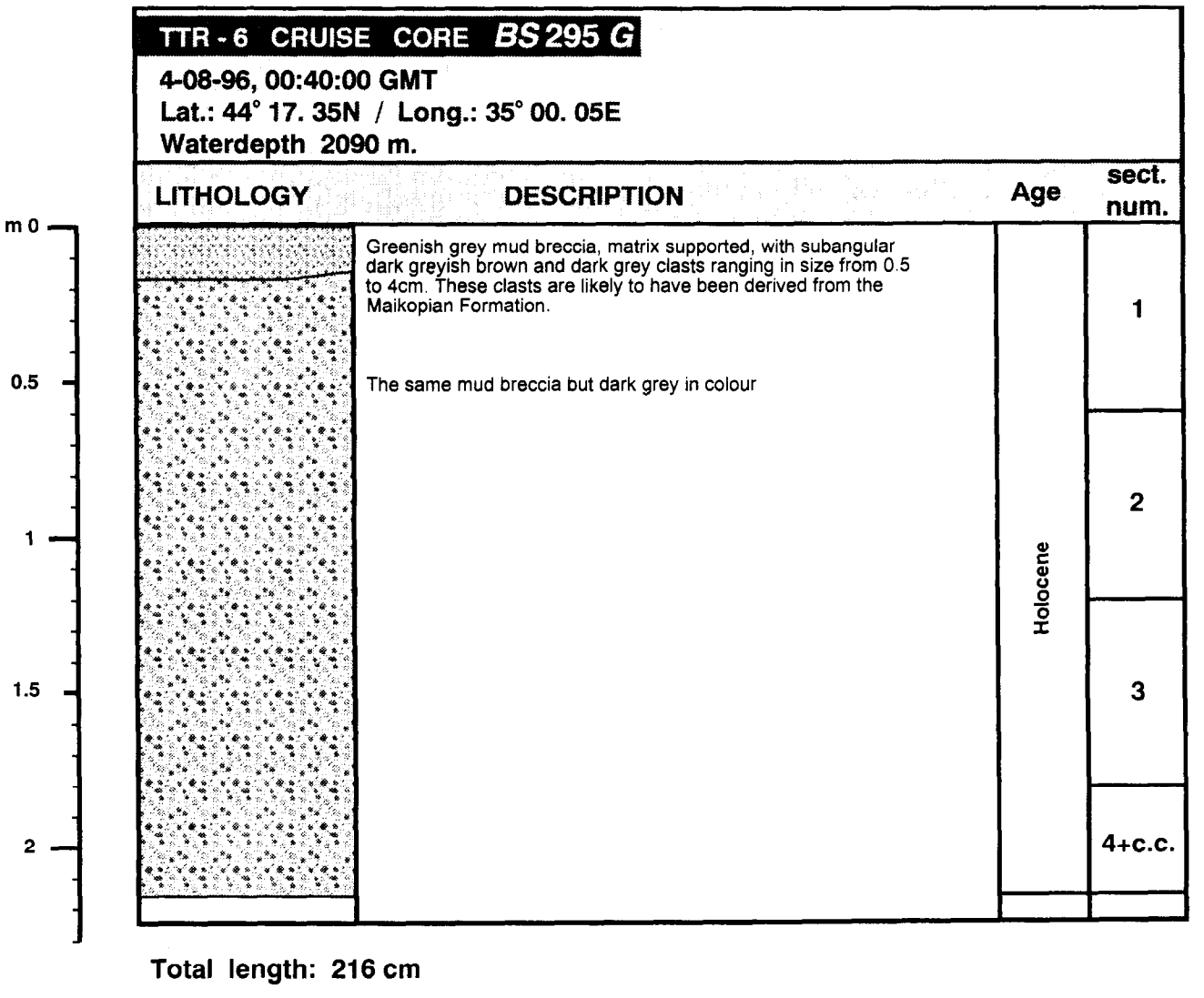

Fig. 85. Core log BS-295G

The following lithological groups/rock types were identified:

(1) marlstone;
(2) grey claystone;
(3) brown claystone;
(4) calcarenite;
(5) carbonate crust;
(6) bioclastic packstone;
(7) siltstone;
(8) sandstone;
(9) quartzite;

(10) microbreccia;
(11) siderite;
(12) chert;
(13) tree bark.

N B: The numbers correspond to the numbers in the statistical figures.

Also the clasts were roughly divided into 4 classes according to the length of their larger axis:
(1) up to 3 mm;
(2) from 3 mm to 2 cm;
(3) from 2 cm to 4 cm;
(4) > 4 cm.

N B: In the graphs, the classes are named as series 1, 2, 3, and 4 respectively.

The bulk rock clast size distribution is shown in Figure 88; and the bulk rock type frequency distribution is illustrated in Figure 89.

The main lithological peculiarities of the rock clasts are described below for the characteristic cores.

BS-284G. The predominance of angular, grey-coloured calcarenite and marlstone clasts. There are also bioclastic packstones with bivalves. One unique marlstone with carbonate crust is present. Special attention should be paid to some well-rounded clasts (group 4 & 6). Pyrite in group 4.

BS-287G. The prevalence of angular, light grey, fine-grained siltstone and grey marlstone. One fragment of carbonate crust is present.

BS-289G. Grey marlstones predominate, but the most interesting feature of the core is the occurrence of 2 well-rounded fragments of sandstone and 2 well-rounded limestone clasts. These clasts could be erupted from a great depth or are derived from a conglomerate.

BS-290G. Brown claystone, subangular to subrounded is the most important group in this core. Probably of the Maikopian age. Pyrite is encountered.

BS-292G. Grey to dark grey, laminated, subangular claystone is the most common clast. Carbonate crust fragments are found.

BS-295G. Grey to dark grey claystone is the dominant group in this core. Unique clasts are a fossilized tree bark and sandstone. Here, the larger clay clasts predominate over the smaller ones.

BS-296G. The predominance of brown claystone, subangular to

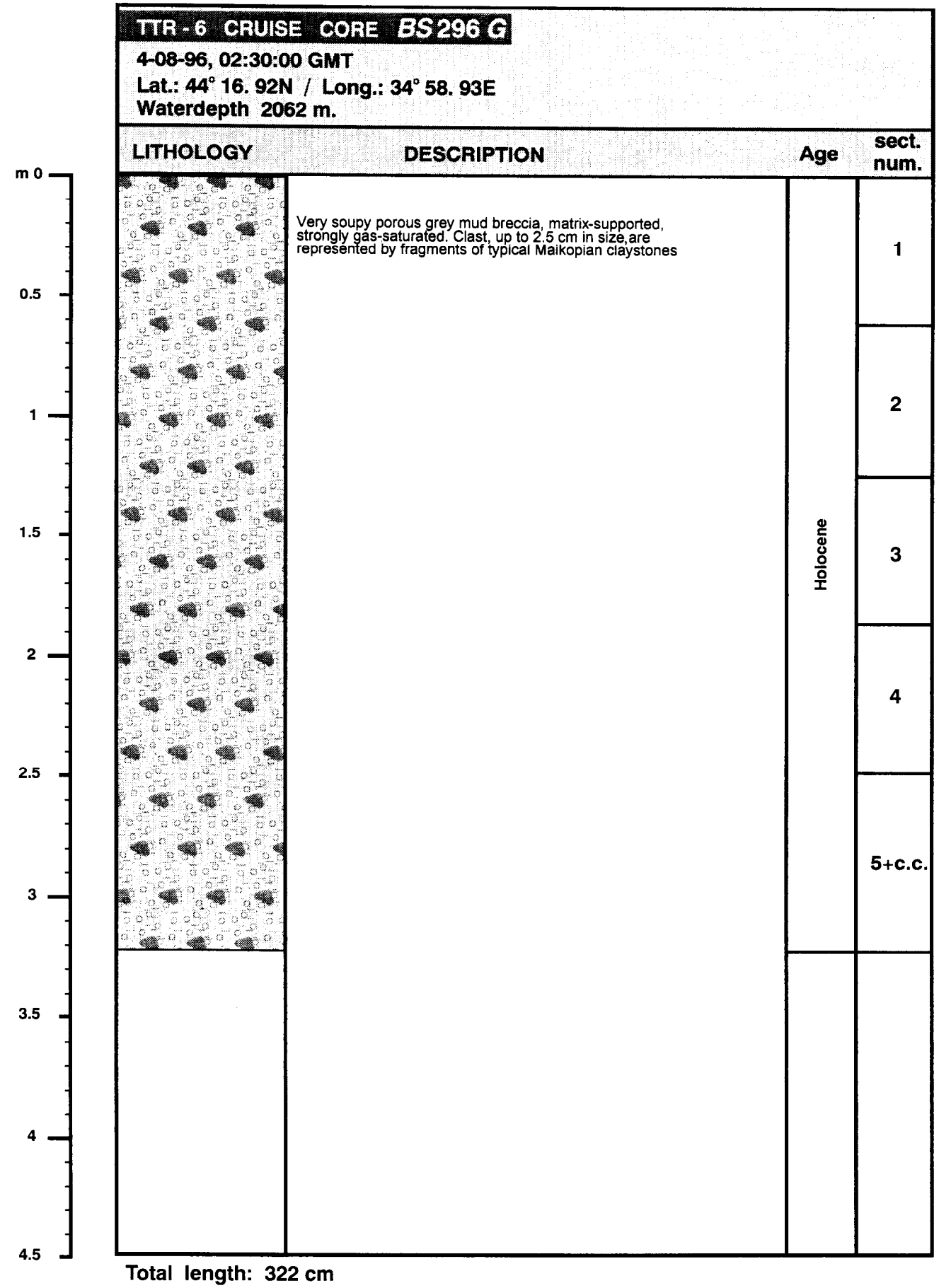

Fig. 86. Core log BS-296G

subrounded, vaguely laminated. Fragments of chert and siderite are present. Some biopackstones with foraminifera. Pyrite in group 6.

Discussion

Most clasts have a size within a range of 3 mm - 2 cm (Fig. 88; class 2). This is apparently the common clast size that could be obtained with the gravity corer of a given diameter, although it is not excluded that this size is a function of their crushing and sorting during the transportation through a mud volcano feeder channel. This size is probably strongly influenced by rock lithology and composition; and one may expect that there is a clear relationship between the hardness and size of the clast.

The majority of clasts are angular. There can be two ways of explanation of this: either the clasts were protected from erosion by the mudflow, which acted as a 'soft cushion' (probably, the gas makes it more easier for the clasts to be transported to the seafloor by the reduced friction), or the clast has been transported only over a short distance.

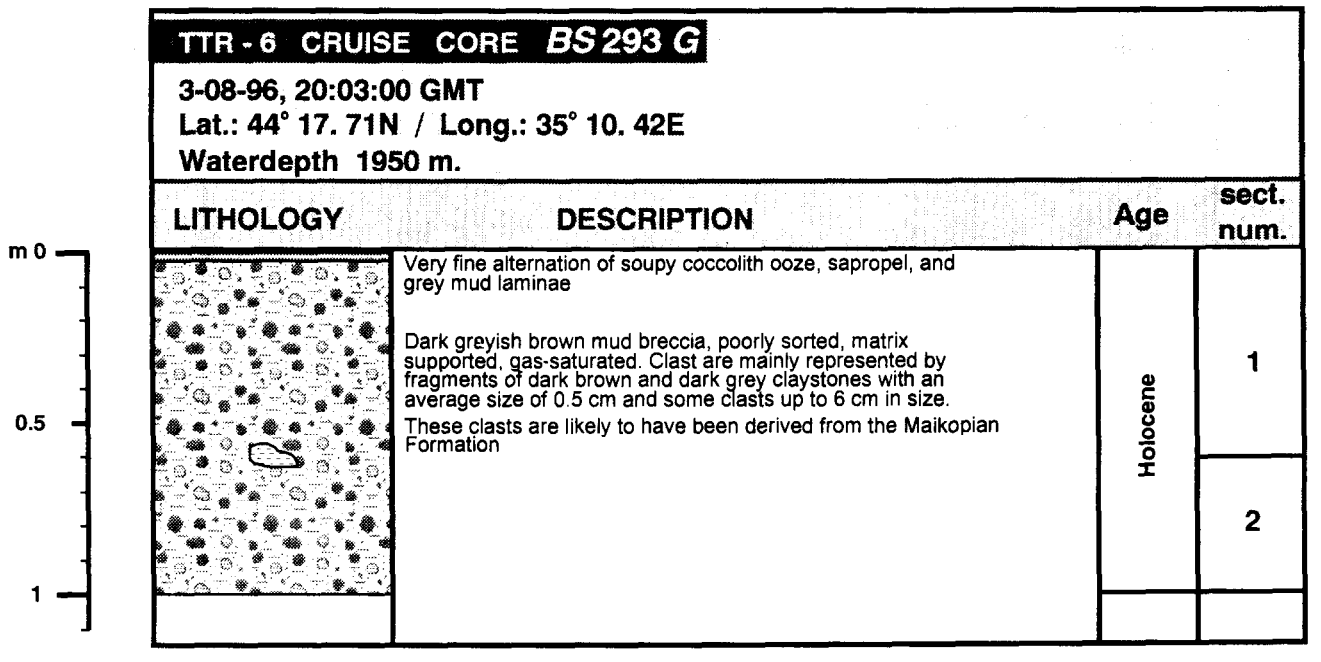

Fig. 87. Core log BS-293G

The rock clasts bulk frequency distribution (in all cores) shows that the most common clasts are those derived from the Maikopian claystones, which are characterized by the occurrence of small mica fragments, dark minerals, and chlorite.

The second important lithology in the area is marlstone. Calcarenite

seems to be also an important group, but this impression results from the presence of numerous relatively small clasts in Core BS-284G.

Some claystones contain pyrite and brown glass shards.

Most clasts were derived from the Maikopian claystones, indicating that this formation is the principal source member for the mud volcanic products in the investigated area. Their dominating role could also be the result of their mechanical properties, because plastic and relatively weakly consolidated clays are more exposed to the detachment by an upward flow of gas-saturated mud than harder rocks, which can not be crushed so easily during a mud volcano eruption.

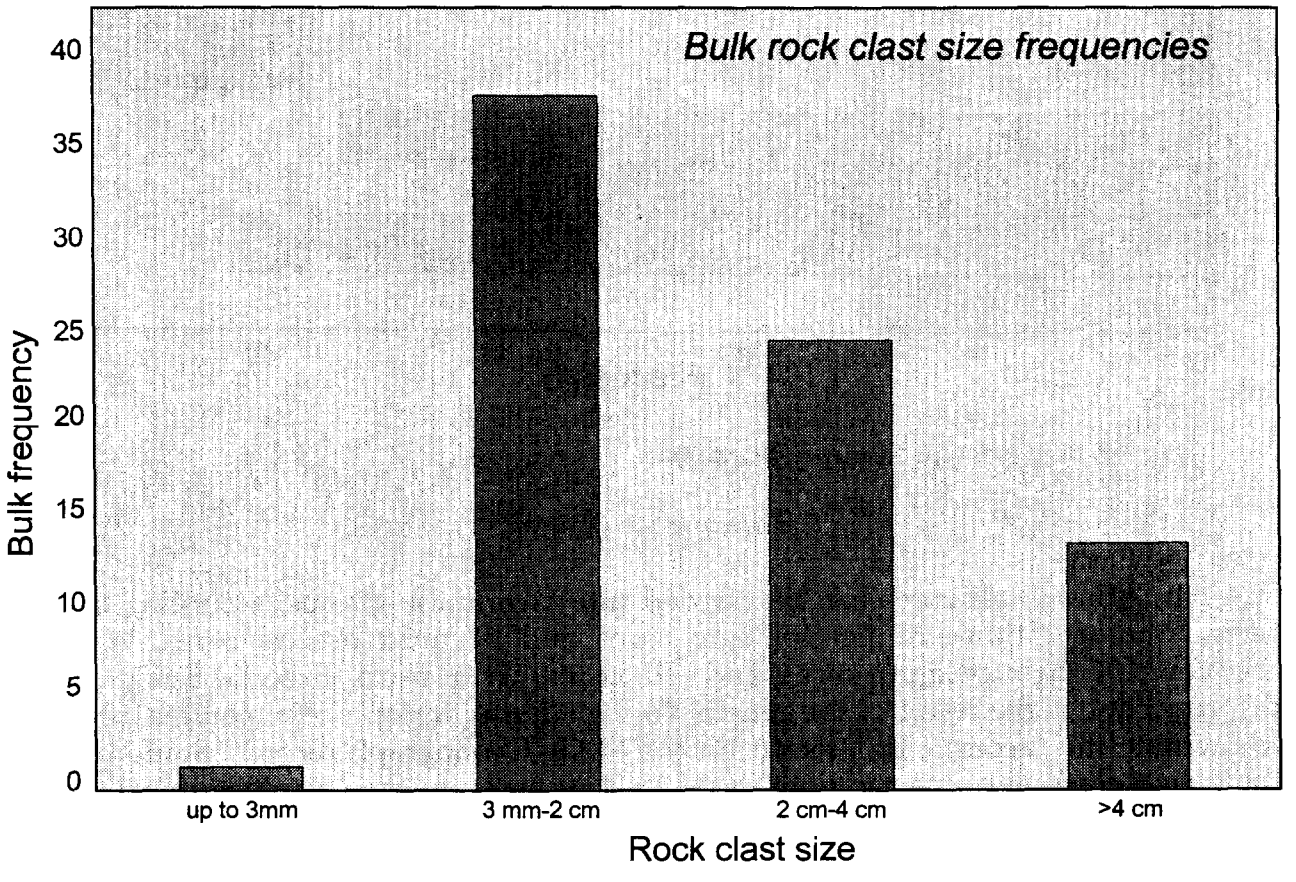

Fig. 88. Bulk rock clast size frequency distribution

It is difficult to say anything about the depth, from which the rock clasts were transported to the seafloor. Their size and roundness are dependant on different compaction of the rocks from the source formation, that is on its depth of lying. The deeper a layer, the stronger and probably bigger the corresponding clasts may be. On the other hand, those clasts have a longer way to go than weaker clasts from shallower depths. How much erosion does a clast get in a matrix-supported position? It should be noted that the frequency distribution of the clast types is based only on the clasts from the recovered cores; and it should be remembered that the cores represent only a minor part of the mud flow system.

The assemblage of rock clasts is very diverse and this is a probable indication of several source formations under the seafloor.

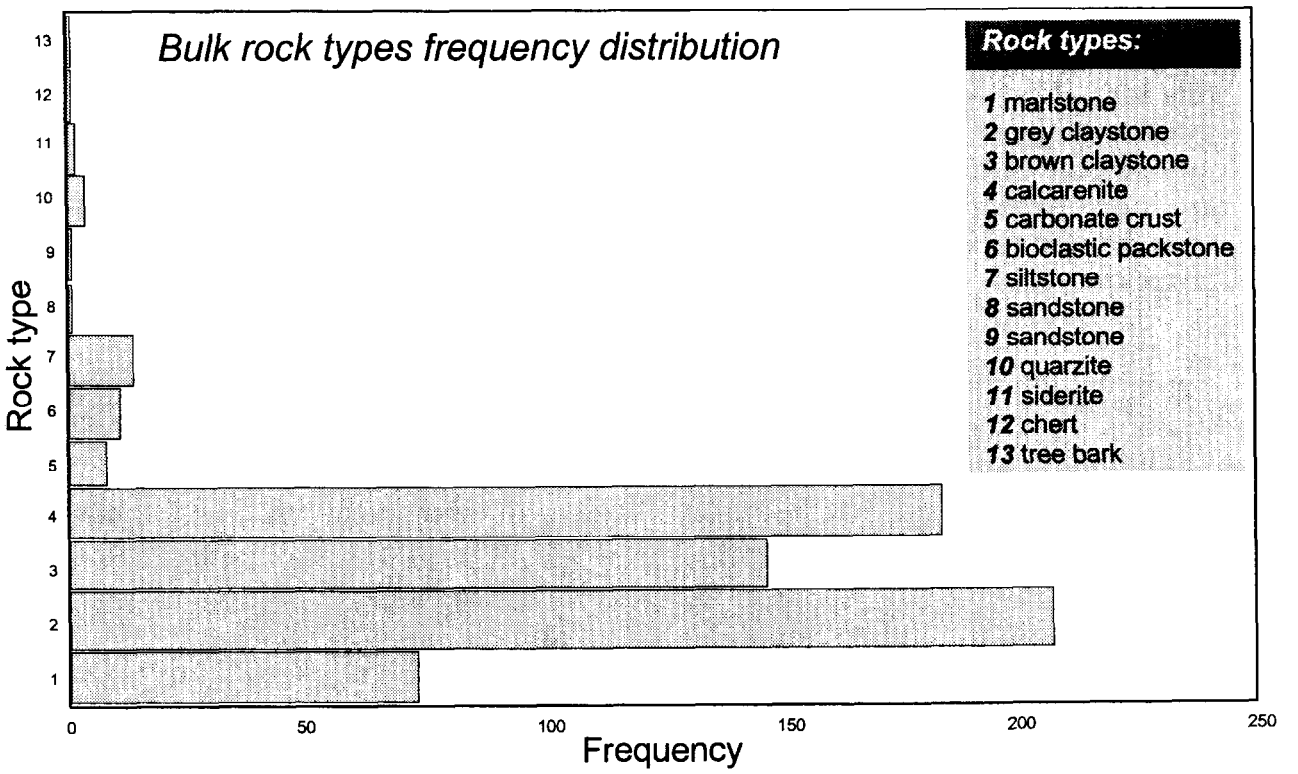

Fig. 89. Bulk rock type frequency distribution

Interpretation

In general, all cores can be divided into two main groups, according to their lithology: those of hemipelagic cores and of mud breccia cores. We recovered 4 hemipelagic cores and 10 cores with mud breccia. Such a disproportion is the result of the general coring strategy which was aimed mainly to calibrate the acoustic facies seen on the MAK-1 sonograph records. Some of the typical cores, as connected with the MAK-1 records, are shown on Figure 90.

Hemipelagic cores

Although we did not manage to take a core especially as a background reference sequence of hemipelagic sediments, 4 cores recovered Holocene and Lower Pleistocene hemipelagic sediments (see correlation chart in Figure 91). Core BS-282G can be considered as the most typical of deep Black Sea sediments. The sequence can be subdivided into three divisions that are as follows (from up to down): (1) fine alternation of coccolith ooze, grey mud, and sapropelic laminae (about 3 kyrs at the bottom; see *Jones and Gagnon, 1994*); (2) grey clay enriched with organic matter that probably indicates the sapropel dilution by clay; dark brown jelly-like sapropel layer (7 kyrs at the bottom; see *Jones and Gagnon, 1994*) was recognized toward the bottom at 2 m; (3) below the sapropel layer, grey clay with an admixture of metastable iron sulphides (hydrotroilite) was recovered.

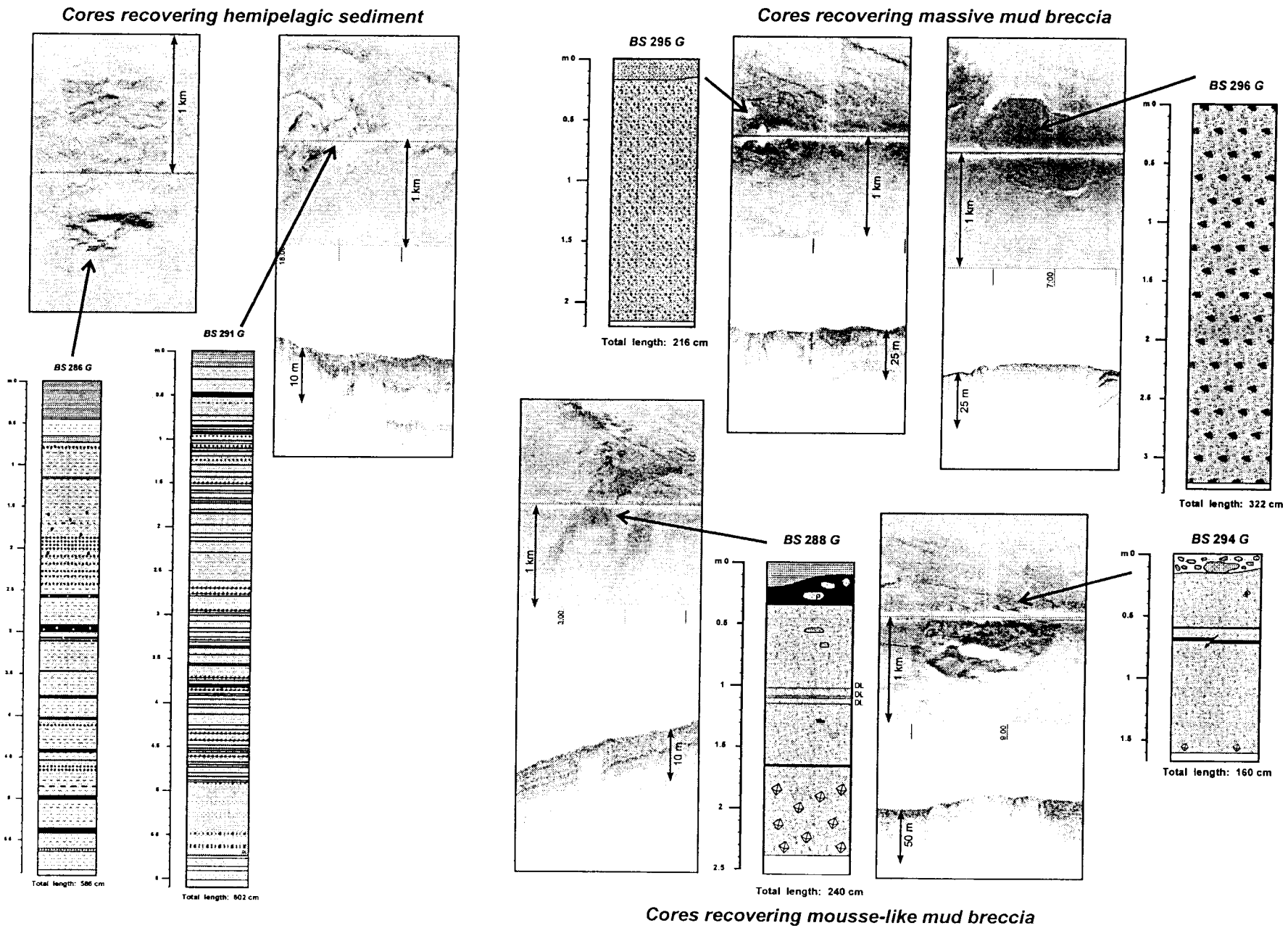

Fig. 90. Typical cores from the Sorokin Trough correlated with the MAK-1 records

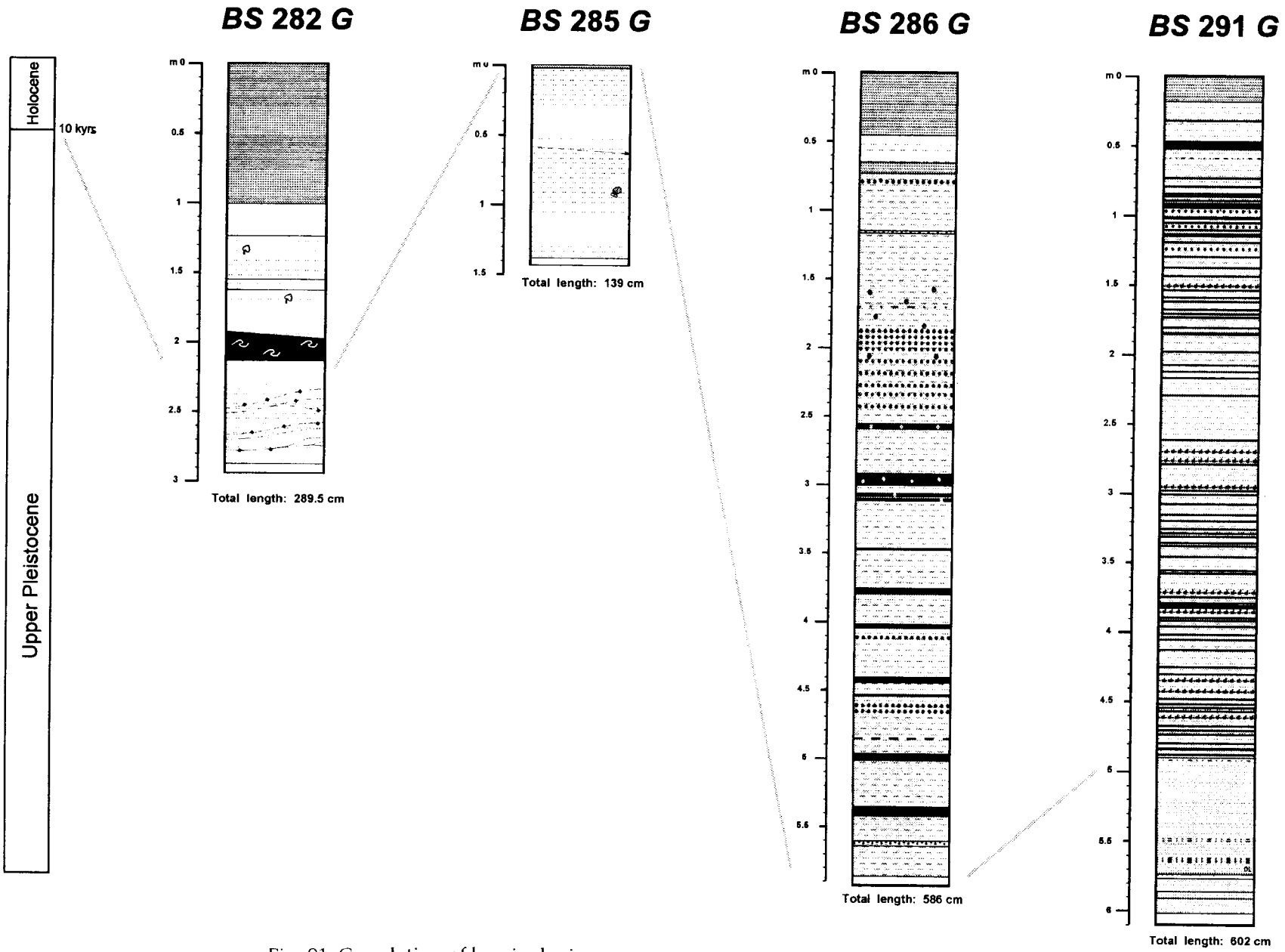

Fig. 91. Correlation of hemipelagic cores

This deepest layer was dated as Pleistocene according to the coccolith assemblage. The same clay was recovered from sampling site BS-285G where it makes up the bulk of the core and is likely to mark an exposure of the Pleistocene clay on the surface within a slump scar, observed by the MAK-1 survey. Cores BS-286G and BS-291G (the longest one) were of the similar appearance and represent a sequence repetition of sapropel layers with various grey clay intervals. Both cores were taken close by assumed mud volcanoes and had a rather high gas content. Core BS-291G recovered 1 m of the typical Pleistocene clay with silty turbidites at the bottom, whereas Core BS-286G did not. The age determination based on micropaleontological data established a Holocene age for the sapropelic layers and the prevalence of Pleistocene species for the grey clay layers interbedded with sapropel layers. From this fact one can conclude that a significant amount of redeposited grey clay was added at the time to the sapropel deposition. The character of the boundaries between the sapropel and clay layers is sometimes transitional for Core BS-286G and rather abrupt for Core BS-291G. This is evidence for a gradual increase in the sedimentary supply in the case of core BS-286G and for a sudden change of deposition from sapropelic to clayey sediments in the case of Core BS-291G. The calculated sedimentation rates for the Holocene are 83 and 70 cm/kyrs for BS-286G and BS-291G respectively. These clay layers are interpreted as muddy turbidites, and, thus, they testify to the Holocene activity of turbidity currents going down the Yalta Canyon located to the northwest of this area.

Mud breccia cores

This group includes 10 cores. On the basis of the matrix consistency and the matrix/clast ratio, they were subdivided into two subgroups (Fig. 92): those containing the mousse-like mud breccia and the typical mud breccia. The first group includes the cores that recovered the mousse-like mud breccia with insignificant amounts of clast and with a high gas content. A total of 4 cores were attributed to this group. Core BS-284G displayed a complicated sequence composed of the mousse-like mud breccia interbedded with layers of the typical mud breccia (at the top and at 1.5 m) and layers of slope breccia. This core was taken from a collapsed structure observed by the MAK-1 survey. Cores BS-287G, BS-288G, and BS-294G are more uniform, representing mainly mousse-like mud breccia sequences. In all cases the mud breccia was overlain by sediments of different types. For example, the mud breccia in Core BS-287G was overlain by younger normal, finely laminated sediments with a thickness of 0.2 m. Core BS-288G recovered a sapropel layer above the mud breccia and more recent soupy sediment as well. The MAK-1 sonograph shows that the core was taken from a mud flow (Fig. 90) and that, according to the coring results, the flow is buried, at least in places.

Core BS-294G has the mousse-like mud breccia with two thin sapropel layers at 0.7 m showing an interruption of the mud volcano activity and the deposition of normal basinal sediments. A broken carbonate crust was found at the top of the core. Some of the carbonate clasts were covered with bacterial mats. Both carbonates and bacterial muds are considered to have developed under the

methane exhaust influence.

The second group included cores containing the typical mud breccia, matrix supported, with numerous rock clasts. In total we took 6 cores with such type of the mud breccia. Almost all of them showed poor recovery, rarely exceeding 2 m. Cores BS-289G and BS-292G included mud breccia with clasts of limestones most of which were Pliocene-Pleistocene in age. Cores BS-290G, BS-293G, BS-295G, and BS-296G recovered mud breccia with clasts of claystones derived from the Maikopian Formation (Oligocene-Lower Miocene), which is widespread in the investigated area and is exposed in many places in the Kerch and Taman Peninsulas. The crater of the Dvurechenskii mud volcano, which was well-expressed on the MAK-1 record, was chosen for sampling site BS-296G. The thickest mud breccia interval taken there was rather soupy and extremely gas-saturated. Sometimes mud breccia intervals were composed of flows of different ages (Core BS-295G).

Micropaleontological investigations of the matrix from all the cores led us to the conclusion that the Pleistocene clays are the main material for the matrix formation, although it might not be excluded that some amount of the Maikopian clays and other lithologies can be present. For instance, the matrix of Core BS-293G was of dark grey colour with a brownish shade and probably contained more clay derived from the Maikopian Formation than other mud breccia cores.

According to the MAK-1 and seismic surveys, almost all of the typical mud breccia cores were taken from a large mud volcano field situated on the top of two zones of the Maikopian clay diapirs. The only exception is Core BS-294G that also belong to this field, but contains the mousse-like breccia. The rest of the cores with the mousse-like mud breccia were obtained from easterly field related to another diapiric zone. In the latter field, the sonographs show that mud flows are often connected with extended fault zones. Thus, it is possible that the mousse-like mud breccia could originate not only through mud volcano eruption but also through fluid venting along weakened zones situated on the Crimean continental slope.

In almost all of the cores the gas presence was detected. Fourteen cores were gas-saturated and often strongly smelled of H_2S. Five of them (BS-288G, BS-289G, BS-290G, BS-292G, and BS-294G) contained gas hydrates. The layer of gas hydrates was probably a serious barrier for the corer to penetrate.

Conclusions

The core samples provided an important information about the nature of the backscattering patterns seen on the MAK-1 sonographs. The coring allowed us to calibrate these images and to distinguish areas of active fluid flow which were normally marked by a strong acoustic backscatter. The main preliminary conclusions are as follows:

(i) The entire area of investigation is characterized by an active gas expulsion through the seafloor associated with the formation of gas hydrates and probably some authigenic carbonates. This fluid expulsion manifests itself also in numerous mud volcanoes and fissure eruptions of mud breccia.

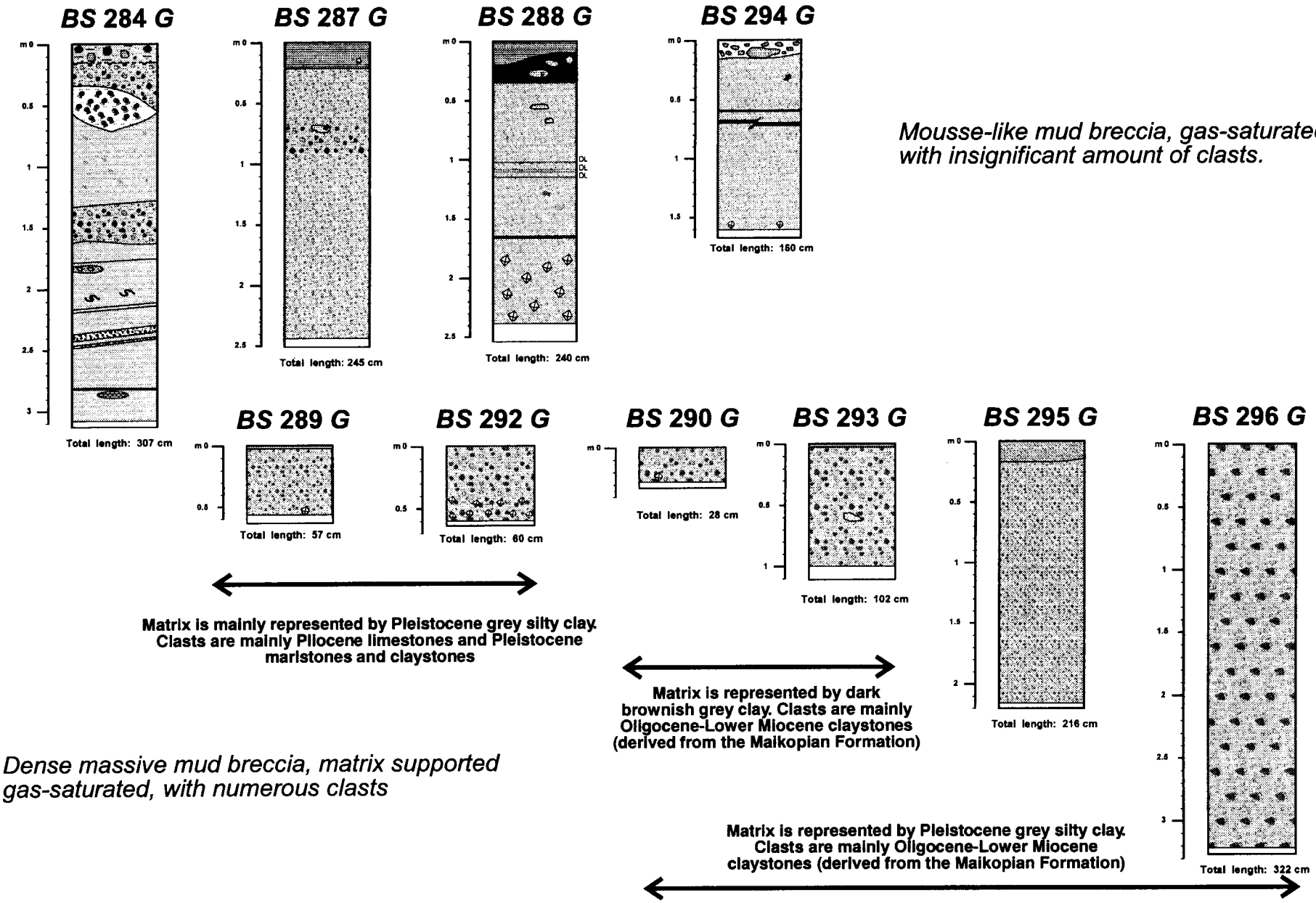

Fig. 92. Cores containing different types of the mud breccia

(ii) The distribution of mud breccia types shows that the mousse-like and typical mud breccias are associated with different fields of fluid expulsion situated on the top of different zones of diapiric folds.

(iii) Mousse-like mud breccia could originate not only through mud volcano eruption, but also through fluid escape along fault zones.

(iv) The Pleistocene clays are the principal material for mud breccia matrix formation.

(v) There is strong evidence for the Holocene turbiditic activity of the Yalta Canyon.

d. PALEONTOLOGICAL AND MICROBIOLOGICAL DATA

S.S. Gablina and A.P. Sautkin

The main aim of paleontological investigations was the dating of sediments. Many samples were taken for this from both the hemipelagic cores and the matrix of the mud volcanic breccia. Although most of them were intended for more accurate study in Moscow, preliminary dating was made on the ship from smear slides taken from all the cores. The assemblages of diatoms and coccoliths identified from the smear slides confirmed the Holocene and Upper Pleistocene age of hemipelagic Cores BS-282G, BS-286G, and BS-291G.

Diatoms are rather abundant in the Holocene deposits as are silicoflagellates. The diatom flora is characterized by typical Holocene warm-water oceanic and neritic species (*Hemiaulus hauckii, Asterompalus robustus, Chaetoceros peruvianus, Thalassiosira oestrupii, Thalassionema nitzschioides, Coscinodiscus* spp.). The presence of brackish-water forms, such as *Cyclotella caspia* indicates that the Holocene Black Sea was of low salinity like the modern one. The unexpected occurrence of littoral and fresh water diatoms could indicate reworking.

The Holocene coccolith assemblage was dominated by *Emiliania huxleyi.* The following species were also found in the Holocene deposits: *Syracosphaera pulchra, Braarudosphaera bigelowi, Umbilicosphaera sibogae, Umbellosphaera* spp., *Cyclococcolithes leptoporus, Gephyrocapsa oceanica, G. caribbeanica.* The three last species are more common in the Pleistocene sediments. An Early Pleistocene age for the matrix in Cores BS-284G, BS-285G, BS-287G, BS-288G, BS-290G, BS-292G, BS-293G, BS-294G, BS-295G, and BS-296G was established on the basis of the coccolith study. *Pseudoemilianeyi lacunosa, Umbilicospaera* spp., *G. caribbeanica, G. oceanica,* and *C. leptoporus* were found there. A clast of carbonate crust with ostracods found in Core BS-287G is most likely of Upper Pliocene age.

It is noteworthy that there are plenty of impressions in the clasts of Arthropods (insects or crustaceans?) and Polychaeta with the remains of a well-preserved chitinous covering. Segments of body and extremities are evident on the imprints. Besides this there are rare Gastropods and many very small bivalve shells (0.1 mm) forming accumulations in depressions on the surfaces of the clasts.

One of most interesting occurrences was of bacterial mats in Cores BS-288G, BS-292G and BS-294G (Fig. 79). The mats from BS-288G and BS-292G are similar but differ significantly from those from BS-294G. They occur in Cores BS-288G and BS-292G on clasts of carbonate crust found in different parts of the core. They look like spherical or round-shaped soft jelly-like deposits of different colours: light-yellow, greenish, rose, light-brown, white, and violet. They fill some small holes and depressions on the surface of the clasts and inside them. The size of mats are 2-3 mm. A smear slide was made of one of these mats. In the microscope (magnification - X1000) the bacteria appear as numerous practically

identical very small semitransparent sticks (size 1-2 μm); but more accurate study shows some typical forms. Some bacilli are structureless, others have small granules inside, and some of them have pointed tops or pinches.

Bacterial mats from Core BS-294G were located at the top on the surface of clast of broken carbonate crust. They form a rather dense and thick (up to several millimetres) cover, which is white on the outside and yellow and rose inside. A thin section of one of these mats shows that it is structureless, but the stick-like bacteria can be seen on the smear slide under the microscope. They are longer and sometimes thicker than bacteria from other cores. Their size is generally about 2-3 μm, but in a few cases up to 10 μm. Many of them are curved or kinked in form. Some granules and partitions could be seen in some of the bacteria.

e. GEOCHEMICAL SAMPLING

A.N. Stadnitskaya

The targets of the geochemical programme and the methods used during the second leg of the cruise in the northern part of the Black Sea on the Crimean continental margin were the same as those described for the Mediterranean Leg.

Sampling

During Leg 2, a total of 6 cores which recovered mud breccia were selected for further geochemical investigation and sub-sampled on board. The cores sampled were taken either from or nearby mud volcanoes (BS-287G, BS-292G, BS-293G, and BS-296G), mud flows (BS- 288G), or from a collapse structure (BS-284G).

According to the lithological description, these cores can be divided into two groups. The first group represents cores which recovered mousse-like mud breccia with insignificant amount of small rock clasts overlain by recent sediments (BS-284G, BS-287G, and BS-288G). These cores contained gas-saturated sediments that crumbled away on the deck under the influence of gas discharge after being extracted from the core barrel. The cores which recovered 'typical' mud breccia (BS-292G, BS-293G, and BS-296G) with clasts visible to the eye were assigned to the second group. All of them were noted for high gas content as well, especially Cores BS-288G and BS-292G, which also contained much gas hydrates.

Gas hydrates

Abundant gas hydrate inclusions from the lower part of Cores BS-288G, BS-292G, and BS-294G were saved and described in a cold laboratory. On a morphological basis, three types of gas hydrates can be distinguished:

(1) tabular fragments of a regular thickness with dimensions of up to 5x3x0.5 cm, characterized by 'a compacted pillar-like' structure (i.e. crystals growing perpendicular to the upper surface). The convex surfaces of these fragments are white in colour and their sides are translucent;

(2) isometric subrounded fragments with dimensions of up to 3x2.5x2 cm. These fragments are probably clasts of a larger tabular gas hydrate body;

(3) branching fragments that look like branching three-dimensional veins with variable thicknesses of up to 0.3 cm.

Preliminary conclusions

According to a preliminary analysis of the data obtained, we can conclude that a higher level of gas saturation is associated with mud volcanoes and fault systems. Some of the gas is undoubtedly of biogenic origin, but the strong link between sediments with an elevated gas content and specific tectonic structures suggests intensive hydrocarbon gas inflow from depth via zones of enhanced permeability.

f. CONCLUSIONS

A.F. Limonov and M.K. Ivanov

The investigations in the Sorokin Trough have led to quite unexpected results that can be summarized as follows:

(1) The diapiric folds in trough have the trends which differ from those inferred before. These trends are controlled by the older Cretaceous-Eocene Tetyaev Rise and Shatskii Ridge. The diapirs seem to have been produced by a lateral tectonic compression from the south. In this process, structural elements formed in the plastic Maikopian clays as a result of being compressed by Cretaceous-Eocene structures acted us a press tool forming against the rigid blocks of the submarine terminations of the Crimean and Caucasian meganticlinoria.

(2) Many diapirs in the trough are crowned by mud volcanoes, and in this respect they are similar to diapiric folds in the Kerch and Taman Peninsulas. Sixteen structures revealed in the MAK-1 sonographs could be centres of mud eruption. Confirmation that 10 of them are mud volcanoes was made directly by bottom sampling. The eruptive centres have different morphology and can be subdivided into four types:

(i) conical mounds with a relatively regular plan shape, a few tens of metres high and 300-600 m across;

(ii) collapsed structures with a diameter of 800-1200 m, which formed by the collapse of a feeder channel after the escape to the seafloor of a large volume of eruptive products;

(iii) 'Barbados type' mud volcano (the only example to be found is the Dvurechenskii mud volcano). It is characterized by steep but low walls, flat top, and eruptive products with a high fluidity;

(iv) large-scale fissure eruptions of mud breccia, found for the first time in the Black Sea and, possibly, in the world.

The Kazakov mud volcano belongs perhaps to a separate type because of its large size and specific location outside the diapiric zone. It is supposed that it could be morphologically similar to some large mud volcanoes in the central Black Sea.

(3) Type (iv) of mud breccia eruption strongly supports our hypothesis that mud volcanoes form under conditions of tectonic compressional stress (*Limonov et al., 1996*). According to this hypothesis, mud breccia can be squeezed out to the seafloor along fault planes under the influence of lateral compression affecting plastic fluid-saturated formations.

(4) Rock clasts in the mud breccia are represented by clay and sandstone from the Maikopian Formation and by fragments of younger deposits. Hence, the Maikopian Formation is a source formation for the mud volcanoes and at the same time a diapir-forming member. This testifies to the close relation of clay diapirism and mud volcanism in this peculiar case, although we know many examples of their separate developments.

(5) The mud breccia from the discovered mud volcanoes contains much gas and often abundant accumulations of gas hydrates. The gas analyses are now

in progress, and we have no evidence yet for its thermogenic origin; however, the link between the mud volcano roots with the deeply buried Maikopian Formation suggests this.

(6) Deep-water chemosynthetic communities, in the form of bacterial mats which have developed in methane vents, may be the first in the world to be found in the strong presence of hydrogen sulphide.

The data obtained significantly increase the evaluation of the gas-and oil-bearing potential of the Sorokin Trough and make it a very promising prospect for discovery of deep-water hydrocarbon pools.

4. The Pallas Uplift area

a. INTRODUCTION

A.F. Limonov

The survey undertaken on the Pallas Uplift was a coopertive activity with ROSKOMNEDRA.

The Pallas uplift is situated off the Kerch Strait, at a waterdepth of about 700-1400 m. It was discovered in the first half of the 1970s as a result of pioneering deep seismic survey by the Yuzhmorgeologiya Association (Gelendzhik). The uplift has dimensions of about 40 by 15 km and it is expressed only in pre-Maikopian deposits, being overlain by slightly deformed younger sediments. Its Paleocene-Eocene top occurs at a depth of the order of 5.5 km, and a significant part of the overlying sequence is represented by Quaternary sediments of the paleo-Don and paleo-Kuban Rivers, which can be as thick as 2-2.5 km (*Tugolesov et al., 1985*). After dividing the Black Sea into national economic zones, the western part of the uplift fell within the Ukrainian zone and the eastern part within the Russian zone.

The Pallas Uplift is considered to be promising for hydrocarbon occurrence. There is a far-reaching plan for possible drilling of some deep commercial holes on the uplift. However, the shallow subbottom structure in the uplift area has been poorly studied previously, and one of the interesting problems was the searching for hydrocarbon seeps above this deeply buried structure.

b. SEISMIC REFLECTION PROFILING

L. B. Meisner, M.K. Ivanov, A. L. Volkonskaya, S.V. Bouriak, and V.G. Gainanov

The principal seismic profiles on the Pallas uplift were shot in a sublatitudinal direction, along the continental slope (Fig. 93). The location of the profiles was dictated by the integration of seismic and multibeam surveys. The line spacing was about 2 km, and the length of each line was about 60 km. Additional lines were run in the central-eastern part of the study area to trace the behaviour of a reflector which could be related to the base of a gas hydrate layer.

In the seismic sections, the complex upper cone of the paleo-Don and paleo-Kuban Rivers shows up as a system of stacked individual fans with channels and levees. The central position in this system is occupied by a relatively small fan, which is situated inside a wide valley. Most of it is overlain to the west and particularly to the east by younger fans (e.g. PS-263, 19:15-19:45; Fig. 94). The width of this fan as expressed on the seafloor is 5.3 km, with a total width of about 16 km. The sediment thickness in the fan is 0.2 km. The related channel is up to 1.8 km wide, and its depth is about 50 m. The channel can be traced from north to south, from line PS-263 to line PS-267 where it is filled with sediments. The western levee is well-seen in northern profiles PS-263 and PS-264. The eastern levee is less well-represented in the seafloor relief. The width of the levees is up to 1 km and the maximum elevation is about 60 m. The fan sediments have a mainly transparent seismic appearance, with two thin groups of parallel reflectors.

The westernmost fan has the largest dimensions and the shallowest depth in the study area. Its width and seafloor relief are 35 km and up to 300 m respectively (Fig. 95). The thickness of the fan sediments reaches 400 m. The fan is cut by three channels. Their widths are up to 1.2 km with depths of 50 to 150 m. From the MAK-1 profiler data, it is seen that the bottom of the eastern channel is eroded, suggesting continuing sediment transit. The accompanying levees have an elevation of up to 90 m. The fan sediments are characterized mainly by two seismic facies. A seismic facies with parallel reflectors lies at a depth of 100-120 m below the seafloor, in the upper part of the sequence. The amplitude of the reflections varies markedly there.

Below this seismic interval, an acoustically transparent seismic facies predominates. In some areas along the eastern front of this cone, a chaotic seismic facies occurs (e.g. PS-263, 18:18-18:40; PS-264, 00:00-00:30). This seismic facies may be caused by a rough erosional surface rising to the seafloor and producing numerous diffractions.

The western margin the fan described above onlaps a buried fan that is well observed in profile PS-267 (14:00-15:00). The upper subsurface sediment of this fan is represented by a group of low amplitude reflections. The main part of the fan is composed of an acoustically transparent seismic facies. In some areas there is a low amplitude chaotic seismic facies developing upward from the base of the fan and probably related to gas migration from the underlying beds. The apparent width of the fan is 7 km, and its sediments are up to 300 m in thickness.

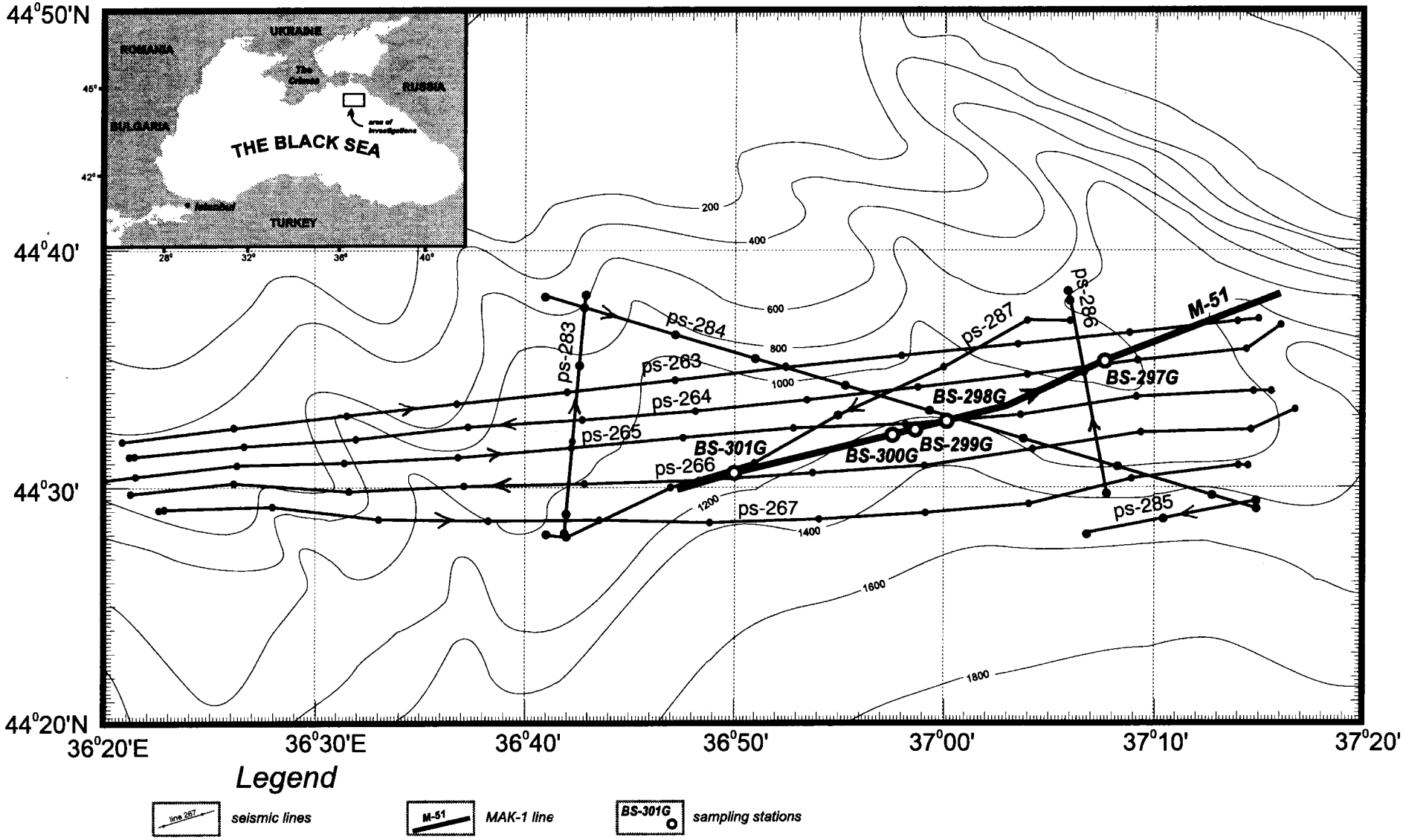

Fig. 93. Location map of seismic lines, MAK line 51, and sampling sites in the Pallas Uplift area. Bathymetry after *IOC-UNESCO (1981)*

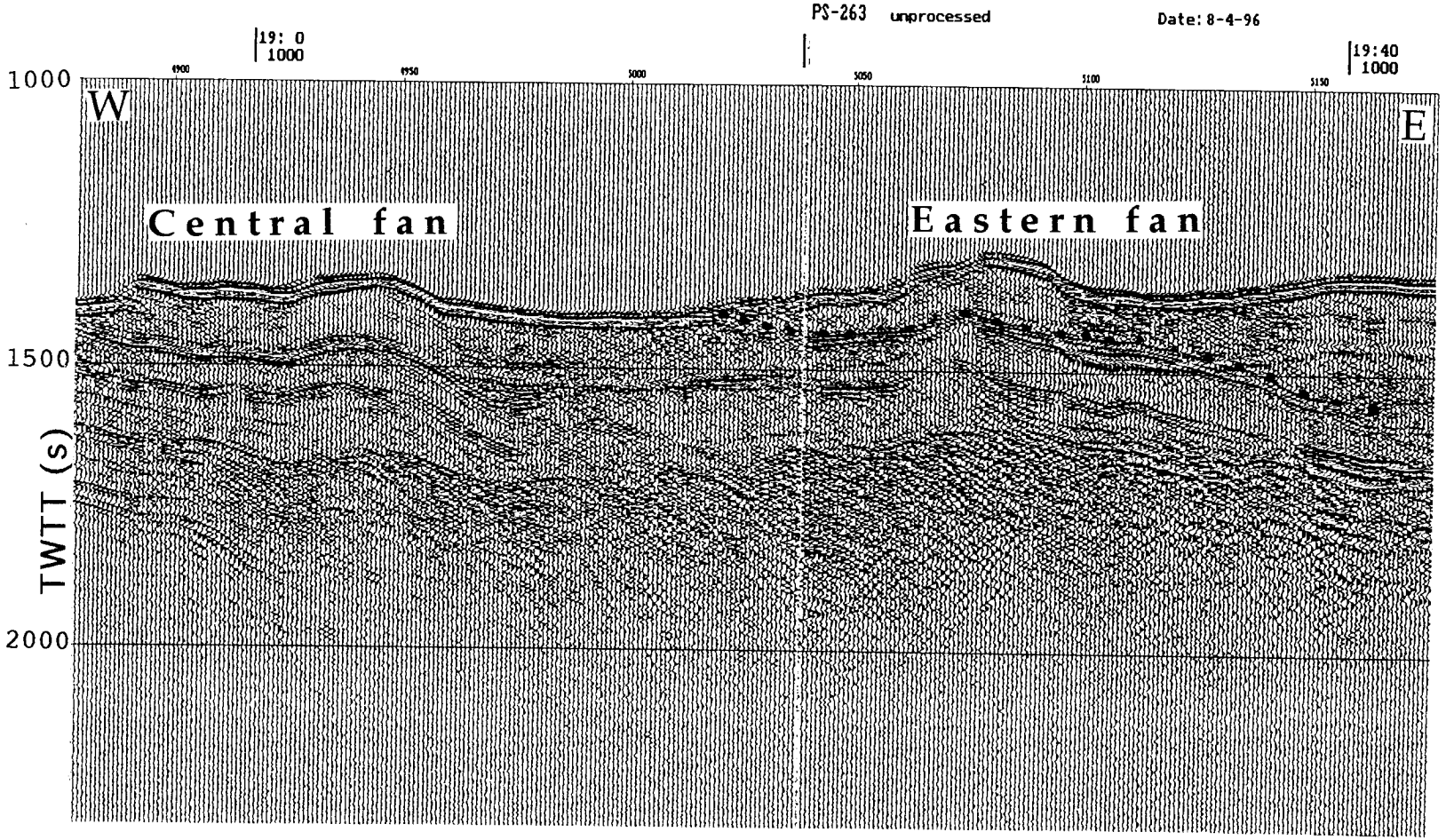

Fig. 94. Detail of seismic profile PS-263 showing the central fan overlain by the eastern younger fan of the paleo-Don/paleo-Kuban Rivers

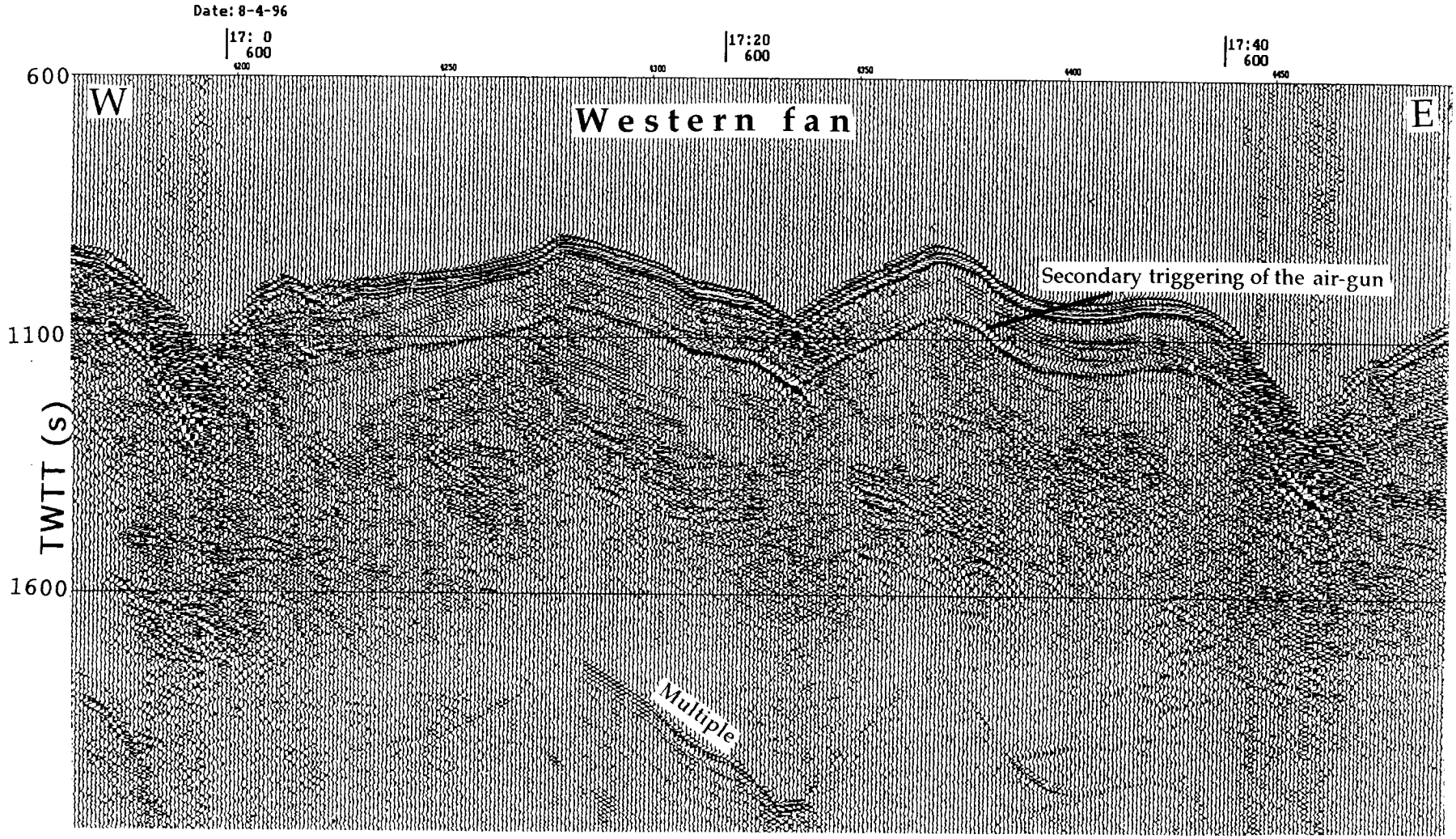

Fig. 95. The western fan in the seismic profile PS-263 is seen to be cut by three valleys

The easternmost fan was imaged incompletely in seismic sections, because the seismic lines terminate in the deep Anapa Canyon, believed to be its principal channel. According to the MAK-1 sidescan sonar and profiler data, the bottom of this canyon is covered by soft undisturbed sediments, suggesting that there is no active sediment transport through it in recent time.

There are no other channels to the north of the western part of this fan, but two rather wide channels are observed in three southern seismic lines (PS-265-267). They seem to be currently inactive. For instance, in profile PS-265 (06:40-06:50), a large slump has dammed up one of the channels. The visible part of the fan is about 23 km wide, and the thickness of its sediments is 300 m. The elevation of the fan in the seafloor relief is 200 m. The seismic pattern is dominated by an acoustically transparent seismic facies which is particularly well seen in profile PS-267. The base of the fan is indicated by a reflector that is clearly expressed in some segments of the profiles, but which has a 'dispersed', discontinuous seismic signature in other segments, and is almost untraceable in profiles PS-266 and PS-267. This reflector approaches the seafloor within the neighbouring valley to the west of the fan, thus marking its western boundary.

As a consequence of the stacking of the fans, their wavy surface, and the presence of erosional valleys, the seabottom in the area of Pallas Uplift represents a rather dismembered surface. This dismembering is reflected in the bathymetric map constructed on the basis of EM-12S multibeam echosounder data. On this map, with contour intervals of 25 m, there are numerous ridges and valleys extending in a NW-SE direction. Within the eastern fan, 6 ridges and 6 valley are observed; the central fan is characterized by 3 ridges and 3 valleys; and the western fan is cut by 5 ridges and 5 valleys. Therefore, the combination of the seismic and multibeam echosounder data provide detailed structural-geomorphological characteristics of the study area.

The formation succession of the individual fans is not clear yet. Evidently, the buried fan in the western part of the study area is the oldest one. The sediments of the central, topographically expressed fan accumulated earlier that those of the topographically expressed western and eastern fans. The timing of the formation of the latter fans can not be established yet. Because the available data indicate that the western fan has an active valley, and an active valley has not been found within the eastern fan, one may assume that the Kuban's sediment discharge migrated mainly westward during recent geological history.

Another as yet unresolved question is the nature of the reflector underlying the sedimentary sequence composing the above described upper fan. In all of the seismic sections recorded in the Pallas Uplift area there is a strongly scattering boundary, above which a normal layered sequence is observed and below which is a zone of acoustic turbidity with poorly seen, discontinuous reflectors. This boundary has a regional distribution over the whole study area. It is most clearly expressed in the western part of the study area, where it approximately follows the seafloor topography. At a waterdepth of about 1100 m, it is observed at a depth of 250-300 ms below the seafloor, but it rises nearer to the seafloor in shallower water. Sometimes, in those areas where the scattering boundary is not traced (that is, where the acoustic turbidity is absent), a

discordant surface is seen at approximately the same depth (e.g. line PS-264, 22:10-22:40; Fig. 96). This scattering boundary is observed in the seismic records to cross lithological boundaries in at least two places: in profiles PS-266 (09:10-09:20) and PS-287 (around 16:50). However, normally this boundary lies parallel to other reflectors, and, hence, we cannot say with confidence whether the boundary is controlled by lithology.

From our standpoint, there are at least two possible interpretations of the observed seismic pattern. First, one may suggest that the described boundary is a BSR, that is the base of the gas hydrate stability zone. In such a case, the acoustic turbidity above it could be explained by gas hydrates forming discrete small lenses, alternating with areas of fluid-saturated rocks, rather than a continuous layer. The lower boundary of such layer would have a discontinuous appearance and a rough relief that would lead to the increased scattering and diffractions observed on the seismic section as acoustic turbidity. The dispersed areas of acoustic turbidity seen at different depths in the eastern part of the study area could be explained by gas saturation of sediments. However, the calculations show that in order to allow the BSR to be situated at such subbottom depths at the indicated waterdepth, one needs to assume that the thermal gradient in the area is anomalously low (approximately one third as much as in the deep Black Sea Basin).

An alternative explanation is that the observed scattering boundary is an erosional surface with essentially rough relief. Then, in those places where the acoustic turbidity passes into the clearly displayed discordance surface, the relief of this boundary would also change for some reason.

Thus, in summary, the seismic sections show the composite upper cone of the paleo-Don and paleo-Kuban Rivers which developed during Pleistocene time. The separate onlapping fans formed a single body with a complex topography. If the scattered boundary is a BSR indeed, one may suppose that the thick gas hydrate layer acts as a caprock for the fluids upwelling from depth. This may be the reason why we do not observe many traces of fluid escape on the seafloor in the area of the Pallas Uplift. Anyway we cannot adequately explain this phenomenon, and this problem needs more detailed analysis of the available data.

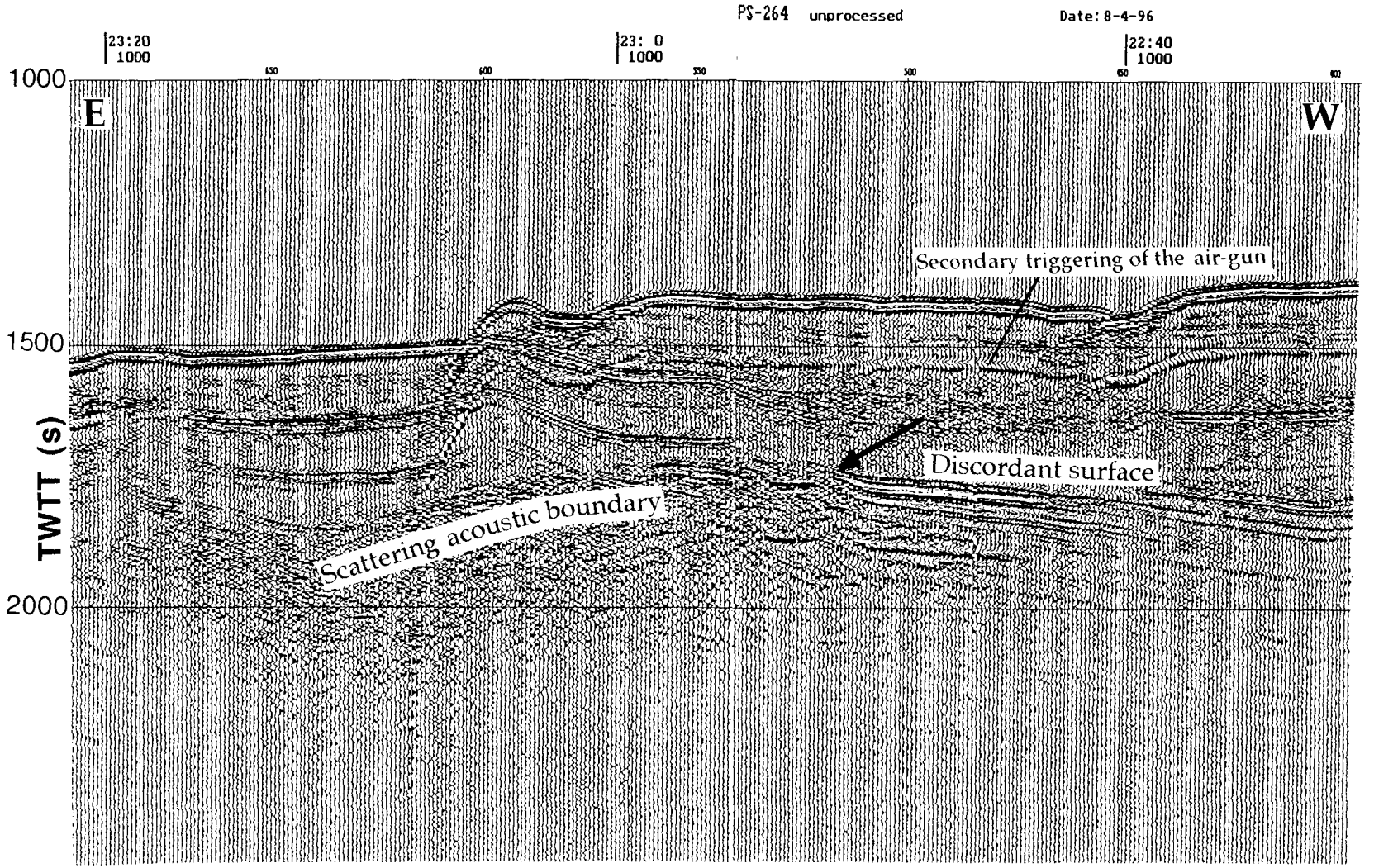

Fig. 96. Transition from the scattering acoustic boundary to the discordant surface (see text for explanation). Seismic profile PS-264

c. DEEP-TOW MAK LINE 51

A. F. Limonov, M. K. Ivanov, and J. M. Woodside

Line M-51 was run over the buried Pallas Uplift (south of the Kerch Strait), from WSW to ENE, across the area, which was previously, during the TTR-6 Cruise, covered by high resolution seismic reflection profiles (Fig. 93). Some seismic profiles showed the presence of a supposed BSR and acoustic turbidity at a depth of 200-300 ms below the seafloor. Hence, the idea was to check whether gas migrates upward from that depth through fault zones, producing some characteristic seafloor features above the uplift.

The MAK line was directed parallel to the regional slope, which is cut by numerous deeply incised but broad valleys belonging to the paleo-Don/paleo-Kuban fan system.

At the beginning, from 20:52 to 21:40, the line crossed a narrow erosional valley trending NW-SE. Both slopes of the valley are covered by large slumps. The slump on the western slope forms an obstacle for sediment transport along the valley and causes the valley to make a turn around the slump mound. Some slump sediments are also seen along the valley course in the left (northern) part of the sonograph. The profile showed highly disturbed sedimentary sequences on both sides of the valley and no acoustic penetration beneath the valley bottom.

Going further upslope over a ridge, the line, from 21:40 to 22:40, demonstrated a very monotonous weak backscatter on the sonograph, which is the result of thick soft sediments blanketing the ridge. The thickness of these well-stratified and almost undisturbed sediments reaches 45 m. They consist of two units. The upper one, up to 15 m thick, is distinguished by strong reflectivity; and the lower one is characterized by low reflectivity and fewer and thick layering.

The eastern slope of this ridge, between 22:40 and 23:55, also shows sediment instability. The MAK image first displayed an area of moderately reflecting, short, sinuous lines, a few tens of metres wide, which were previously interpreted as 'tension fractures' (see Section II.3.b). The tension fractures pattern is replaced downslope (from 23:00 to 23:55) by an area with a mottled acoustic backscatter. High reflectivity patches, of up to 100 m across, are arranged in arcuate lines across the sonograph swath. The general background of the backscatter is enhanced (Fig. 97).

On the sonograph, one can observe a consistent thinning of the stratified sedimentary sequence downslope, to its complete pinching out at 23:55. The sediments are deformed by frequent, small folds due to their downslope gliding. The tension fractures area corresponds to some acoustic turbidity in the upper acoustic member. In the area of the mottled backscatter, no acoustic anomalies are observed. The distal part of this sedimentary apron appears to be detached. It is brought up short against a slightly uplifted block were no subbottom reflectors were recorded in the profile. The block is traced until 01:00. Although the surface of this block is marked by enhanced backscatter on the sonograph and by strong reflectivity on the profile, suggesting possible shallow gas occurrence, no

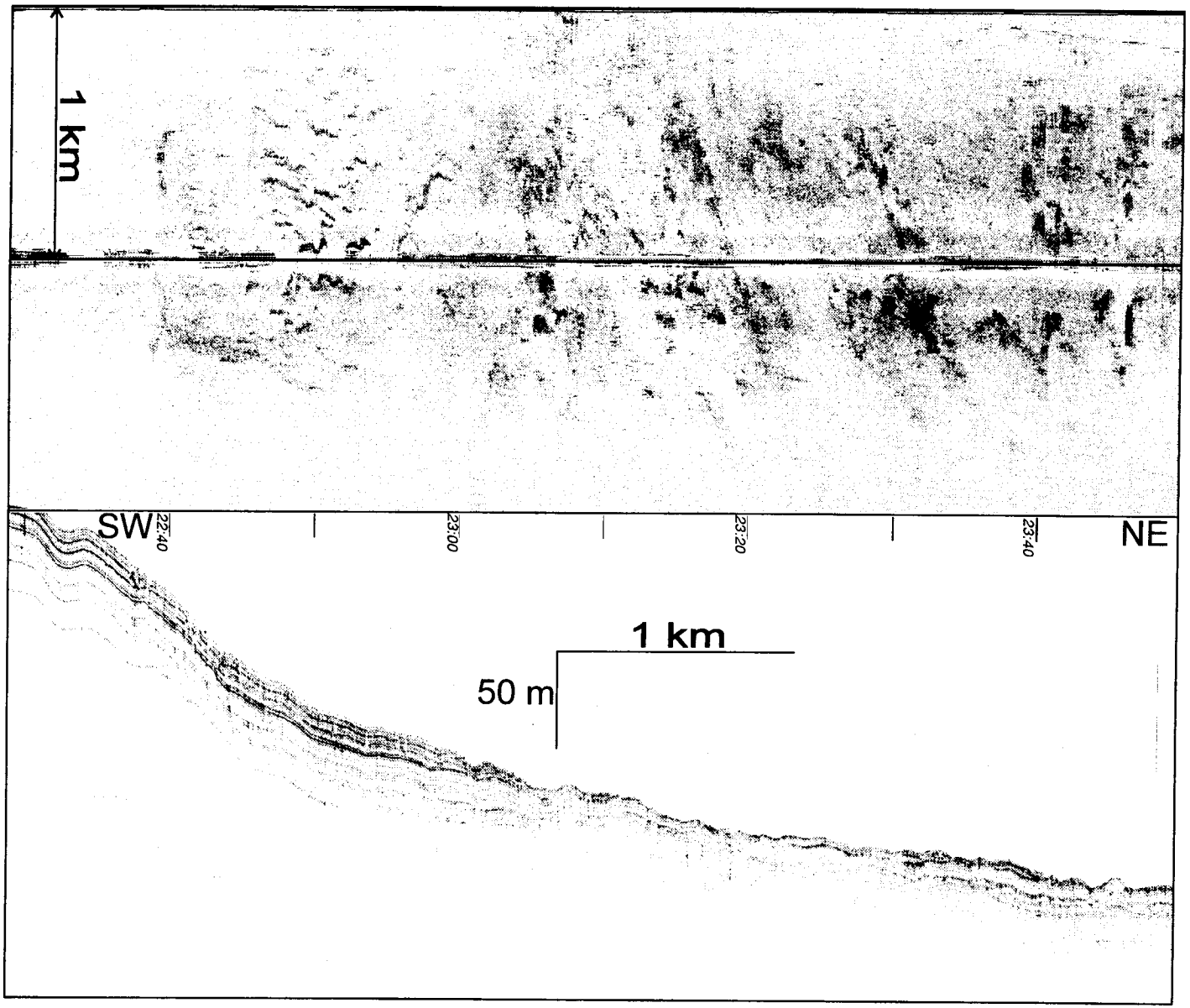

Fig. 97. Successive stages of surficial sediment slumping: from initial tensional fractures on the upper slope to an almost completely detached sedimentary apron at the foot of the slope. MAK line M-51

perceptible quantity of gas was detected in the core raised from this area. The strong reflectivity was conditioned by the stiff Novoeuxinian clay virtually exposed on the seafloor. Hence this block was interpreted as an area of active erosion inside a large valley.

From 01:00 to 05:00, the sonograph demonstrated variable patterns of acoustic backscatter. Most of them were produced by large-scale slumping down either regional or local slopes. The slump scars are clearly seen, for example between 02:25- 02:55 and between 03:45-04:08. The latter scar was left by a large, isometric block that slid in place. It is characterized by strong backscatter and is believed to be related to an active fault marked by very strong backscatter. The fault obliquely crosses the northern side of the sonograph at 03:40.

At least three erosional valleys were recorded along this portion of the MAK line. All of them have roughly the same, NNW-SSE, orientation. The valley, at 01:50, cuts through a layered sequence of unconsolidated sediments to a depth of about 15 m, and its bottom is characterized by low backscatter. In contrast to this, the valley at 03:27, which is incised to a depth of about 25 m into unstratified sediments, is notable for strong backscatter. There is an impression that the valley closes up in its upper reaches, visible at the very margin of the northern scan. The active fault described above continues just to that place. Thus, alternatively, the valley could be a linear slump trail, and the slumped sediments were cut off by the active fault. The fault in this place is also observed in the corresponding seismic section.

The valley at 04:40 has a clear erosional nature, but it probably also developed along a fault, as observed in the seismic profile. The seafloor reflectivity is high inside the valley both on the sonograph and the subbottom profile. The valley depth is more than 30 m. Its long eastern slope is complicated by a terrace, whereas the western one is steep and short. The terrace disappears upward the valley course, where the valley changes its trend more to the southwest. No subbottom reflectors are observed beneath the valley.

A large ridge stretches right perpendicular to the fish track across the sonograph between 01:30 and 03:20. Its summit has low reflectivity on the subbottom record, but some poorly seen, disturbed reflectors appear downward the western slope, accompanied by the gradual increase of the seafloor reflectivity. Unlike this, the surface of the eastern slope is notable for enhanced reflectivity on the subbottom profile. On the sonograph, the summital part of the ridge is marked by a very weak backscatter, the area of the weak backscatter abruptly widening both northward and southward from the sonograph centre. This low backscatter is apparently caused by thick unconsolidated bottom sediments. Between the weekly backscattering areas on both slopes of this feature, there are areas of moderate (to the west) and strong (to the east) backscatters, which are evidently related to slumping. The slumping might be initiated by two parallel faults cutting the ridge.

The most peculiar feature on the subbottom profile is a weak reflector which can be traced from 01:00 to 03:08 at a depth of 20 to 45 m below the seafloor. The reflector to some extent simulates the seafloor relief but in a very exaggerated form. In some places, there are something like acoustic voids where this reflectors approaches the seafloor (e.g. at 01:10 and 01:25). The reflector may

be related to shallow gas occurrence, but we did not get any evidence for this from the bottom sampling.

Between 05:00 and 07:00 the line crossed an uplifted plateau covered by undisturbed sediments with a constant thickness of about 20 m. On its gentle western slope, the sonograph showed a field of 'tension fractures' that can be considered as an initial stage of slumping on a gentle relief.

Further along the line, until 07:25, no seafloor features were recorded on the sonograph, partially the possible result of towing the fish too high above the seafloor.

From 07:02 to 04:05, the line crossed the eastern steep and step-like slope of the plateau. Again, the slope is characterized by large-scale slumping and the presence of large detached blocks with disturbed layering. An U-shaped erosional valley with steep slopes cuts the seafloor between two such blocks. It is well displayed on the sonograph as a feature with strong backscatter, bounded by straight walls with even stronger backscatter. The valley depth is more than 40 m, and the width is about 300 m. The valley bottom texturing implies that it is probably still active or has been active recently. The distal visible part of the valley on the south scan seems to be covered by soft sediments.

The eastern slope of the plateau is at the same time the slope of the large Anapa Canyon (named on the IBCM by strange name 'Kumani Canyon') whose eastern wall is observed at the very end of the line. The canyon depth is more than 200 m. It has a flat bottom covered by a 40-45 m layer of thinly stratified undisturbed sediments. The sediments are notable for a very high reflectivity on the profile but they show a low backscattering strength on the sonograph. A sedimentary apron enters the canyon from the northeast. The pattern of sedimentation in the Anapa Canyon clearly implies that it is inactive today.

Summarizing these observations, one may conclude that active fluid escape above the Pallas Uplift, if there is any, has an extremely limited scale.

d. CORING RESULTS

A. M. Akhmetjanov, G. G. Akhmanov, A. V. Korkin, E. V. Kozlova, S.S. Gablina, A. P. Sautkin, A. J. Doets, S. Woodside, I.Yu. Belen'kaya, and A.N. Stadnitskaya

Introduction

The area called the Pallas Uplift lying off the Kerch Strait was the focus of interest of the second part of Leg 2 (Figs. 93 and 98). We took 5 gravity cores there, recovering a total of 20.5 m of sediment. Generalized core logs are shown in Figures 99-103. The sampling sites were selected after the preliminary interpretation of the MAK-1 sonograph and profile M-51. The main objectives of the bottom sampling were: (i) to calibrate the acoustic facies on the M-51 sonograph sedimentologically; (ii) to elucidate whether the uppermost bottom sediments are gas-charged; and (iii) to determine recent sediment transport processes.

Ground-truthing MAK Line 51

Core BS-297G

The core was taken from a local high slightly west of the Anapa Canyon (Fig. 98). The sonograph showed moderate acoustic backscatter; and well-layered subbottom sediments were seen on the profiler record to a depth of 45 m bsf. This sampling site had been chosen to provide a reference core in which the sedimentary sequence might be typical of the region in general.

The core recovered 5.9 m of sediment, all hemipelagic (Fig. 99). Three sedimentary units typical of the Black Sea sediments were observed as follows: (i) a fine alternation of coccolith ooze, sapropel and grey clay laminae to a depth of 1.3 m; (ii) a greenish grey sapropel layer with the upper half obviously diluted with clay and the lower boundary at 2.1 m; and (ii) an interval of grey dense silty clay with hydrotroilite admixture down to the end of the cored section. The last interval had a streaked appearance due to the presence of darker hydrotroilite-rich layers some of which were also silty. The frequency of occurrence of dark layers approached to about 20 layers per 10-cm interval. A well-expressed and rather thick black layer of hydrotroilite-rich clay was observed at 3.4-3.8 m. The last 10 cm taken out from the core catcher was obviously porous, probably as a result of gas saturation, although there was no H_2S smell.

Core BS-298G

This core was sampled from the flat top of a strongly acoustically backscattering slump block (Fig. 98), situated within an erosional valley. Almost no penetration was seen on the subbottom profiler record. The core, 2.77 m long, consisted of hemipelagic sediments (Fig. 100). Its sequence included only the upper and lower sedimentary units found in Core BS-297G. A finely-laminated interval was observed in the upper 10 cm, whereas the rest of the section was

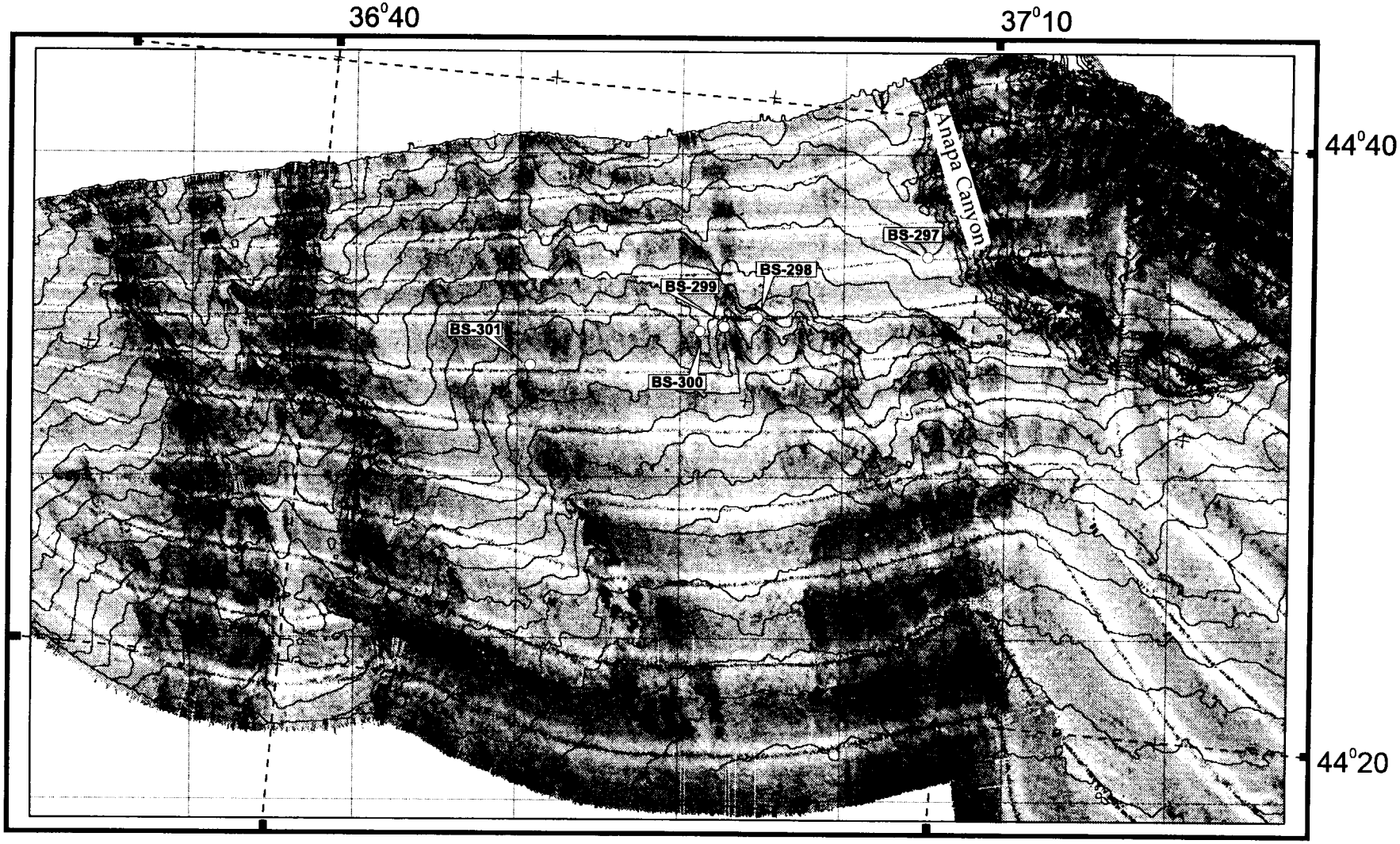

Fig. 98. Location of sampling sites on the Simrad EM-12S bathymetric and seafloor reflectivity map of the Pallas Uplift area

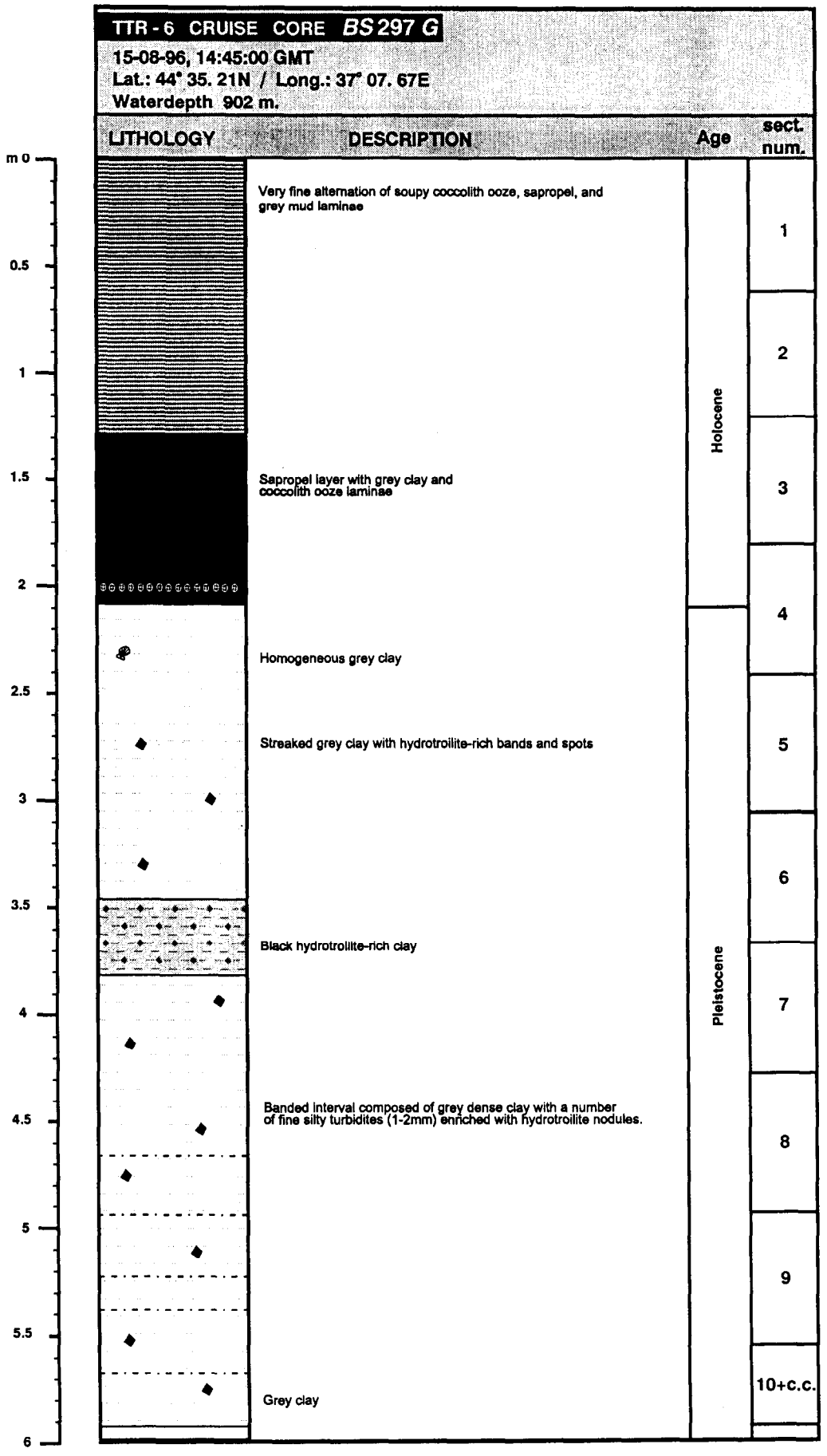

Total length: 591.5 cm

Fig. 99. Core log BS-297G

represented by grey, dense, streaked clay with hydrotroilite. A black layer of hydrotroilite clay was observed at 0.9-1.4 m. The interval was disturbed by numerous cracks and microfaults, some of which were filled with hydrotroilite nodules and sometimes appeared to be surrounded by dark haloes.

Core BS-299G

This core was taken from the same valley as BS-298G, about 3 km to the west-southwest. A similar acoustic pattern was seen on the sonograph and subbottom profiler records. A section of hemipelagic sediments with a thickness of 2.62 m was recovered (Fig. 101), with the same set of the sedimentary units as in Core BS-298G. A grey clay interval with a black layer of hydrotroilite-rich clay at 0.9-1.2 cm was overlain by a finely-laminated interval with a thickness of 5 cm. A number of cracks and microfaults developing in the black clay layer was observed in the middle of the interval.

Core BS-300G

This site was situated on the crest of a local mound lying 2 km to the west-southwest of Site BS-299G (Fig. 98). A low acoustic backscatter was recorded on the MAK-1 sonograph, while the subbottom profiler showed a penetration of 20 m through vaguely stratified sediments. The core was hemipelagic also, and 5.4 m of sediments was recovered (Fig. 102). A full set of the same sedimentary units as in Core BS-297G was found. The lower boundary of the finely-laminated interval was observed at 0.55 m, while the lower boundary of the sapropel layer was found to lie at 1.3 m. The finely-laminated layer appeared to be more diluted with terrigenous clay in its lower half. The rest of the section was represented by streaked grey clay with hydrotroilite-rich layers. No single, thick, black hydrotroilite-rich clay layer was found.

Core BS-301G

The core was taken from the bottom of a canyon next to the southwest end of line M-51 (Fig. 98). The MAK-1 sonograph displayed a streaked pattern on the seafloor, suggesting active erosion by turbidity currents, while the subbottom profiler recorded a broad valley incised into well-stratified sediments and with almost no penetration below the seafloor. The core was hemipelagic, with a total recovery of 3.1 m (Fig. 103). Finely-laminated and grey clayey intervals were recovered, the lower abrupt boundary of the former being found at 0.25 m. A grey silty-clay interval with the remains of *Dreissena* sp. shells was observed directly below this boundary down to the bottom of the section. A black hydrotroilite-rich layer was found at 0.4-0.5 m.

Interpretation

According to their geomorphologic settings, all the cores can be divided into two groups. The cores taken from the canyons differ essentially from those taken from the divides (Fig. 104).

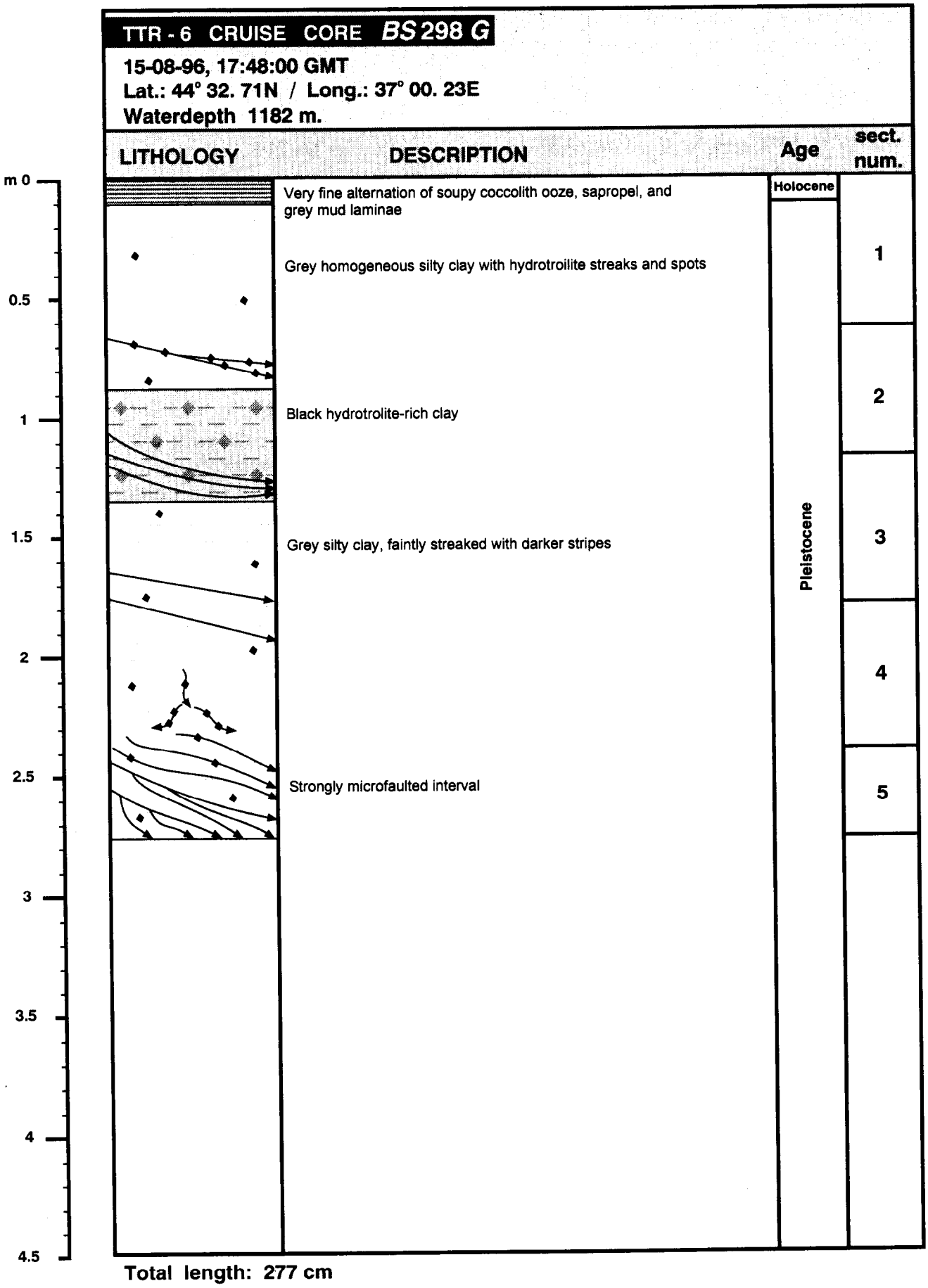

Fig. 100. Core log BS-298G

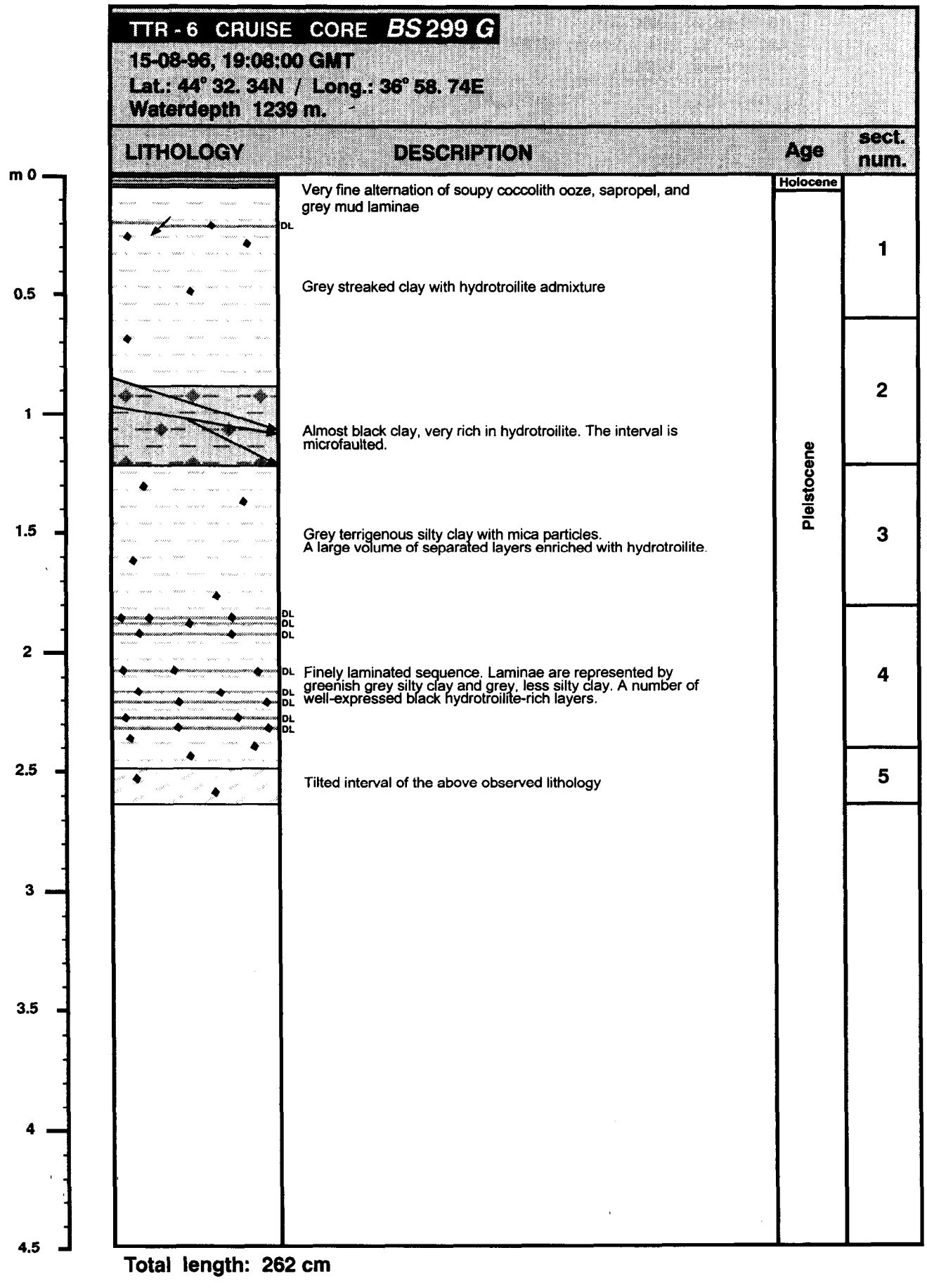

Fig. 101. Core log BS-299G

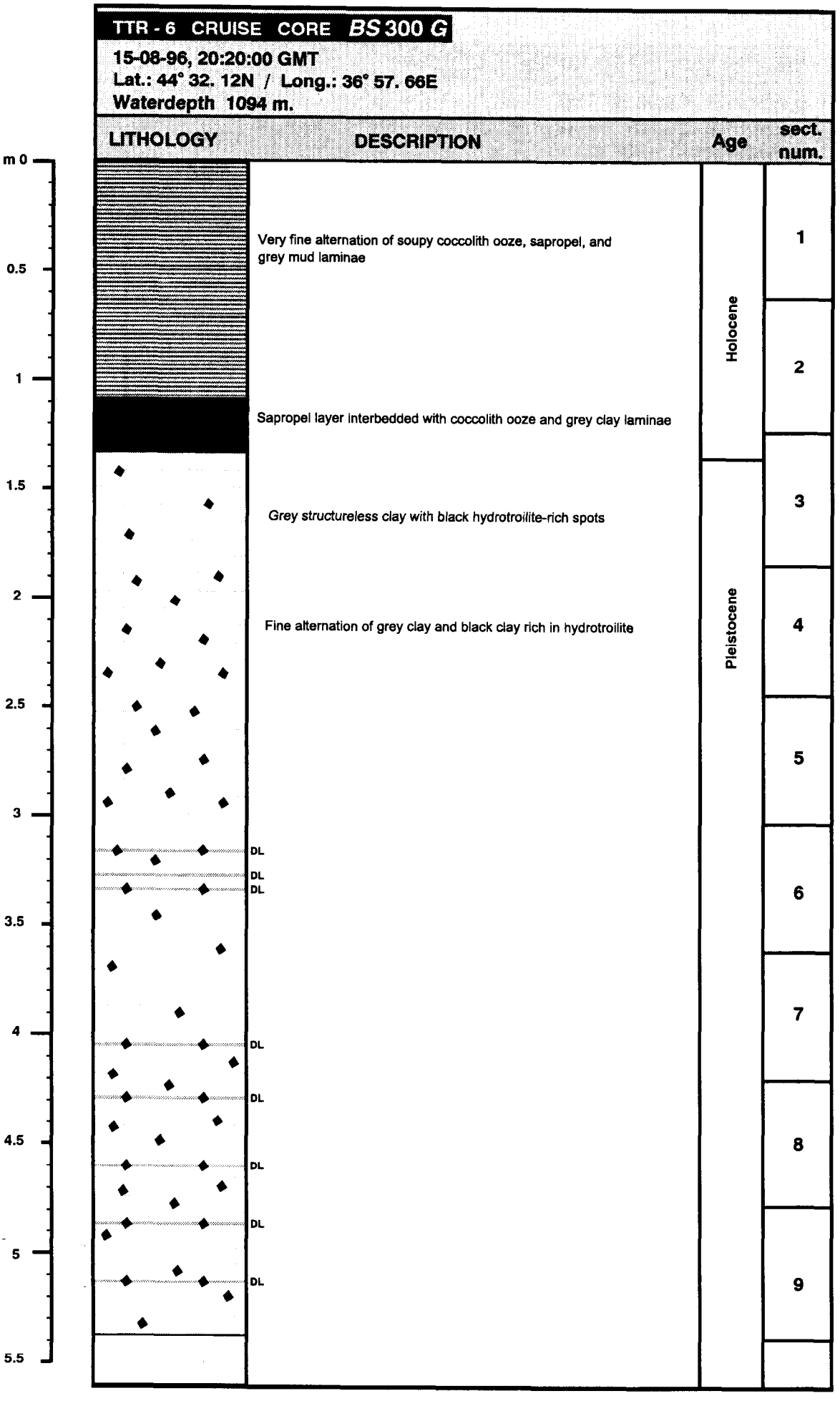

Total length: 540 cm

Fig. 102. Core log BS-300G

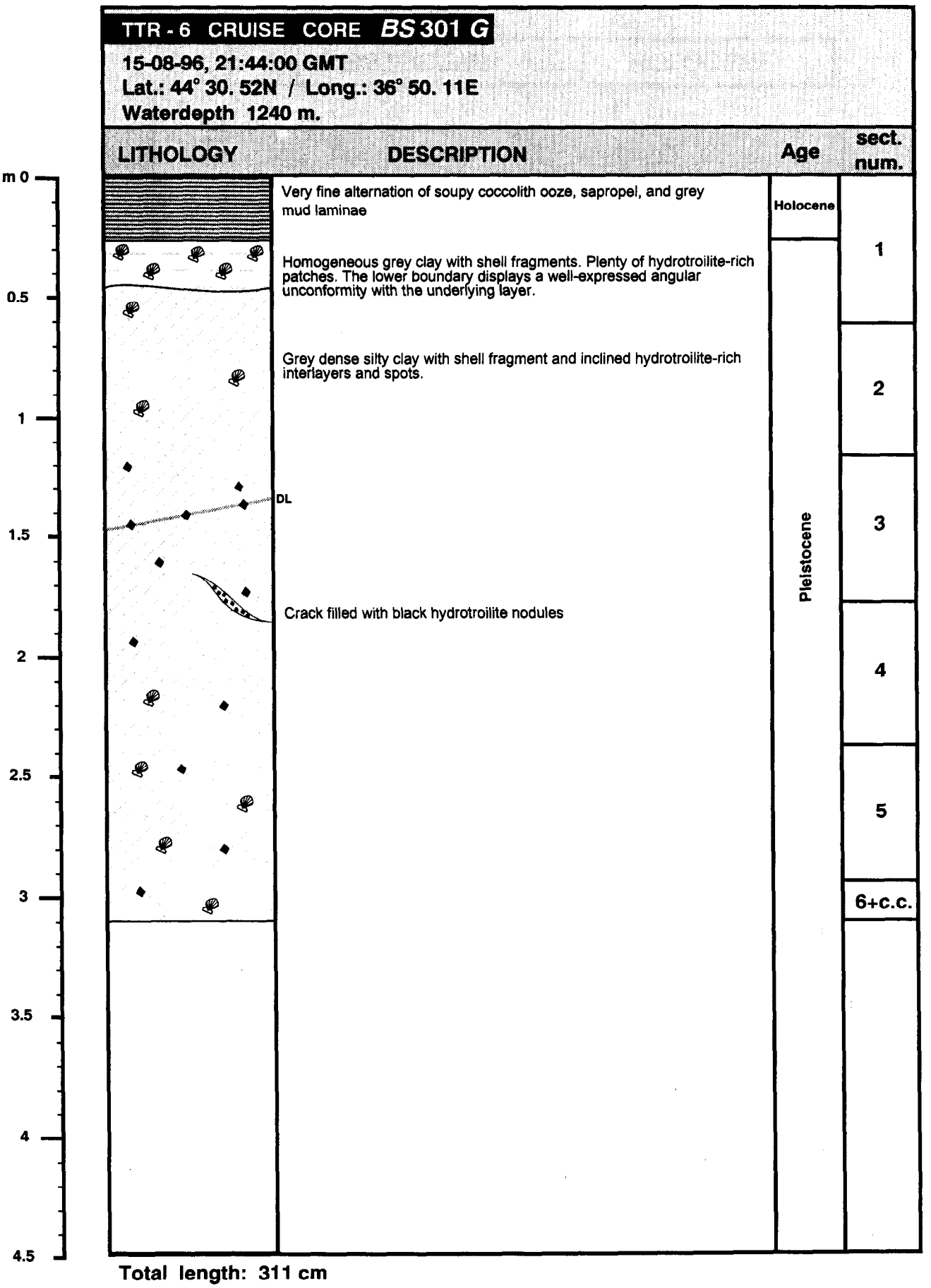

Fig. 103. Core log BS-301G

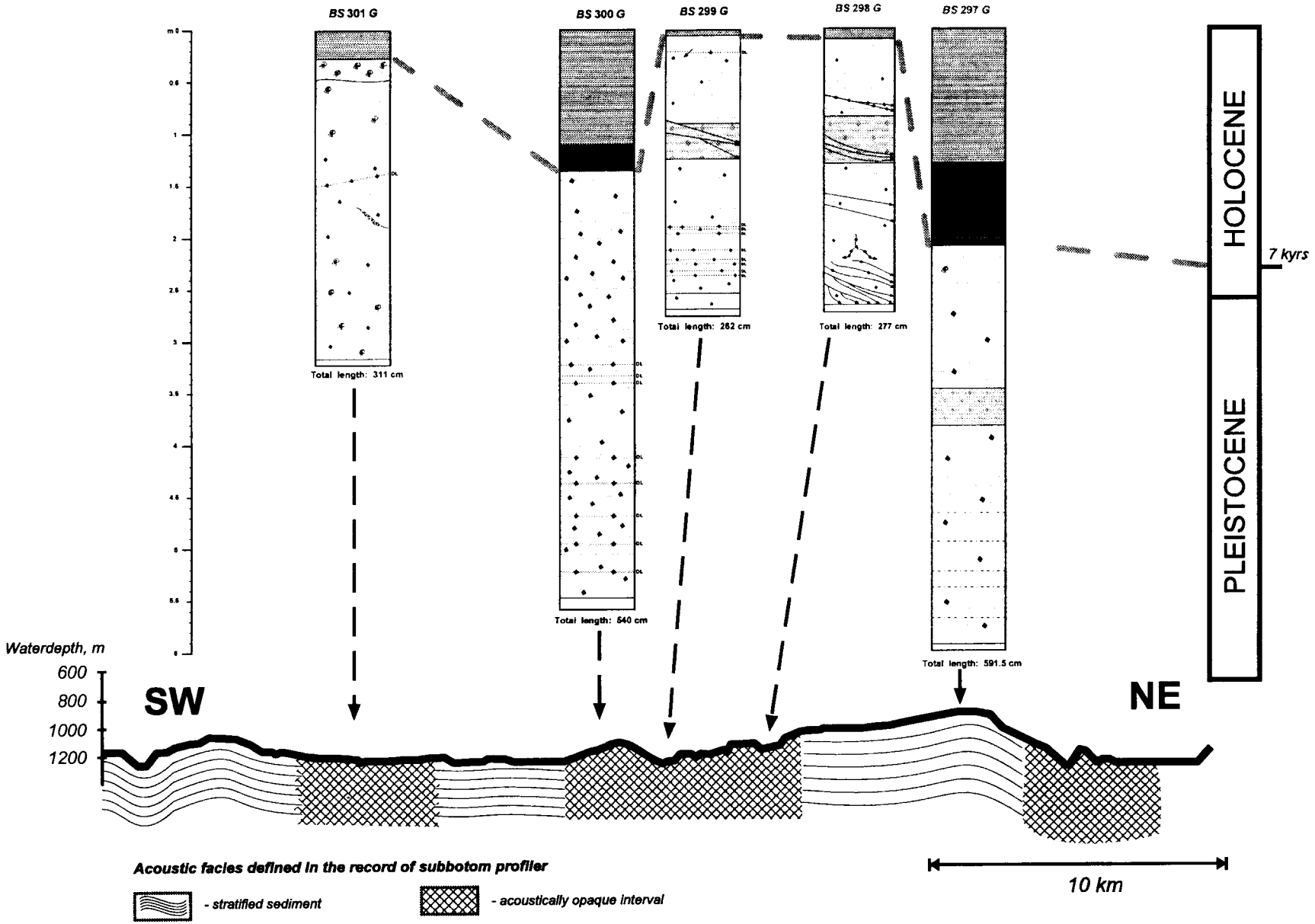

Fig. 104. Correlation of the cores recovered in the Pallas Uplift area along MAK line M-51

Cores taken from divides

Cores BS-297G and BS-300G belong to this group. A complete hemipelagic sequence was obtained in reference Core BS-297G, as was expected; and three units typical of the Black Sea Quaternary sediments were observed. The thickness of the Holocene sediments is comparable to that in the cores collected from the central part of the Black Sea (*Limonov et al., 1994*). The second core also recovered all of these units. This core contained a thinner sapropel layer (0.25 m) in comparison with Core BS-297G (0.7 m). The sedimentation rate for the Holocene sediments was estimated to vary from 15 cm/kyrs for Core BS-300G up to 20 cm/kyrs for Core BS-297G.

Cores taken from canyons

The cores belonging to this group (BS-299G and BS-301G) were obtained from valleys which are well-expressed in the seafloor topography. The bottoms of these canyons are usually characterized either by the absence of acoustic penetration or by penetration of a few metres on the subbottom profiler records. A reduced sequence of the Holocene sediments was the main distinguishing feature of the cores. No sapropel layer was recovered, and the whole sequence is represented by Pleistocene grey clays overlain by a relatively thin veneer (10-30 cm) of Recent sediments. Much evidence for sediment slope instability was recognized in almost all cores, largely in the form of microfaults and cracks disturbing the Pleistocene clays. Some of these disturbances are considered to be pathways for solutions responsible for the formation of the hydrotroilite nodules that are often located along cracks and microfaults. Core BS-301G contained abundant fragments of bivalve shells which are likely to have been derived from the adjacent shelf areas. This core is also remarkable because of the presence of an unconformity. On the basis of these observations, the canyon from which this core was taken can be considered to have been very active in the Pleistocene. Such conclusions were later also confirmed when the seafloor reflectivity map had been constructed on the basis on the multibeam echosounder data (Fig. 98).

Conclusions

The sampling data allowed us to better understand sedimentation processes in the area of the Pallas Uplift and to determine the causes of the backscatter patterns observed. Hence, the analysis of the sedimentary sequences sampled from different sea bottom features led us to the following conclusions:

(1) The channel system expressed in the modern relief in the area of the Pallas Uplift was active during Pleistocene time and it retains some minor activity to date.

(2) Holocene channel activity is mainly of erosive character and has resulted in the redeposition of sediments from the slope further toward the abyssal plain, although relatively coarse material derived from the adjacent shelf has accumulated in some channels in the Pleistocene.

(3) The enlarged thickness of Holocene hemipelagic sediments covering

local highs and divides is believed to be the main reason for the unexpectedly low backscattering level observed on the MAK-1 records.

(4) No evidence for gas escape was found, although it was expected from the seismic data.

5. Bathymetric mapping of the Russian Black Sea economic zone

A.F. Limonov

Similar to the survey undertaken on the Pallas Uplift, the bathymetric mapping of the Russian economic zone was essentially a coopertive activity with ROSKOMNEDRA. Only a brief general description of the results obtained is adduced below.

Simrad EM-12S mapping in the Black Sea was carried out for the first time. Bathymetric and navigation maps previously available were based on discrete soundings and conventional echosounder data along dispersed profiles.

The mapping was executed along approximately 25 profiles, within a zone roughly parallel to the Caucasian coast, from the area off the Kerch Strait to about 43°02′ N (Fig. 105). This zone includes the continental shelf, slope, and part of the abyssal plain, from a waterdepth of 250 m to more than 2200 m. This resulted in the construction of two bathymetric maps at scales of 1 : 200 000 and 1 : 300 000, with depth contours of 25 and 50 m respectively, and a bottom reflectivity map. All data were recorded in a digital form on a magneto-optical disk; and, therefore, there remains the possibility of constructing maps at any scale and with any contour interval within the accuracy limits of the observations.

The Caucasian continental slope is cut by numerous canyons generally trending in a NE-SW direction. At a depth of about 1800 m, this trend is abruptly superimposed by a NW-SE direction, which is defined by the presence of frequent linear folds of the Tuapse Trough. The trough occupies most of the lower continental slope and rise and is filled with the Maikopian Formation producing clay diapirs. It has the same structural position with respect to the Caucasus as the Sorokin Trough with respect to the Crimea.

All the canyons of the Caucasian margin are related to numerous currently or recently active rivers. Sometimes it is difficult to define to which river a canyon is linked, because a canyon head, as a rule, is shifted relative to a river mouth, and the canyons are supplied with sediments by along-shore transport. In many cases canyons are developing under the influence of the combined discharge of several small rivers.

The largest canyons in the mapped area are the Anapa, Pshada, Betta, Bzhid, Nechepsukho, Tuapse, Shakhe, Khosta, and Mzytma. Their average width reaches 8 km and the depth varies from 200 to 400 m. They can be traced from the shelf break to a depth of greater than 2000 m. Sometimes they cut across the diapiric folds of the Tuapse Trough.

The related fans form an almost continuous system on the continental rise, but their individual elements are expressed in the seafloor relief. On the reflectivity map, the canyons and fans show up as areas of strong reflectivity because of exposures of bedrocks on the flanks of the canyons and turbidite accumulation. Turbidite pathways are often displayed as a seafloor striation. The peculiarities of the structure of this wide turbidite system are not yet known and represent a first-order priority for future work.

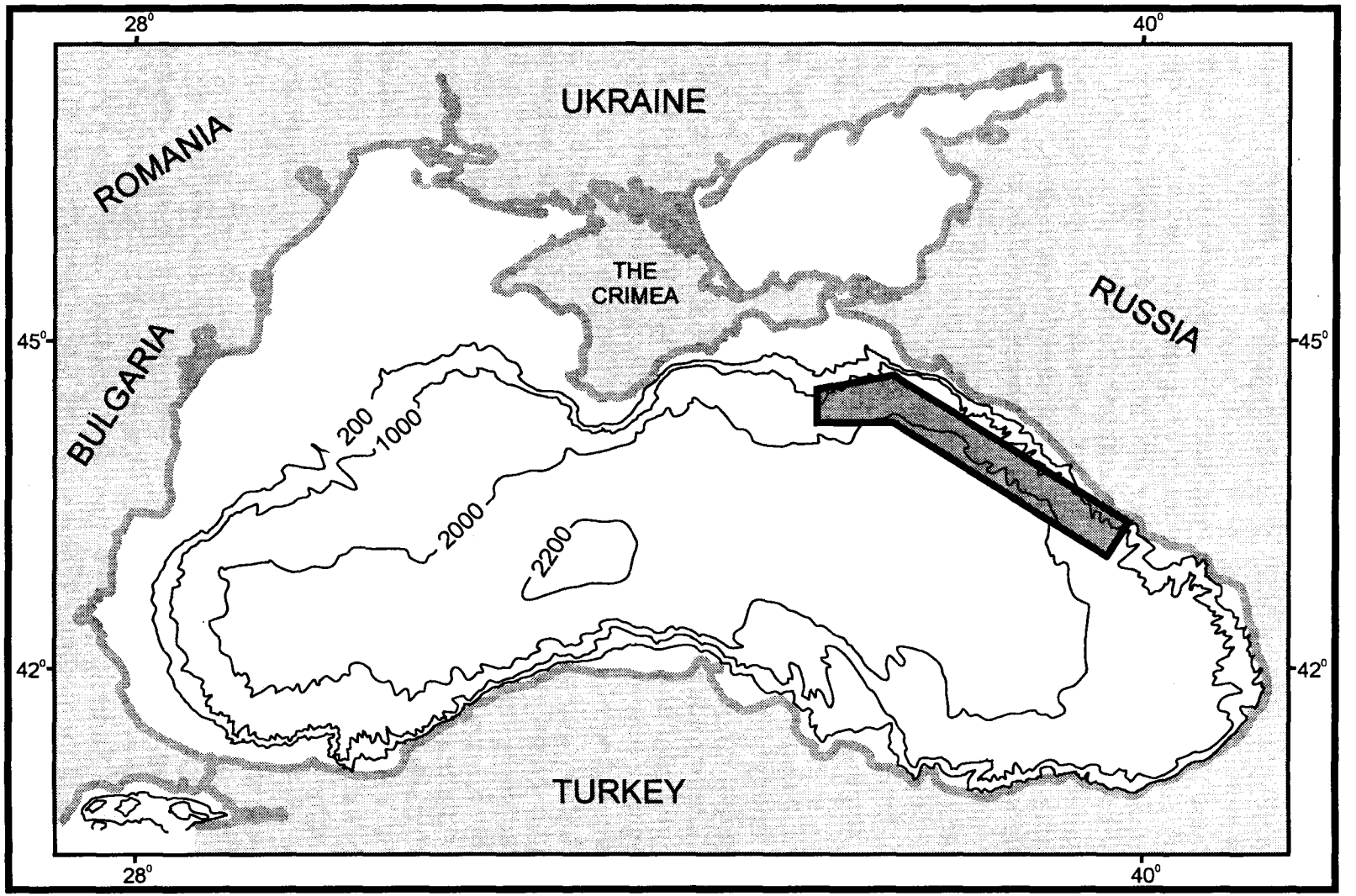

Fig. 105. Bathymertically mapped area within the Russian economic zone on the Caucasian margin

Diapiric structures recorded in the bathymetric maps have a length of up to 20 km, a width of about 2 km, and they rise to 200 m above the surrounding seafloor. As compared with similar folds in the Sorokin Trough, they are more linear and of higher amplitude. On the reflectivity map, there are also some isometric high reflective patches, 1 km or so across, which could be mud volcanoes. A clear relationship between them and the diapiric folds is not observed, and these features need more detailed study.

6. Coring results on the Caucasian margin

M.K. Ivanov, A.M. Akhmetjanov, G.G. Akhmanov, A.V. Korkin, E.V. Kozlova, S.S. Gablina, A.P. Sautkin, S. Woodside, I.Yu. Belen'kaya, and A.N. Stadnitskaya

On the Caucasian margin, within the bathymetrically mapped zone, three cores were taken from areas previously sampled during students' training cruises (mid 1980s, R/V *Feodosia*). All sampling sites (BS-302G - 304G) were positioned on the seaward-facing slopes of topographically expressed diapiric folds (Fig. 106) in order to exclude the influence of turbidite sedimentation from the Caucasian continental slope and to recover the Maikopian clays composing the diapirs. Nevertheless, all three cores contained turbidite sediments, and were disturbed to different degrees by slump processes.

The 5.36 m long *Core BS-302G* (Fig. 107) consisted from top to bottom of recent soupy sediments (0-0.24 m) underlain by a thick sapropel layer, a clay interval (0.51-2.08 m) with several turbidite interlayers, debris flow deposits represented by clay pebbles and angular clasts of sapropel, clay, and ooze between 2.08 and 2.5 m, and underlying sediments made up of clay with some turbidites. Another sapropel layer lies at the bottom of the core.

Core BS-303G was a 5.86 m long core taken from the same diapir. It is characterized by numerous sapropel layers and interlayers (Fig. 108). The uppermost soupy sediments were missing. Slump intervals containing coccolith ooze and slope breccia in a sapropel matrix were observed at 1.7-1.8 m and 4.06-4.11 m respectively. The lower part of the core (about from 2.5 m to the bottom) smelled of hydrogen sulphide.

Core BS-304G was obtained from another diapiric fold, northwestwards of the coring sites described above (Fig. 109). Turbidites were found throughout the core length (5.74 m), starting with the recent soupy sediments (Fig. 109). The sapropel layer is thick (80 cm), but it includes several thin interlayers of grey clay.

Thus, in summary, turbidity currents on the Caucasian margin demonstrate their periodic activity throughout the Pleistocene-Holocene. The diapiric folds serve as barriers on their way, but turbidity flows are capable to carry clastic material over them. The turbidite pathways and accumulations are clearly seen as dark areas on the corresponding seafloor reflectivity chart (Fig. 106).

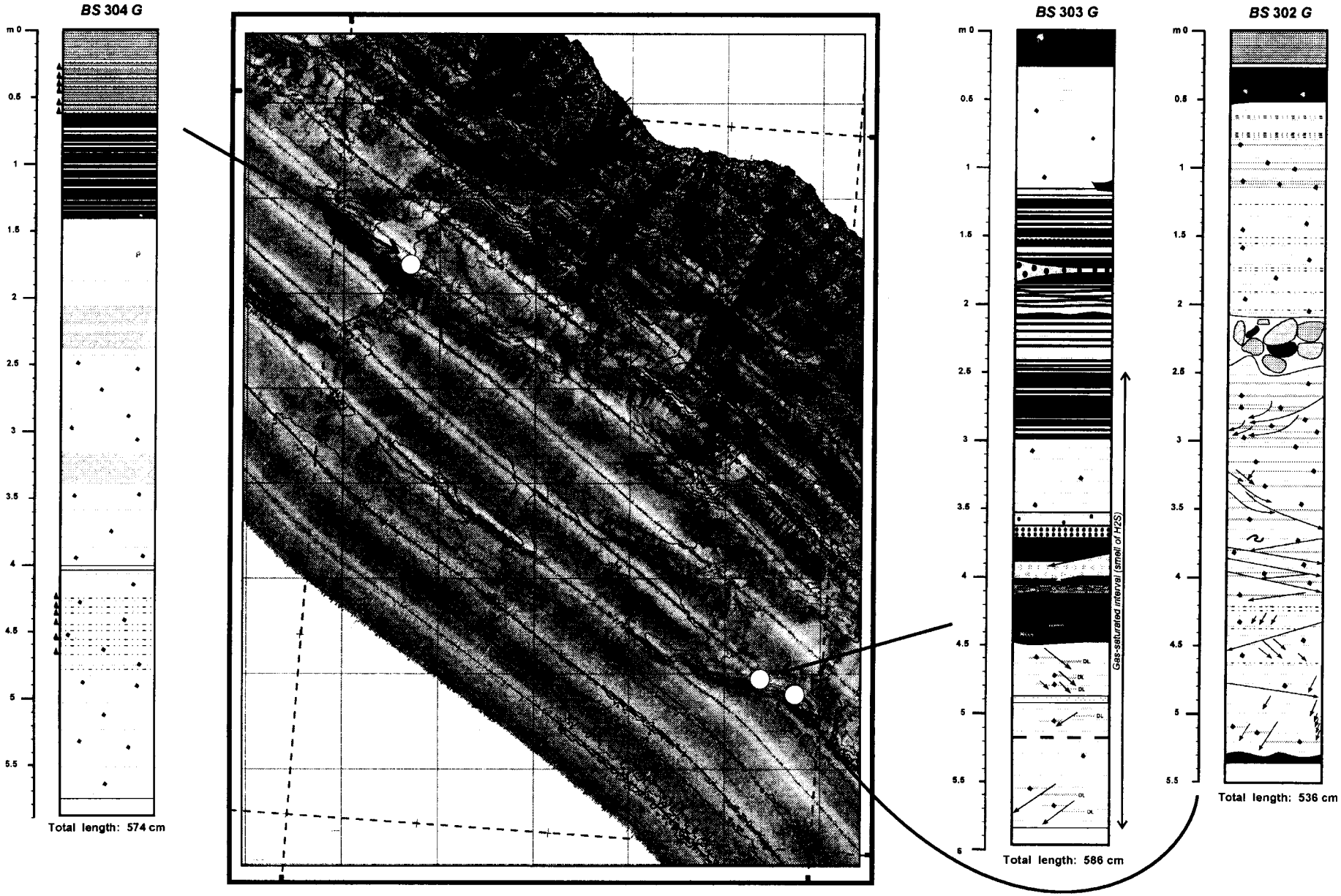

Fig. 106. Detail of the seafloor reflectivity chart of the Caucasian margin with the location of sampling sites

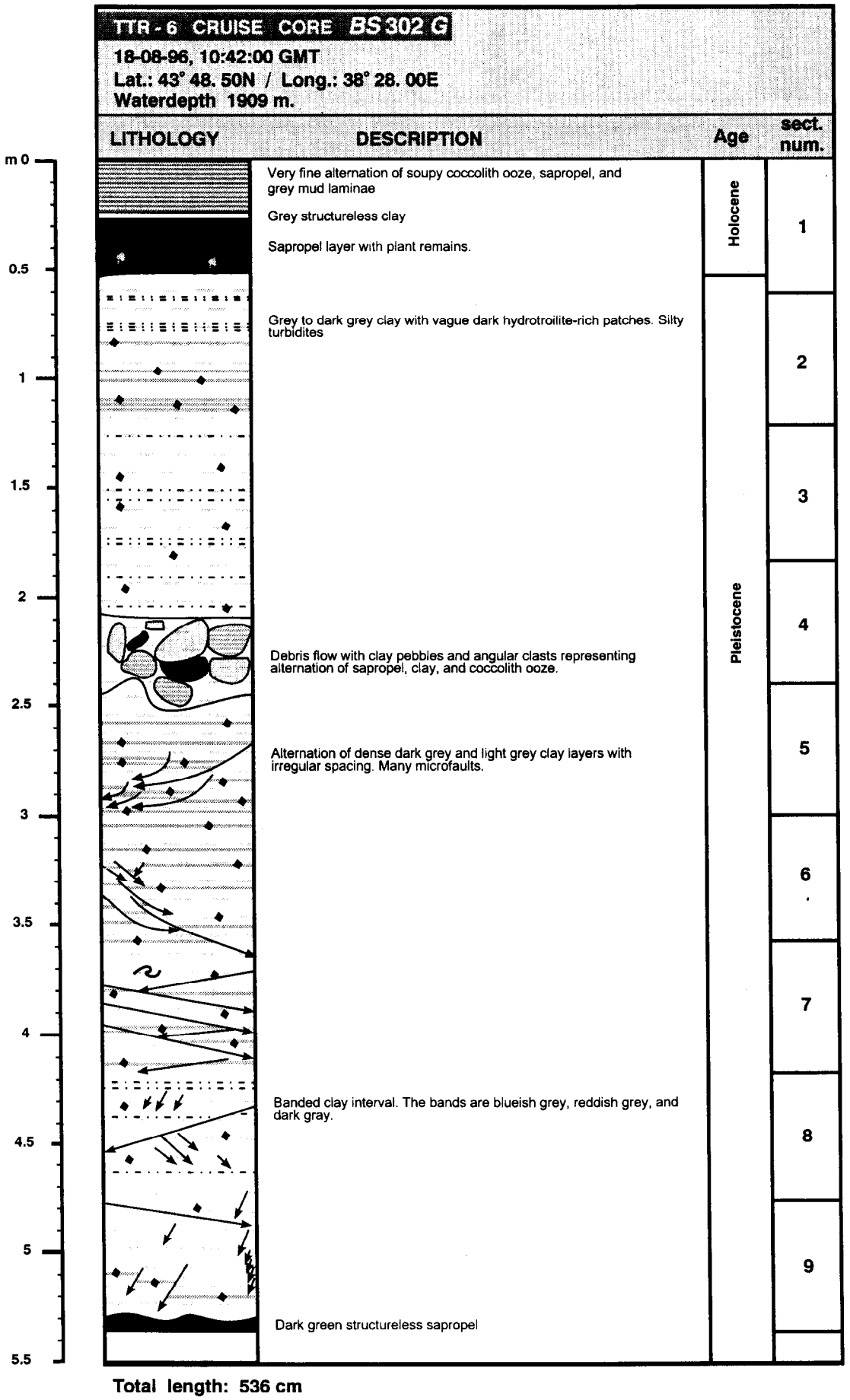

Total length: 536 cm

Fig. 107. Core log BS-302G

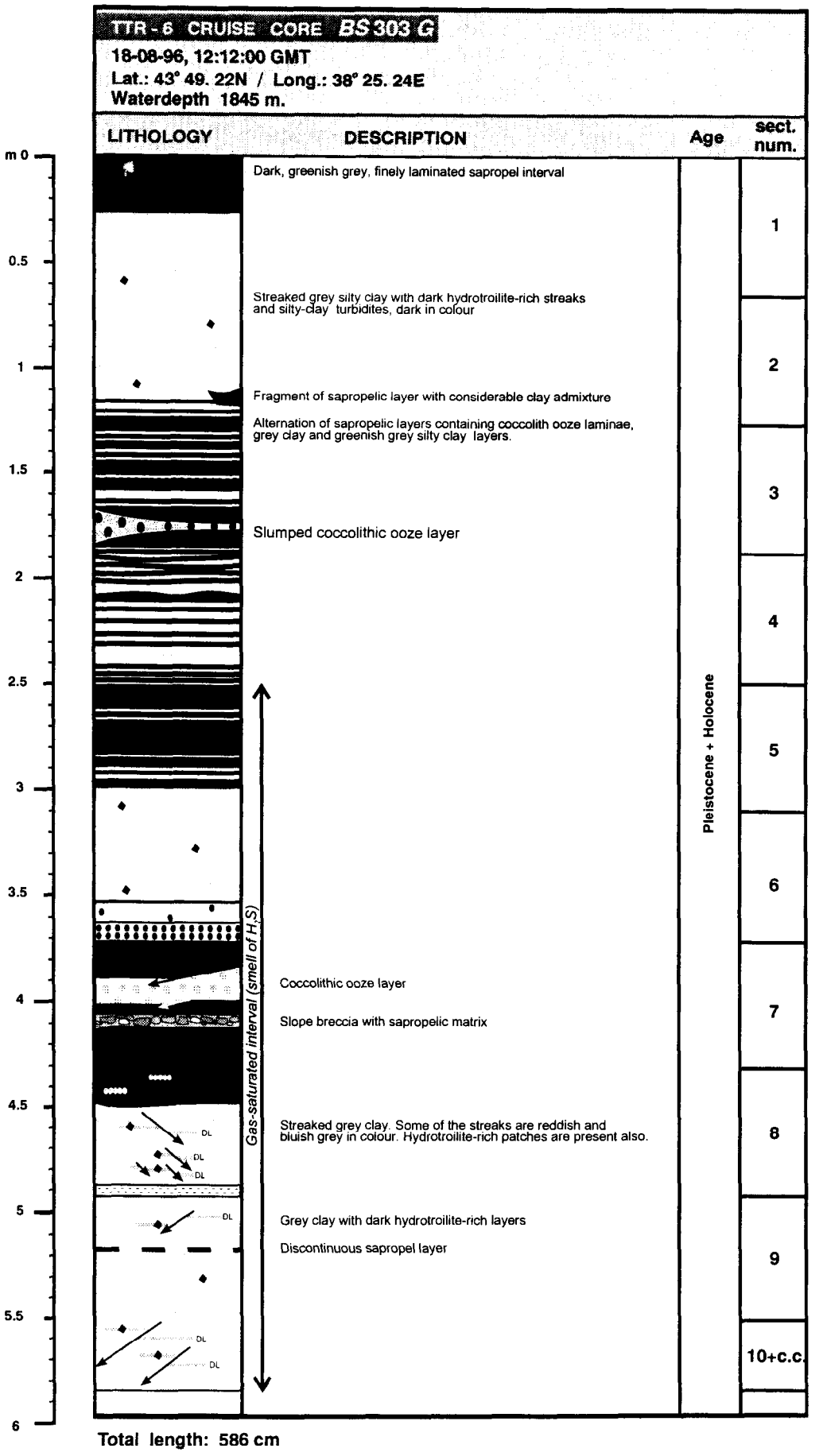

Fig. 108. Core log BS-303G

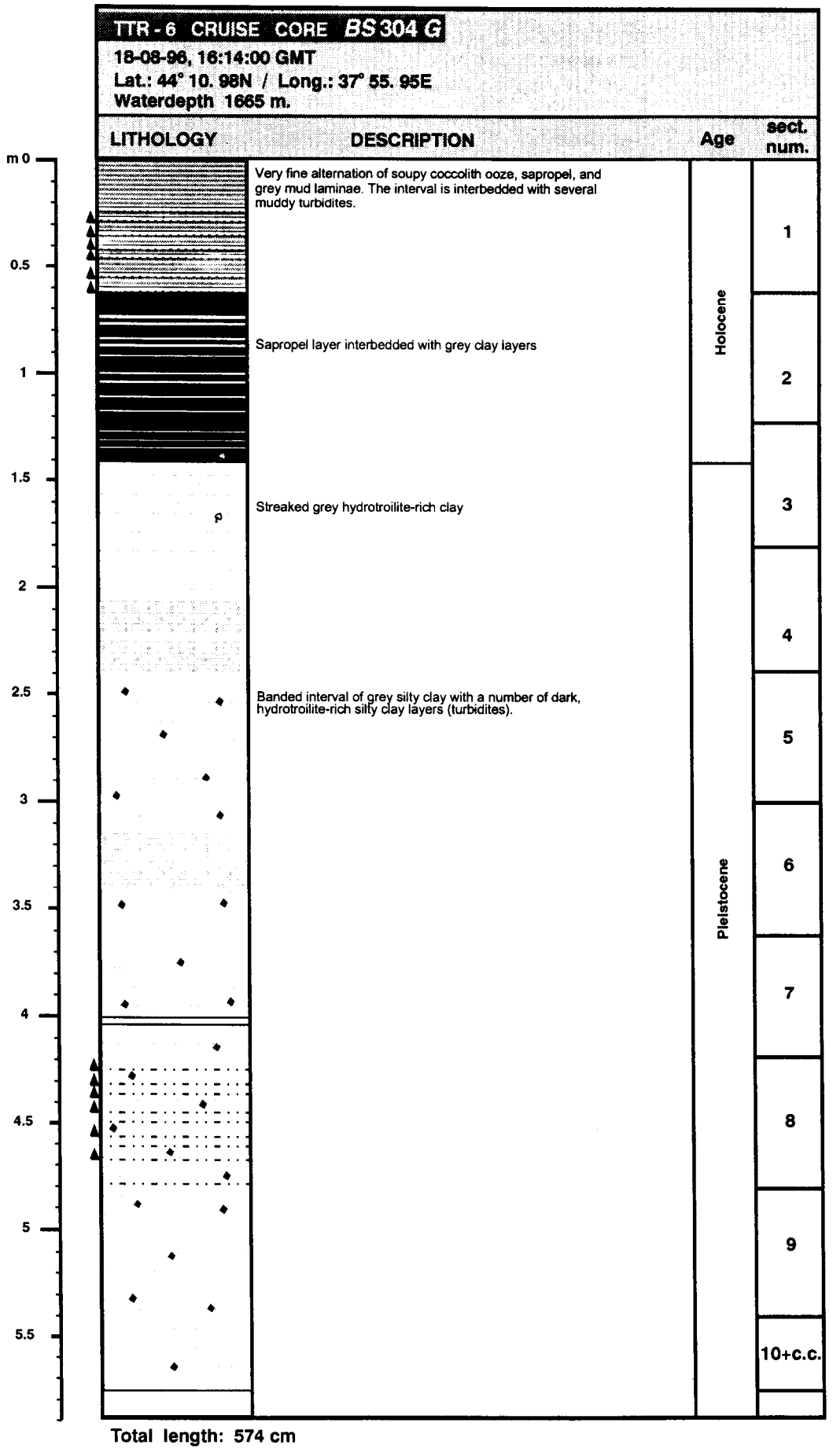

Fig. 109. Core log BS-304G

REFERENCES

Barka, A., Reilinger,R., Saroglu. F, and Sengör, M.C., 1995. The Isparta Angle: its evolution and importance in the tectonics of the Eastern Mediterranean region. IESCA-1995, Programme and Abstracts, Izmir-Güllük, Turkey, 9-14. October 1995: 6.

Bellaiche, G., 1993. Sedimentary mechanisms and underlying tectonic structures of the northwestern Mediterranean margin, as revealed by comprehensive bathymetric and seismic survey. Mar. Geol., 112: 89-108

Buyukasikoglu, S., 1979. Sismolojik verilere gore Anadolu ve dogu Akdeniz'de Avrasya/Afrika levha sinirlarmin ozellikleri. Doktora Tezi, I.T.U., Istanbul, Turkey.

Cita, M.B. and Camerlenghi, A., 1992. The Mediterranean Ridge as an accretionary prism in collision context. Mem. Soc. Geol. It., 45: 463-480.

Cita, M.B., de Lange, G.J., and Olausson, E., 1991. Anoxic basins and sapropel deposition in the Eastern Mediterranean: past and present. Mar. Geol., 100: 1-4.

Cita, M.B., Ivanov, M.K., and Woodside, J.M. (Eds.), 1996. The Mediterranean Ridge Diapiric Belt. Mar. Geol. (spec. volume), 132(1/4): 273 pp.

Clube, T.M.M., and Robertson, A.H.F., 1986. The paleorotation of the Troodos microplate, Cyprus, in the Late Mesozoic - Early Cenozoic plate tectonic framework of the eastern Mediterranean. Surv. in Geophysics, 8: 375-437.

Corselli, C. and Basso, D., 1996. First evidence of benthic communities based on chemosynthesis on the Napoli mud volcano (eastern Mediterranean). Mar. Geol., 132: 227-239.

De Capitani, L. and Cita, M.B., 1996. The "Marker-bed" of the Mediterranean Ridge diapiric belt: geochemical characteristics. Mar. Geol., 132: 215-225.

Emery, K.O., Heezen, B.C., and Allen, T.D., 1966. Bathymetry of the eastern Mediterranean Sea. Deep-Sea Res., 13: 173-192.

Ginsburg, G.D., Kremlev, A.N., Grigoriev, M.N., Larkin, G.V., Pavlenkin, A.D., and Saltykova, N.A., 1990. Filtrogenic gas hydrates in the Black Sea. 21th Cruise of R/V Evpatoria. Geologiya i Geofizika, 3: 10-19 (in Russian).

Gutnic, M., Monod, O., Poisson, A., and Dumont, J.-F., 1979. Géologie des Taurides occidentales (Turquie), Mém. Soc. Géol. France, LVIII: 1-112.

Huchon, P., Lyberis, N., Angelier, J., Le Pichon, X., and Renard, V., 1982.. Tectonics of the Hellenic Trench: a synthesis of Sea-Beam and submersible operations. Tectonophysics, 86: 69-112.

IOC-UNESCO, 1981. International Bathymetric Chart of the Mediterranean. Scale 1 : 1 000 000. Leningrad, Ministry of Defence.

Ivanov, M.K. and Limonov, A.F., 1996. Mud volcanism in the Black and Mediterranean Seas. In: B.A. Sokolov (Ed.). Oil/Gas-Bearing and Coal-Bearing Basins in Russia. Moscow, MGU: 205-231 (in Russian).

Ivanov, M.K., Limonov, A.F, and Cronin, B.T. (Eds.), 1996a. Mud Volcanism and Fluid Venting in the Eastern Part of the Mediterranean Ridge. Initial results of geological, geophysical and geochemical investigations during the Fifth UNESCO-ESF 'Training-through-Research' Cruise of R/V Professor Logachev (July-September 1995), UNESCO Reports in Marine

Science, 68: 127 pp.

Ivanov, M.K., Limonov, A.F., and van Weering, Tj.C.E., 1996b. Comparative characteristics of the Black Sea and Mediterranean Ridge mud volcanoes. Mar. Geol., 132: 253-271.

Ivanov, M.K., Limonov, A.F., and Woodside, J.M. (Eds.), 1992. Geological and Geophysical Investigations in the Mediterranean and Black Seas. Initial results of the 'Training-through-Research' Cruise of R/V Gelendzhik in the Eastern Mediterranean and the Black Sea (June-July 1991). UNESCO Reports in Marine Science, 56: 206 pp.

James, G.A. and Gagnon, A.R., 1994. Radiocarbon chronology of Black Sea sediments. Deep-Sea Res., 41(3): 531-557.

Jongsma, D., and Mascle, J., 1981. Evidence for northward thrusting southwest of the Rhodes Basin. Nature, 293: 49-51.

Kuznetsov, A., 1992. Samples from the Anaximander Mountains. Poster. XXXIIIe Congress and Plenary Assembly of CIESM, Trieste, 12-17 October 1992.

Le Pichon, X., Foucher, J.P., Bouleque, J., Henry, P., Lallemant, S., Benedetti, M., Avdik, F., and Mariotti, A., 1990. Mud volcano field seaward of the Barbados Accretionary Complex: a submersible survey. J. Geophys. Res., 95: 8931-8943.

Limonov, A.F., 1997. Shallow structure of the eastern segment of the Mediterranean Ridge deduced from seismic and sidescan sonar data. Geo.-Mar. Lett. (in press).

Limonov, A.F., Kenyon, N.H., Ivanov, M.K., and Woodside, J.M. (Eds.), 1995. Deep-Sea Depositional Systems of the Western Mediterranean and Mud Volcanism on the Mediterranean Ridge. Initial Results of geological and geophysical investigations during the Fourth UNESCO-ESF 'Training-through-Research' Cruise of R/V Gelendzhik (June-July 1994). UNESCO Reports in Marine Science, 67: 171 pp.

Limonov, A.F., van Weering, Tj.E.C., Kenyon, N.H., Ivanov, M.K., and Meisner, L.B., 1997. Seabed morphology and gas venting in the Black Sea mudvolcano area: observations with the MAK-1 deep-tow sidescan sonar and bottom profiler. Mar. Geol., 137: 121- 136.

Limonov, A.F., Woodside, J.M., Cita, M.B., and Ivanov, M.K., 1996. The Mediterranean Ridge and related mud diapirism: a background. Mar. Geol., 132: 7- 19.

Limonov, A.F., Woodside, J.M., and Ivanov, M.K. (Eds.), 1994. Mud Volcanism in the Mediterranean and Black Seas and Shallow Structure of the Eratosthenes Seamount. Initial results of the geological and geophysical investigations during the Third UNESCO-ESF 'Training-through-Research' Cruise of R/V Gelendzhik (June-July 1993). UNESCO Reports in Marine Science, 64: 173 pp.

Makris, J. and Wang, J., 1994. Bouguer gravity anomalies of the eastern Mediterranean Sea. In: V.A. Krasheninnikov and J.K Hall (Eds.), Geological structure of the Northeastern Mediterranean (Cruise 5 of the Research Vessel 'Akademik Nikolaj Strakhov'). Jerusalem: 87-98.

Mascle, J., Le Cleac'h, and Jongsma, D., 1986. The eastern Hellenic margin from

Crete to Rhodes: Example of progressive collision. Mar. Geol., 73: 145-168.

MEDRIFF Consortium, 1995. Newly discovered brine lakes in the seabed of the Mediterranean Ridge, southwest of Crete. Rapp. XXXIVe Congr. C.I.E.S.M., Résumés des Communications, 34: 111.

Morgunov, Yu.G., Kalinin, V.V., Gainanov, V.G., Kalinin, A,V., Pivovarov, B.L., and Limonov, A.F., 1976. Diapiric folds in the Black Sea south of the Mountainous Crimea. Doklady Akad. Nauk SSSR, 228(5): 1159-1162 (in Russian).

Oral, B., 1994. Global Positioning System (GPS) Measurements in Turkey (1988-1992): Kinematics of the Africa-Arabia-Eurasia Plate Collision Zone. PhD Thesis, Massachusetts Institute of Technology, Cambridge, USA: 344 pp.

Parisi, E., 1987. Carbon and oxygen isotope composition of *Globigerinoides ruber* in two deep-sea cores from the Levantine Basin (Eastern Mediterranean). Mar. Geol., 75: 201- 219.

Parisi, E., Erba, E., and Cita, M.B., 1987. Stratigraphy and sedimentation in the anoxic Bannock Basin (Eastern Mediterranean). Mar. Geol., 75: 93-117.

Robinson A.G., Rudat J.H., Banks C.J., and Wiles R.L.F., 1996. Petroleum geology of the Black Sea. Mar. and Petrol. Geol., 13(2): 195-223.

Rotstein, Y. and Ben-Avraham, Z., 1985. Accretionary processes at subduction zones in the eastern Mediterranean. Tectonophysics, 112: 551-561.

Rotstein, Y. and Kafka, A.L., 1982. Seismotectonics of the southern boundary of Anatolia, eastern Mediterranean region: subduction, collision, and arc jumping, J. Geophys. Res., 87(B9): 7694-7706.

Southward, E.C., Tunnicliffe, V., Black, M.B., Dixon, D.R., and Dixon, L.R.J., 1996, Ocean-ridge segmentation and vent tubeworms (Vestimentifera) in the NE Pacific. In: C.L. MacLeod, P.A. Tyler, and C.L. Walker (Eds.). Tectonic, Magmatic, Hydrothermal and Biological Segmentation of Mid-Ocean Ridges, Geol. Soc. Spec. Publication, 118: 211-224.

Thunell, R.C., Williams, D.F., and Belyea, P.R., 1984. Anoxic events in the Mediterranean Sea in relation to the evolution of late Neogene climates. Mar. Geol., 59: 105-134.

Tugolesov D.A., Gorshkov A.S., Meisner L.B., Solov'ev V.V., and Khakhalev E.M., 1985. Tectonics of the Mesozoic-Cenozoic Deposits of the Black Sea Basin. Nauka, Moscow: 216 pp. (in Russian).

Vine, F.J., Poster, C.K., and Gass, I.G., 1973. Aeromagnetic survey of the Troodos igneous Massif, Cyprus. Nature, Phys. Sci., 244: 34-38.

Woodside, J.M., 1976. Regional vertical tectonics in the eastern Mediterranean. Geophys. J.R. Astr. Soc., 47: 493-514.

Woodside, J.M., 1977. Tectonic elements and crust of the Eastern Mediterranean Sea. Mar. Geophys. Res., 3: 317-354.

Woodside, J.M., 1995. ANAXIPROBE-95. Report of the l'Atalante Expedition, 4-11 August 1995, Heraklion, Crete to Port Said, Egypy. Amsterdam, Vrije Universiteit (unpublished).

Woodside, J.M., Ivanov, M.K., and Shipboard Scientific Party, 1992. The Anaximander Mountains: linking the Hellenic and Cyprus Arcs. Rapp. et Proc.-Verb. des Réunions, 33. Monaco: 155.

Woodside, J.M., Ivanov, M.K., and shipboard scientists R/V Gelendzhik 1992 Training Through Research Cruise, 1993. Is the African Plate tearing between the Hellenic and Cypriot Arcs?. Terra Abstracts supplement 1 to Terra Nova, 5. Oxford, Blackwell Scientific Publications: 272.

Young, C.M., Vaquez, E., Metaxax, A., and Tyler, P.A., 1996. Embryology of vestimentiferan worms from deep-sea methane/sulphide seeps; Nature, 381: 514-516.